THE UNIVERSITY
of EDINBURGH

Nutrient Cycling in the Arctic and Subarctic Oceans: A Stable Isotope Study

Margot Debyser

Thesis submitted for the degree of Doctor of Philosophy

School of Geosciences

The University of Edinburgh

2022

Declaration

I certify that this work is solely my own, except where otherwise stated, and has not been submitted for any other degree or professional qualification at this or any other University.

……..……..

Margot Debyser

Edinburgh, August 28th 2022

Acknowledgments

First and foremost, I would like to thank my supervisory team for their advice and support throughout this project and particularly through this fast-paced summer.

My primary supervisor, Prof Raja Ganeshram for entrusting me with a fascinating research project and for all the polar fieldwork opportunities you have given me since I was 19; they have given me a true passion for my work. Thank you also for pushing my scientific capabilities beyond what I thought myself capable of and for readying me to the world of academia.

My second supervisor, Dr Laetitia Pichevin, for your continued scientific advice, laboratory skills and spectrometric expertise, particularly at the early stages of my PhD, and for the freedom and trust you have given me to get to know and use the mass spectrometer where I was able to develop unvaluable skills.

My third supervisor, Dr Robyn Tuerena, for your expertise on nutrients, laboratory expertise and for always making me feel supported, even while you were on leave. Through your hard-work, energy, positivity and passion, you are a personal inspiration inside and outside of academia.

This work was funded by UKRI, the Changing Arctic Ocean program and SAGES. I would like to thank Colin Chilcott and Louisa Norman for their analytical support. Paul Dodd, Penny Holliday, Igor Yashayaev, Igor Semiletov, Clare Johnson and the ARISE team are gratefully acknowledged for their scientific support in acquiring and interpreting data for this project. Thank you to all the captains, officers, crews and scientists that made my introduction to oceanographic expeditions unforgettable life experiences.

Thank you to the fellow students in our small isotope world, Antonia, Adam, Philip and Marta, as well as my PhD cohort friend Dylan, who have endured all these long hours in the offices and labs by my side. I thank you all for the good spirits, laughter and the niche geochemistry patter which would have be lost on the rest of the world.

From the bottom of my heart, I would like to thank all of my incredible friends for keeping me sane over these trying years and particularly through the last few months. For all the memories we share of these last eight years in Edinburgh. Thank you for the laughs, the food, the wheels and the roofs, for your love of the outdoors and always keeping high spirits on gloomy days. In no specific order: Flavie, Helen, Fiona, Emily, Anna, Sam K., Sam P., Alex, Marianne & Molly. You mean the world to me. A particularly big shout out to Nicky & Pete for being incredible flatmates and friends this last month. You are remarkable people and a joy to live with.

Finally and most importantly, thank you to my family for being there for me since the start and whenever I need it the most. My dad, Pascal, my mom, Valérie and my brother, Thomas. These last years have been a long and tough journey, and I could not have gotten here today without your love, your help and your continued support.

Thesis Abstract

Anthropogenic global warming is actively changing nutrient supply and the food web of the Arctic Ocean and the subpolar regions. This study uses the stable isotopes of dissolved silicon and nitrate, two vital nutrients for marine life, to investigate the marine biogeochemical cycling of nutrients in these regions. This work analyses datasets acquired from 7 oceanographic expeditions in three key regions: the Laptev Sea shelf, polar outflow waters of the Fram Strait (79˚N) and a full transect across the subpolar North Atlantic (50-60˚N). Hydrographic data, alongside concentrations of nitrate (NO_3), dissolved silicon (DSi) and their isotopic composition ($\delta^{15}N\text{-}NO_3$, $\delta^{18}O\text{-}NO_3$, $\delta^{30}Si(OH)_4$) is presented to provide spatially and temporally integrated information on biogeochemical cycling in these regions. The overall objective of this work is to determine the processes which control nutrient budgets and cycling in the Arctic Ocean, export to the subpolar regions and the sensitivity of these processes to ongoing climate change.

On the shallow Eurasian shelves of the Arctic Ocean, nitrogen is strongly depleted. This results from intense biological utilisation and significant benthic denitrification in the coastal regions, coupled with nitrogen-poor freshwater sources. Primary production in these regions is limited by N availability as a result of this. This puts a biological control on the extent of DSi utilisation in surface waters and modulates its export to the central Arctic Ocean. Over 40% of riverine DSi supplied by the Lena river is consumed and buried into the sediments of the Laptev shelf, enabled by vigorous recycling of nitrogen. Extrapolating these burial rates to the Eurasian shelf leads to an excess riverine DSi export of 3.10 ± 0.71 kmol/s through the Transpolar Drift to the central Arctic Ocean and outflowing currents.

Consequently, Eurasian rivers significantly contribute to the DSi inventory of outflow polar surface waters, providing 40 ± 4% of the total DSi. By contrast, Pacific sources, which were previously estimated to be an important source of export of DSi, only contribute to 8 ± 1% of the total inventory. Glacial DSi influence from melting of the Greenland Ice sheet was found to be negligible. The Si budget is thus primarily controlled by biological processes on Arctic shelves, which currently act to

enrich the $\delta^{30}Si(OH)_4$ outflowing water masses by 0.1‰ compared to Atlantic inflow (1.7‰). Climate change is increasing riverine inputs of DSi faster than N. As the export of DSi from the Arctic Ocean is dependent on N-availability, outflow waters could transport a larger flux of DSi in the future, with lowered isotopic signature.

In the subpolar North Atlantic, nutrient properties of surface waters are integrated into the deep through convective water mass formation. Thus, biological assimilation and regeneration of nutrient stocks at high and low latitudes impact the nutrient inventory of North Atlantic deep waters. Surface waters of the North Atlantic have lighter $\delta^{30}Si(OH)_4$ (1.7‰) than predicted considering its nutrient deplete nature. Important processes at low latitudes act to dilute DSi concentrations of Atlantic surface waters and dampen their isotopic signature. This signal is integrated with the one of heavily utilised surface waters from the subpolar regions and the Nordic Seas into the deep North Atlantic. In recent years, deviation of the Labrador Current to the subpolar North Atlantic has reduced N assimilation. The freshwater content of the subpolar regions is predicted to increase from increased glacial melt and freshwater supply. This can act to increase stratification and decrease primary production of the region in the future. Due to the interconnectivity of the subpolar regions on the global scale, this can be reflected into the deep convective waters of the Atlantic and affect nutrient availability in the Eurasian Arctic.

Lay Summary

Around half of all photosynthesis on our planet happens in the oceans. Photosynthesis is carried out by algae in surface waters, which need nutrients to grow. Global warming in the Arctic regions and the North Atlantic is affecting the supply of these essential nutrients to the surface ocean. Algae are the base of the marine food chain, and their future is uncertain under current climate change scenarios.

This work examines the sources of two vital nutrients, nitrate and silicic acid, to the Arctic Ocean and the North Atlantic. Arctic rivers are found to be an important source of silicic acid to the Arctic Ocean. Biological activity controls the distribution of nutrients in the Arctic. Low concentrations of nitrate in the coastal seas of the Arctic limit biological activity, which allows silicic acid to leak out of the Arctic Ocean into the North Atlantic. As river discharge increases because of climate change, an increasing amount of silicic acid is expected to be transported out of the Arctic Ocean.

In the Atlantic Ocean, recent freshening events have reduced biological activity in surface waters, with far-reaching impacts to the Arctic regions and deep waters of the North Atlantic. The results from this study can be used to understand how humans have impacted algae growth in our oceans and to predict how Arctic and North Atlantic marine food chains will be impacted in the future.

Thesis Overview

Chapter 1 provides an introduction to the marine silicon and nitrogen cycles as well as stable isotope systematics and their use in the oceanographic context. It also provides an introduction to nutrient cycling in the Subpolar North Atlantic and Arctic Ocean, and a literature review of our current knowledge on isotope systematics in these regions.

Chapter 2 describes the fieldwork undertaken for this study and the seven oceanographic cruises from which samples were analysed. Methodology, analyses and data quality checks associated with this study are described in this chapter.

Chapter 3 is based on a manuscript submitted to *Biogeosciences* and examines the biogeochemistry of the Fram Strait region of the Arctic Ocean. The isotopes of nitrate and silicon are examined to understand the nutrient origins of outflowing polar waters. The improved mechanistic understanding of nutrient supply to the Fram Strait is used to discuss how nutrient availability and changing supply may affect downstream ecosystems and nutrient stoichiometry in the context of global warming.

Chapter 4 is based on a manuscript aimed for submission in *Global Biogeochemical Cycles* and focusses on the delivery of dissolved silicon and its cycling on Eurasian shelves, with an emphasis on the distribution of silicon isotopes in the Laptev Sea and the export of its signature through the Transpolar Drift. The documentation of shelf burial of silicic on Eurasian shelves is used to update the silicon isotope budget of the Arctic Ocean. The biological controls of the Arctic's Silicon (Si) budget is discussed in the context of climate change. The distribution of Nitrogen (N) isotope species for the Laptev Sea is also presented in an appendix to Chapter 4.

Chapter 5 describes the biogeochemistry of the subpolar North Atlantic regions through N and Si isotopes to understand the mechanisms of low-latitude and high-latitude (Arctic) nutrient supply which eventually contribute to North Atlantic Deep Water inventory through convective water mass formation. This is examined in the context of recent freshening events to the subpolar regions and Atlantification of the Eurasian Arctic Ocean. The findings of Arctic and subarctic nutrient cycling from

this thesis are put into the global context of the meridional overturning circulation of the Atlantic Ocean.

Chapter 6 summarises the main findings from this thesis, focusing on how they refine our current scientific understanding of the biogeochemistry of the Arctic and subarctic regions. A critical evaluation of this study is presented, and future research priorities to address existing gaps in our understanding of marine nutrient cycling are identified.

Table of Contents

Acronyms

Water masses & currents of the Atlantic Ocean

AABW – Antarctic Bottom Water

AAIW – Antarctic Intermediate Water

DSOW – Denmark Strait Overflow Water

ISOW – Iceland Strait Overflow Water

IW – Irminger Water

LC – Labrador Current

LSW – Labrador Sea Water

MOW – Mediterranean Outflow Water

NAW – North Atlantic Water (from the North Atlantic current)

NADW – North Atlantic Deep Water (layer of multiple water masses)

NEADW – NorthEast Atlantic Deep Water

WTOW – Wyville-Thomson Overflow Water

WGC – West Greenland Current

Water masses & currents of the Arctic Ocean

AAW – modified Arctic Atlantic Water

AW – Atlantic Water inflow

DW – Deep Water (Fram Strait)

LFP – Lena river Freshwater Plume

OSW – Old Shelf Water (Laptev shelf)

PSW – Polar Surface Water

SAMW – Sub-Antarctic Mode Water

SFL – Surface Freshwater Layer (Laptev shelf)

TPD – Transpolar Drift

Other terms

AOU - Apparent Oxygen Utilisation

BSO – Barents Sea Opening

CTD – Conductivity Temperature Depth

CPND – Coupled Partial Nitrification Denitrification

DOC – Dissolved Organic Carbon

DON – Dissolved Organic Nitrogen

DSi – Dissolved Silicon

MAGIC – MAGnesium Induced Co-precipitation

MLD – Mixed Layer Depth

MOC – Meridional Overturning Circulation

OM – Organic Matter

OMZ – Oxygen Minimum Zone

PN – Particulate Nitrogen

PON – Particulate Organic Nitrogen

PSi – Particulate Silicon

TDN – Total Dissolved Nitrogen

1. Introduction

Nitrate (NO_3) and silicic acid ($Si(OH)_4$) are two vital nutrients for marine life. Biological production from microbes and algae converts inorganic carbon and nutrients to organic matter in the surface of the ocean (photic zone) through photosynthesis. The biological availability and physical transport of nutrients regulates the distribution and abundance of these organisms around the global ocean. This cycling is referred to as the "marine biological carbon pump", which regulates atmospheric CO_2 through the trapping of Carbon (C) into the deep ocean by biological activity. Anthropogenic global warming is drastically changing the environment of the Arctic Ocean, thus actively changing nutrient supply to primary producers in these regions. This study investigates the biogeochemical cycling of Silicon (Si) and Nitrogen (N) in the Arctic Ocean & Subpolar North Atlantic. The objective of this work is to determine which processes control nutrient budgets and cycling in the Arctic Ocean, export to the subpolar regions and the sensitivity of these processes to ongoing climate change.

1.1 An Introduction to the marine silicon cycle

Dissolved Silicon (DSi), primarily in the form of silicic acid, is a key nutrient to silicifiers. Silicifiers are an important type of primary producers which constitute the base of the marine food chain (diatoms, silicoflagellates, siliceous sponges…). These organisms use DSi to precipitate biological Si (opal) into their internal and/or external structures. Diatoms globally consume vast amounts of DSi along with N and inorganic carbon, and are estimated to contribute to around 40% of the total primary production in the oceans and 20% of all photosynthesis on Earth combined (Benoiston et al., 2017; Field et al., 1998). Historically, research has primarily focused on C and N in the context of anthropogenic-induced environmental changes, limiting our understanding of the cycling of Si which sustains nearly half of all marine productivity. Additionally, diatoms are highly efficient at sequestrating carbon, and are thus intertwined with the CO_2 inventory of the atmosphere on geological timescales (Pichevin et al., 2014; Pondaven et al., 2000; Sarmiento et al., 2004; Tréguer et al., 2018).

1.1.1 Sources of marine DSi

Silicon is the second most abundant element in the Earth's crust, but is only available to primary producers in its dissolved form. All four DSi sources (continental, aeolian, hydtrohermal and sedimentary) to the ocean are ultimately derived from the weathering of the Earth's crust (Frings et al., 2016; Tréguer and De La Rocha, 2013).

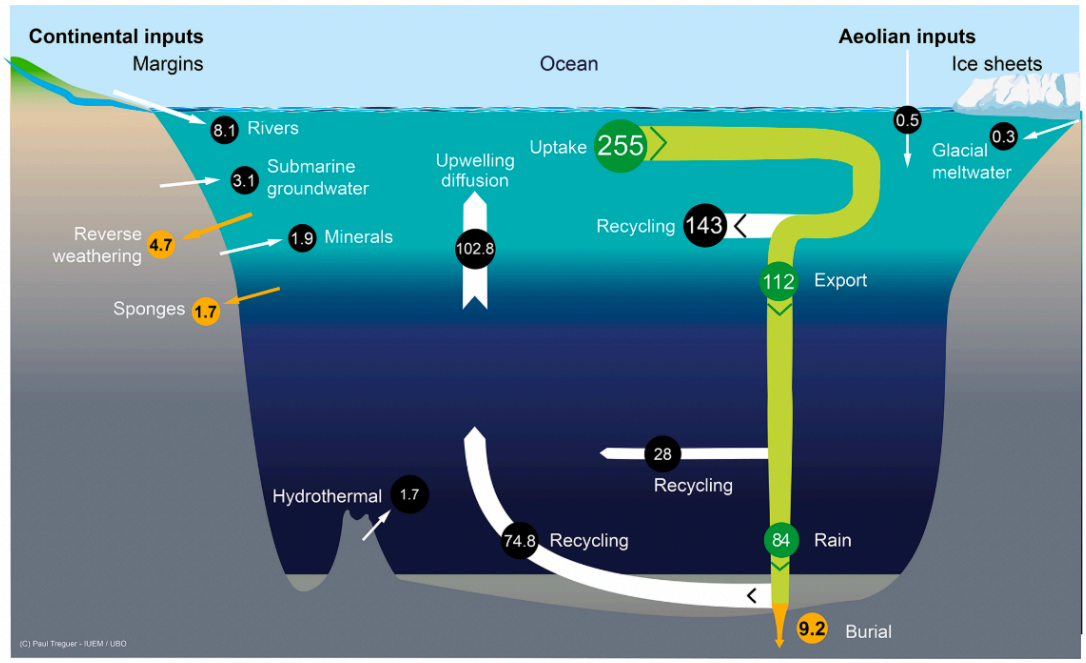

Figure 1.1. Schematic of the modern marine dissolved Si cycle and the magnitude of its fluxes. All fluxes are in Tmol Si/yr. Taken from Tréguer et al. (2021).

Chemical weathering of the continental crust produces DSi and particulate amorphous silica. These fluxes of DSi along with dissolvable biogenic silica are transported to coastal areas via river, glacier and submarine discharge of groundwater. Submarine groundwater is not well characterised in the ocean, but can be of the same order of magnitude as riverine input (Georg et al., 2009a) with significant mineral dissolutions. River and submarine discharge fluxes combined constitute >70% of the total inputs of DSi to the oceans (Tréguer et al., 2021). The fluxes of marine DSi and their magnitude are schematically shown on Figure 1.1.

Aeolian dust inputs of DSi via particle deposition and subsequent dissolution can be an important source of DSi in coastal areas but is not well constrained. The North Atlantic and the Western North Pacific receive significant Particulate Silicon (PSi)

inputs from the Sahara and Gobi deserts respectively, however it is uncertain how much dissolves to become bioavailable (Tréguer and De La Rocha, 2013).

Deep-sea hydrothermal vents leach silicon-rich fluids from the oceanic crust, albeit cooling of these fluids quickly removes DSi via precipitation of secondary clay minerals. This source is not well characterised nor constrained but may be regionally important along the mid-Atlantic ridge (Brzezinski and Jones, 2015) and the deep Arctic Ocean around major hydrothermal vents (Liguori et al., 2020). It is estimated to contribute to around 10% of all marine DSi.

The final source of DSi to the ocean is from low-temperature dissolution of siliceous minerals both in seawater and from the sediments. Lithogenic dissolution happens through 1) the dissolution of riverine lithogenic particles deposited along the continental margin and shelves and 2) the deep dissolution of basaltic glass in seawater. Non-biogenic dissolution of sedimentary Si leads to an estimated flux of 1.9 Tmol Si/yr (Frings et al., 2016; Tréguer et al., 2021).

1.1.2 Biological fluxes of DSi

Biological Si (opal) is produced from DSi by photosynthesizing organisms in the surface ocean. Over half of biological Si is internally recycled within the upper ocean to DSi, while the remaining opal is exported to the deep ocean. The biological uptake of DSi in the global ocean is 255 TmolSi/yr (Tréguer et al., 2021 and references therein), and by far the largest flux of DSi in the marine environment, illustrating the strong biological control on the marine Si cycle. Gross and net primary production of opal distinguish between the apparent and total flux of Si which is internally cycled. Concentrations and stoichiometric parameters struggle to resolve the latter, and the isotope of DSi is a useful complementary tool to capture this component.

Diatoms thrive in nutrient-rich turbulent conditions, and thus are prevalent at high latitudes and coastal upwelling regions (Nelson et al., 1995; Tréguer et al., 2018). Studies suggest that below 5 μM of ambient DSi and in the absence of N-limitation, kinetic limitation occurs (Krause et al., 2018). Thus, DSi availability sometimes become limiting to diatom growth before DSi is fully consumed (Giesbrecht et al.,

2022). At high latitudes, diatoms are typically the first phytoplankton group to bloom during the spring (Reigstad et al., 2002), but sub-optimal conditions favour the growth of other phytoplankton species and non-silicifiers as DSi stocks become deplete over the growth season.

1.1.3 Sinks of marine DSi

The main loss of DSi from the oceans is through its assimilation by plankton to form biogenic silica, and its subsequent long-term burial into the sediments. Unlike the remineralisation of Particulate Organic Nitrogen (PON), water-column and sedimentary dissolution of opal is much smaller, and thus sedimentary burial accounts for 60% of all sinks of DSi (Tréguer et al., 2021). Sedimentary burial rates are tied to the distribution and density of organic matter, and are highest in the Southern Ocean, equatorial Pacific and coastal and continental margin zones (DeMaster, 2002). Post-depositional distribution sedimentary processes strongly affect the preservation of opal in sediments, which can lead to large bias in their estimation (Geibert et al., 2005; Hayes et al., 2021) and a 46% increase in its estimated flux linked to this bias (Tréguer et al., 2021; Tréguer and De La Rocha, 2013). The burial of opal is also particularly high in estuarine and river plume environments, where river-borne nutrients fuel diatom blooms. The high rates of organic matter formation, sedimentation and export lead to particularly high burial rates of Si in these environment.

Sponges are also a sink of DSi as they slowly accumulate biological Si over their lifetime, into the sediments upon sponge death. The difference between sponge DSi demand and the much smaller flux of DSi from sponge skeletal dissolution on the continental shelf is estimated at 1.7 ± 1.6 Tmol Si/yr (Maldonado et al., 2019). Nevertheless, this flux is associated with large uncertainty and geographical sponge distribution remains poorly constrained.

The final sink of DSi, reverse weathering, occurs primarily in estuaries and river plumes. Riverine PSi and DSi fuels authigenic clay formation ubiquitously in the global ocean which removes additional DSi from the system (Ehlert et al., 2016; Michalopoulos and Aller, 2004). Combined with the high burial rates, this make

deltaic environments particularly important for the fate of continental DSi to the open ocean.

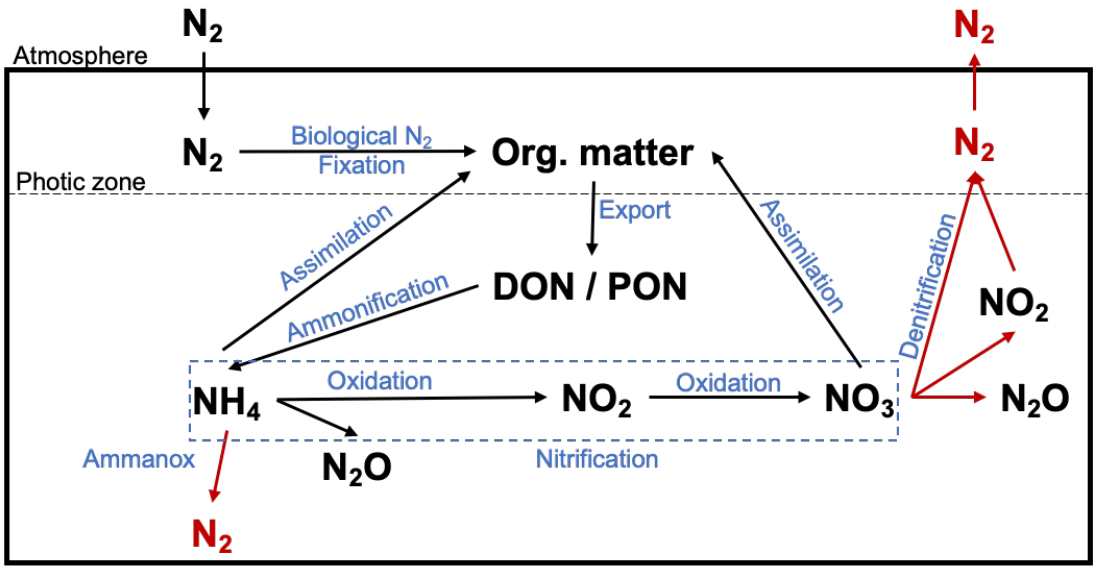

Figure 1.2. Schematic of fixed nitrogen cycling in the ocean. Black arrows show aerobic processes, red arrows anaerobic processes.

1.2 An Introduction to the marine nitrogen cycle

Fixed nitrogen (in the forms of nitrate, ammonium and nitrite) is a major nutrient required by all primary producers in the oceans and its availability regulates marine productivity in large parts of the world's surface oceans. Fixed nitrogen is often fully consumed in surface waters, acting as the limiting nutrient to phytoplankton growth in the majority of the ocean (Moore et al., 2008, 2013), thus shaping oceanic biogeochemistry, carbon export and eventually global climate (Gruber, 2004).

The marine cycle of N is biologically mediated, making it relatively more complex than that of Si. Its cycling in the marine environment is described on Figure 1.2. Processes can act to add fixed nitrogen to the marine pool (biological nitrogen fixation) or remove it (denitrification), with internal cycling processes (assimilation, remineralisation) regulating its speciation within the system. The principal form of fixed N in the ocean is nitrate (NO_3), which accounts for ~90% of the marine N reservoir (Gruber, 2004)

1.2.1 Sources of Fixed N

The most abundant form of nitrogen in the oceans is inert N_2 (94%), and is not bioavailable to most primary producers. Diazotrophs, N_2 fixing species (mainly cyanobacteria from the *Trichodesmium* species), fix atmospheric nitrogen into ammonia which is subsequently available to other primary producers.

Biological nitrogen fixation is the main source of fixed nitrogen to the ocean (140 Tg N/yr, Voss et al., 2013), occurring primarily at low-latitudes and upwelling zones in tropical and subtropical waters. Nitrogen is also added to the oceans via atmospheric deposition (30Tg/yr, Fowler et al., 2013) and riverine discharge (40-60 Tg N/yr, Voss et al., 2013), and are particularly important N sources to coastal areas. While the distribution of atmospheric deposition is not well constrained, these two inputs have been nearly doubling from anthropogenic activity (Fowler et al., 2013) and are expected to continue rising.

1.2.2 Sinks of Fixed N

The main sink of marine fixed N is through denitrification, an anaerobic process relying on anaerobic bacteria which use nitrate as a source of energy. In low oxygen conditions (Oxygen Minimum Zones, OMZ or Oxygen Deficient Zones, ODZ), where O_2 is below 4-5µM, anaerobic metabolisms are activated (Codispoti et al., 2001). In these conditions, organisms use NO_3 as electron acceptors instead of O_2, which yields the next highest energy level in the oxidation process, and produces N_2 as a by-product.

Denitrification occurs both in the water column and within the sediments (benthos). Strong oxygen minimum zones are indicative of water-column denitrification, such as in the Eastern tropical Pacific and Arabian Sea (Codispoti et al., 2001; Gruber and Sarmiento, 1997). Suboxic conditions in the benthos occur when the rate of molecular diffusion of oxygen from the water above the sediments is lower than the rate of oxygen demand from organic matter breakdown. Benthic denitrification occurs more uniformly across oceanic basins, with an estimated loss of 200-250 Tg N/yr compared to 100 Tg N/yr for water column denitrification (Brandes and Devol, 2002). The rates of benthic denitrification is tightly linked to the supply of organic

matter, and are thus highest near continental margins over shallow water columns. Additional pathways also exist in the conversion of fixed N to N_2. Fixed nitrogen (nitrite and ammonia) is also lost via anammox (anaerobic ammonium oxidation) to a smaller extent in anaerobic conditions during CO_2 fixation. Unlike denitrification, annamox does not produce N_2O during incomplete reactions, a potent greenhouse gas. Overall, incomplete nitrification and denitrification represent 30% of the total atmospheric inventory of N_2O, further linking the Earth's climate to marine nutrient cycling (Codispoti et al., 2001).

The cycling of N is highly dynamic, and the balance between sources and sinks is kept by a negative feedback loop, roughly dictated by N_2 fixation and denitrification respectively. Given that these processes are spatially separated in the ocean, the feedback system between the two processes ties to the meridional overturning circulation on timescales around 1000 years (Gruber and Sarmiento, 1997).

1.2.3 Internal Cycling

The dominating process of the marine N cycle is assimilation, where nitrate is taken up by primary producers during photosynthesis in the photic zone of the surface ocean, producing organic matter. Assimilation occurs at an estimated rate of 320 Tg N/yr across the global ocean (Voss et al., 2013).

Organic matter is eventually degraded into Dissolved Organic Nitrogen (DON) and PON. The particulate pool is mainly remineralised within the water column or the sediments, leaving only a small part to be buried into the sediments. The remineralisation to nitrate occurs in multiple steps of oxidation from ammonium to nitrite and eventually nitrate. Ammonification is the biologically mediated conversion of organic matter to ammonium by heterotrophic bacteria which lack the enzymes required to fully carry out the oxidation to nitrate.

The next two steps, referred to as nitrification, complete the oxidation process through chemo-autotrophic bacteria which use the oxidation of N species as their source of energy. The remineralisation of nitrate takes place in oxic conditions, and is most efficient at the bottom of the euphotic zone in low light availability, which

gives an advantage to nitrifying bacteria over phytoplankton assimilation. In well mixed environments, nitrification and assimilation often co-occur in surface waters (Rafter et al., 2019).

The tracer N* (calculated as $NO_3 – 16*PO_4$, modified from Gruber and Sarmiento, 1997) represents the excess or deficit of nitrate relative to phosphate compared to the Redfield stoichiometry from processes of denitrification or N fixation. N* is an extremely valuable water mass tracer, however it still has a few disadvantages: It is a concentration based approach and thus only considers the net source and sink of nutrients and these processes are underestimated while occurring in close proximity. Additionally, this concentration based approaches overlook important internal cycling processes, thus nitrate isotope signatures are useful additional tracers to N-cycling and constrain its internal processes.

1.2.4 Coupling of the marine N and Si cycles

Both the cycles of DSi and N are strongly biologically regulated. All phytoplankton, including silicifiers, require nitrate and phosphate to grow, and in most of the global ocean, phytoplankton growth is limited by nitrate availability (Moore et al., 2013). In the subpolar north Atlantic and the Arctic Ocean, DSi can also act as the limiting nutrient to diatom growth when nitrate remains in excess (Agustí et al., 2018; Krause et al., 2019).

Phytoplankton consume nitrate and phosphate following near-Redfield ratio (N:P = 15-16), which is remineralised quasi-conservatively in the water column. The consumption of DSi with respect to N is more variable (DSi:N ≈ 1), and DSi tends to be remineralised deeper in the water column through dissolution rather than decomposition of soft tissues. This highlights the biogeochemical importance of diatoms which rapidly sink out of the photic zone and export organic matter to the deep ocean, fuelling new production in the surface ocean. Upon depletion of DSi stocks, a shift towards non-diatom primary producers leads to the use of an increased proportion of regenerated nutrients within the photic zone, and hence an increased proportion of uptake from regenerated nutrients as opposed to pre-formed nutrients (Yool and Tyrrell, 2003). The stoichiometric tracer Si* (= $DSi – NO_3$, Sarmiento et

al., 2004) is derived from typical DSi:N uptake ratios by diatoms and is conserved if both nutrients are equally remineralized. Negative Si* are expected during the preferential remineralization of nitrate or non-siliceous organisms, while positive Si* may indicate strong denitrification.

Ambient nutrient concentrations impact the ratio in which diatoms uptake DSi:N, shifting from 1.7:1 in nutrient replete conditions to 1:1 in limited conditions in the Atlantic sub-Arctic (Krause et al., 2018), hence affecting the nutrient uptake by total phytoplankton community over the growth season. Thus, both nitrate and DSi availability impacts the total production and composition of phytoplankton growth, as well as the efficiency and stoichiometry to which nutrients are exported to deep waters.

1.3 An Introduction to the Subpolar North Atlantic & Arctic Oceans

1.3.1 Physical Circulation & Processes

Nutrient distribution and cycling in the global ocean is tightly linked to the physical transport of water masses, through lateral transport, upwelling, convection and mixing which acts to resupply nutrients to surface waters. Here a brief overview of the physical oceanographic setting of the subpolar North Atlantic Ocean and the Eurasian Arctic is provided as a baseline for the interpretation of geochemical parameters within this study.

1.3.1.1 The Subpolar North Atlantic

The subpolar North Atlantic is an important area of sea-air exchange, and feeds into the global thermohaline circulation as an area of deep water formation. Deep waters in these regions form through cooling of northward flowing high salinity waters and deep winter convection of surface and intermediate waters, entraining carbon and nutrients from the surface to the deep. These dense, deep waters are subsequently exported through the Labrador Sea and form the southward flowing limb of the Meridional Overturning Circulation (MOC), as schematically shown on Figure 1.3.

The MOC is important to the climate system as it carries heat and carbon northward, and from the surface to the deep ocean, sequestrating C from the atmosphere and nutrients from surface waters.

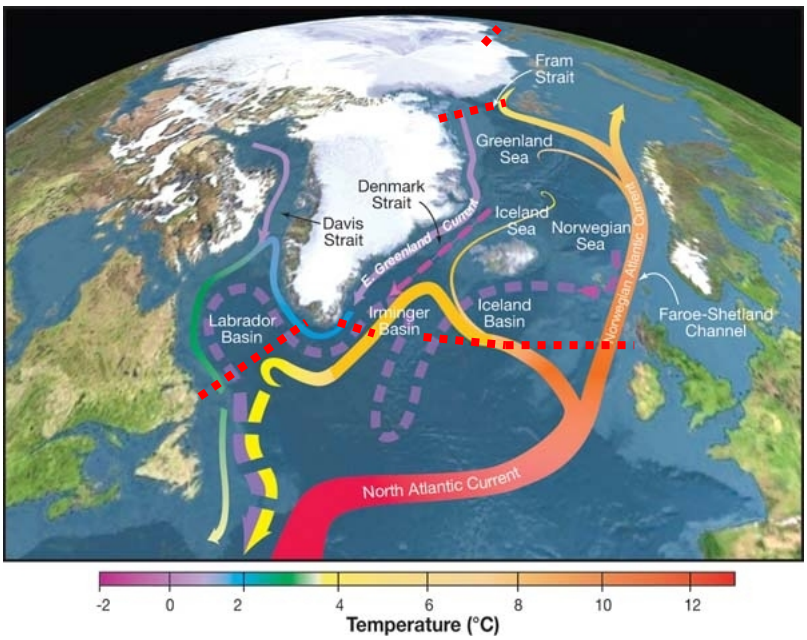

Figure 1.3. Map of the subpolar basins with schematic circulation of the Atlantic Meridional Overturning Circulation (MOC) as surface currents cool and sink to form deeper southward flowing waters. Surface/intermediate currents are displayed with solid arrows and deep currents with dashed arrows. Red dotted lines show the approximate location of oceanographic transects of this thesis with respect to the convective basins and Arctic currents. Adapted from Curry and Mauritzen (2005).

In the North Atlantic, the MOC is characterised by a northward flux of warm waters in surface and intermediate waters, North Atlantic Waters (NAW) from the North Atlantic current which extends from the Gulf Stream. NAW is compensated by a southward flux of cool deep waters (Li et al., 2021; Lozier et al., 2019). NAW either continues flowing northward into the Nordic Seas to eventually reach the Arctic Ocean (<40%), or is incorporated into NADW. Across the sector, the warmest, saltiest branch of NAW is found over the Rockall Trough, with waters becoming increasingly fresher and cooler westward as they circulate through the subpolar regions. The hydrography of the surface North Atlantic is characterised by two gyre system, the subtropical and subpolar gyres, with contrasting hydrographic features. The subtropical gyre is stratified year-round, while the subpolar gyre experiences

deep winter mixing and ventilation, thus affecting the biogeochemistry of the upper water column.

Deep water formation occurs in the Nordic basin, Irminger basin and the Labrador basin. Overflow of cold, dense water in the Nordic Seas across the ridge between Greenland and Scotland forms Denmark Strait Overflow Water (DSOW), the main component of NADW and deep limb of the MOC, which spreads into the Labrador Sea. The deep waters of the Iceland basin host Iceland-Scotland Overflow Water (ISOW), where cold, dense water in the Nordic seas overflow along the crest of the Iceland-Scotland ridge, spreading southwards (Saunders, 2001).

The Labrador Sea is the coldest and freshest basin of the North Atlantic Ocean. Two fresh and cold Arctic Ocean currents pass around the Labrador Sea margins: the Labrador Current (LC) and the West Greenland Current (WGC). Offshore of the continental slopes, warm, saltier waters are found, the final destination of NAW from the North Atlantic Current system. NAW has undergone significant cooling and freshening during their transit through the subpolar gyre, reducing stratification of Atlantic Water (AW), although steep density gradients between polar and Atlantic originating currents are still observed. This leads to strong lateral and horizontal mixing, exchanging heat and freshwater, contributing to the in situ formation of Labrador Sea Water (LSW). Thus, strong surface cooling forms the intermediate water mass of LSW, which is a key component of upper NADW (Yashayaev, 2007; Yashayaev et al., 2015; Yashayaev and Loder, 2009). The production of LSW displays strong interannual variation linked to ocean-air interactions, with convective depths varying between 500-1100m, and occasionally reaching down to 1600m (Yashayaev, 2007; Yashayaev and Loder, 2009). Upon formation, LSW spreads southwards into the Atlantic towards the Equator, although a large branch recirculates into the subpolar basins, dominating the intermediate depths of the water column in all four basins of the subpolar North Atlantic.

1.3.1.2 The Arctic Ocean & its shelves

The Arctic Ocean is nearly completely landlocked and water exchange to the Atlantic & Pacific Ocean is restricted to three shallow straits (the Barents Sea

Opening, Bering Strait and the Davis Strait) and one deep strait: the Fram Strait. Over 7sv of Atlantic water from the North Atlantic current flows into the Arctic Ocean through the Barents Sea Opening and the Fram Strait, delivering oceanic heat to the central Arctic (Tsubouchi et al., 2012). Freshwater and sea ice is exported out of the Arctic Ocean primarily through polar surface currents, namely from >1Sv of low salinity Pacific inflow through the Bering Strait, precipitation and riverine freshwater (Aagaard and Carmack, 1989; Haine et al., 2015).

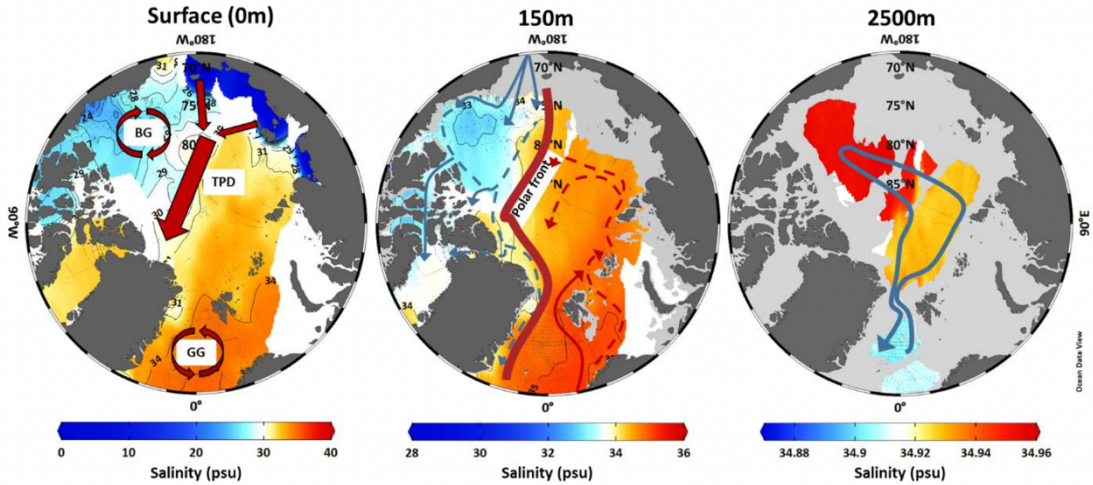

Figure 1.4. Schematic of the circulation and salinity of surface currents as regulated by atmospheric processes (left), at 150m as a summary of halocline driven circulation (middle) and intermediate/deep circulation (right) of waters around the Arctic Ocean. Red arrows represent warm, saline Atlantic waters, and purple/blue represent the relative cooling and freshening of water masses. BG = Beaufort Gyre, GG = Greenland Gyre, TPD = Transpolar drift.

The bathymetry of the Arctic Ocean is dictated by its proximity to land. Shallow continental shelves cover more than half of the Arctic Ocean, with depths shallower than 500m (Jakobsson, 2002), and deep basins (>4000m) occupying the central Arctic Ocean. The hydrography of these shallow shelves is heavily influenced by rivers with large watersheds draining the North American and Eurasian continents. The Arctic Ocean is relatively small, containing 1% of the global ocean's volume, yet receives >10% of global riverine discharge, principally from 8 major rivers: the Yukon, Mackenzie, Ob, Yenisey, Lena and Kolyma rivers (Aagaard and Carmack, 1989; McClelland et al., 2012) which bring freshwater and nutrients to the Arctic shelves. Along with fresh Pacific water, the low density runoff creates strong salinity

stratification with the denser AW underneath. This halocline is a dominant feature of the upper hydrography of the Arctic Ocean (middle panel of Figure 1.4), shoaling towards the Atlantic inflows, restricting deep convection and separating Atlantic heat from the surface, sea ice and the atmosphere (Tsubouchi et al., 2012). General circulation patterns of the Arctic Ocean are further illustrated on Figure 1.4.

AW flows into the Arctic Ocean through two major branches, East of the Fram Strait and through the Barents Sea Opening (BSO). As the Barents Sea Shelf is shallow (<250m), AW is cooled by the atmosphere and becomes denser further north. Concurrently, the heat content of AW leads to sea-ice melt, which combined with riverine discharge, leads to the formation of shelf waters with a large salinity range which flow counterclockwise around the Barents shelf, Kara Sea and the Laptev Sea, before being transported into the central Arctic (Rudels et al., 2004). The inflow of AW at Fram Strait is relatively deeper, with minimum heat loss to the atmosphere. These two AW branches are important for the evolution and ventilation of Arctic intermediate waters (Haine et al., 2015). Shelf waters are transported into the central Arctic via the Beaufort gyre, a clockwise oceanic current driven by wind in the Canadian Basin, which transports ice, Pacific & riverine freshwater and the Transpolar Drift (TPD), a strong, southwest-ward flowing current which transports ice and Siberian shelf freshwater to the Nordic Seas (Charette et al., 2020; Karcher and Oberhuber, 2002; Woodgate, 2018). The TPD quickly transports freshwater to the Eurasian Arctic with a short residence time (<2 years), while freshwater are concentrated in the Canada basin via the Beaufort gyre (Charette et al., 2020; Holmes et al., 2002) and eventually exported to the Labrador Sea through the Canadian Arctic archipelago.

1.3.2 Macronutrient distribution & primary productivity

Physical properties of Arctic waters are significantly modified from Atlantic inflow through cooling, mixing and freshening as waters circulate northward and through the Arctic basin. Alongside this, the chemical properties of Arctic water masses are modified from inflowing AW, owing to changing nutrient sources, pathways and cycling in the Arctic Ocean. Here, the biochemical cycles of nitrate and DSi in both

regions are outlined. This provides a basis for evaluating the impact of climate change and climate variability onto marine biogeochemsistry and productivity in these regions.

1.3.2.1 The Subpolar Regions

N and DSi are supplied to the surface ocean through upwelling or lateral transport, with N_2 fixation as an additional mechanism for N. In the Atlantic ocean, nutrients are supplied to the tropics and subtropics by the northward transport of subantarctic water masses (Sarmiento et al., 2004). Intermediate water masses of Antarctic Intermediate Water/ Sub-Antarctic Mode Water (AAIW/SAMW) are particularly important in supplying southern-sourced DSi (De Souza et al., 2012) and nitrate (Tuerena et al., 2015) from the subsurface, tightly linking the MOC to nutrient distribution, as shown on Figure 1.5. The North Atlantic current, a northern extension of the Gulf stream, further transport these nutrients to the subpolar North Atlantic regions and eventually to the Arctic Ocean. Consequently, the upper water column of the Eastern subpolar North Atlantic is relatively rich in nutrients from subtropical influence, while nutrient-deplete fresh currents from the Arctic and Nordic seas become of increasing influence towards the Western basins of the Irminger and Labrador Seas. In the deep Iceland basins and Rockall Trough, the high DSi concentrations are observed (>20 μM), the northern-most influence of pre-formed DSi in Antarctic Bottom Water (AABW), leading to the most positive Si* (>5 μM) of the water column.

The subtropical gyre is oligotrophic from year-round stratification, and is a significant area of N_2 fixation without seasonal blooms (Marconi et al., 2015; Moore et al., 2008, 2013). By comparison, winter convection seasonally re-supplies nutrients from the subsurface to the photic zone in the subpolar gyre. This leads to strong diatom spring blooms and a significant flux of carbon to the deep ocean in the subpolar regions (Allen et al., 2005; Martin et al., 2011) with only partial consumption of N and potential Fe limitation instead (Moore et al., 2013). North Atlantic Deep Water (NADW) is relatively deplete in both N and DSi compared to Southern-sourced waters as it forms from surface and intermediate waters which are highly utilised in the subpolar regions and are further diluted by Arctic sources.

Therefore, it is important to constrain the cycling of both nutrients upstream in the Arctic regions and in situ of the subpolar North Atlantic, as surface properties are directly incorporated into deep water masses and have a direct impact on the nutrient inventory and stoichiometry of NADW.

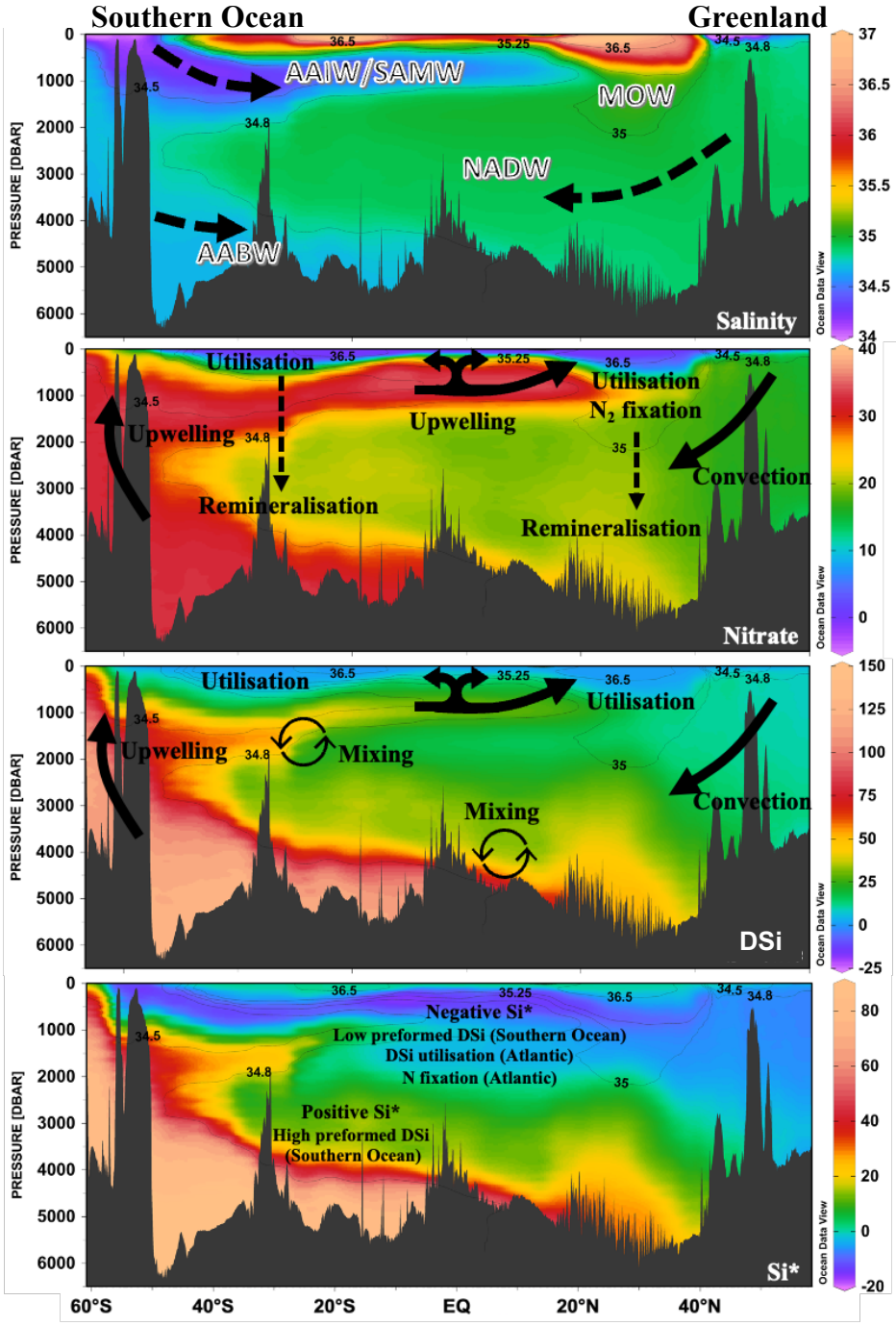

Figure 1.5. General physical distribution of water masses in the Atlantic Ocean and its nutrient distribution. Salinity (top), Nitrate (middle top), DSi (middle bottom) and Si* distribution across the meridional Atlantic Ocean from the Southern Ocean (60˚S) to the Labrador Sea (60˚N)

linked to MOC and regional patterns of upwelling and primary productivity. Data from GLODAPv2 (Olsen et al., 2016).

1.3.2.2 The Arctic Ocean

Nitrate and phosphate is imported to the Arctic Ocean through AW in the Barents Sea Opening and Fram Strait as a direct extension of the North Atlantic current, while the main inflow of DSi is via the Bering Strait from the Pacific Ocean (Torres-Valdés et al., 2013). Nutrients are primarily exported via the Davis Strait through the Canadian Arctic Archipelago. While nitrate fluxes are approximately balanced, the Arctic is a net exporter of DSi to the North Atlantic Ocean (15.7 ± 3.2 kmol DSi/s, Yamamoto-Kawai et al., 2006). Owing to N loss within the Arctic Ocean, low N* waters are exported to the North Atlantic which supports >16% of nitrogen fixation in the North Atlantic Ocean (Yamamoto-Kawai et al., 2006). Pacific-waters imported through the Bering Strait experience extensive denitrification (Granger et al., 2011), and further large-scale benthic denitrification occurs on Arctic shelves (Chang and Devol, 2009; Fripiat et al., 2018; Granger et al., 2018; Mctigue et al., 2016).

Riverine discharge from Arctic rivers play a large role in replenishing Arctic N inventory as it remains balanced or nearly-balanced despite the large denitrifying sink (Torres-Valdés et al., 2013; Yamamoto-Kawai et al., 2006). The Arctic ocean receives a disproportionally large volume of freshwater relative to its area (>10% of the world's riverine discharge) from several of the world's largest rivers, such as the Ob, Yenisei, Lena and Kolyma rivers. These four major rivers provide 1755 km^3 of freshwater to Arctic shelves annually, along with large supplies of C, 135 x 10^9 g of nitrate and 4816 x 10^9 g of DSi (Holmes et al., 2012). Along with Pacific DSi-rich waters, rivers play an important role in supplying excess DSi to the Atlantic Ocean. The strongest export of this terrestrial supply of organic matter and nutrients is through the TPD (Charette et al., 2020; Stedmon et al., 2011), transporting nutrients from the Eurasian shelves through the Fram Strait.

Glacial sources to Arctic waters are generally poor in N and are not considered to have an impact on the Arctic N budget but may significantly contribute to its DSi budget. Recent work suggests the Greenland Ice sheet is a significant exporter of

DSi, both in the dissolved and the amorphous phase (Hatton et al., 2019; Hawkings et al., 2015, 2017). The Greenland Ice sheet has been estimated to provide 37% of the riverine fluxes of Si to the coastal regions of Arctic Seas (Hawkings et al., 2017). However, these studies are based on glacial stream measurements, and could overestimate DSi contributions by ignoring important fjord cycling processes of biological uptake, precipitation and reverse weathering (Hopwood et al., 2020). In addition to these sources, lithogenic supply of DSi to Arctic shelves was recently documented in the Barents Sea sediments (Ward et al., 2022a, 2022b), as well as potential addition of DSi from hydrothermal vents (Edmonds et al., 2003; Liguori et al., 2020). The magnitude of these fluxes is unknown but likely to be small compared to riverine and marine fluxes, and their distribution on a basin-wide scale is poorly characterised.

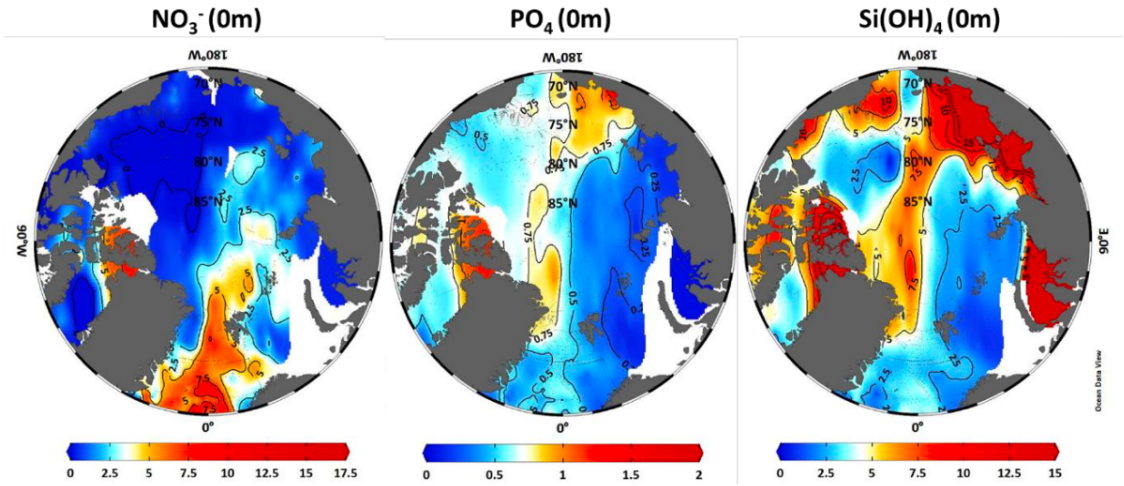

Figure 1.6. Mean nutrient concentrations in the surface Arctic Ocean from 2000 – 2010. Dataset from GLODAPv2 (Olsen et al., 2016).

The advection of nitrate from AW and DSi supplied by Pacific originating-waters and rivers on the Eurasian shelf is clearly reflected in surface nutrient concentrations as shown on Figure 1.6. Elevated phosphate and DSi concentrations in the central Arctic Ocean also clearly illustrate the mechanism of the TPD in transporting nutrients from Arctic shelves to the Atlantic Ocean (Charette et al., 2020).

Primary productivity in the Arctic Ocean is dominated by diatoms which contribute to >50% of primary production (Giesbrecht et al., 2019; Giesbrecht and Varela, 2021; Sakshaug, 2004). In the Arctic regions, primary production is controlled by

complex interactions between light and nutrient availability in the euphotic zone (Giesbrecht and Varela, 2021; Popova et al., 2012; Yool et al., 2015). Nutrient limitation is highly variable both spatially and temporally due to the large gradients in temperature and light.

Regimes shift from ice-free, thermally stratified environments into seasonal and permanent sea ice covers towards the central Arctic ocean, which affects nutrient availability, phytoplankton communities and production. Sea ice reduces light availability with shallower euphotic depths. Strong phytoplankton blooms occur in spring as productivity shifts from light limitation towards nutrient limitation, with an associated peak in biomass production. Nitrogen is the primary limiting nutrient for primary production in Arctic waters (Codispoti et al., 2013; Krisch et al., 2020; Randelhoff et al., 2018; Tuerena et al., 2021a) and sedimentary denitrification on shallow Arctic shelves play an important role in limiting nitrogen availability (Fripiat et al., 2018; Granger et al., 2018). In AW, phytoplankton generally experience DSi limitation instead (Agustí et al., 2018; Krause et al., 2018, 2019) due to the DSi-deplete origins of AW from its subpolar origins.

The strength of water column stratification controls nutrient resupply to the euphotic zone from deep nutrient stocks. The water column of thermally stratified waters is easily destabilised by atmospheric cooling in winter, resupplying nutrients from the subsurface waters (Codispoti et al., 2013; Randelhoff et al., 2018). By comparison, salinity stratified waters (when freshwater lenses sit at the surface of the water column) minimises mixing from ocean-atmosphere interactions due to the large density gradients which are not easily overcome. This restricts deep winter convection and limits nutrient resupply to the euphotic zone, creating oligotrophic conditions in the central Arctic Ocean (Sakshaug, 2004). >90% of all Arctic productivity is constrained to thermally-stratified waters (such as AW) and coastal areas (Codispoti et al., 2013), with terrestrial nutrients sustaining a third of all Arctic primary productivity (Terhaar et al., 2021). Thus, it is key to understand nutrient cycling in these two keys Arctic regions, AW and the Eurasian shelves, and how climate change will affect them and modify exported nutrient inventories from the Arctic Ocean.

1.3.3 Variability in the Subpolar North Atlantic

The surface hydrography of the subpolar North Atlantic is controlled by two gyres with vastly different nutrient regimes: the subpolar and subtropical gyres. The relative strength of these gyres fluctuates through time from changing wind patterns and ocean-air interactions (Foukal and Lozier, 2017; Koul et al., 2020). Properties of nutrients supplied to the region are a function of the relative contribution from subpolar and subtropical waters entrained by the gyre systems (Hátún et al., 2005; Holliday et al., 2008). As the subpolar gyre contracts, the NAW path migrates westward, entraining more warm, saline oligotrophic AW to enter the Nordic Seas and Arctic Ocean and thereby reducing nutrient stocks (Hátún et al., 2017; Johnson et al., 2013).

Over the last 20 years, a decrease of 1.5-2 μM DSi in the North Atlantic and Nordic Seas has been observed as a result of weakening subpolar gyre (Hátún et al., 2017). As AW in the Arctic Ocean is DSi limited (Krause et al., 2019), a further decrease in the DSi inventory has the potential to increase pressures on DSi demand and shift primary production towards non-silicifying species, with implications on carbon export.

Over the last decade, the Eastern subpolar North Atlantic has undergone the largest freshening recorded in 120 years (Holliday et al., 2020), starting in 2012 and reaching its peak in 2016 over the Iceland basin and with surface salinities lowered by 0.1 psu. While the origins of this freshening are still uncertain (Bryden et al., 2020; Fox et al., 2022; Holliday et al., 2020), it has potentially diverted nutrient supply and has had large-scale impacts on water column stratification and primary productivity in these regions (Holliday, pers. comm.). The origins of this freshening are important, as diversion of subpolar waters rich in nutrients to the eastern basins have been shown to increase productivity in the past and stimulate ecosystems (Hátún et al., 2017).

Overall, this illustrates that the subpolar regions regularly experience strong variability in its surface hydrography and the deep convective water masses of the North Atlantic directly reflect the nutrient properties of surface water. Therefore, it is

important to 1) have a mechanistic understanding of nutrient cycling in the subpolar region and 2) characterise the impact of climate variability and large scale freshening events onto the biogeochemistry and ecosystems of the region.

1.3.4 Arctic Biogeochemistry in the Context of Climate Change

The impact of climate change onto the Arctic Ocean are threefold: 1) Increased heat content in surface waters, 2) loss of sea ice and 3) increased freshwater content. All three factors have repercussions on biogeochemistry and hence primary productivity of the Arctic Ocean.

The Arctic is warming twice faster than the global mean (IPCC, 2021), leading to drastic sea ice loss as a direct result of climate warming from anthropogenic forcings (Notz and Stroeve, 2016). Models predict that the Arctic Ocean will experience summers free of sea ice in under 30 years (Notz and Community, 2020). This increases sea surface temperatures and enhances advection of warm Atlantic waters (Bekryaev et al., 2010), which leads to increased sea-air interactions and weakening water column stability (Barton et al., 2018). The loss of sea ice is increasing solar absorption in the surface ocean, thus warming the upper Arctic Ocean further as a feedback loop (Ivanov et al., 2019). Additionally, the heat budget of the Arctic Ocean has been increasing as the advection of heat from the Pacific via the Bering Strait (Woodgate, 2018) and from AW (Arthun et al., 2012; Lind et al., 2018; Polyakov et al., 2017). AW has warmed by 1.4˚C since the 1980ies, and has been expending northward.

Combined, the loss of sea ice and increasing influence of AW to the Eurasian Arctic is referred to as “Atlantification” of the Arctic Ocean (Arthun et al., 2012; Barton et al., 2018; Ingvaldsen et al., 2021; Lind et al., 2018) describing a shift of both hydrography and ecosystems from polar towards Atlantic-like conditions. The increase in heat weakens stratification of the halocline, thus increasing mixing, heat and nutrient resupply to the surface, thereby increasing rates of sea ice melt (Polyakov et al., 2017). Atlantification has led to a poleward expansion of temperate phytoplankton species such as the calcifying *E. huxleyi* and the retreat of polar

diatoms species further north (Neukermans et al., 2018; Oziel et al., 2020), thereby also shifting the polar foodweb. These combined shifts in ecosystems and nutrient inventories have also led to a shift in biogeochemistry and increasing summer drawdown of N in AW to near-deplete concentrations (Tuerena et al., 2021c).

Climate warming is actively altering the hydrological regime of the Arctic Oceans, with direct repercussions on nutrient supplies and impacting the nutrient inventories of growth-limiting nutrients in the Arctic Ocean (Tuerena et al., 2021c). Riverine fluxes are increasing freshwater discharge by >30% to the Arctic Ocean, particularly in the Eurasian basin (Mcclelland et al., 2006; Rawlins et al., 2010), and precipitation and sea ice melt is increasing (Haine et al., 2015) with repercussions on water column stability near coastal regions. Warming temperatures on land have increased the rate of permafrost thaw, increasing the discharge of organic matter and nutrients to coastal regions (Carey et al., 2020; Frey and McClelland, 2009; Kendrick et al., 2018; Kipp et al., 2018; Pokrovsky et al., 2020).

Primary productivity regimes are highly spatially variable in the Arctic Ocean, owing to vastly varying hydrography and nutrient regimes (Giesbrecht and Varela, 2021; Pabi et al., 2008; Terhaar et al., 2021). Altogether, increased light penetration, reduced stratification and enhanced nutrient supply to surface waters near Arctic shelves has doubled primary productivity (Arrigo et al., 2008; Arrigo and van Dijken, 2015). However longer seasons of active primary productivity increases nutrient demand on already low nutrient inventories, and a shift towards non-silicifying primary producers will increase N-demand in the Eurasian Arctic (Tuerena et al., 2021c). The increased advection and riverine supply of nutrients onto shelves may increase denitrification in the Arctic Ocean, further reducing N inventories (Mctigue et al., 2016). Combined with reducing DSi concentrations through the inflow of AW (Hátún et al., 2017), the future ability of the Arctic Ocean to sustain these levels of primary productivity is uncertain, with potential changes to the nutrient inventory of exported water masses to the subpolar North Atlantic. To understand how climatic changes will affect future Arctic foodwebs, it is vital to first understand how nutrients supplied to Arctic shelves are used and cycled prior to their export through Arctic outflow waters via the TPD.

1.4 Stable Isotope Tracers in Marine Geochemistry

Naturally occurring physical, chemical and biological processes will fractionate the stable isotopes of a given element. This occurs through equilibrium or kinetic processes. In the marine environment, stable isotopes of dissolved nutrients (i.e DSi & N) act as tracers of spatially and temporally integrated nutrients processes. They have the advantage of providing insights on large scale changes in nutrient biogeochemistry.

During the chemical transformation of an element from one form to another, such as when silicic acid is transformed to opal by diatoms, or when PN is remineralised, kinetic fractionation occurs. The isotopic effect (ε) of a reaction can be defined by the rates at which isotopes are converted from the reactant to the product phase using the equation below:

$$\varepsilon(‰) = \left(\frac{{}^{a}k}{{}^{b}k} - 1\right) \times 1000 \qquad \textit{Eq. 1.1}$$

From Hayes (2004), where ^{a}k and ^{b}k are the rate coefficients for the separate isotopes of a given element (i.e ^{14}N & ^{15}N and ^{28}Si & ^{30}Si).

The fractionation of stable isotope is described by two idealised models: the Rayleigh (closed-system) model and the open-system model. They describe the isotopic composition of reactant and product phases as a function of ε and initial conditions.

The Rayleigh model describes a closed system with no resupply of the reactant, leading to exponential fractionation. It is defined using the following equations:

$$\delta^{a}X_{\text{reactant}} = \delta^{a}X_{\text{initial}} - \varepsilon \ln(f) \qquad \textit{Eq. 1.2}$$

$$\delta^{a}X_{\text{instantaneous}} = \delta^{a}X_{\text{reactant}} - \varepsilon \qquad \textit{Eq. 1.3}$$

$$\delta^{a}X_{\text{integrated}} = \delta^{a}X_{\text{initial}} + \varepsilon \left(\frac{f}{1-f}\right) \ln(f) \qquad \textit{Eq. 1.4}$$

Where $\delta^{a}X$ is the isotope of a given element ($\delta^{15}N$ or $\delta^{30}Si$), f = fraction of reactant remaining, and $\delta^{a}X_{initial}$ is the initial isotopic composition of element X. In the marine environment, closed system fractionation assumes no input or output of nutrients to the photic zone available for utilisation (Mariotti et al., 1981). This is often representative of strongly stratified surface waters and spring blooms, as can be found in the Arctic Ocean. Intermittent mixing of water masses, remineralisation of organic matter and destratification events supply additional inorganic nutrients to the photic zone. In this scenario, nutrient utilisation is better described by an open model instead, where the isotopic effect leads to a linear trends of fractionation:

$$\delta^{a}X_{reactant} = \delta^{a}X_{initial} + \varepsilon\,(1 - f) \qquad \textit{Eq. 1.5}$$

$$\delta^{a}X_{product} = \delta^{a}X_{initial} - \varepsilon\,(f) \qquad \textit{Eq. 1.6}$$

The open model is a steady state system where consumption of nutrients is irreversible but is balanced by resupply with a constant isotopic signature. Both system of fractionation for Si and N are described in Figure 1.7.

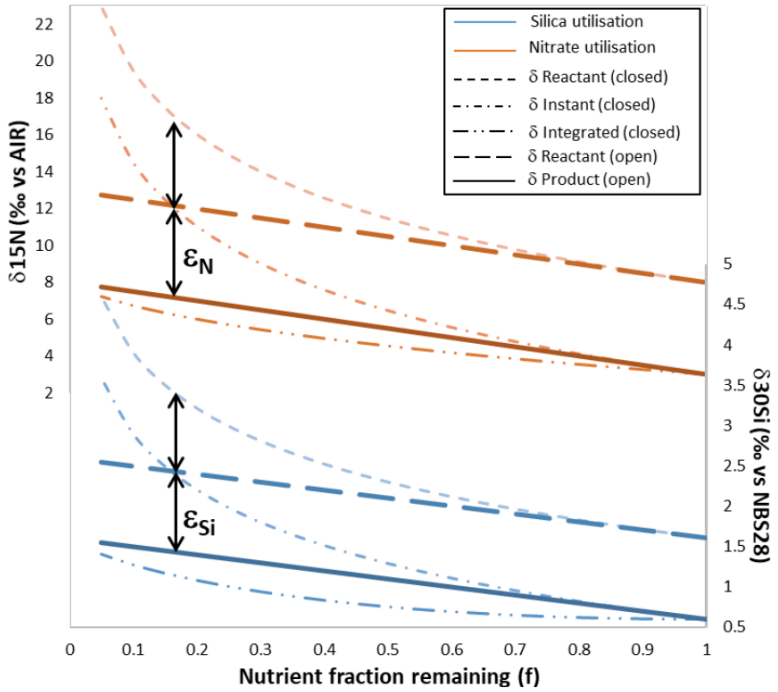

Figure 1.7. Isotopic fractionation of nitrogen (orange) and silicon (blue) for reactants and products in a unidirectional reaction for open and closed systems. The figure shows fractionation factor (ε) of 5‰ for $\delta^{15}N$ and 1‰ for $\delta^{30}Si$, representative of isotopic fractionation during biological uptake in the open ocean.

The nitrogen and silicon cycles within the ocean are highly variable seasonally and spatially. A snapshot may be obtained from studying processes such as N_2 fixation or phytoplankton composition from shipboard studies, but these measurements may overlook the importance of temporal processes over the course of a season. In highly remote areas such as the Arctic Ocean, where sea-ice cover restricts access, frequent inter-seasonal measurements are unrealistic. By using integrative tracers, the upscaling of occasional shipboard measurements can be used to capture processes over the course of a season and internal cycling processes.

Thus, by combining isotopes of nitrate and DSi, a comprehensive assessment of Si and N cycling in the Arctic Ocean and subpolar regions can be gained, whilst contrasting the separate dynamics of total primary production (N isotope) and total silicifier production (Si isotope).

1.4.1 Principles of silicon isotopes

Silicon has three stable isotopes: ^{28}Si (92.22%), ^{29}Si (4.68%) and ^{30}Si(3.08%). The mass difference between each isotope leads to distinct rate coefficients where $^{28}k > {}^{29}k > {}^{30}k$. The isotopic composition of Si varies because of mass-dependent isotopic fractionation based on exchange reaction and kinetic effects. The isotopic signature of Si within a sample is traditionally defined as the relative proportions of ^{28}Si and ^{30}Si in relation to the universal standard NBS28 (Barnes et al., 1975). It is expressed in permil (‰) and denoted by the δ^{30}Si notation.

$$\delta^{30}\mathrm{Si} = \left(\frac{\left(\frac{^{30}\mathrm{Si}}{^{28}\mathrm{Si}}\right)_{\mathrm{sample}}}{\left(\frac{^{30}\mathrm{Si}}{^{28}\mathrm{Si}}\right)_{\mathrm{NBS28}}} - 1 \right) \times 1000 \qquad \textit{Eq. 1.7}$$

Because of analytical difficulties, isotopic signature of Si are sometimes reported in the literature as δ^{29}Si instead (Cardinal et al., 2003, 2005). In seawater, the abundance of δ^{29}Si with respect to δ^{30}Si is close to theoretical fractionation laws (Grasse et al., 2017; Young et al., 2002) and can be converted to δ^{30}Si for comparability (Fripiat et al., 2011a, 2011b; Liguori et al., 2021).

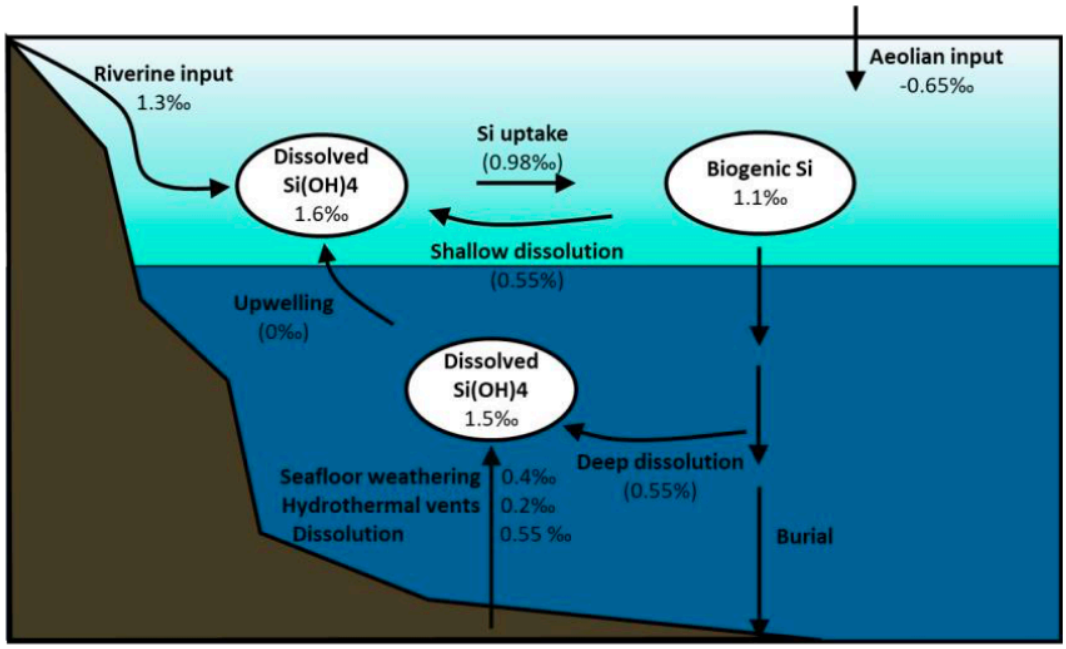

Figure 1.8. Overview of isotopic fractionation during marine Si cycling. Numbers in brackets show typical fractionation effects using $^{30}\varepsilon$ listed in Sutton et al., 2018 and references therein.

1.4.1.1 Marine silicon isotope sources & water column distribution

The largest source of Si to the oceans come from freshwater inputs. On the whole, freshwater is enriched in ^{30}Si relative to the Earth's crust. This is because Si from chemical weathering is removed from solution as it is incorporated into clay minerals and $bSiO_2$. The formation of clay minerals discriminate against the heavy isotopes of Si by 0.5-3.0‰ as ^{30}Si is preferentially incorporated in the secondary phase (Opfergelt and Delmelle, 2012 and references therein). This leads to variable, but isotopically heavier riverine waters (from -0.2 to +4.5‰), while groundwater is associated with lighter $\delta^{30}Si(OH)_4$ from secondary mineral dissolution (Georg et al., 2009b, 2009a). The fractionation factor $^{30}\varepsilon$ associated with the formation of clay minerals is variable but estimated around ~1.6‰ (Frings et al., 2016; Opfergelt and Delmelle, 2012; Sutton et al., 2018a). The DSi flux associated with aeolian dust dissolution has been estimated ~-0.65‰, however quantification is sparce and still requires empirical measurements in the modern world (Frings et al., 2016).

Non-continental sources of DSi to the ocean include seafloor weathering and contribution from hydrothermal vents. Dissolution and fractionation of isotopically light minerals within the sediments is an isotopically light source of DSi (-0.9‰,

Ward et al., 2022b) and lighter signatures are sometimes measured near the seafloor and continental slopes (Liguori et al., 2020), indicative of weathering, although the significance of this flux on a basin scale remains unconstrained (Frings et al., 2016). Hydrothermal contribution of DSi is a significant contributor to the marine DSi budget (>10%, Tréguer et al., 2021), yet few isotopic studies have characterised the impact of hydrothermal activity on Si isotopes (Brzezinski and Jones, 2015; De La Rocha et al., 2000; Liguori et al., 2020). Hydrothermal fluids have high DSi concentrations and low $\delta^{30}Si(OH)_4$ (-0.30‰, De La Rocha et al., 2000), and have been associated with a lowering of ambient $\delta^{30}Si(OH)_4$ near hydrothermal vents, albeit within analytical error (Brzezinski and Jones, 2015; Liguori et al., 2020). The impact of DSi fluxes from oceanic basalts on the isotopic budget of the modern ocean remains unconstrained and very poorly understood (Frings et al., 2016).

From these combined continental and non-continental fluxes, seawater is enriched in ^{30}Si relative to the Earth's crust, reflecting the dominating impact of cumulative incorporation of lighter silicon isotopes during weathering and biological processes on the continent. Variation in seawater $\delta^{30}Si(OH)_4$ are primarily driven by biological fractionation by diatoms in the upper ocean combined with large-scale oceanic circulation. The heaviest $\delta^{30}Si(OH)_4$ within the water column are found within the euphotic zone from the fractionation of $\delta^{30}Si$ by diatoms (>3‰) (Cardinal et al., 2005; Varela et al., 2004). Below this, $\delta^{30}Si(OH)_4$ distinguishes between water masses. The average subsurface marine $\delta^{30}Si(OH)_4$ vary regionally between 1.2‰ in Antarctic Bottom Waters (AABW) and 1.9‰ in the Arctic Ocean, which has the heaviest $\delta^{30}Si(OH)_4$ signature in the modern ocean (De Souza et al., 2012; Varela et al., 2016).

1.4.1.2 Biological opal production

Diatoms fractionate the isotopes of Si as they are taken up within their opal frustules. As such, $\delta^{30}Si(OH)_4$ can be used as a proxy for DSi utilisation over a growth season. In the euphotic zone, $\delta^{30}Si(OH)_4$ has been used to quantify annual DSi uptake and vertical nutrient supply rates (Fripiat et al., 2011b) and give insight into the biological Si pump of the modern ocean (Brzezinski et al., 2021; Giesbrecht et al.,

2022; Varela et al., 2004). Biological opal production has an associated $^{30}\varepsilon$ of -1.10 ± 0.4‰ in a laboratory environment (De La Rocha et al., 1997), which is close to average global estimates from field based studies (Giesbrecht et al., 2022 and references therein), although $^{30}\varepsilon$ on a local scale are varying (-0.33‰ to -2.09‰, Sutton et al., 2013; Varela et al., 2016). Variation in $^{30}\varepsilon$ are linked to a range of mechanisms seasonally and locally. Diatom species, size and temperature were not originally thought to impact the isotope effect of Si fractionation (De La Rocha et al., 1997; Reynolds et al., 2007). Recent studies however show that diatom assemblage composition may have a large impact on the isotope effect, particularly in polar environments with the largest variations between subpolar and polar diatom species (Giesbrecht et al., 2022; Sutton et al., 2013), linked to DSi uptake rate . Diatom studies in the Canadian sector of the Arctic Ocean suggest particularly low isotopic effect ($^{30}\varepsilon$ = -0.59 ± 0.07‰) if a closed-system model is considered. Using open-system models, an isotopic effect close to global ocean values ($^{30}\varepsilon$ = -1.19 ± 0.11‰) is measured instead (Giesbrecht et al., 2022; Varela et al., 2016). The difference in $^{30}\varepsilon$ for closed systems between the Arctic and the global mean is potentially linked to the effect of fractionation by sea-ice diatoms (Giesbrecht et al., 2022; Varela et al., 2016), although dilution may also artificially lower isotopic effects. The variability between both isotopic effects highlight the significant bias associated with both isotopic models, and that care needs to be applied when choosing models and initial conditions in the Arctic Ocean.

1.4.1.3 Remineralisation of biogenic opal

The dissolution of biogenic opal from diatoms, both in the water and the sediments, is also argued to affect water column $\delta^{30}Si(OH)_4$ distribution. During dissolution, lighter isotopes are preferentially dissolved, with $^{30}\varepsilon$ = -0.55‰ (Demarest et al., 2009). Nonetheless, isotopic fractionation linked to dissolution of biogenic opal within the water column and sediments is still debated and is sometimes not associated with significant fractionation (Egan et al., 2012; Frings et al., 2014; Varela et al., 2004; Wetzel et al., 2014).

In the subpolar North Atlantic, no significant effect from dissolution is observed in deep $\delta^{30}Si(OH)_4$ measurements (Giesbrecht et al., 2022; De Souza et al., 2012; Sutton et al., 2018b). In the Arctic Ocean, benthic efflux and water column dissolution were found to have a significant impact in lowering $\delta^{30}Si(OH)_4$ in deep basins (Brzezinski et al., 2021) and on shelves (Ward et al., 2022b). The efflux was not linked to any fractionation compared to water-column biogenic Si material, likely due to complete dissolution of opal (Giesbrecht et al., 2022; Varela et al., 2016). Given the variability and seasonality of particulate Si, the net impact of sedimentary efflux and water column dissolution on water column $\delta^{30}Si(OH)_4$ in the Arctic Ocean remains uncertain.

1.4.2 Principles of nitrate isotopes

Nitrogen has two stable isotopes, ^{14}N (99.63%) and ^{15}N (0.37%). Their mass difference lead to distinct rate coefficients, where $^{14}k > {}^{15}k$. Because of these differences in rate coefficients, biogeochemical N processes discriminate between the two isotopes. Almost all processes associated with the marine N cycle are biologically mediated and lighter isotopes are preferentially used owing to their lower energy requirements.

The isotopic signature within a sample is defined as the relative proportions of ^{14}N and ^{15}N in relation to N(AIR), a universal standard of known isotopic composition. It is expressed in ‰ and denoted by the $\delta^{15}N$ notation.

$$\delta^{15}\mathrm{N} = \left(\frac{(\frac{^{15}\mathrm{N}}{^{14}\mathrm{N}})_{\mathrm{sample}}}{(\frac{^{15}\mathrm{N}}{^{14}\mathrm{N}})_{\mathrm{AIR}}} - 1 \right) \times 1000 \qquad \textit{Eq. 1.8}$$

Using the same principle, oxygen has three stable isotopes ^{16}O (99.8%), ^{17}O and ^{18}O. The isotopic signature of oxygen is denoted by the $\delta^{18}O$ notation and is reported in ‰ relative to the Vienna Standard Mean Ocean Water (VSMOW) universal standard.

1.4.2.1 Marine nitrate isotope sources & water column distribution

δ^{15}N-NO_3 in the subsurface ocean is a balance of sources of N to the ocean (mainly as N_2 fixation) and isotopic fractionation from sinks (principally denitrification), leading to an average deep ocean δ^{15}N-NO_3 of 5.16‰ (Fripiat et al., 2021). During biological N_2 fixation, uptake of atmospheric N_2 is not associated with an isotopic effect, and the composition of fixed nitrogen is close to atmospheric N_2 (-2 to 0‰, Carpenter et al., 1997), relatively light compared to subsurface δ^{15}N-NO_3 values. Bacterial nitrogen fixation is balanced by water column denitrification, a nitrate sink with an isotope effect of 20-30‰ (mean $^{15}\varepsilon$ = 25‰ Altabet et al., 1999; Sigman et al., 2009a).

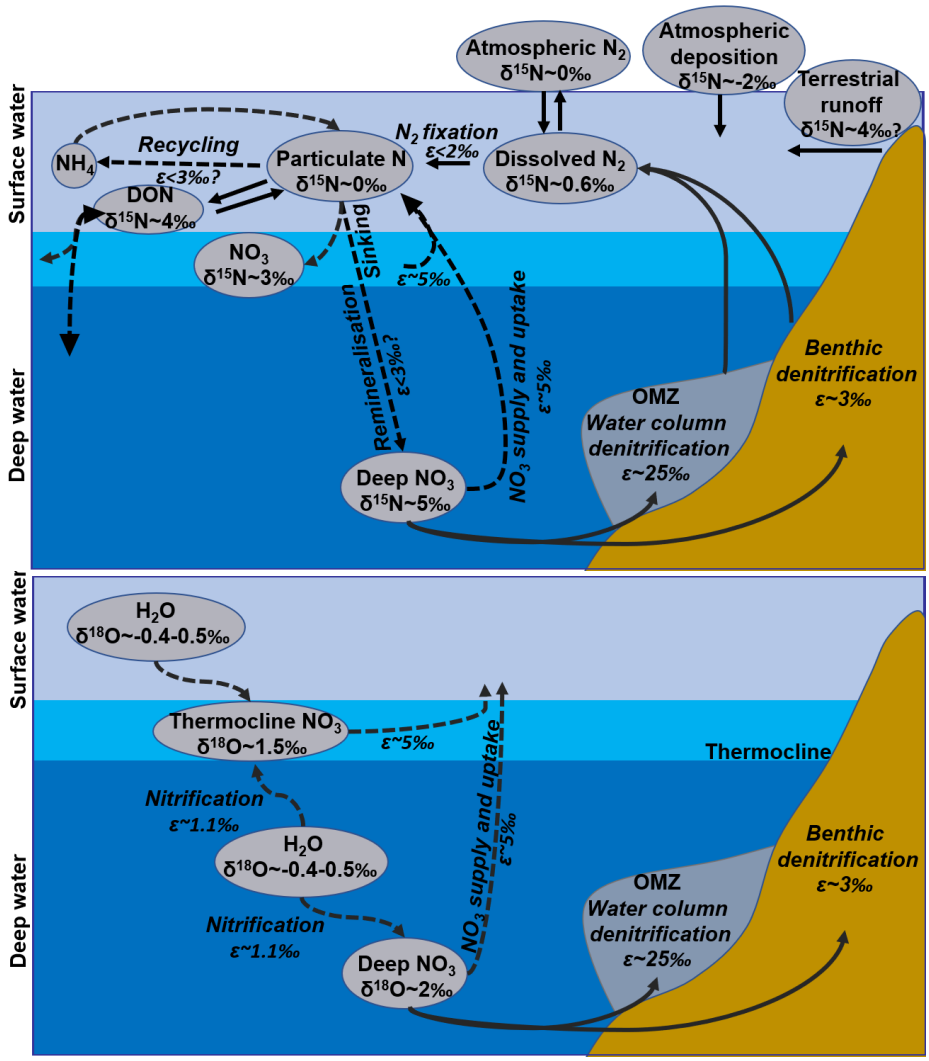

Figure 1.9. Overview of isotopic fractionation during marine N cycling for δ^{15}N-NO_3 (top) and δ^{18}O-NO_3 (bottom) along with their associated isotopic effect. Taken from Doncila, 2020.

Broadly in the open ocean, nitrate is depleted by phytoplankton and limits primary production (Moore et al., 2008, 2013). The complete uptake and remineralisation of nitrate has little impact on subsurface $\delta^{15}N\text{-}NO_3$ (Sigman et al., 2000). Because of the near-complete drawdown of nitrate, variations in subsurface $\delta^{15}N\text{-}NO_3$ carry signatures of remote large-scale N processes, and the mean signature observed is a balance of light-sourced $\delta^{15}N$ and heavy isotopic fractionation by denitrification.

1.4.2.2 Nitrate consumption

Nitrate is lost from the water column via two processes: consumption by phytoplankton and denitrification. Phytoplankton preferably consume the light isotopes of nitrate, thereby enriching the residual nitrate pool of $\delta^{15}N\text{-}NO_3$, with a $^{15}\varepsilon$ close to 5‰ in the open ocean (Altabet and Francois, 2001; Tuerena et al., 2015). Where nitrate is fully consumed by phytoplankton (low latitudes), it does not impact the $\delta^{15}N\text{-}NO_3$ of subsurface waters. Where nitrate is partially consumed (seasonally or locally), the relationship between nitrate concentrations and ambient isotopes can be used to determine utilisation through fractionation models (Sigman et al., 2000), and deviation from these trends can be used to investigate the various physical and biogeochemical processes leading to this.

Water column denitrification is the largest sink of N, and in suboxic conditions has a high $^{15}\varepsilon$ (20-30‰) (Altabet et al., 1999; Sigman et al., 2003), strongly enriching the residual nitrate pool of $\delta^{15}N\text{-}NO_3$. In contrast, benthic denitrification leads to negligible fractionation. $\delta^{18}O\text{-}NO_3$ is fractionated with the same isotopic effect as $\delta^{15}N\text{-}NO_3$ during consumption via nitrate reduction (Casciotti et al., 2002; Granger et al., 2004). If denitrification or nitrate assimilation alone is taking place in the water column, both isotopes of nitrate become increasingly enriched along a 1:1 trajectory (Rafter et al., 2013).

1.4.2.3 Nitrate remineralisation

The production of nitrate impacts $\delta^{15}N\text{-}NO_3$ and $\delta^{18}O\text{-}NO_3$ differently, decoupling both isotopes. N atoms are a fixed pool, and are internally cycled within the ocean. Fixed N is added to the ocean through the remineralisation of PON. The isotopic

signature of remineralised nitrate varies depending on the source of organic material. N_2 fixers have an isotopic signature of around -1‰. PON in non-nitrogen fixers reflect N uptake from ambient seawater source. If partially consumed, this will be lighter than $\delta^{15}N\text{-}NO_3$, while in nitrate-deplete environments, this will be close to source $\delta^{15}N\text{-}NO_3$ from the integrated product. In low oxygen zones, remineralised nitrate may have high $\delta^{15}N\text{-}NO_3$ from denitrification. $\delta^{15}N\text{-}NO_3$ is set by the fixed N pool at time of nitrification, “memorising" ambient conditions.

O atoms of nitrate are obtained from ambient seawater and O_2. Therefore, newly nitrified $\delta^{18}O\text{-}NO_3$ is “reset”, and loses signatures from previous enrichments by denitrification or partial assimilation. “New” nitrate has a $\delta^{18}O\text{-}NO_3$ signature around 1.1‰ above the $\delta^{18}O\text{-}H_2O$ (Sigman et al., 2009a). Nitrification is an absolute input of O, therefore the deviation of $\delta^{18}O\text{-}NO_3$ from $\delta^{15}N\text{-}NO_3$ can inform on the importance of processes that affect both isotopes separately (nitrification, fixation) versus consumption in the surface ocean. Where nitrification dominates, a lowering of Δ(15-18) below the global average of 3‰ is expected.

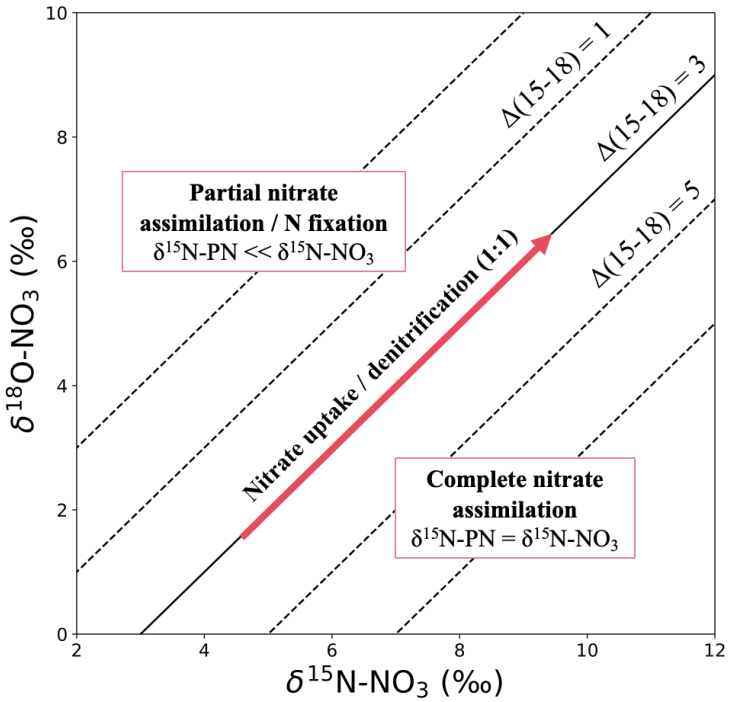

Figure 1.10. The fractionation of $\delta^{15}N\text{-}NO_3$ and $\delta^{18}O\text{-}NO_3$ during N cycling and the resulting impact on Δ(15-18). When nitrate is remineralised, O atoms are sourced from $\delta^{18}O\text{-}H_2O$ (+1.1‰) and $\delta^{15}N\text{-}NO_3$ depends on N_2 fixation and the extent of utilisation.

Thus, combined with stoichiometric parameters, the two isotopes of nitrate and their derived parameter Δ(15-18) are powerful tools to constrain the complex internal cycling of nitrate and to trace the different sources of remineralised nitrate across the ocean (Rafter et al., 2013). A summary of the processes described above and the way they impact Δ(15-18) are shown on Figure 1.10.

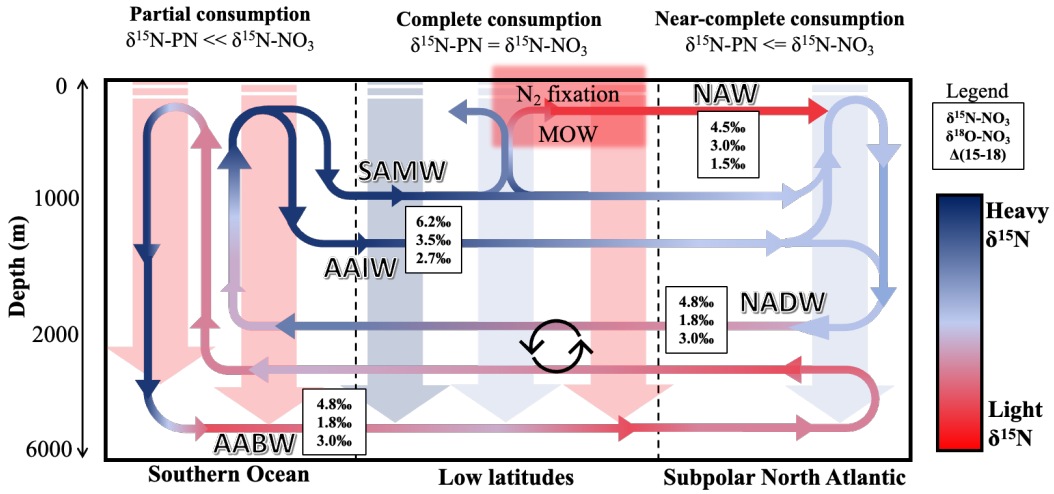

Figure 1.11. Schematic of the $\delta^{15}N$ of nitrate and PN coupled to the Meridional Overturning Circulation (MOC) of the Atlantic Ocean, highlighting key biological and physical processes shaping the N isoscape. Endmembers isotopic characteristics from Marconi et al. (2019) and Deman et al. (2021). Transparent vertical arrows show the relative isotopic composition of sinking particulate nitrogen, as controlled by the extent of utilisation of the nitrate pool in surface waters.

1.4.3 Marine patterns of N & Si isotopes

1.4.3.1 In the Subpolar North Atlantic

The average subsurface oceanic $\delta^{15}N\text{-}NO_3$ is around 4.80‰ in the deep North Atlantic, and is 1.80‰ for $\delta^{18}O\text{-}NO_3$ (Marconi et al., 2019). It can roughly be interpreted as a balance between the isotopic fractionation associated with N_2 fixation and denitrification (Sigman et al., 2009b). In the Atlantic Ocean, $\delta^{15}N\text{-}NO_3$ is closely related to the Meridional Overturning Circulation (MOC), as schematically shown on Figure 1.11. In the Southern Ocean, concentrations of both DSi and N remain high due to iron limitation during photosynthesis, leading to high export concentrations of nutrients in Southern Ocean intermediate and deep waters to the Atlantic (Boyd et al., 2007; Boyd and Law, 2001; Moore et al., 2013; Sunda and

Huntsman, 1995). Partially utilised N in SAMW/AAIW leads to elevated $\delta^{15}N\text{-}_{NO3}$. This signal propagates northwards, and lowers $\delta^{15}N\text{-}NO_3$ in the deep ocean through the remineralisation of light PN during partial consumption at Southern latitudes (Marconi et al., 2019). The heavy $\delta^{15}N\text{-}NO_3$ isotopic signature in these intermediate water masses is largely erased by the remineralisation of nitrate with low $\delta^{15}N\text{-}NO_3$ in the tropical North Atlantic instead, presumably through N_2 fixation (Marconi et al., 2015), although the Mediterranean Outflow also appears to lower $\delta^{15}N\text{-}NO_3$ in the Eastern North Atlantic (Deman et al., 2021; Marconi et al., 2019).

In the subpolar North Atlantic, assimilation by phytoplankton is the primary control on nitrate isotopes in the seasonally warmed surface layer. In subsurface waters at high latitudes, the co-occurrence of partial nitrate assimilation and nitrification lead to diverging $\delta^{15}N\text{-}NO_3$ and $\delta^{18}O\text{-}NO_3$ as it affects the O isotope budget while leaving the N unchanged (Sigman et al., 2009a). The cycling of N between nitrate assimilation and nitrification has no net effect on $\delta^{15}N\text{-}NO_3$, but the $\delta^{18}O$ consumed is initially lower (down to -3‰) than $\delta^{18}O\text{-}NO_3$ produced by nitrification (+1.1‰ from ambient $\delta^{18}O\text{-}H_2O$).

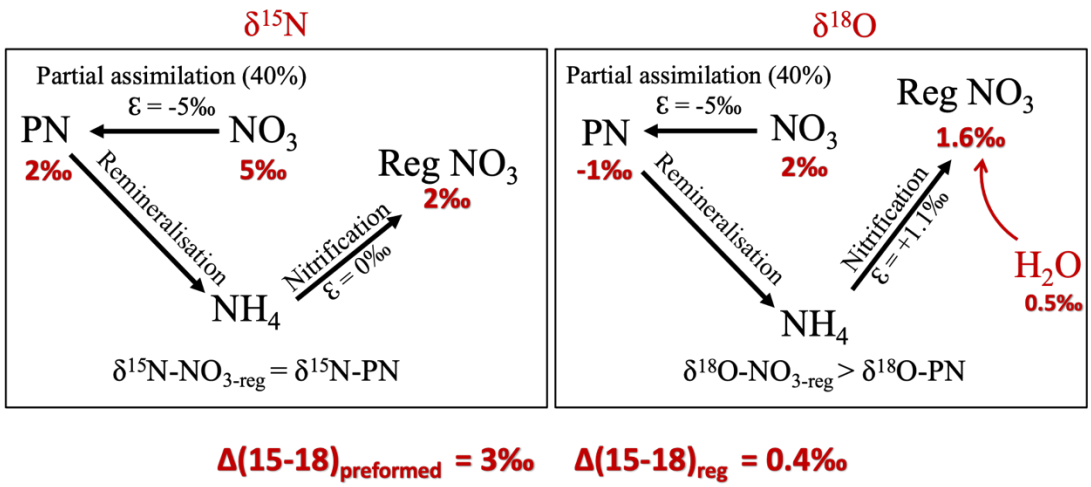

Figure 1.12. Schematic of assimilation and nitrification when nitrate is partially consumed, with the distinct impact on $\delta^{15}N$ (left) and $\delta^{18}O$ (right). Red values show theoretical impact of processes on preformed nitrate ($\delta^{15}N\text{-}NO_3$ = 5‰ and $\delta^{18}O\text{-}NO_3$ = 2‰) if approximately 40% of the N pool is utilised following Rayleigh fractionation where ambient $\delta^{18}O\text{-}H_2O$ = 0.5‰.

The co-occurrence of partial nitrate assimilation and nitrification therefore raises $\delta^{18}O\text{-}NO_3$ while $\delta^{15}N\text{-}NO_3$ remains constant, thereby lowering $\Delta(15\text{-}18)$ below the global average of 3‰ in the upper water column of the subpolar North Atlantic (Deman et al., 2021; Van Oostende et al., 2017; Peng et al., 2018). Where nitrate is fully consumed, $\Delta(15\text{-}18)$ increases instead, as regenerated nitrate has lower $\delta^{18}O$ than its preformed pool (as $\delta^{18}O\text{-}PN = \delta^{18}O\text{-}NO_3$), as illustrated on Figure 1.12.

The isotopic distribution of DSi is relatively simpler by comparison, as Figure 1.13 illustrates. $\delta^{30}Si(OH)_4$ in surface waters of the North Atlantic is primarily controlled by biological fractionation of DSi during uptake by diatoms (Brzezinski and Jones, 2015). Below 300m, $\delta^{30}Si(OH)_4$ is tied to the distribution of water masses. It traces the MOC through a gradient between Southern Ocean sourced DSi in AABW, SAIW & AAIW ($\delta^{30}Si(OH)_4$ = 1.2‰) and nutrient-poor waters from the North Atlantic and the Nordic seas ($\delta^{30}Si(OH)_4$ >1.6‰, De Souza et al., 2012).

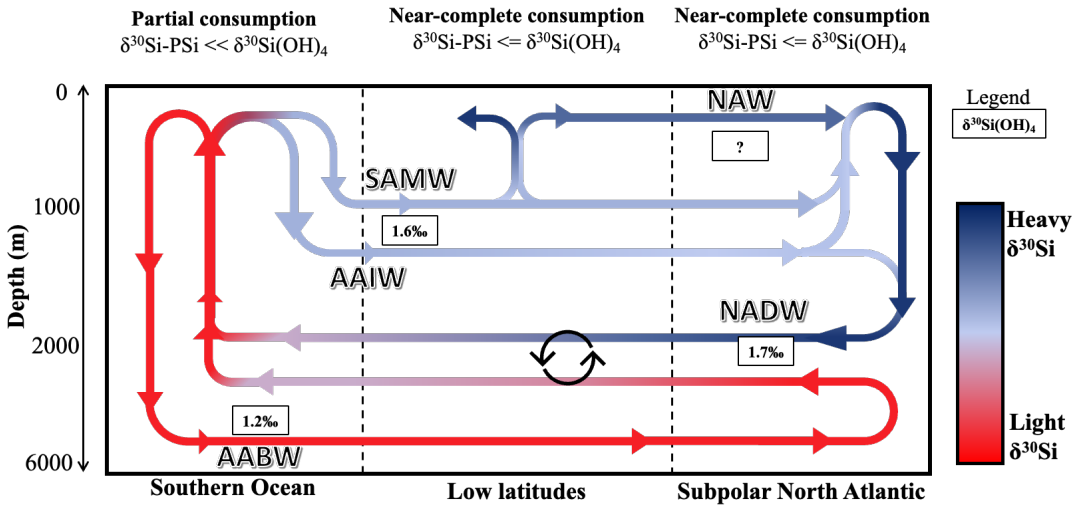

Figure 1.13. Schematic of the $\delta^{30}Si$ of silicic acid coupled to the Meridional Overturning Circulation (MOC) of the Atlantic Ocean, highlighting key physical and biological processes shaping the DSi isoscape and gaps in knowledge. Endmembers isotopic characteristics from De Souza et al. (2012). Unlike for N, sinking PSi dissolution at depth does not significantly impact deep $\delta^{30}Si(OH)_4$ signatures.

As shown on Figure 1.14, the distribution of $\delta^{30}Si(OH)_4$ behaves quasi-conservatively between the two isotopically-light, high nutrient and low nutrient, isotopically-heavy endmembers, attributed primarily to heavily fractionated

SAIW/AAIW transport in the upper limb of the MOC (De Souza et al., 2012, 2015). Other studies hypothethise an important source of isotopically heavy DSi from the Pacific and Arctic Ocean to the Nordic Seas due to restriction from shallow sills and intensive utilisation by diatoms (Brzezinski and Jones, 2015). This Arctic-sourced DSi is reflected in particularly isotopically heavy LSW, contributing to enriching North Atlantic $\delta^{30}Si(OH)_4$ (Sutton et al., 2018b). All studies mentioned above however faced significant gaps in knowledge, particularly from the lack of measurements of the upper limb of the MOC in the subpolar North Atlantic and of the Arctic Ocean due to analytical restrictions at very low DSi concentrations, thereby limiting our knowledge in nutrient depleted areas.

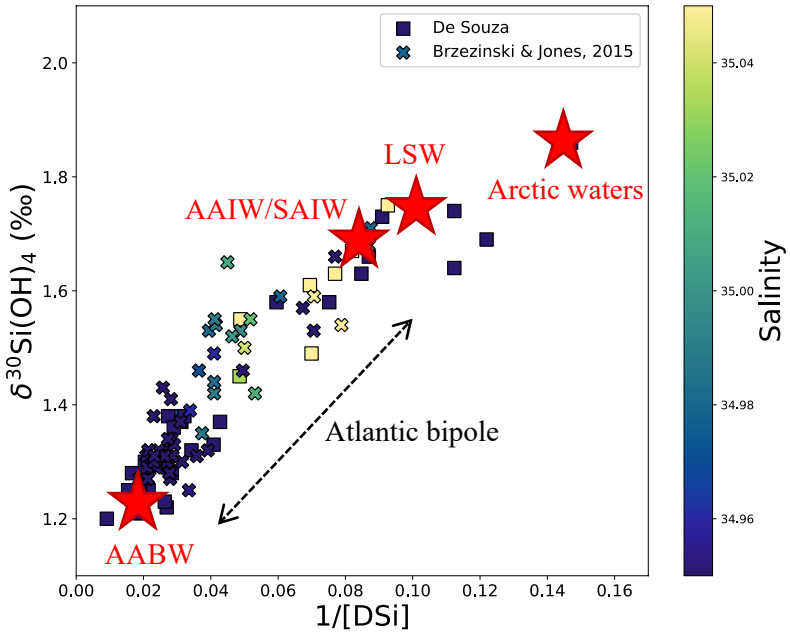

Figure 1.14. The silicon isotope bipole in the Atlantic Ocean between endmember waters masses in the Southern Ocean (AABW) and Arctic/Nordic Sea waters (red stars). Datasets from De Souza et al. (2012) and Brzezinski & Jones (2015), for depths >1000m, corrected for the 0.22‰ offset observed between studies in the latter publication. Colorscale shows salinity.

The N and DSi isoscapes across the Atlantic oceans differ as they are controlled by different mechanisms. $\delta^{15}N\text{-}NO_3$ in the deep ocean is nearly uniform (4.8‰), while $\delta^{30}Si(OH)_4$ displays a strong meridional gradient (Marconi et al., 2019; De Souza et al., 2012). Due to the biogeochemical nature of these two tracers, the isoscape of

both nutrients is strongly related to the extent of their utilisation in surface waters. The remineralisation of PN at depths impacts ambient isotopic signatures (Marconi et al., 2019) and thus depends on the extent of utilisation in surface waters. N is limiting across much of the Atlantic Ocean (Moore et al., 2008, 2013), and complete utilisation of the nutrient pool implies the isotopic signature of PON is equal to the one of ambient seawater (Sigman et al., 2000, 2009a). As N is also required by diatoms, this limits DSi utilisation to near-deplete conditions across much of the ocean, implying the exported isotopic signature of PSi is significantly fractionated from ambient seawater, increasing surface $\delta^{30}Si(OH)_4$ during assimilation. Contrarily to PON, sinking PSi does not appear to significantly lower ambient $\delta^{30}Si(OH)_4$ through dissolution (De Souza et al., 2012).

1.4.3.2 Isotopic signatures of source waters to the Arctic Ocean

Inflow of Atlantic waters through Fram Strait and the Barents Sea Opening carry a roughly similar isotopic signature varying from 4.7 – 5.1‰ for $\delta^{15}N\text{-}NO_3$ and 2.4 – 3.0‰ for $\delta^{18}O\text{-}NO_3$ (Tuerena et al., 2021b, 2021a), leading to an average $\Delta(15\text{-}18) <$ 3‰. This is comparable to the signature of NADW (Marconi et al., 2015; Sigman et al., 2009a) and the subpolar North Atlantic thermocline (Van Oostende et al., 2017; Peng et al., 2018). In the subpolar North Atlantic, $\delta^{30}Si(OH)_4$ range from 1.6-1.7‰, as a result of the quasi-conservative mixing between heavy Nordic Seas and Arctic-sourced nutrients and light Southern Ocean sources (Brzezinski and Jones, 2015; De Souza et al., 2012). The $\delta^{30}Si(OH)_4$ of Atlantic water inflow to the Arctic Ocean is believed to closely align with (>1.7‰ Brzezinski et al., 2021; Liguori et al., 2020), although direct measurement are still lacking and mechanisms of transformation within the Nordic Seas are unknown.

The Pacific inflow of nitrate through the Bering strait isotopically reflects the signal of far-field denitrification ($\delta^{15}N\text{-}NO_3$ = 6.5‰, $\delta^{18}O\text{-}NO_3$ = 3.2‰, $\Delta(15\text{-}18) >$ 3‰, Granger et al., 2011). It is easily distinguished from Atlantic waters both through its nutrient stoichiometry and nitrate isotopic signature. The $\delta^{30}Si(OH)_4$ of Pacific waters is light and controlled by the utilization from diatoms (+1.4 ± 0.2‰, Reynolds et al. 2006). This rich source of DSi is traced through the Bering strait and becomes

increasingly modified into the upper halocline waters of the Arctic Ocean, thereby increasing $\delta^{30}Si(OH)_4$ further (Brzezinski et al., 2021; Giesbrecht et al., 2022).

Riverine discharge supply terrestrial N and Si to the Arctic Ocean. The isotopic signatures of riverine discharge are highly spatially and temporally variable due to

1. Geology, soil type and permafrost content of each river catchment
2. Riverine concentration and lability of organic matter
3. Downstream biological processes (uptake, denitrification)
4. Seasonality (most Arctic rivers experience annual freeze – thaw cycles and spring freshets)

The $\delta^{15}N\text{-}NO_3$ of Arctic rivers ranges from 0-5‰ (Francis, 2019), resulting from the remineralisation of light (<0‰) land-derived dissolved and organic particulate nitrogen whereas denitrification increases $\delta^{15}N\text{-}NO_3$. $\delta^{18}O\text{-}NO_3$ ranges from -19‰ to -3‰ (Francis, 2019), reflective of light ambient $\delta^{18}O\text{-}H_2O$ (~ -20‰, Yi et al., 2012) and vigorous cycling in recent thaw zones. $\delta^{18}O\text{-}NO_3$ becomes heavier with proximity to estuaries due to denitrification processes, but remains much lighter than sources of marine nitrate. The $\delta^{30}Si(OH)_4$ of Arctic rivers are light from weathering of basalt bedrock, secondary clay dissolution and degradation of terrestrial biological material. Measured riverine $\delta^{30}Si(OH)_4$ range from 0.4 – 2.5‰, with an average source riverine signature of 1.3 ± 0.3‰ for all major Arctic rivers (Georg et al., 2006a; Pokrovsky et al., 2013; Sun et al., 2018). Glacial meltwaters are a light source of $\delta^{30}Si(OH)_4$ (-0.3 to +1.4‰, Hatton et al., 2019; Hawkings et al., 2018) with lower DSi concentrations compared to glacial rivers.

In addition to marine and terrestrial sources, benthic supply of isotopically light DSi to shelf waters is observed in the Barents Sea (Ward et al., 2022a, 2022b), as well as potential light contribution from hydrothermal vents (Liguori et al., 2020) although the magnitude of these fluxes on a basin-wide scale are currently unknown.

1.4.3.3 Nutrient cycling on Arctic shelves and export to the North Atlantic

Over the Bering and Chukchi shelves and the East Siberian Seas, $\delta^{15}N\text{-}NO_3$ increases while $\delta^{18}O\text{-}NO_3$ decreases nearly towards 0‰ (Brown et al., 2015; Fripiat et al., 2018; Granger et al., 2018). Biogeochemical cycling over Arctic shelves is vastly different from the central Arctic Ocean as they are highly productive shallow environments which receive a high supply of organic matter (OM) exported from surface waters during the vegetative season or supplied by rivers. High rates of export of OM to the seafloor drives sedimentary remineralisation which exceeds the rates of sedimentary nitrification (Granger et al., 2011). As OM degrades, NH_4 builds up and diffuses to shelf bottom waters. Sedimentary remineralisation has high O_2 requirements, driving the denitrification horizon close to the sediment-water interface, such that the two processes overlap.

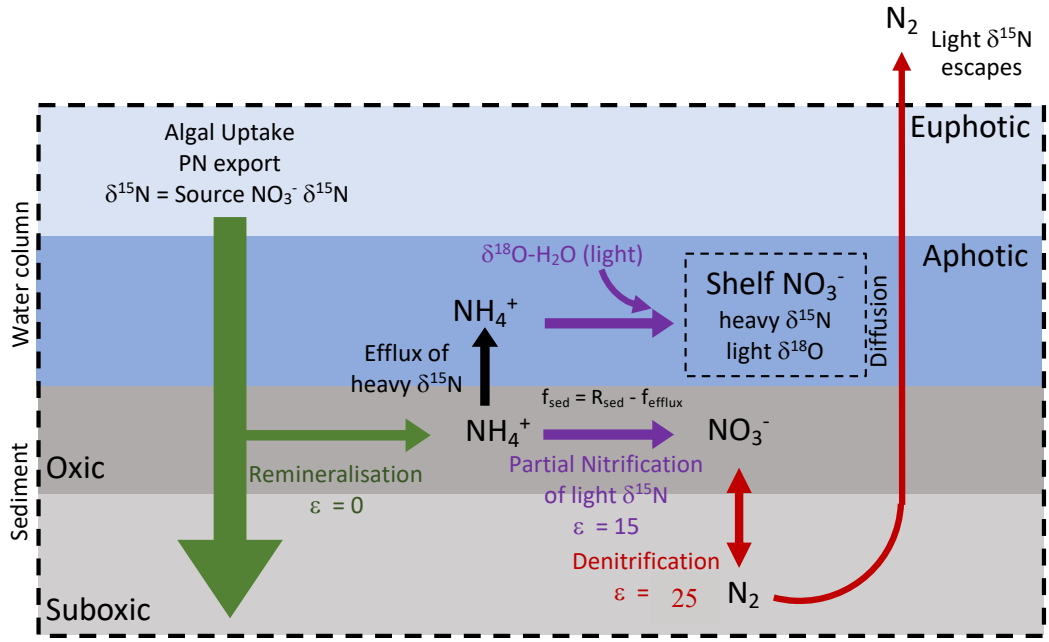

Figure 1.15. Schematic representation of Coupled Partial Nitrification Denitrification (CPND) on Arctic shelves. Green arrows show organic matter export to the sediments and subsequent remineralisation to NH_4^+ close to exported PON $\delta^{15}N$ and advected $\delta^{15}N$ (as most N is consumed in the euphotic layer). If benthic remineralisation is larger than nitrification, accumulated NH_4^+ diffuses into the water column (f_{efflux}). The fraction nitrified within the sediments (f_{sed}) is the residual fraction of N remineralised (R_{sed}) after efflux. Light NH_4^+ is preferentially oxidised to nitrate within the substrate and quantitively denitrified to N_2 in suboxic conditions; isotopically light N_2 escapes the system as it diffuses to the atmosphere. The residual pool of NH_4^+ after

sedimentary nitrification has high $\delta^{15}N$, and the heavy isotopic signature is carried into the overlaying shelf waters. Adapted from Doncila (2020) and Fripiat et al. (2018).

During benthic denitrification, light $\delta^{15}N$ escapes the fixed N pool as inert N_2 gas, thereby enriching the $\delta^{15}N$ of the remaining dissolved inorganic nitrogen pool. As such, when NH_4 diffuses out of the sediments and is eventually nitrified, $\delta^{15}N\text{-}NO_3$ of the water column increases. During nitrification, N atoms are internally recycled while oxygen atoms are sources from ambient O_2 and seawater, in general providing a "reset" signature of $\delta^{18}O\text{-}H_2O$ + 1.1‰ (Buchwald et al., 2012; Sigman et al., 2009b) and a divergence of both isotopes from traditional 1:1 ratio.

This chain of reaction is named Coupled Partial Nitrification Denitrification (CPND) and leads to increasing Δ(15-18) which can be used to trace N cycling and evolution of shelf waters across the Arctic Ocean (Fripiat et al., 2018; Granger et al., 2018). A schematic representation of this process on Arctic shelves is shown on Figure 1.15. This is a wide-scale process in the Arctic Ocean documented across the Bering and Chukchi shelves and the East Siberian Seas (Brown et al., 2015; Fripiat et al., 2018; Granger et al., 2018) with an imprint on polar waters exported to the North Atlantic (Lehmann et al., 2019; Tuerena et al., 2021a).

The $\delta^{30}Si(OH)_4$ of Arctic waters in the deep basins and surface outflows are heavy (>1.8‰). Two main hypothesis have been formulated to explain the mechanisms of this enrichment: inflow of isotopically heavy halocline and intermediate waters of Atlantic origins through Fram Strait (Varela et al., 2016) or biological uptake and modification of $\delta^{30}Si(OH)_4$ within the Arctic Ocean (Brzezinski et al., 2021; Liguori et al., 2021). The inflow shelves of the Bering, Chuchki and Barents Seas highly particularly with large diatom abundance (Codispoti et al., 2013; Giesbrecht and Varela, 2021; Sakshaug, 2004). The $\delta^{30}Si(OH)_4$ of Pacific-originating DSi increases with decreasing concentrations across the shelf, indicative of biological removal. The conservation of this heavy isotopic signature in surface waters implies burial of isotopically light opal in sediments of highly productive shelves. Direct measurements of the Fram Strait and Arctic shelves are however still lacking to determine whether the control of $\delta^{30}Si(OH)_4$ exported out of the Arctic Ocean are

physical or biological. Both are subject to change in the context of climate warming, with knock-on impact on North Atlantic ecosystems and nutrient stoichiometry.

1.5 Thesis aims

The overall aim of this thesis is to increase the current understanding of biogeochemical cycling of DSi and N in the Arctic Ocean and the subpolar North Atlantic to understand the impact of climate change on primary production. This work also contributes to filling in gaps in the global marine datasets of nitrate isotopes and $\delta^{30}Si(OH)_4$. The key research areas investigated in this work and the questions it aims to answer are outlined below.

1.5.1 Characterise DSi and N isoscapes of the Eurasian Arctic

The isotopic budget of Arctic Si is currently unconstrained (Brzezinski et al., 2021). It is unknown whether the heavy isotopic enrichment of Arctic waters is due to physical water mass mixing of heavy intermediate inflow waters or biological activity modifying nutrient budgets.

The first research aim is to measure nitrate isotopes and $\delta^{30}Si(OH)_4$ in the Laptev Sea and Fram Strait to interpret the importance of various DSi and N cycling processes in these area which affects the exported nutrient inventory in surface waters of the Arctic. Mapping of the isoscape of inflow and outflow waters at Fram Strait is discussed in Chapter 3. This aims to determine the isotopic signature of inflow waters to the Arctic ocean and thus constrain the origins of heavy isotopic enrichment of Arctic waters.

1.5.2 The fate and export of riverine DSi on Arctic shelves

The isoscape of the Lena delta and the Laptev Sea is discussed in Chapter 4. The fate of riverine DSi is traced from the Lena delta to the continental slope, eventually feeding into the TPD. This work constrains biological Si burial on Arctic shelves. The isotope Si budget of the Arctic is updated based on findings from 1.5.1 and 1.5.2.

1.5.3 High vs low latitude nutrient supply to the subpolar North Atlantic

Convective water masses in the subpolar North Atlantic have a global impact on nutrient distribution and directly depend on nutrient origins and utilisation of surface waters of the Atlantic. In chapter 5, a transect across the convective basins investigates nutrient origins and the biogeochemical controls on this highly productive region using DSi and N isotope data.

1.5.4. Biogeochemical cycles in the context of climate change

Isotope and nutrient stoichiometry is used to evaluate the impact of climate variability (Chapter 5) and global warming (chapter 3 & 4) onto the biogeochemistry of the Arctic and the subpolar regions, with future implications on nutrient inventories and primary productivity.

1.5.5 Linkages between N and Si cycles

The combined use of nutrient isotopes constrains the impact of nutrient limitation during assimilation by phytoplankton in different regions of the Arctic and subarctic regions. In chapter 3, 4 and 5, this is used to examine the linkages between N and Si cycles and how they shape nutrient distribution and primary productivity in the marine environment.

2. Fieldwork & laboratory methods

Three sectors under polar water influence are examined to characterise the biogeochemical cycling of Si and N within the Eurasian Arctic Ocean and the sub-polar North Atlantic. These are the Lena river delta and the Laptev Sea (highlighted in red on Figure 2.1), the Fram Strait at 78.5˚N (highlighted in green on Figure 2.1) and the subpolar North Atlantic convective zone at 50-60˚N (highlighted in orange on Figure 2.1) where water samples were collected along 7 oceanographic sections.

This work was funded under the ARISE project (UK Changing Arctic Ocean program), which uses C & N isotopes to examine the changing ecosystems of the Arctic Ocean on different trophic levels. Crucial in this context is the isotope value of ambient seawater at the base of the food chain, called the isoscape. The isoscape is affected by environmental characteristics and is spatially and temporally variable, therefore, ARISE aimed to gain observational constraints on environmental variability of the isotope composition of the Eurasian Arctic Ocean over cruises targeting the Fram Strait and the Barents Sea (2017 – 2019), with additional sampling in the North Atlantic regions. An overview of all samples collected for this project is shown on Figure 2.1. The sampling of Si isotope on UK cruises and sampling on international cruises for this project was supported by the UKRI NERC Doctoral Training Program and SAGES. In measuring Si & N stable isotopes for this region, we significantly increase the number of measurements within the Arctic and Atlantic basins, filling in crucial gaps of the Arctic isoscape and adding to our understanding of biogeochemical cycling of biologically important elements within these regions.

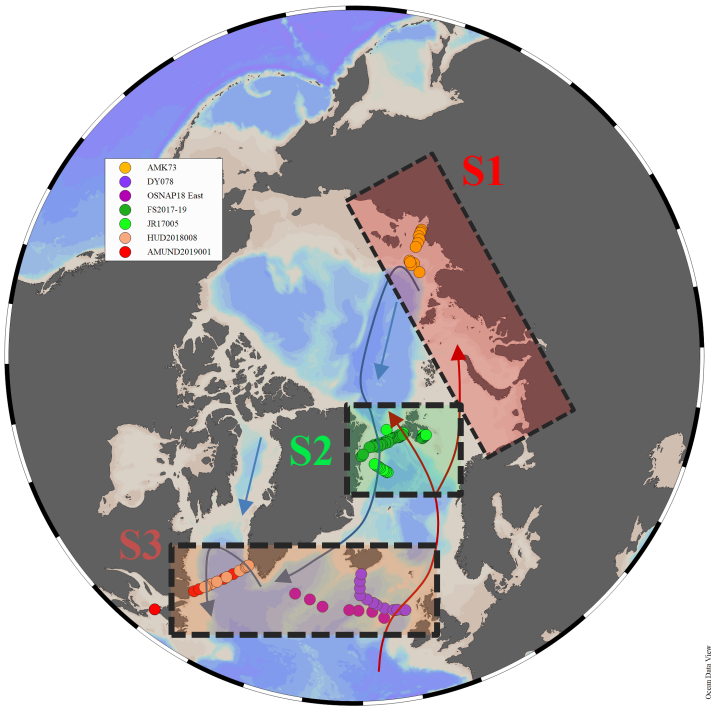

Figure 2.1. Map of the study region. CTD stations sampled for isotopes are highlighted by dots. Arrows show generalized surface circulation patterns for Atlantic-originating waters (red) and polar waters (blue). Dotted squares highlight the three main sectors studied in this project. S1 (red) = the Eurasian shelf sector (Lena Delta & Laptev Sea), S2 (green) = the Arctic-Atlantic gateway sector (Fram Strait) and S3 (orange) = the subarctic convective zone sector (full OSNAP transect).

2.1 Oceanographic expeditions

2.1.1 Fieldwork: Fram Strait

Fram Strait is the largest gateway to the Arctic Ocean and the only area of deep water exchange with the Atlantic. It is both an inflow and an outflow gateway. The annual Fram Strait Arctic Outflow Observatory (Norwegian Polar Institute) targets 30 annually repeated stations between 10˚W and 10˚E at Fram Strait in August/September at 78.5˚N. This samples both inflowing AW (West Spitbergen Current) East of Fram Strait, and outflowing PSW at the West of Fram Strait and over the East Greenland shelf. Each year, hydrographic and tracer measurements are collected and used to separate different types of freshwater in the Arctic Outflow at Fram Strait. If sea ice conditions are favorable, additional transects on the East Greenland Shelf are conducted. Data presented in this thesis were collected onboard three repeats of the Fram Strait Outflow Observatory cruises: Samples were collected

by the author onboard FS2017 (24th August – 13th September 2017) on RV Lance, FS2018 (25th August – 11th September 2018) on RV Kronprins Haakon, FS2019 (1-16 September 2019) on RV Kronprins Haakon. CTD station locations and profiles are shown on Figure 2.3 and Figure 2.4.

The repeat of the Fram Strait section at Fram Strait across years allows to monitor interannual variability of the biogeochemistry of Fram Strait. Isotopic samples were also collected in the early summer of 2018 onboard cruise JR17005 (9th May – 9th June) by other members of the ARISE team in Fram Strait at 79˚N, parallel to the 78.5˚N NPI transect. CTD stations from JR17005 are shown on Figure 2.2. Collection onboard JR17005 allowed to track seasonal variation in the biogeochemistry of Fram Strait.

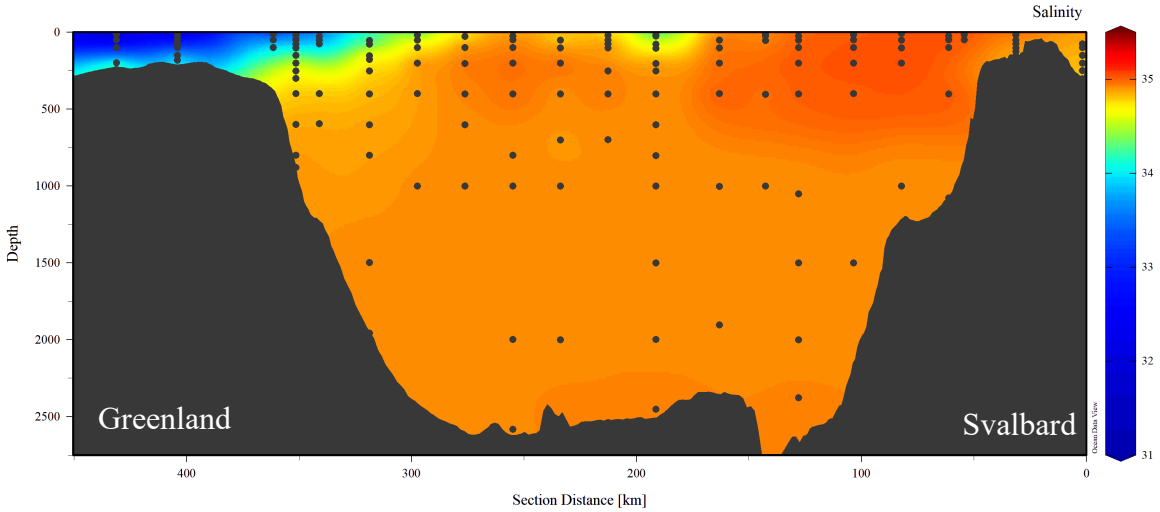

Figure 2.2. Hydrographic section (salinity) of the main Fram Strait JR17005 CTD transect. Black dots show isotope sample location in the water column.

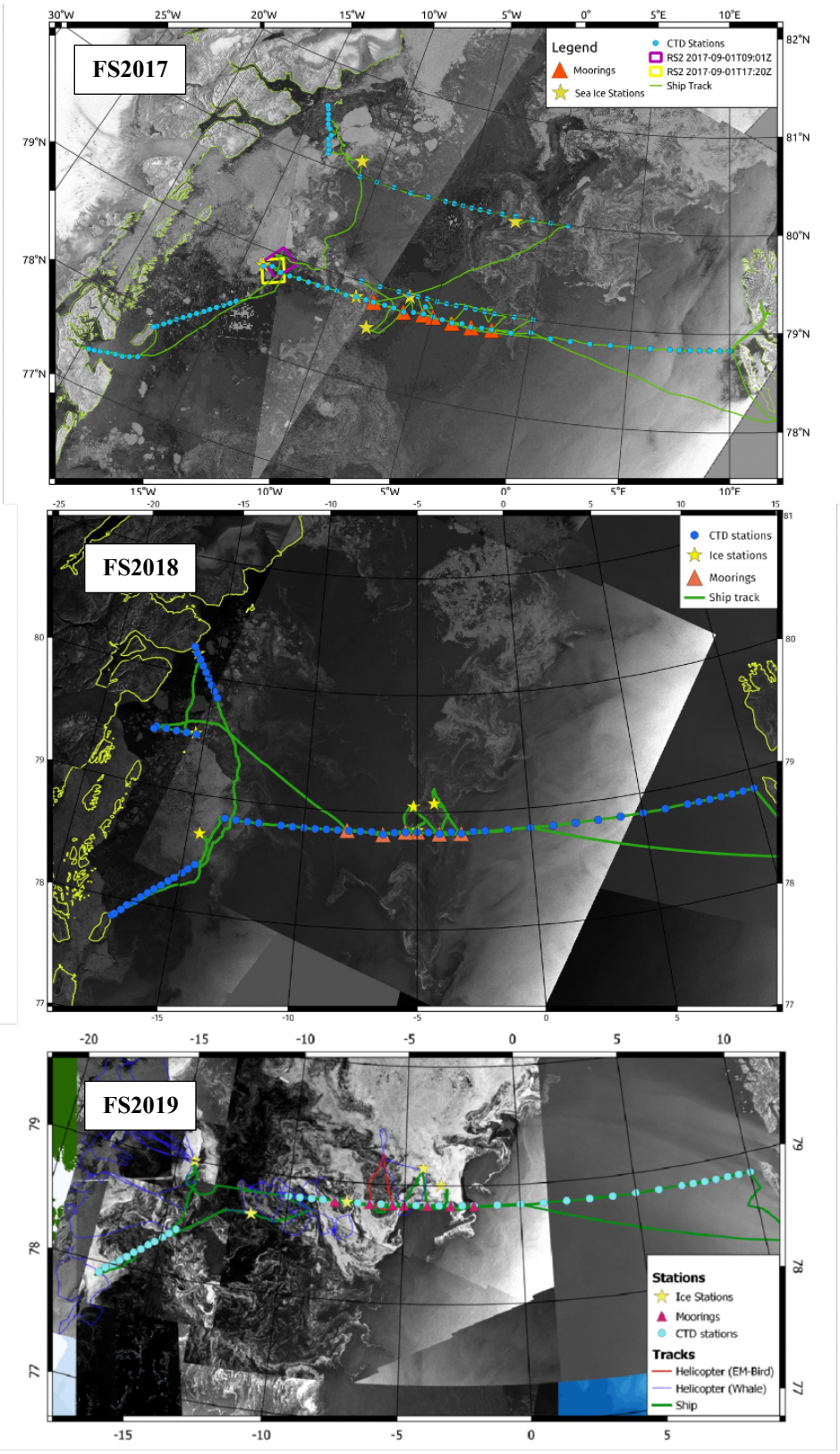

Figure 2.3. Cruise tracks and CTD stations of FS2017 (top), FS2018 (middle) and FS2019 (bottom) overlain onto satellite imagery of the sea ice conditions at the time of sampling. Figure adapted from (de Steur, 2017, 2018, 2019).

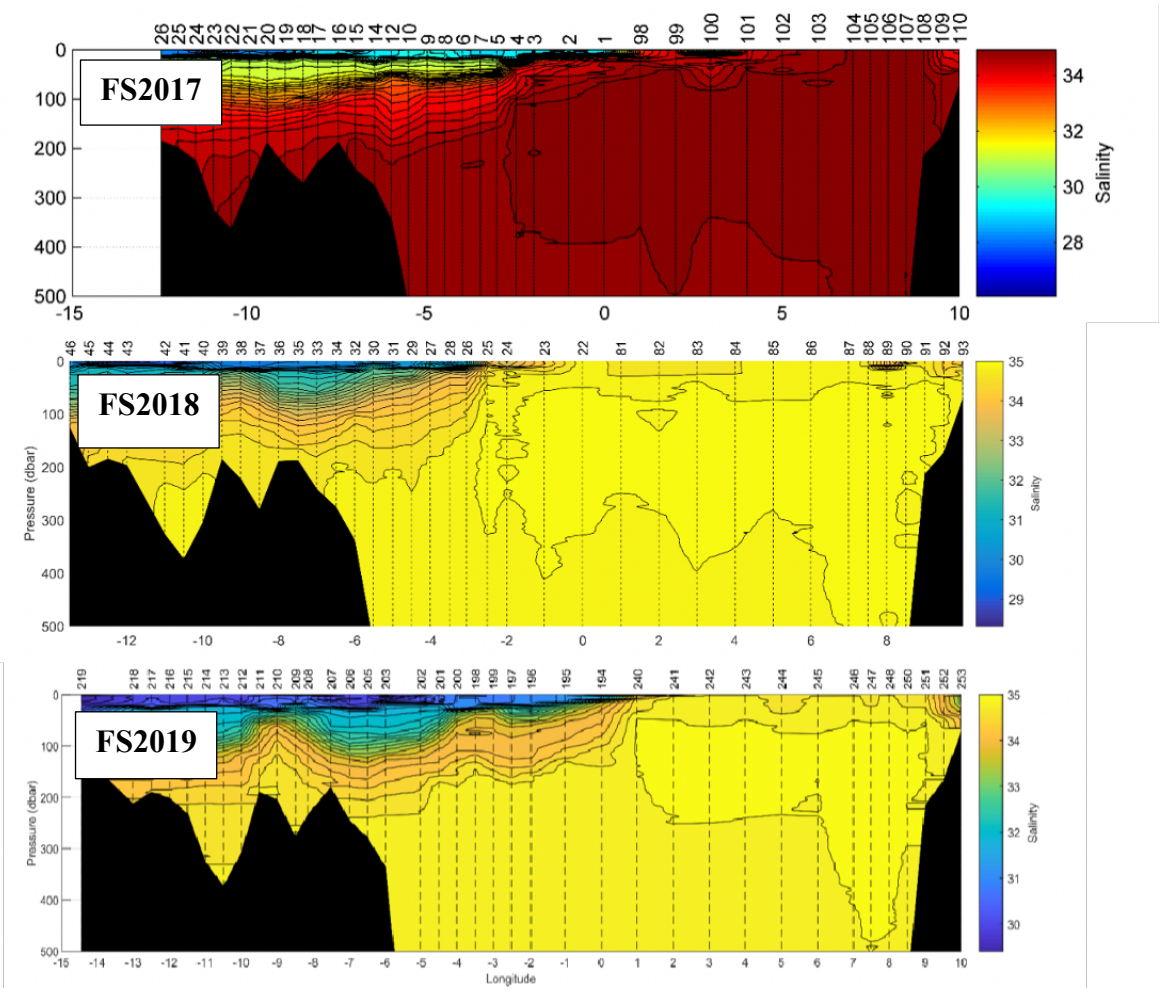

Figure 2.4. CTD measurements of salinity along the main Fram Strait section for FS2017 (top), FS2018 (middle) and FS2019 (bottom) along 78.5°N. Measurements from the primary salinity sensors, station numbers are indicated above sections. Figure adapted from (de Steur, 2017, 2018, 2019)

2.1.2 Laptev Sea & the Eurasian shelf (AMK73)

The Arctic Ocean is a shelf sea, around 50% of the Arctic basin is composed of shallow shelves, where unique and intensive biogeochemical processes occur. To capture and understand nutrient transformation on the Eurasian shelves, samples were collected in October 2018 during the 73rd expedition of R/V *Akademik Mstislav Keldysh* (AMK73). The main CTD transect is located in the Laptev Sea along the Lena estuary, shelf area and the upper part of the continental slope. Underway samples were also collected during transit covering the Eurasian shelf at its surface,

as shown on Figure 2.5. The hydrography and isotope sample location of the CTD transect from the Lena Delta onto the continental slope is shown on Figure 2.6.

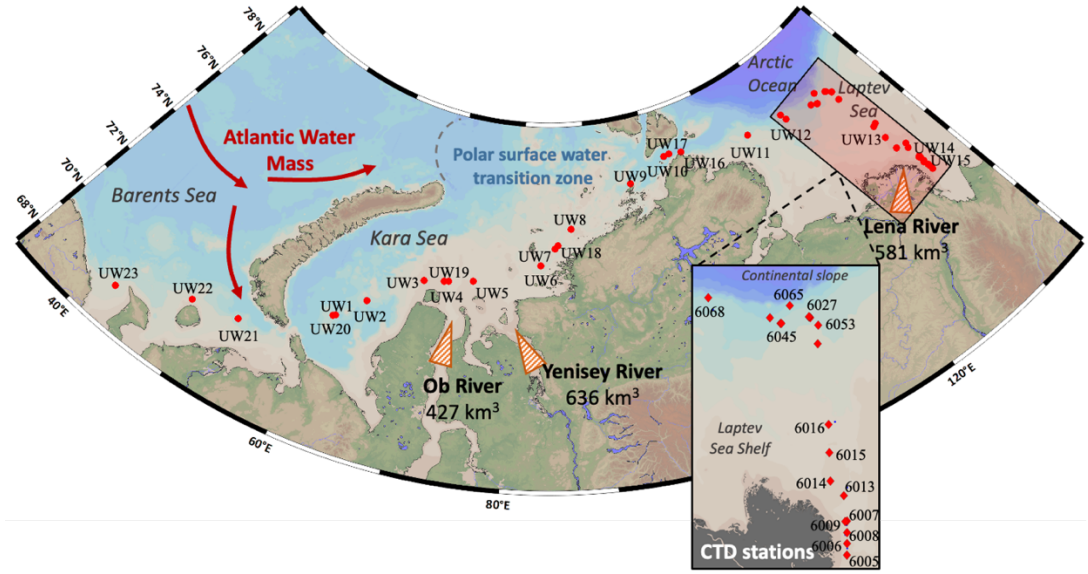

Figure 2.5. Sampling location of AMK73. Underway sites are labelled as UWX. The shaded red area highlights the CTD section and its station numbers. Map modified from Ocean Data View.

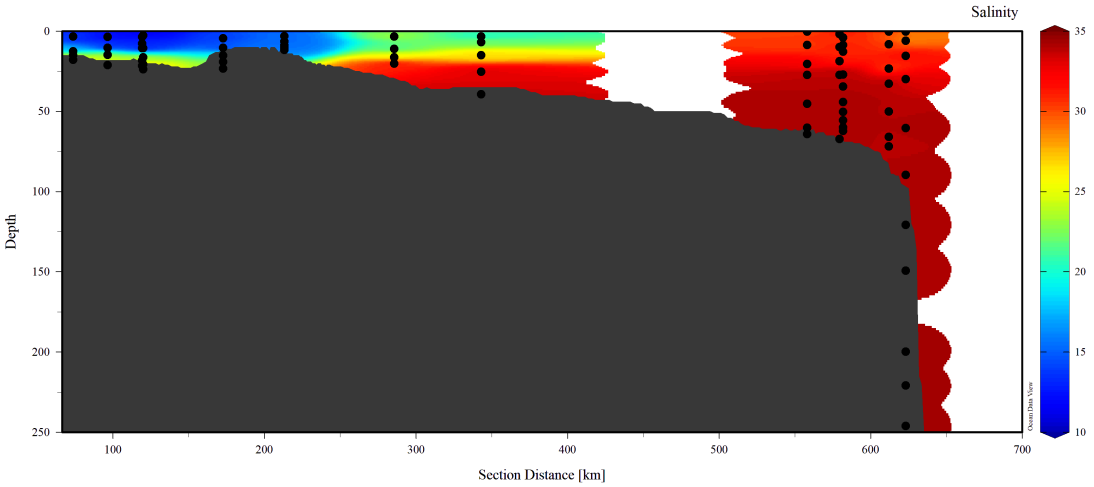

Figure 2.6. Hydrographic section (salinity) of the AMK73 CTD transect. Black dots show isotope sample location in water column.

2.1.3 The subpolar North Atlantic (DY078, OSNAP18-E, HUD2018-008, HUD2019001)

Samples from the subpolar North Atlantic were collected along three oceanographic transects to sample inflowing waters to the Arctic and polar waters and area of deep water formation in the North Atlantic through ongoing international programs.

Isotopes were used to monitor differences in water masses between three convective basins: the Labrador Basin, Iceland Basin and the Irminger Basin.

DY078 was sampled onboard RRS Discovery (6th-28th May 2017) through the Extended Ellett Line program, a long-term monitoring program of the Subpolar North Atlantic across the Rockall Trough and the Iceland Basin. The Rockall Trough is the main route of import of AW into the Nordic Seas and the Arctic Ocean. The Iceland basin is an area of deep convection and deep water formation, and exports waters from polar origins.

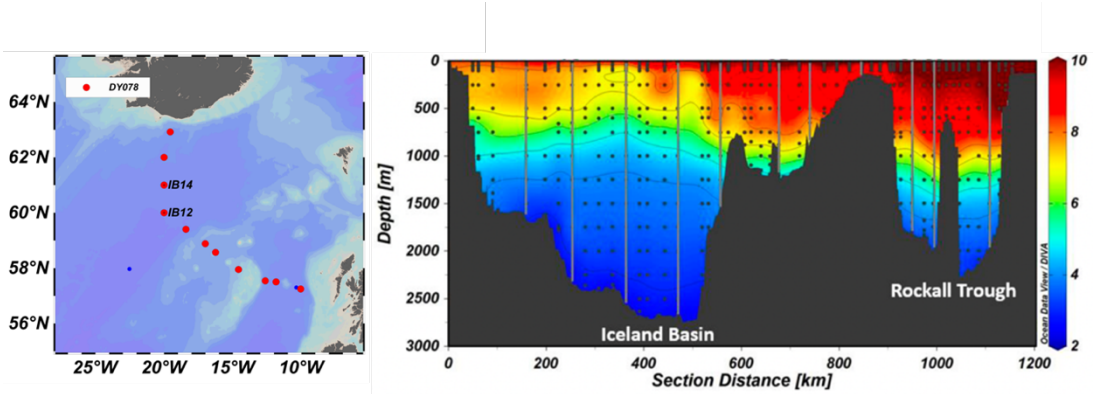

Figure 2.7. Map (left) displays CTD stations location from DY078 measured for nitrate isotopes. Labelled stations are stations with silicon isotope measurements. Hydrographic section (left, temperature ˚C), of the transect. Black dots show sample location in water column, adapted from Doncila (2020).

The AR30-004 cruise (referred to onwards as OSNAP18-E) is a continuation of the extended Ellett line transect, from the UK over the Rockall Trough to Western Greenland under the international OSNAP program. Samples were collected during OSNAP18-E onboard RV Neil Armstrong (1-29th July 2018). The Overturning in the Subpolar North Atlantic Program (OSNAP) is an international observing system, providing a record of the full-water column, trans-basin fluxes of heat, mass and freshwater in the subpolar North Atlantic. It also traces the pathways of overflow waters to assess connectivity of currents crossing the OSNAP line. Its Eastern leg (OSNAP East) extends from the southeastern tip of Greenland to Scotland.

OSNAP18-E targets the same water masses as DY078, with the additional sampling of the Irminger Basin, to also target Denmark Strait Overflow Water.

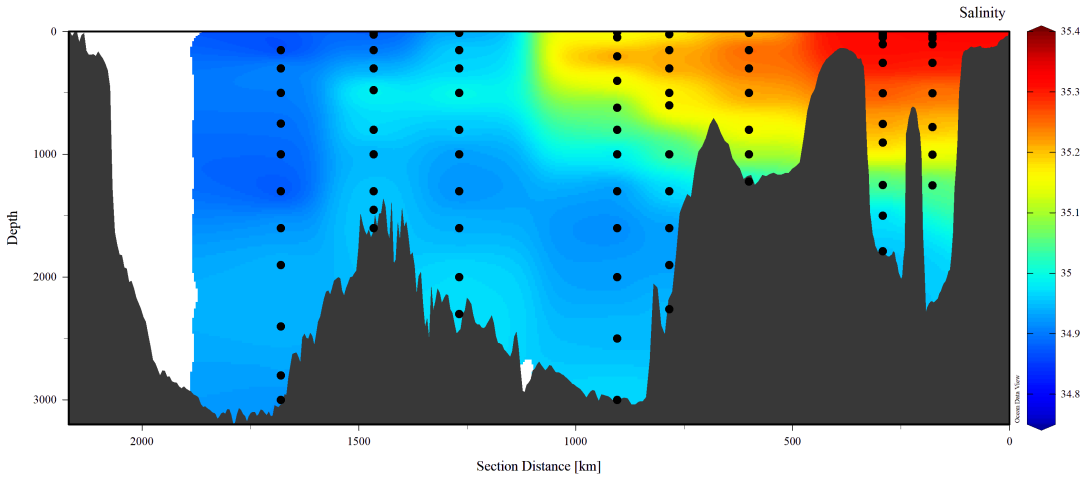

Figure 2.8. Hydrographic section (salinity) of the OSNAP18-E transect. Black dots show isotope sample location in water column. Section location is shown on Figure 2.1.

For the same purpose as DY078 and OSNAP18-E, samples were also collected along the AR7W transect in the Labrador Sea. The AR7W transect runs from the Labrador to Greenland, and provides observations of key oceanic characteristics to understand physical and biogeochemical connectivity between the Labrador Sea and Canadian Arctic. This targets Labrador Sea Water (LSW) formation, NEADW, and the Denmark Strait Overflow Water (DSOW) situated at depth, as well as surface currents from polar origins. Samples were collected on cruise HUD2018008 onboard CCGS Hudson (25th April – 22nd May) under the Atlantic Zone Monitoring Program (AZOMP), ran by the Canadian Department of Fisheries and Oceanography (DFO). As LSW forms through deep winter convection with large differences in convective depth on an interannual basis (Kieke and Yashayaev, 2015; Yashayaev, 2007), interannual variability was accounted for through the sampling of a second AZOMP cruise in 2019 during AMUND2019001 onboard CCGS Amundsen (30th May – 23rd June), led by the Ocean and Ecosystem Sciences Division of the Bedford Institute of Oceanography. Cruise track for AMUND2019001 is shown on Figure 2.9. The same stations were occupied under the AZOMP program during HUD2018008. The hydrography and isotope sample location for both cruises is shown on Figure 2.10.

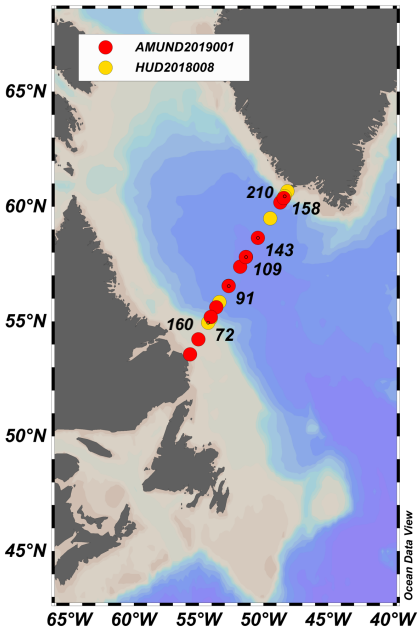

Figure 2.9. Cruise track of HUD2018008 and AMUND2019001. Dots show CTD stations along the AR7W transect where nitrate isotope samples were taken. Labelled stations are where silicon isotopes were also measured.

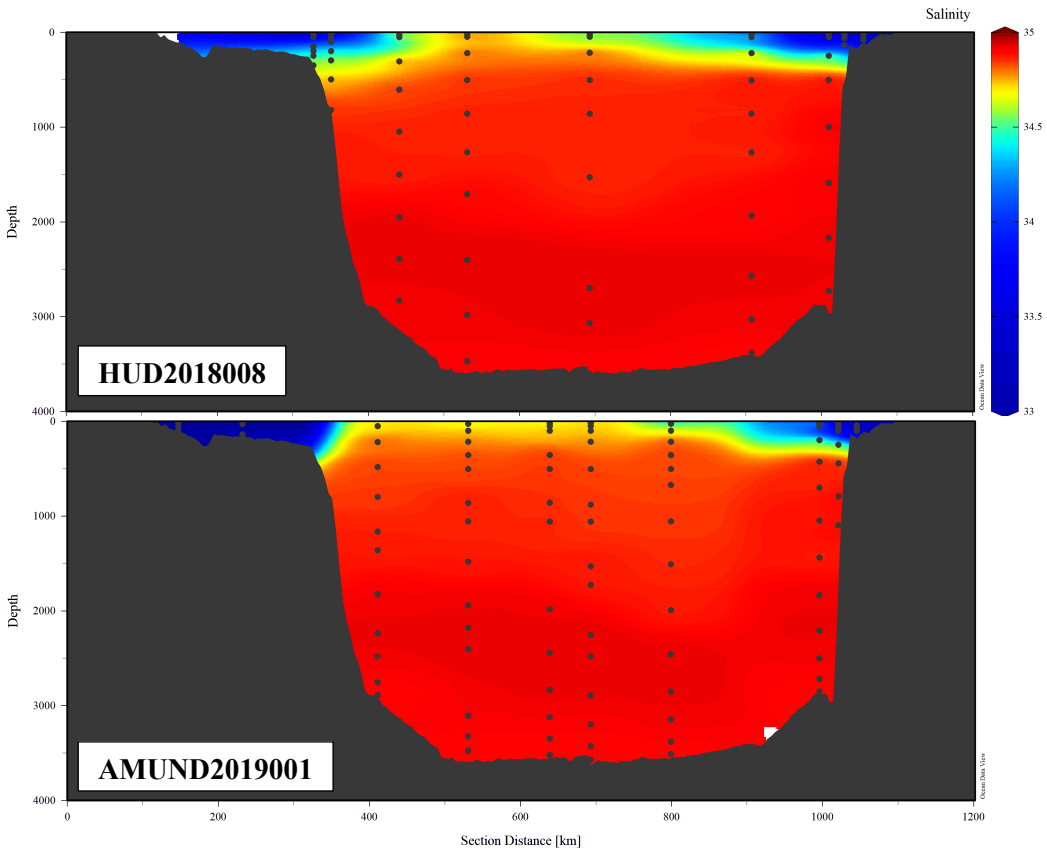

Figure 2.10. Hydrogrphic section (salinity) of the AR7W transect in the Labrador Basin. Black dots show isotope sample location in water column for HUD2018008 (top) and AMUND2019001 (bottom).

2.2 Sample & data collection

2.2.1 Hydrography and sensor measurements

Standard CTD (conductivity, temperature, depth) measurements and sampling were performed using a stainless steel rosette (12 Niskin bottles for FS2017, 24 for all other cruises), equipped with a full sensor array and 20 liter OTE bottles. CTD packages were equipped with a SBE911plus CTD system recording multiple parameters (conductivity, temperature, pressure & salinity). Salinity was calibrated on-board using a Guildline Portasal salinometer or Autosal 8400B. Dissolved O_2 was determined using a Seabird SBE 43 and calibrated onboard using a photometric Winkler titration system (Carritt and Carpenter, 1966). Tracer water samples were collected at selected stations for the standard depths of 5, 15, 25, 50, 75, 100, 150, 200, 250, 400 dbar and at the bottom of each cast for Fram Strait cruises, and at depths targeting regional water masses for all other cruises, with higher resolution in the upper 500m of the water column to document the upper ocean biological processes.

From physical parameters, the Mixed-Layer Depth (MLD) was calculated. MLD is identified as the maximum depth at which the potential density was within 0.1kgm^{-3} of the shallowest measurement (Peralta-Ferriz and Woodgate, 2015). MLD governs the depth for which nutrients are resupplied to the surface waters and to which planktons are mixed (Yool et al., 2015).

2.2.2 Nutrients and nutrient isotope sampling

Dissolved inorganic nutrient concentrations for all cruises were collected and determined on autoanalysers following the GO-SHIP protocol using standard colorimetric methods and calibrated using international standards and certified reference materials (Becker et al., 2020; Grasshoff et al., 1983). Samples for dissolved inorganic nutrient analysis were collected from Niskin bottles and either analysed live onboard or stored in pre-cleaned HDPE bottles for subsequent analysis in laboratories. Samples for isotopic analysis were collected following GEOTRACES protocols. Water from the Niskin bottles was filtered inline using Nuclepor polycarbonate membranes (0.4µm pore size) into acid-cleaned

polypropylene bottles and stored at -20℃ (nitrate isotopes) or acidified at 0.1% v/v with 12M HCl and stored at 4°C (silicon isotopes).

2.2.3 Particulate matter

2.2.3.1 Particulate Nitrogen

Prior to collection, filters were muffle-furnaced at 450˚C for 4h to remove any potential organic contamination, individually weighed on a microbalance, wrapped in aluminium foil, and sealed in a plastic container for transportation. Sampling depths were chosen based on the chlorophyll maximum observed in real time, or from the ship's underway system where sample volumes from Niskin bottles were limited. Seawater samples were collected from the underway system into acid-cleaned carboys and filtered through combusted GF/F filters (0.7µm pore size) within 2h of collection on the filtration system described on Figure 2.11. The filters were stored at -80°C until analysis. All equipment was rinsed with Milli-Q and stored in 10% HCl acid bath overnight prior to being used for a different sample. Prior to analysis the filters were freeze-*dried*, wrapped in tin foil cones (OEA Laboratories) and pelletised.

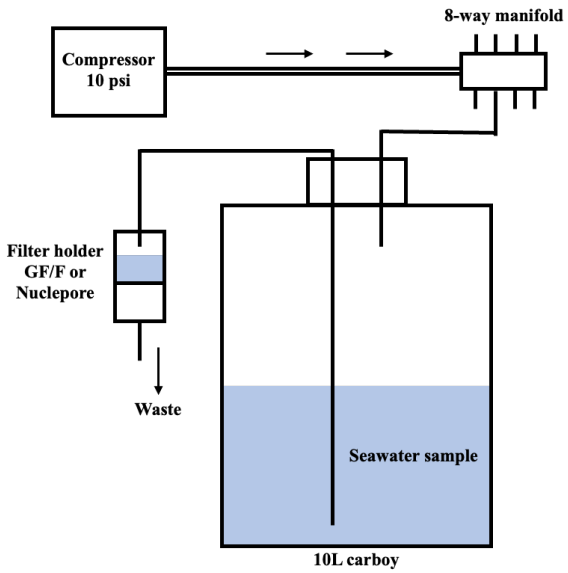

Figure 2.11. Filtration set up for onboard collection of suspended particulates in seawater. Samples were pressure filtered using a compressor at 10-psi. Up to eight water samples can be filtered simultaneously with the manifold.

2.2.3.2 Particulate Silicon

Seawater samples were collected from the underway system or niskin bottles into acid-cleaned polyethylene bottles and immediately filtered through Nuclepore filters (0.8μm pore size) on the filtration system described on figure 2.11. The filters were stored at -80°C until analysis. All equipment was rinsed with Milli-Q and stored in 10% HCl prior to being used again. Cleaning and dissolution of particulate silica was adapted from Morley et al. (2004). Filters were rinsed with MQ and collected particles were dried in digestion vials. 0.5ml of 10% HCl was added to dissolve carbonates overnight and evaporated at 100˚C. 0.2ml of concentrated H_2O_2 was added to dissolve organic compounds overnight and fully evaporated at 120˚C. 1ml of 0.1M NaOH was added to dissolve the particulate silica overnight. Solution was neutralized with HCl and eluted to 5ppm Si. The solution was subsequently processed through resin columns and analysed for $\delta^{30}Si$ on MC-ICP-MS as per the method of analysis of $\delta^{30}Si(OH)_4$ described in section 2.3.

2.3 Dissolved stable silicic acid isotopes

DSi is present in low concentrations in the modern ocean (0-60μmol/L) with respect to other major ions. To accurately analyse the isotope of DSi in seawater, $\delta^{30}Si(OH)_4$, finely-tuned concentration and purification steps are required. Preconcentration of DSi avoids traditional methods which rely on fluoration of silicon and determination using gas source mass spectrometry, a complicated method requiring the use of hazardous chemicals such as HF to convert DSi to $BaSiF_6$ (Brzezinski et al., 2006; De La Rocha et al., 1996). Purification steps allows for the use of Multi-Collector Inductively Coupled Plasma Mass Spectrometer (MC-ICP-MS) instead but this requires DSi to be in a relatively pure solution for subsequent ionization (Georg et al., 2006b).

A range of precipitation methods is currently used for the preparation of $\delta^{30}Si(OH)_4$ (Mg-induced with NaOH, Mg-induced with purified ammonia, TEA-moly precipitation, etc.) with no significant differences in resulting isotopic measurements

if all DSi is fully precipitated (Grasse et al., 2017). For this work, we use a pre-concentration protocol originally based on the Magnesium Induced Coprecipitation (MAGIC) method described in Karl and Tien (1992) with NaOH, as it requires non-hazardous and readily available chemicals. A drawback of pre-concentration steps however is that it creates a relatively high salt matrix effect, particularly at low dilution volumes.

Since DSi concentrations are very low in the Arctic ocean (<10μM), previous protocols from Brzezinski et al. (2003) and Reynolds et al. (2006) did not yield high enough DSi concentrations post-precipitation for accurate analysis in MC-ICP-MS. For this thesis, the method described in De Souza et al. (2012) was further optimised to allow measurements at concentrations below 10μM down to 1μM, and to increase the sensitivity and reproducibility of measurements in the very low concentration range. This was achieved through modification of the pre-concentration steps, and exploring a range of purification and spiking techniques to reduce contamination. The steps of the fully optimized protocol are described below.

2.3.1 DSi determination

As co-precipitation of samples is dependent on accurate determination of DSi concentration in the sample, DSi concentration was separately analysed for all $\boldsymbol{\delta}^{30}Si(OH)_4$ samples prior to sample preparation. This was determined from the $\boldsymbol{\delta}^{30}Si(OH)_4$ samples using the ultra-low range silica by Heteropoly Blue method where silica is complexed with molybdate ions to form a yellow coloured compound: silicon-molybdic acid. The addition of molybdate ions also complexes phosphate to form yellow phosphomolybdic acid and interferes with dissolved silica determination. Phosphomolybdic acid is hence decomposed using a small amount of citric acid (in excess). Amino acid is then added to the solution to reduce molybdic acid to a blue colour, determined with spectrophotoscopy. The HACH molybdate blue method provides a quick and highly reproducible method for low dissolved silica concentrations within the range of 0.2-100ppm Si (HACH, 2011), using a very low volume of sample. These were analysed after 1h in the spectrophotometer in 1cm cell at a wavelength of 812nm. Calibration curves are obtained from CRM SiO_2 (0.5ppm

Si) and in-laboratory standard of fresh Fiji water (85ppm Si) using concentrations shown in Table 2.1 below. For quality control, 10% of samples were measured in triplicates and standard deviation was calculated, and deep seawater samples of known DSi concentrations were measured across runs for intra-run comparability. Where data is available, concentrations are compared to those obtained from the cruise-organising institutions for data quality control.

Table 2.1. Standard calibration used for quick HACH DSi determination.

Standard	Volume standard (µl)	Volume MQ (µl)	Concentration (ppm)
Blank	0	3000	0
SiO_2 (0.5ppm Si)	250	2750	0.04
SiO_2 (0.5ppm Si)	500	2500	0.08
SiO_2 (0.5ppm Si)	1000	2000	0.17
SiO_2 (0.5ppm Si)	2000	1000	0.33
SiO_2 (0.5ppm Si)	**3000**	**0**	**0.50**
Fiji water	**50**	**3950**	**1.06**
Fiji water	100	3900	2.13

2.3.2 Pre-concentration

Pre-concentration increases DSi concentration in the sample, while decreasing the associated salt cation and anion matrix by over two orders of magnitude. This later enables the use of smaller cation exchange column, thus enabling faster processing of samples (Reynolds et al., 2006). The MAGIC method relies on the precipitation of brucite ($Mg(OH)_2$) in basic solutions (~pH10) using 1M metal-grade suprapur NaOH. As magnesium is a conservative element in the global ocean (Broecker and Peng, 1983), no artificial spiking of samples is required, avoiding contamination through artificial introduction of magnesium. Brucite forms in excess in basic solutions, scavenging silicic acid without fractionating Si isotopes above the detection limit of the method of analysis when scavenging is higher than 98% (Brzezinski et al., 2003). If less than 98% of DSi has been co-precipitated, the precipitate was excluded from analysis.

The adapted method for pre-concentration of very low concentration samples is described below, adapted for DSi concentrations between 1-10μM. To 40ml of previously acidified sample in an acid-cleaned centrifuge tube, 220μL of 1M trace-metal grade NaOH is added in order to neutralise the pH of the sample, previously acidified upon collection. A further 420μL of NaOH is added to make the solution basic, forming a white, jellyfish-like precipitate. This is left to shake for 1h at 100rpm to optimize silica recovery, and left to settle for 24h.

The next day, sample is centrifuged (5min, 3000T/min), and the supernatant is transferred into a second acid-cleaned centrifuge tube and 400μL NaOH is added. This is to prevent re-dissolution, observed over periods of time greater than 24h (Cassarino, pers. comm.). The supernatant is pipetted, not poured, to avoid any disturbance of the deposit. The sample is left to shake for 1h again and left to settle.

On the 3rd day, the 2nd precipitate is recovered by centrifugation and removal of the supernatant (via pipetting to avoid disturbance). Both precipitates are dissolved in a small volume of 6M HCl (~120μL, until solution is clear, slightly acidic), combined and diluted to a SiO_2 concentration of 2ppm with MQ water. The amount of MQ water added is calculated based on the sample's original concentration. Careful handling of the samples is required at the stage to avoid loss or fractionation of the separate aliquots. Successful precipitation of DSi was confirmed by testing the supernatant for DSi using the protocol described above.

The increased precipitation volumes used for low concentration determination of $\delta^{30}Si(OH)_4$ leads to reduced purity of the samples and higher salt matrix. To further reduce salt content from the precipitate, a weak 0.2M NaOH rinse stage of the precipitate is sometimes introduced (Cassarino, pers. comm.). Agitation of the precipitate however was found to lead to significant leaching of DSi into the NaOH solution, causing substantial DSi loss and fractionation of $\delta^{30}Si$ as the lighter isotopes are preferentially returned to the solution. Because of uncontrolled fractionation, this rinsing step was not found favorable, and salt-matrix effects induced from higher precipitation volumes were addressed at the analysis stage instead.

Table 2.2. Column chemistry procedure for $\delta^{30}Si(OH)_4$ purification adapted from Georg et al., 2006b.

Solution	Volume (ml)	Collect/Discard	Note
3M HCl	1	Discard	Clean resin
6M HCl	1	Discard	
3M HCl	1	Discard	
MQ	Fill	Discard	Repeat x3 Check pH is neutral
Sample	0.5	Collect	
MQ	0.5	Collect	Elution, repeat x3
MQ	1	Collect	Elution
3M HCl	2	Discard	Clean resin
6M HCl	2	Discard	
3M HCl	2	Discard	
MQ	Fill	Discard	

2.3.3 Purification

Pre-concentrated samples were further purified using a cation exchange resin column to separate DSi from other ionic species, following the method described in Georg et al. (2006) and applied to seawater in Reynolds et al. (2006). Purification of samples by removing other ionic species suppresses potential mass-bias effects and interferences upon analysis in the MC-ICP-MS (Albarède et al., 2004; Rehkämper et al., 2001). Between pH2-8, DSi is found prevalently under two species: non-ionic monosilicic acid ($Si(OH)_4$) and anionic silicate species ($H_3SiO_4^-$), neither of which will be retained by cation-exchange columns (Georg et al., 2006b). On the day of column chemistry, samples' pH are neutralised with 0.2M NaOH. 0.5ml of sample is loaded onto a pre-cleaned Biorad 50W-X8 cation-exchange resin column at pH 6-7 to remove cations and subsequently eluted to 3ml.

The full column chemistry procedure is shown in Table 2.2 above. Between uses, columns were stored in 1.5M HCl and resin was cleaned with twice-distilled HCL and

used 3 times between cleaning with stronger acids (HF and HNO_3).

2.3.4 Analysis

Resulting solutions were analysed on a Nu Plasma II MC-ICP-MS at the University of Edinburgh for all 3 isotopes of Si: ^{28}Si, ^{29}S and ^{30}Si, using standard-sample bracketing protocol (Georg et al., 2006b). Standard-sample bracketing is used to control error from reference material as well as standard deviation upon analysis. Analysis was done in pseudo-medium resolution to separate Si from various N and NO interferences, using a desolvator in pseudo-dry plasma, as per Pichevin et al. (2014). A bracketing of 3 sample measurements with 4 standard measurements is used to produce an average signature with an estimate of the standard deviation within bracketing. This allows to correct for drift in the instrumentation over time and avoids subsequent measurement bias. Each analysis is composed of 3 blocks of 15 measurements integrated over 5 seconds (45 individual measurements in total). Each sample or standard is bracketed with the primary isotopic standard NBS28.

δ^{29}Si was calculated in permil notation in deviation from NBS28, as calculated per the equation below:

$$\delta\ {}^{x}\mathrm{Si}(‰) = \left(\frac{({}^{x}\mathrm{Si}/{}^{28}\mathrm{Si})_{\mathrm{sample}}}{({}^{x}\mathrm{Si}/{}^{28}\mathrm{Si})_{\mathrm{NBS28}}}\right) \times 1000 \qquad \textit{Eq. 2.1}$$

where ^{x}Si is either ^{28}Si or ^{29}Si.

The international solid standard Big Batch and either high and low concentration GEOTRACES seawater standards $Aloha_{1000}$ and $Aloha_{300}$ were used as reference materials for measurement precision and method reproducibility at low concentrations in each sample run to monitor accuracy and provide an estimate of external reproducibility. The seawater standards were prepared in the same way as Arctic samples, including the MAGIC method steps.

2.3.5 Data correction

During analysis of pre-concentrated ALOHA standards, offset was measured from the standard published values on the $\delta^{30}Si$, but not the $\delta^{29}Si$, with ratio of $\delta^{29}Si/\delta^{30}Si$ diverging from the theoretical expected ratio of around 1.96 (Young et al., 2002). As BigBatch $\delta^{30}Si$ and $\delta^{29}Si$ was measured within error of published measurements and expected ratio, and as the $\delta^{29}Si$ of both ALOHA standards did too, this offset was not due to fractionation during laboratory preparation or from tuning/half peak offset selection in the MC-ICP-MS. This diversion was observed in seawater standards, but not the solid standard BigBatch, linking it to isobaric or anionic interferences during analysis linked to the matrix of seawater samples. Reanalysis of the same standards across runs on different days showed varying offsets for $\delta^{30}Si$ depending on the geometry of the torch, coil and cone position, which are not easily characterized, particularly in the low concentration standard $ALOHA_{300}$ as samples with low DSi have a higher matrix : DSi ratio.

As $\delta^{29}Si$ consistently remained unaffected by this interference effect, and the ratio of $\delta^{29}Si$: $\delta^{30}Si$ in the modern ocean is relatable, $\delta^{29}Si$ was converted to $\delta^{30}Si$. This allows comparison with other published datasets while reducing measurement error and increasing reproducibility. For the dataset produced in this thesis, $\delta^{29}Si$ was converted to $\delta^{30}Si$ using a theoretical conversion factor of 1.96, as calculated from the kinetic fractionation law (Young et al., 2002). As per other studies in areas of low DSi concentrations, this correction was applied to all measurements conducted within this thesis to avoid variable interferences on $\delta^{30}Si$ measurements from the low concentrations and high interference effect (Fripiat et al., 2011a, 2011b; Liguori et al., 2021) resulting from the increased precipitation volumes in our modified protocol.

For a period of the runs, the MC-ICP-MS geometry showed no offset between $\delta^{29}Si$ & $\delta^{30}Si$ (ratio around 2). The theoretical conversion ratio was still used to convert $\delta^{29}Si$ to $\delta^{30}Si$ to ensure consistency across the dataset. Nonetheless, this confirms that sample processing does not cause fractionation of the two isotopes.

2.3.6 Data quality

Here we examine the accuracy and long-term reproducibility of the adapted laboratory methods for analysis of $\delta^{30}Si(OH)_4$ at the University of Edinburgh laboratories by comparing measurements from this thesis to international reference materials. Table 2.3 shows the theoretical values for standards BigBatch, the high DSi concentration $ALOHA_{1000}$ (113 µmol/L, 1000m depth) and the low concentration standard $ALOHA_{300}$ (9 µmol/L, 300m depth), as well as the mean $\delta^{30}Si(OH)_4$ measured for each standard over the course of analysis for this work (2019-2021). Our measurements were ±0.04 ‰ or better within consensus values (Grasse et al., 2017; Reynolds et al., 2007). A slight enrichment (0.03-0.04 ‰) towards heavy isotopic values is measured in seawater, however this is well within the traditionally accepted standard deviation of replicates of ±0.2‰. Compared to prior inter-calibration studies such as Grasse et al. (2017), the analysis of lower DSi concentrations does not increase measurement error or offset from the consensus value. As $ALOHA_{300}$ has DSi concentration of the same order of magnitude as DSi concentrations in the Arctic & Sub-Arctic regions, this confirms the method was successfully adapted to create accurate and repeatable measurements of $\delta^{30}Si(OH)_4$ in the low concentration range.

Table 2.3. Isotopic values of silica standards. (1) From Reynolds et al., 2007., uncertainties at 1SD (2) From Grasse et al., 2017, uncertainties at 1SD. Also presented are the measured $\delta^{29}Si$ and converted $\delta^{30}Si$ using the theoretical fractionation factor 1.96. Standard deviations are 1 standard deviation in measurements over the course of the study (2019-2021).

Standard	Published $\delta^{29}Si$ (‰)	Published $\delta^{30}Si$ (‰)	Measured $\delta^{29}Si$ (‰)	Converted $\delta^{30}Si$ (‰)	Analysis n
Big Batch(1)	-5.34 ± 0.15	-10.45 ± 0.27	-5.35 ± 0.03	-10.48 ± 0.09	65
$Aloha_{300}$(2)	0.85 ± 0.05	1.66 ± 0.15	0.86 ± 0.03	1.69 ± 0.05	30
$Aloha_{1000}$(2)	0.65 ± 0.05	1.25 ± 0.10	0.66 ± 0.04	1.29 ± 0.08	59

To confirm that laboratory processing of samples is not fractionating $\delta^{29}Si$ with respect to $\delta^{30}Si$, we examine the relationship between $\delta^{29}Si$ and $\delta^{30}Si$ in runs where no interference on $\delta^{30}Si$ is measured (Figure 2.12 and Figure 2.13). It is important to verify isotopes are not artificially fractionated during sample processing, as this would otherwise indicate loss of DSi during processing and lead to bias when converting $\delta^{29}Si$ to $\delta^{30}Si$. Over the complete period of analysis of this work, we observe a good relationship between $\delta^{29}Si$ to $\delta^{30}Si$ (slope = 0.5196, $R^2 = 0.99$), in very close agreement to expected kinetic fractionation values (0.5092). This relationship still holds strongly in samples which contain a seawater matrix (when BigBatch measurements are excluded, slope = 0.5065, $R^2 = 0.99$). This is a good indicator that (1) no polyatomic interferences during MC-ICP-MS measurements are present, (2) laboratory processing is not significantly altering $\delta^{29}Si$: $\delta^{30}Si$ ratio, indicating that DSi is conserved.

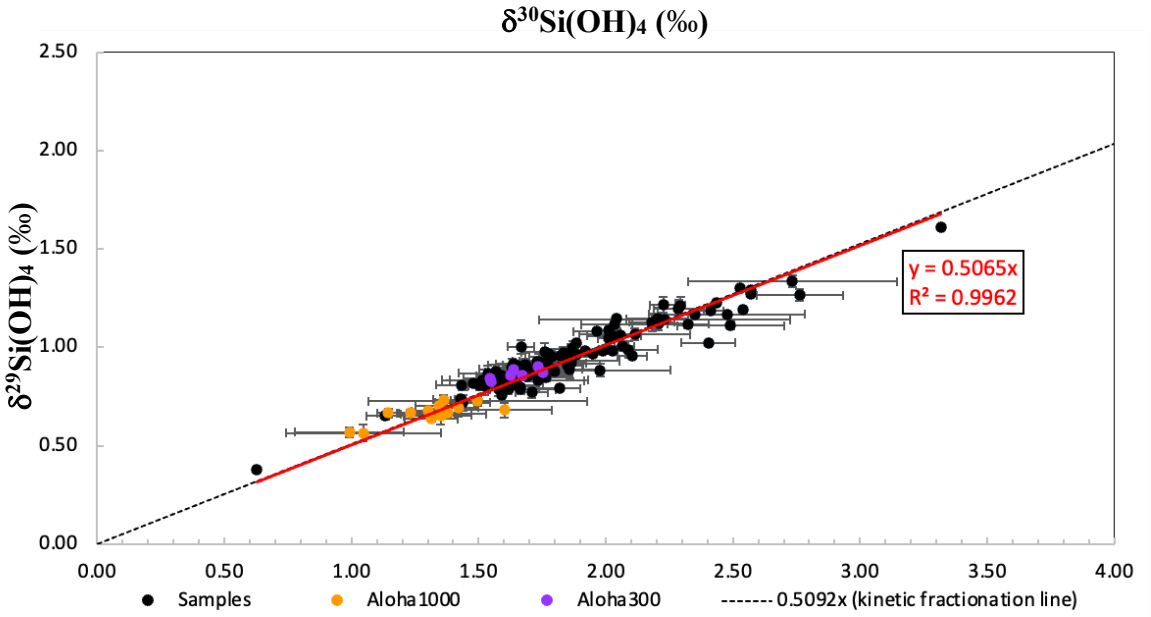

Figure 2.12. Plot of $\delta^{30}Si(OH)_4$ vs $\delta^{29}Si(OH)_4$ for seawater samples (black dots), $ALOHA_{1000}$ (orange dots), $ALOHA_{300}$ (purple dots) and BigBatch (blue dots) for all runs where no salt matrix interference was present . Error bars are one standard deviation. Solid red line is the least square regression, with a slope of 0.5156 ($R^2 = 0.999$). The theoretical kinetic fractionation line is shown in black dots (slope = 0.5092, see Reynolds et al., 2007).

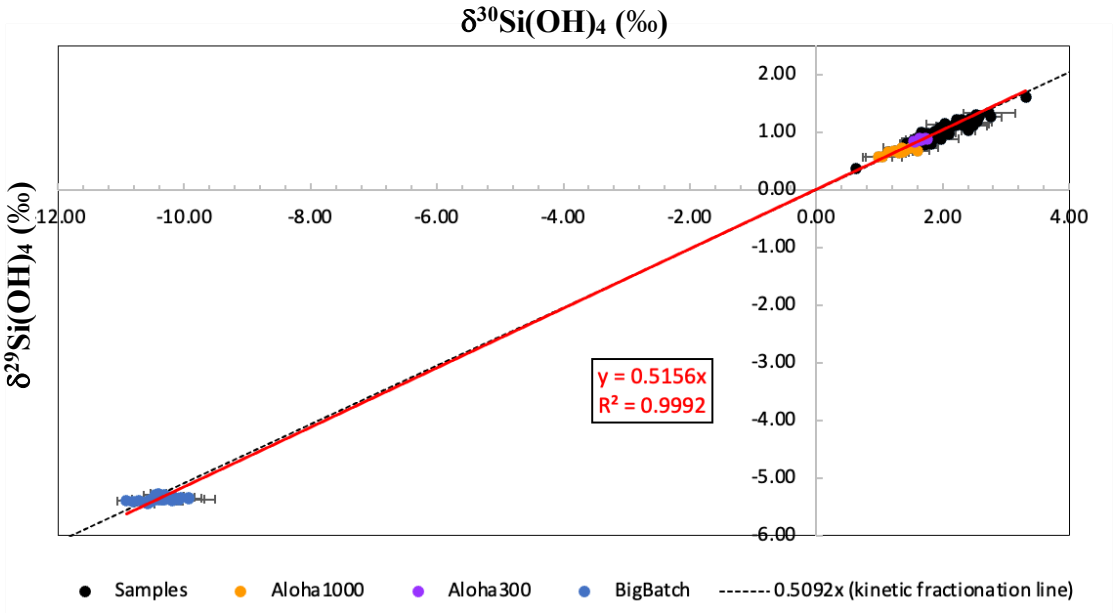

Figure 2.13. As per Figure 2.12, excluding the BigBatch standard. Solid red line is the least square regression, with a slope of 0.5065 (R^2 = 0.996). The theoretical kinetic fractionation line is shown in black dots (slope = 0.5092, see Reynolds et al., 2007).

2.3.7 Characterising analytical interference

During analysis of HUD2018008 samples with low DSi, interference because of the high sample matrix with increased precipitation volumes was observed analytically on $\delta^{29}Si$ and a spiking method was used during sample analysis. Matrices can be artificially matched in all samples through spiking with salt ions to concentrations order of magnitudes higher than their original post-column residual concentrations (Grasse et al., 2017). Where interference was observed through a positive offset in the ALOHA (seawater) standard but not in BigBatch (MQ), interference is present and spiking can be introduced to match this matrix (Van Den Boorn et al., 2009; Hughes et al., 2011). Samples and standards are spiked with 3500ppm HCl and 500ppm of H_2SO_4 following the method in Ng et al. (2020), to alleviate the interference effect. Average BigBatch measurements for the duration of the analysis with spiking was 5.36 ± 0.02‰ ($\delta^{30}Si$=10.51‰) and 0.69 ± 0.02‰ ($\delta^{30}Si$ = 1.35‰) for $ALOHA_{1000}$. We measure a 0.03-0.06‰ heavy enrichment in these sets of standards compared to non-spiked measurements over the course of this study. This could potentially be linked to the acid spiking of the samples, however this is well within analytical error and accepted inter-laboratory error (±0.2‰).

An experiment was carried out to further understand the impact of salt matrices on isotopic measurements, and is briefly outlined below. A series of test were conducted using Low-Nutrient Seawater (LNS) and Big Batch standard. 40ml of LNS were precipitated using the MAGIC method. They were then diluted at a range of volumes similar to the range of dilutions required for low-nutrient Arctic samples (1 to 15ml) to recreate a range of typical matrices during sample preparation after precipitation, and spiked to 2ppm of Big Batch prior to column chemistry. A high concentration sample was spiked to 15ppm Si. 10ml volumes of LNS were also precipitated and diluted to 5 and 10ml. An aliquot of the 10ml precipitated, 5ml dilution sample was passed through columns at low pH (3) to test the impact of pH on column chemistry. All other samples were neutral.

All samples were measured in the MC-ICP-MS following the analysis protocol described below. Results are shown on figure 2.14. It can be observed that the initial volume of seawater precipitated, and therefore the size of the C, N or salt matrix, appears to control the amplitude of the offset in isotopic signature measured. A combination of low precipitation and high dilutions volumes lead to the smallest deviation from standard values. In areas of high DSi, like upwelling regions of the Southern Ocean or North Pacific, it is therefore advisable to use low volumes of sample for precipitation and increase the dilution volume when the solution is diluted down to 2ppm prior to analysis.

Due to the extremely low concentrations of the Arctic and Sub-Arctic regions, a large volume of precipitation is required. 40ml was used for all samples so that the matrix effect was kept as similar as possible across samples.

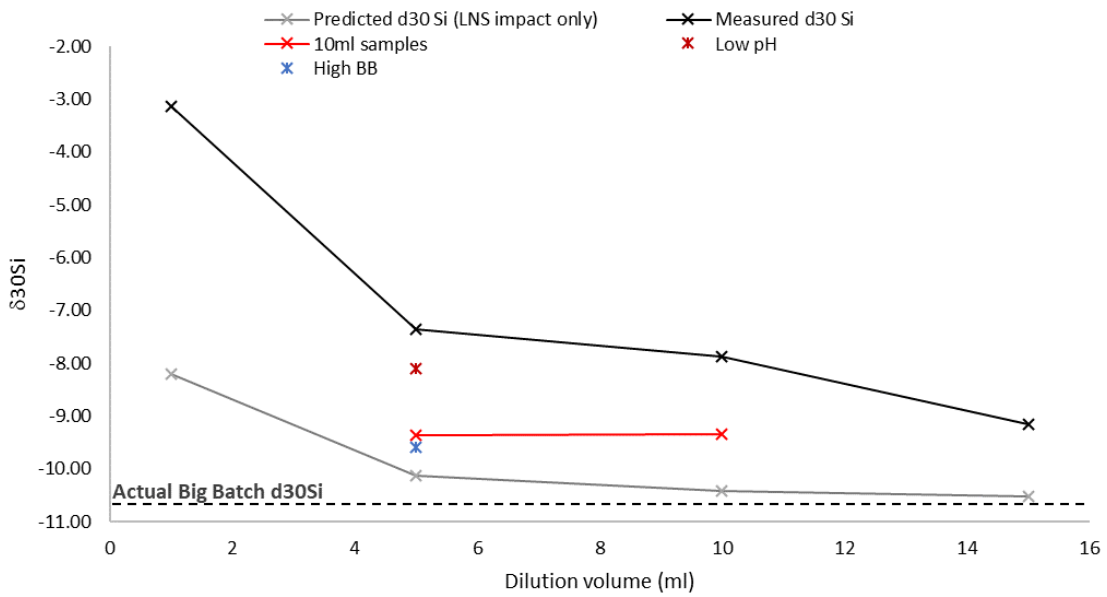

Figure 2.14. δ^{30}Si measured against dilution volume of LNS (+ spiked with 2ppm BigBatch). Black line shows samples with original volume precipitated of 40ml, red line shows 10ml initial volume. The grey line shows the predicted impact of the silicon concentration present in LNS. While it has a significant impact at low concentrations, this does not account for the full offset measured, with anion matrix showing significant contribution.

A second observation is that at low dilution samples (very low concentrations), the impact of the salt matrix becomes increasingly high. This is to be expected as the same total amount of salt ions will be present in samples of the same volume precipitated, but increased dilution will reduce their final concentration, thus creating less interference with the silicon signal. This is further confirmed with the high BB sample, which shows a BB signature much closer to the actual signature as the ratio of Si:Salt is higher within the sample. Finally, the low pH sample shows a large deviation from its isotopic signature, stressing the importance of using pH neutral solutions during column chemistry. While the original volume of sample precipitated can be kept constant for the entire dataset, the dilution volume of samples cannot, as running samples of different concentrations in a mass spectrometer creates measurement bias. This can lead to substantially different matrix effects that cannot be individually corrected for as shown on figure 2.14. This would introduce "random" error and render the data produced unusable.

The intensity of the matrix effect and subsequent offset observed in samples appears dependent on the plasma torch position relative to the sample cone. This is dependent on the relative position of the torch, coil and cone within the instrument and can not easily be controlled or parameterized, but it can be monitored through the various standards. Spiked standards display a set offset which may be characterized from the divergence of BigBatch and Aloha from their standard measured values across runs. While the standards average offset is run-dependent (depends on the position of the torch relative to cone and coil), but not signature-dependant, as shown on figure 2.14, sample signatures can be corrected with it to ensure homogeneity and reproducibility across runs without introducing bias. Data resulting from each run where interference was observed was thus corrected for the spiking-induced offset observed from the according standards during the run. This method however, assumes no laboratory fractionation of the ALOHA standards, and no longer allows to use them for international comparison of method accuracy.

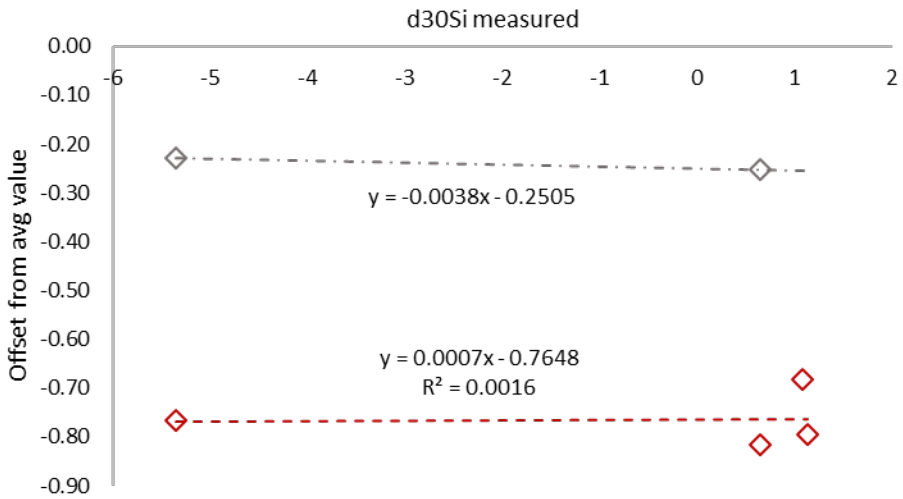

Figure 2.15. Spiking introduced offset of measurements. The grey line shows data measured on run #11 and red on run #2. Both trends show no significant relationship with $\delta^{30}Si$.

2.4 Nitrate stable isotopes: the Denitrifier method

The two isotopes of nitrate, $\delta^{15}N\text{-}NO_3^-$ and $\delta^{18}O\text{-}NO_3^-$ were determined using the Denitrifier Method (Casciotti et al., 2002; Sigman et al., 2000) and the protocol established at the University of Edinburgh laboratories by Dr Robyn Tuerena (2012-

2014). This relies on bacteria *P.aureofaciens*, a denitrifying bacterium which converts nitrate and nitrite into nitrous oxide (N_2O) while conserving an identical isotopic signature to the original state when fully converted. N_2O is extracted from the sample using a purging rack and trap system (Sigman et al., 2009a), and subsequently analysed with gas chromatography and mass spectrometry. Mass spectrometry measures the ratios of the two isotopes ($^{15}N/^{14}N$ & $^{18}O/^{16}O$) within the material analysed relative to a universal reference material with a constant ratio. In this instance, we use tanks of Air (AIR) for nitrogen and the Vienna Standard Mean Ocean Water (VSMOW) for oxygen linked to the IRMS as standards. The isotope ratios of samples of standards analysed are reported in delta notations (δ) in units of permil (‰), which refers to the part per thousand deviation from the universal reference material, determined using equations below:

$$\delta^{15}\mathrm{N}(‰) = \left(\frac{(^{15}\mathrm{N}/^{14}\mathrm{N})_{\mathrm{sample}}}{(^{15}\mathrm{N}/^{14}\mathrm{N})_{\mathrm{standard}}}\right) \times 1000 \qquad \textit{Eq. 2.2}$$

and

$$\delta^{18}\mathrm{O}(‰) = \left(\frac{(^{18}\mathrm{O}/^{16}\mathrm{O})_{\mathrm{sample}}}{(^{18}\mathrm{O}/^{16}\mathrm{O})_{\mathrm{standard}}}\right) \times 1000 \qquad \textit{Eq. 2.3}$$

2.4.1 Laboratory procedure for Inorganic Nitrogen Isotopic Determination

Clean laboratory conditions are required for all methods described below. All working surfaces and gloves are cleaned with 70% ethanol prior to laboratory work. All labware has to be sterilised and acid-cleaned to remove bacterial and nitrate contamination.

Briefly, *Pseudomas aureofaciens* (stock kept frozen at -80C) are streaked onto clean agar plates (500ml MQ water, 0.5g KNO3, 0.125g (NH4)SO4, 2.5g KH2PO4, 15g Tryptic Soy Broth (TSB) and 15g Tryptic Soy Agar (TSA) autoclaved at 105C for 30min) and left to grow in a dry, dark, sterilized box until distinct colonies form (2-3 days). Using these, a second plate is streaked and left to grow until distinct colonies

form. Bacteria can be used from plate 2 (for homogenous colonies) until plate 4 (after which mutation are likely) for the Denitrifier Method. Bacterial colonies are then inoculated in 10ml of bacterial media (2L MQ water, 2g KNO_3, 0.5g $(NH_4)_2 SO_4$, 10g KH_2PO_4, and 60g Tryptic Soy Broth (TSB), autoclaved at 121˚C for 30min) left to grow overnight on a shaker table. 1ml of the starter media is injected into 150ml of bacterial media, left to grow in the dark on a shaker table until all nitrate was consumed, and when the media turned cloudy (6-10days).

Bacterial media is tested for traces of nitrite (120µl of Sulphanilamide + HCl and NED reagents into 1ml of media). If the media turns pink, bacterial concentrations are not high enough yet and it is left to grow for longer. When no colour change is observed, media is ready for vial preparation. The bacteria is concentrated by centrifugation of 350ml of bacterial media split into eight 50ml centrifuge tubes (5000rpm, 14min) and the supernatant is removed. The solid pink/brown bacteria is diluted back into 150ml of nitrate-free media (1L MQ water, 0.25g $(NH_4)_2 SO_4$, 5g KH_2PO_4, and 30g TSB, autoclaved at 105C for 30min). 0.1ml of nitrate-free antifoam is added to the solution.

3ml of the nitrate free media and bacterial solution are pipetted into 50 acid-cleaned 15ml glass vials and crimped sealed with a butyl stopper. To ensure anaerobic conditions and remove residual N_2O, vials are placed on a nitrogen gas bubbling rig with a venting needle and left to purge the bacteria for 3hours to produce anaerobic conditions and remove any of N_2O resulting from bacterial activity with the nitrate-rich media during growth. This set up is further described on Figure 2.16. After purging, all vials are injected for 20nmol of nitrate ($V_{inj}=20/[NO_3]$ where V_{inj} is the sample injection volume and $[NO_3]$ is the concentration of nitrate in the sample) to produce 10nmol of N_2O and yield a constant sample-to-blank ratio, to avoid sample size effects and reduce mass spectrometer non-linearity (Weigand et al., 2016). Bacteria are left to consume the nitrate overnight in the upturned vials to improve gas retention. Bacterial consumption is stopped the next day by lysing with 0.1ml of 10M NaOH.

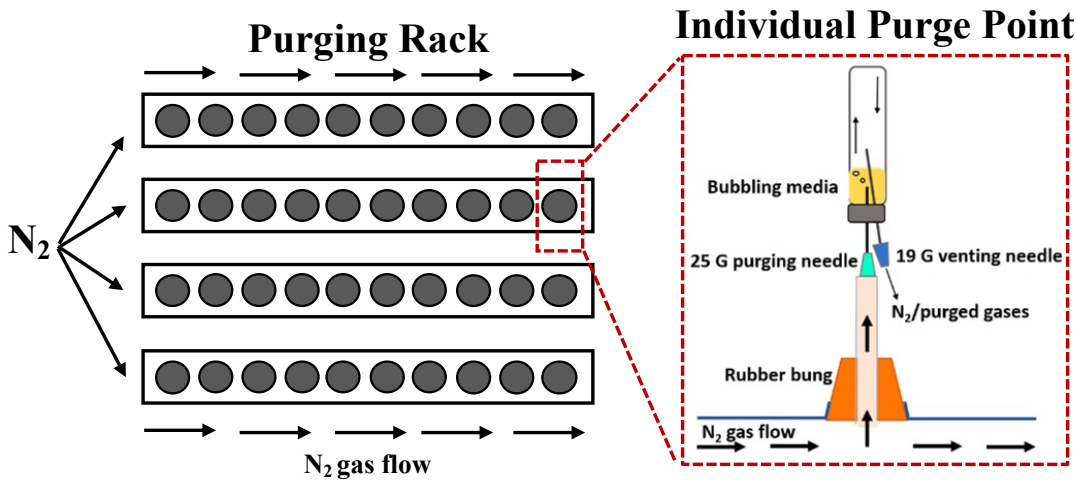

Figure 2.16. Schematic of the vial purging system for the Denitrifier method for 40 vials at the University of Edinburgh (current set up can take up to 50 vials). Each grey circle on the rack (left) represents a purging vial point (right schematic). Adapted from Doncila (2020).

2.4.1.1 Total Dissolved Nitrogen

The $\delta^{15}N$ of total dissolved N ($\delta^{15}N$-TDN) was also measured in nitrate isotope samples by peroxidation of TDN to NO_3 and subsequent N isotope analysis through the Denitrifier Method. This follows the method described in Knapp et al. (2005) and used for the Bering Sea shelf in Granger et al. (2011). Measurement accuracy and reproducibility was checked with international organic standards U40 (L-glutamic acid) and in-house standard Glycine in each run. Three sets of standards are used in this protocol: a set of N3 and U34 standards without the persulfate solution to correct for the IRMS measurements (injected at 20nmol in triplicates), a set of N3 and U34 standards with the persulfate solution to correct for N contamination from the persulfate (injected at 5, 10 and 20nmol), and organic standards (20nmol) to monitor measurement accuracy and reproducibility.

Briefly, bacteria was grown as per the method described above, with modified bacterial media prepared using a 3x increase in KH_2PO_4 to provide additional buffering in the solution. To ensure that the potassium persulphate (KPH) used in the organic N digestion step was free of nitrogen, we use a triple recrystallization step of the potassium persulphate for purification. This procedure eliminates trace amounts of nitrogen in the persulphate 100g of potassium persulphate (Nitrogen free grade) was dissolved into 600ml of MQ water at 60˚C. This temperature should not be

exceeded to avoid loss of persulphate. The mixture was subsequently rapidly cooled into a cold water tub until crystals formed (5˚C). The solution is then filtered using a vacuum pump, and the process was repeated until crystals have been recrystallized 3 times on the day of analysis, with a ratio of crystal: water mass of 1:4-1:5 on each subsequent recrystallization to dissolve the crystals. Lower water volume usage for dissolving the crystals minimizes the loss of persulphate in each recrystallisation step. Crystals can be stored in a beaker within a vacuum desiccator, but further recrystallisation should be carried out on the day of analysis as nitrogen is absorbed by the crystals over time.

Prior to the sample injection step to purged vials, all N was converted to nitrate using an organic N digestion step. An alkaline persulphate solution is prepared on the day of analysis (75ml of MQ water, 25ml of 2M NaOH (N free grade), 1g of triple-filtered potassium persulphate). This solution is discarded after use to limit N contamination. 0.33ml of the solution per sample/standard is pipetted into muffled ampoules (3 aliquot per ampoule for standards, 2 for organic standards and samples) and are flamed sealed. Ampoules with internal standards U40 and Glycine were injected with 60nmols of N (1.5ml of standard), sample ampoules were injected with a volume of sample relating to the TDN concentration present (= 20/[TDN] * 2), prior to flame sealing. All ampoules were autoclaved (105˚C, 30min) and rinsed with MQ water to remove any N contaminant deposited on the outside of the ampoule. At this stage, all DON in the sample/standard is converted into DIN. Once cooled, ampoules are neutralized with 4M HCl and 2M NaOH and injected into the purged nitrogen-free media vials. Ampoules containing the persulphate solution only (for standards) are split evenly between 3 vials, while sample and organic standard ampoules are split in two.

2.4.2 Analysis and data correction

Nitrous oxide produced by the bacteria in the headspace of the sample vials were analysed using a Combi PAL autosampler coupled to a Thermo Fisher Scientific GasBench II to a Delta V Advantage stable isotope ratio mass spectrometer (detection limit <0.5ppm) at the University of Edinburgh laboratories. Reference

standards used are IAEA N3 and US34. For analytical precision and quality control, samples are duplicated within a batch and ran along with replicates of USG34 and IAEA-NO_3 reference nitrate solutions, made up in MQ and low nutrient seawater, to allow the reporting of $\delta^{15}N$ against AIR and $\delta^{18}O$ against VSMOW. The standards are analysed at a range of nitrate concentrations that bracket the sample's concentration analysed (Weigand et al., 2016). A bacterial blank and gas blank are also analysed to control laboratory and analytical contamination of samples. The analytical precision for seawater sample $\delta^{15}N$-NO_3 was ±0.2‰ and for $\delta^{18}O$-NO_3 ±0.6‰ over the 4 years course of analysis, which is comparable to other studies for these isotopes (Fripiat et al., 2018; Granger et al., 2018; Lehmann et al., 2019; Sigman et al., 2001, 2005). Internal standards of North Atlantic seawater were also analysed across runs to check inter-run variability and validity of each run's measurements. Analytical precision and reproducibility for seawater sample $\delta^{15}N$-TDN was 0.25‰, within standard measurements within error of published standards (see table 2.4). Samples with very low concentrations (<2µM, Section 4, Appendix 1) were analysed following the same laboratory procedure at 5nmol instead (V_{inj}=5/[NO_3]) on a low detection mass spectrometer at the University of Edinburgh laboratories (AMK73 and surface samples). Standard reproducibility for this was ±0.2‰ and ±0.4‰ for $\delta^{15}N$-NO_3 and $\delta^{18}O$-NO_3 respectively.

Table 2.4. Published isotopic values of nitrate isotope standards and measured isotopic values over the course of this study. Uncertainty is shown to 1 standard deviation.

Standard	$\delta^{15}N$ – published (‰)	$\delta^{18}O$ - published (‰)	$\delta^{15}N$ – measured (‰)	$\delta^{18}O$ - measured (‰)	Analysis number (n)
USGS34	-1.8 ± 0.2	-27.9 ± 0.6	-1.8 ± 0.3	-27.7 ± 1.0	176
USGS40	-4.5 ± 0.1		-4.2 ± 0.1		4
Glycine	1.1 ± 0.2		1.0 ± 0.1		3
IAEA-N3	4.7 ± 0.2	25.6 ± 0.6	4.7 ± 0.2	25.7 ± 0.8	175

Table 2.5. Published isotopic values of seawater nitrate isotope internal standards and measured isotopic values over the course of this study. Error are shown to 1 standard deviation.

Internal Seawater Standard	$\delta^{15}N$ – published (‰)	$\delta^{18}O$ - published (‰)	$\delta^{15}N$ – measured (‰)	$\delta^{18}O$ - measured (‰)	Analysis number (n)
16-2	4.9 ± 0.2	1.9 ± 0.6	5.0 ± 0.2	1.9 ± 0.4	52
66-3	6.7 ± 0.2	3.4 ± 0.6	6.7 ± 0.1	3.5 ± 0.2	3
80-5	6.3 ± 0.2	3.8 ± 0.6	6.5 ± 0.2	4.1 ± 0.6	8

Output data from the mass spectrometer is filtered and corrected to homogenise datasets following the Sigman correction scheme (2007). Only data with peak start time over 1200 seconds are considered (lower peak areas would suggest a blockage and potential interference with CO_2). Measurements are corrected as per Sigman et al. (2001), by creating a regression line between measured and published standard values to obtain corrected standardised isotopic values. Measured isotopic signatures are also corrected for injection volume and for the expected $\delta^{18}O$-H_2O of water masses. Long term reproducibility of standards and internal standards is shown in Table 2.4 and Table 2.5. On the whole, a small positive bias of +0.1‰ and +0.2‰ is observed for $\delta^{15}N$ and $\delta^{18}O$ respectively, however, this is well within the range of published and accepted isotopic values.

2.4.3 Correction of $\delta^{15}N$-TDN

Output values from the MS for $\delta^{15}N$-TDN are filtered for erroneous values as described above. Additionally, any sample with peak area intensity values greater than 2 from the standards in the run were discarded. IRMS calibrated $\delta^{15}N$ values were produced using US34 and IAEA-N3 set of standard free from persulfate solution, using the standard regression line between measured and published standard values. Using the set of US34 and IAEA-N3 standards injected with persulfate solution, a straight line against inverse peak area value is generated. The two slope and intercept values obtained were used to characterise the $\delta^{15}N$ and area intensity of the KPS solution,

and IRMS adjusted values were then corrected using these to produce final KPS-corrected δ^{15}N-TDN. The accuracy of these measurements are checked with the two internal organic standards. Additionally, triplicate blanks of the persulfate solution are present in each run, peak area should be <0.6 to confirm that the persulfate was properly purified. Blank percentage in sample final values should be less than 10%.

2.4.4 δ^{15}N-PN analysis

δ^{15}N-PN was determined by EA-IRMS using a Costech Instruments Elemental Analyser coupled to Thermo Scientific Delta V Advantage mass spectrometer fitted with Conflo IV gas handling system by Louisa Norman (NOC). The instrumentation was operated using ISODAT 3.0 isotope ratio MS software. L-glutamic acid standards USGS 40 and USGS 41a (US Geological Survey, Reston Stable Isotope Laboratory) were run alongside the samples and were used both for data processing and to assess the performance of the instrumentation. An internal standard consisting of freeze-dried, finely powdered prawn was also used as a further 'check standard'. A 10-point calibration using standard USGS 40 was measured to provide the linear regression equation which was used to derive PON concentrations from the respective peak areas. µg/L concentrations were then then calculated using the concentration obtained from the whole filter and volume of seawater filtered. The detection limit for PON was 10µg.

2.5 Data processing

The semi-conservative tracers N* & Si* were calculated from inorganic nutrient concentrations where $N^* = NO_x - PO_4^- \times 16$, adapted from Gruber & Sarmiento (1997), and $Si^* = DSi - NO_x$ (Sarmiento et al., 2004). Both tracers are indicative of nutrient deviation from typical Redfield ratio, and highlight additional sources or processes through which nutrient become deficit (i.e Negative N* shows nitrate deficit in comparison to phosphate). The isotopic parameter Δ(15-18) is calculated as $\Delta(15\text{-}18) = \delta^{15}N\text{-}NO_3 - \delta^{18}O\text{-}NO_3$. Δ(15-18) captures variation in both isotopes, tracing sources and modification of nitrate (Rafter et al., 2013).

Dataset processing and plots presented in this work was achieved using a combination of excel, matlab, python & ODV (Schlitzer, 2021). Where relevant, interpolation of discrete measurements was done using Data-interpolating Variational Analysis (DIVA) gridding mode for biogeochemical parameters in the ODV software and in Matlab for physical datasets. In Matlab & ODV, derived parameters were calculated using the Gibbs-Seawater Oceanographic toolbox, using TEOS-10 equations for seawater (McDougall and P.M. Barker, 2011).

2.6 Ancillary data

Hydrographic and sensor data was collected and quality control checked following international standards by the Norwegian Polar Institute (FS2017-FS2019), the British Oceanographic Data center (DY078, OSNAP-E, JR17005), Igor Semiletov (AMK73) and Igor Yashayaev (HUD2018008, HUD2019001). Inorganic nutrients were measured by Colin Stedmon (DTU) for FS2017-2019, Louisa Norman (NOC) for JR17005, DY078 and OSNAP18-E, Robyn Tuerena (SAMS) for AMK73 and provided by Igor Yashayaev for HUD2018008 and HUD2019001. All particulate matter concentrations and PN isotope analysis presented in this thesis were analysed and corrected by Louisa Norma (NOC). All PSi isotope analysis were done by Laetitia Pichevin at the University of Edinburgh following an adapted method from Morley et al., (2004) and is further described in Chapter 3.2.4.1.

Unless stated below or referenced in text, all isotopic data presented in this thesis were analysed by myself. Nitrate stable isotopes measurements for JR17005 were obtained from Robyn Tuerena for JR17005 (data available in Tuerena et al., 2021), and from Antonia Doncila for part of the DY078 stations (data available in Doncila, 2020). All data was measured in the laboratories of the University of Edinburgh using the Denitrifier Method and corrected using the procedure described above (2.4). Ancillary datasets were corrected using the same internal and international standards, and sample stations were cross-checked for reproducibility across analysers.

2.7 Inter-comparison of datasets

An additional quality check for accuracy and reproducibility for the method of analysis of nutrient isotopic measurements described in sections 2.3 and 2.4 is to compare our data to deep oceanic measurements of other published datasets at nearby locations. The central Labrador basin as a few profiles measured for both nitrate isotopes (Deman et al., 2021; Lehmann et al., 2019, 2022) and $\delta^{30}Si(OH)_4$ (Giesbrecht et al., 2022; De Souza et al., 2012; Sutton et al., 2018b) which crossover stations measured in this study along the AR7W transect.

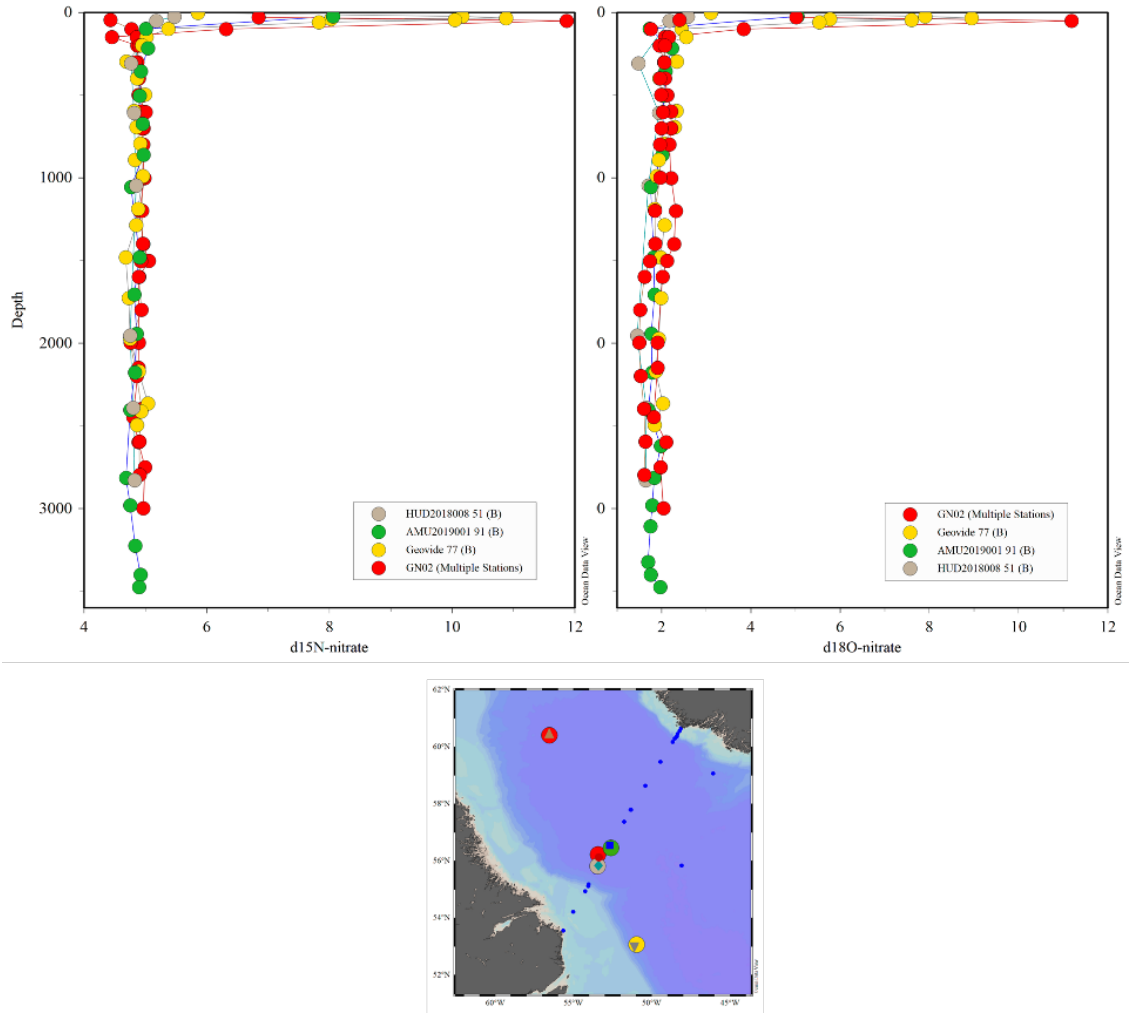

Figure 2.17. Data from the Labrador sea (CTD casts 51 & 91) during the HUD2018008 and AMUND2019001 expeditions compared with stations 69 and 77 from the GEOVIDE expedition in 2014 (Deman et al., 2021) and stations LS2 and K1 from the GEOTRACES GN02 expedition in 2015 (Lehmann et al., 2019, 2022) at nearby locations. $\delta^{15}N\text{-}NO_3$ (left top panel) and $\delta^{18}O\text{-}NO_3$ (right top panel). Station location in the basin is shown on map.

Figure 2.17 shows nitrate isotope profiles from this study (grey & green) in comparison to nearby measurements from GEOVIDE and GEOTRACES expeditions (Deman et al., 2021; Lehmann et al., 2019, 2022). Below the photic zone subject to seasonal variations, all profiles agree very well with each other, within the standard uncertainty associated with the Denitrifier method (0.2‰ for $\delta^{15}N\text{-}NO_3$ and 0.6‰ $\delta^{18}O\text{-}NO_3$). There is little variation in deep $\delta^{15}N\text{-}NO_3$, but for $\delta^{18}O\text{-}NO_3$, datasets all reproduce the same trends of enrichment between 500-1000m and 1000-2000m. The use of international and internal standards, and the reproducibility of seawater characteristics obtained for nitrate isotopes validates interpreting differences in isotopes both within our datasets and between publications of seawater nitrate isotopes.

Figure 2.18 shows the same dataset inter-comparison in the Labrador Sea for $\delta^{30}Si(OH)_4$ (Giesbrecht et al., 2022; De Souza et al., 2012; Sutton et al., 2018b). Ensuring inter-comparability of datasets is particularly important for $\delta^{30}Si(OH)_4$ in the Atlantic Ocean as offsets larger than 0.2‰ have been reported in the past (Brzezinski and Jones, 2015; Sutton et al., 2018b), linked to analytical methods. The left panel of Figure 2.18 shows that in the deep Ocean, all four datasets are within the accepted laboratory offset of ±0.2‰ (Grasse et al., 2017; Reynolds et al., 2007). The datasets from this study are in particularly good agreement to datasets from both De Souza et al. (2012) and Giesbrecht et al. (2022), and reproduce trends within profiles, while measurements reported in Sutton et al (2018) are consistently lighter. The right panel of Figure 2.18 shows the alignment of uncorrected measurements from this study to the published deep Atlantic measurements from the studies cited above. Again, data from this project appears in very good alignment with global trends and well within the expected range of isotopic measurements for water masses of the North Atlantic without the need for offset correction. Since the laboratory inter-comparaison exercise in Grasse et al. (2017), the use of ALOHA seawater international standards appear to largely address offset between datasets. However, care still needs to be taken when comparing to datasets prior to the use of ALOHA standards, and not to over-interpret offset under 0.2‰ when the data is produced

from laboratories with differing instruments and analytical methods (Grasse et al., 2017).

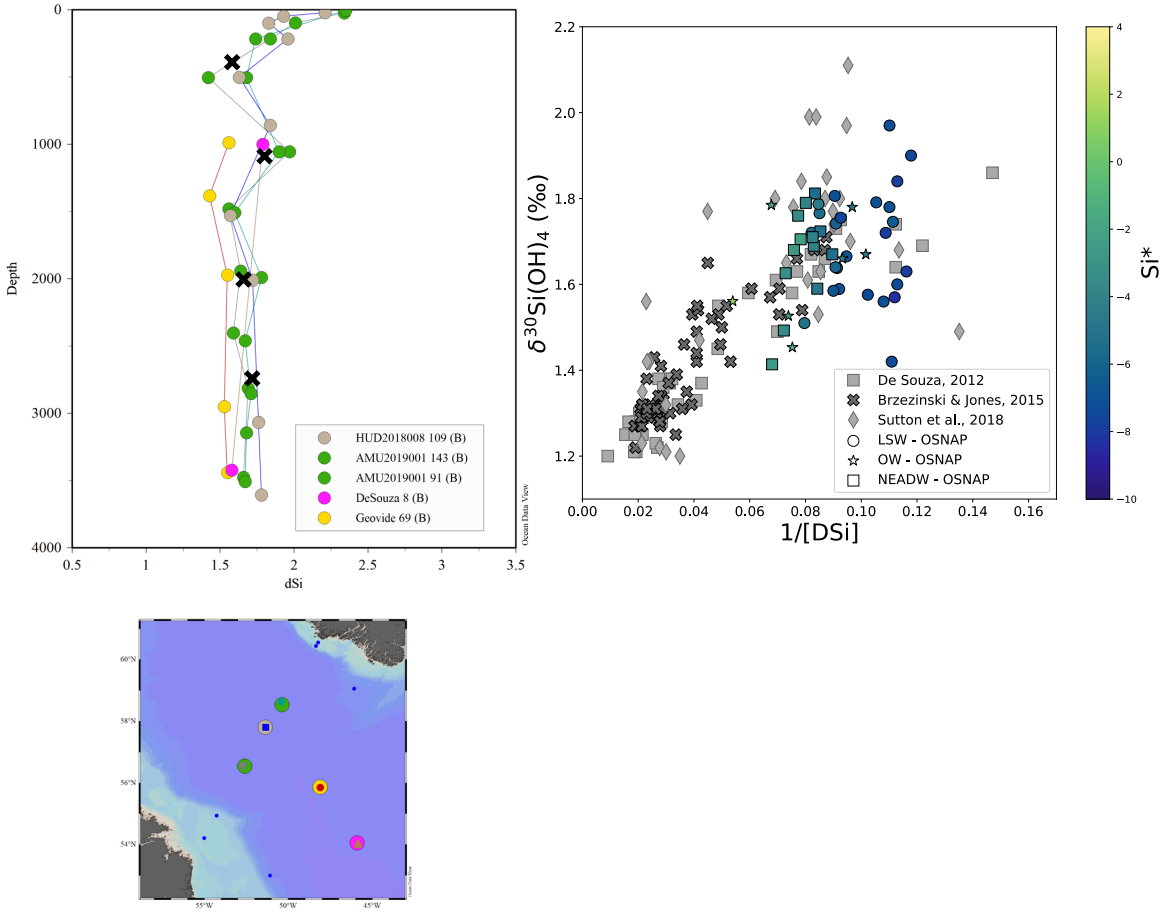

Figure 2.18. Top left panel shows δ30Si(OH)4 data from the Labrador sea (CTD casts 109 & 143) during the HUD2018008 and AMUND2019001 expeditions compared with uncorrected δ30Si(OH)4 data from stations 69 from the GEOVIDE expedition in 2014 (Sutton et al., 2018b) and station 8 from expedition 64PE319 in 2010 (De Souza et al., 2012). Endmember water mass signatures from station K1 during the GEOTRACES GN02 expedition in 2015 are shown in black crosses (Giesbrecht et al., 2022) at nearby locations. Station location in the basin is shown on map. Top right panel shows uncorrected δ30Si(OH)4 measurements from the subpolar North Atlantic from this study for deep samples (>1000m, colorscale = Si*) against 1/DSi. Grey symbols show all other published δ30Si(OH)4 measurements across the Atlantic Ocean (Brzezinski and Jones, 2015; De Souza et al., 2012; Sutton et al., 2018b). Due to documented offsets between the three publications prior to the use of seawater δ30Si(OH)4 standards, datasets from Brzezinski and Jones (2015) and Sutton et al. (2018) were corrected to De Souza et al. (2012) using the offsets reported in Sutton et al. (2018): -0.22‰ and +0.25‰ respectively for the right panel only.

3. Eurasian Arctic biogeochemical cycles and nutrient export through the Fram Strait

This chapter is based on a manuscript currently in review in the journal *Biogeosciences*.

Margot C.F. Debyser[1], Laetitia Pichevin[1], Robyn E. Tuerena[2], Paul A. Dodd[3], Antonia Doncila[1], Raja S. Ganeshram[1]

Affiliations

[1]School of Geosciences, University of Edinburgh, Edinburgh, EH9 3FE, United Kingdom

[2]Scottish Association for Marine Science, Dunstaffnage, PA37 1QA, United Kingdom

[3]Norwegian Polar Institute, Tromsø, 9296, Norway

Contribution

Author – M.C.F Debyser

Research design – M.C.F. Debyser, R.S Ganeshram, R.E Tuerena, P.A. Dodd & L. Pichevin

Sample collection – M.C.F Debyser, R.E Tuerena & P.A. Dodd

Sample analysis – M.C.F Debyser, R.E Tuerena & L. Pichevin

Scientific interpretation and manuscript implementation – M.C.F Debyser, R.E Tuerena, R.S. Ganeshram, L.Pichevin & P.A Dodd

Abstract

Nutrient cycles in the Arctic ocean are being altered by changing hydrography, increasing riverine inputs, glacial melt and sea-ice loss due to climate change. In this study, combined isotopic measurements of dissolved nitrate ($\delta^{15}N\text{-}NO_3$ and $\delta^{18}O\text{-}NO_3$) and silicic acid ($\delta^{30}Si(OH)_4$) are used to understand the pathways that major nutrients follow through the Arctic ocean. Atlantic waters were found to be isotopically lighter ($\delta^{30}Si(OH)_4$= +1.74‰) than their polar counterpart ($\delta^{30}Si(OH)_4$= +1.85‰) owing to partial biological utilisation of dissolved Si (DSi) within the Arctic ocean. Coupled denitrification and nitrate regeneration on Eurasian Arctic shelves leads to the enrichment of $\delta^{15}N\text{-}NO_3$ and lighter $\delta^{18}O\text{-}NO_3$ in the polar surface waters ($\delta^{15}N\text{-}NO_3$ = 5.44‰, $\delta^{18}O\text{-}NO_3$ = 1.22‰) relative to Atlantic waters ($\delta^{15}N\text{-}NO_3$ = 5.18‰, $\delta^{18}O\text{-}NO_3$ = 2.33‰). Using a pan-Arctic DSi isotope dataset we find that the input of isotopically light $\delta^{30}Si(OH)_4$ by Arctic rivers and the subsequent partial biological uptake and burial on Eurasian shelves are the key processes that generate the enriched isotopic signatures of DSi exported through Fram Strait. A similar analysis of $\delta^{15}N\text{-}NO_3$ highlights the role of N-limitation due to denitrification losses on Arctic shelves in generating the excess DSi exported through Fram Strait. We estimate that 40% of DSi exported in Polar surface waters through the Fram Strait is of riverine origin. As the Arctic ocean is broadly N-limited and riverine sources of DSi are increasing faster than nitrogen inputs, a larger export through the Fram Strait is expected in the future. Arctic riverine inputs therefore have the potential to modify the North Atlantic DSi budget and are expected to become more important than variable Pacific and glacial DSi sources over the coming decades.

3.1 Introduction

The dissolved macronutrients nitrate (NO_3^-) and silicic acid ($Si(OH)_4$) are key nutrients in sustaining marine primary production in the Arctic ocean, and have distinct sources from the Atlantic and Pacific Oceans (Tremblay et al., 2015). Additionally, river and coastal erosion contribute dissolved silicon (DSi) and nitrate which fuel approximately 30% of Arctic-wide net primary productivity (Terhaar et

al., 2021). The Greenland Ice Sheet has also been suggested as an important source of DSi to the Arctic ocean (Hatton et al., 2019; Hawkings et al., 2017). It has been estimated that >85% of DSi from riverine sources is not consumed by phytoplankton (Le Fouest et al., 2013) and is exported out instead, but the controlling processes of this remain unclear. Thus, an integrated understanding of the relative importance of sources to the internal cycling of DSi and the controls on the export of DSi to the North Atlantic is lacking.

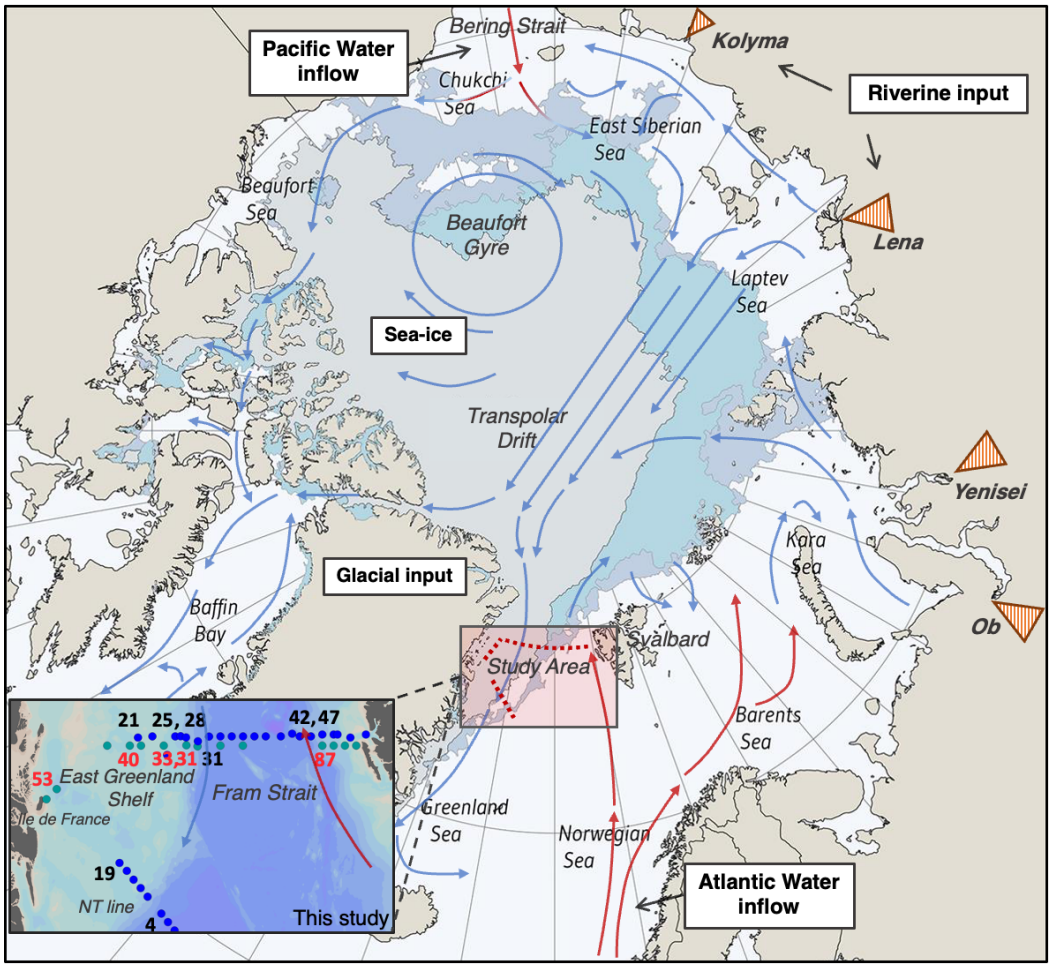

Figure 3.1: Map of the Arctic ocean showing the study area of this research and general surface circulation patterns within the Arctic ocean. Red arrows represent warm, saline currents of the Atlantic and Pacific, and blue arrows represent fresh, cold water modified within the Arctic ocean (adapted from Tremblay et al., 2005). Orange triangles show the river deltas of the Ob, Yenisei, Lena & Kolyma rivers. Shaded areas shows September sea ice extent for 2006 (dark blue), 2017 (light blue) and 2020 (grey-blue). Figure adapted from NSIDC, 2020. Inset: Nitrate isotope sample stations are shown with blue dots (JR17005) and green dots (FS2018). The station numbers for silicon isotope profiles are shown in red for FS2018 & black for JR17005.

Stable isotope measurements of nitrate ($\delta^{15}N\text{-}NO_3$ & $\delta^{18}O\text{-}NO_3$) and dissolved silicon ($\delta^{30}Si(OH)_4$) can provide useful insights into nutrient sources and cycling within the ocean (Brzezinski et al., 2021; Sigman et al., 2000; Varela et al., 2016), particularly when both isotopes are combined (Grasse et al., 2016; De Souza et al., 2012). In this study, we present the first full profiles of $\delta^{30}Si(OH)_4$ measurements in Fram Strait and over the East Greenland shelf in conjunction with nitrate isotopes to examine the controls on DSi export through Fram Strait and suggest potential future scenarios.

In the Arctic ocean, primary production is controlled by complex interactions between light availability and nutrient limitation (Giesbrecht and Varela, 2021; Popova et al., 2012; Yool et al., 2015) which are highly variable both spatially and temporally. Nitrogen is the primary limiting nutrient for primary production in the Eurasian Arctic (Krisch et al., 2020; Tuerena et al., 2021a) and sedimentary denitrification on shallow Arctic shelves play an important role in limiting nitrogen availability (Fripiat et al., 2018; Granger et al., 2018) making the Arctic ocean a net sink of nitrate overall (Yamamoto-Kawai et al., 2006). In contrast, there is an excess of DSi in the Arctic ocean and a disproportionally large amount of DSi is exported to the North Atlantic via Fram Strait and the Canadian Arctic Archipelago. Budget estimates have shown that the Arctic ocean contributes more than 10% of the DSi entering the North Atlantic (Torres-Valdés et al., 2013).

The excess of DSi in the Arctic Ocean's DSi budget is primarily attributed to Pacific water, which enters the Arctic through the Bering Strait, but also freshwater sources, as highlighted in Figure 3.1. The Arctic ocean receives a disproportionally large volume of freshwater relative to its area (>10% of the world's riverine discharge) from several of the world's largest rivers, such as the Ob, Yenisei, Lena and Kolyma rivers which discharge onto the Eurasian shelves. These four rivers alone provide 1755 km^3 of freshwater to Arctic shelves annually, along with 135 x 10^9 g of nitrate and 4816 x 10^9 g of DSi (Holmes et al., 2012), which fuels coastal and Arctic-wide productivity, subsequently transported through the Transpolar Drift (TPD) (Charette et al., 2020; Terhaar et al., 2021). Arctic glacial meltwaters provide a potentially

significant contribution to the Arctic's nutrient budget (Hatton et al., 2019; Meire et al., 2016), with DSi and amorphous Si inputs from the Greenland Ice sheet estimated to constitute around 37% of riverine fluxes in the coastal regions of Arctic Seas (Hawkings et al., 2017). However, the fraction that is exported from Greenland and Svalbard fjords into the open ocean remains poorly documented (Hopwood et al., 2020).

Atlantification is leading to changes in sea-ice cover and stratification of the Eurasian basin (Arthun et al., 2012; Lind et al., 2018) and increasing nutrient availability in the surface ocean (Randelhoff et al., 2018; Tuerena et al., 2021a). Meanwhile, DSi concentrations from Atlantic Waters (AW) are decreasing in the sub-Arctic regions (Hátún et al., 2017) as nutrient demand increases, and the inflow of Pacific water is increasing (Woodgate, 2018). Riverine freshwater inputs have been increasing in the Eurasian sector (Mcclelland et al., 2006) and nutrient fluxes are increasing in rivers with degrading permafrost (Frey et al., 2007; Frey and McClelland, 2009; Zhang et al., 2021). All of these changes have widespread impact on phytoplankton dynamics (Ardyna and Arrigo, 2020). In response, the nutrient budgets of the Arctic ocean are expected to change, with potential repercussions on downstream ecosystems and Atlantic nutrient budgets. In order to predict such impacts, a better understanding of the relative importance of Arctic nutrient sources and internal cycling is needed.

Fram Strait is both an inflow and outflow gateway and a key area of exchange between the Arctic and the North Atlantic. On the Eastern side, warm, saline AW originating from the subpolar and subtropical gyre of the North Atlantic flows northward in the surface intensified West Spitsbergen Current. On the Western side, Polar Surface Water (PSW) carries cold, fresh Arctic-originating water and sea-ice into the Subpolar North Atlantic Ocean in the upper (ca. 250m) part of the water column (Dodd et al., 2012; Rudels et al., 2002; de Steur et al., 2009). PSW is relatively low in nitrate, carrying the signal of Pacific nutrient stroichiometry and benthic denitrification to the Atlantic Ocean through low N:P ratio (Dodd et al., 2012). In contrast to PSW, AW has relatively high nitrate concentrations but is poor in DSi (≅ 5µM) as this key nutrient is depleted in the Atlantic through uptake by

silicifying phytoplankton species during its northward movement. The stoichiometry of DSi availability compared to nitrate (DSi:N <1) in AW in Fram Strait suggests phytoplankton blooms experience DSi limitation prior to nitrate limitation (Krause et al., 2018, 2019; Tuerena et al., 2021a).

Nitrate removal processes within the Arctic ocean are reflected in the nitrate isotopic signatures of 5.5 ± 0.4‰ for $\delta^{15}N\text{-}NO_3$ and 1.3 ± 0.4‰ for $\delta^{18}O\text{-}NO_3$ of PSW (Tuerena et al., 2021a), which are significantly different from incoming AW signatures of 5.1 ± 0.2‰ for $\delta^{15}N\text{-}NO_3$ and 2.4 ± 0.3‰ for $\delta^{18}O\text{-}NO_3$. The difference between these two water masses reflects benthic denitrification on shallow Eurasian shelves, also termed coupled partial nitrification-denitrification (CPND), which increases $\delta^{15}N\text{-}NO_3$ while decreasing $\delta^{18}O\text{-}NO_3$ producing an associated increase in the parameter Δ(15-18), defined as $\delta^{15}N\text{-}NO_3$ - $\delta^{18}O\text{-}NO_3$, through the release of isotopically heavy ammonia from sediments (Fripiat et al., 2018; Granger et al., 2018).

PSW transports high DSi concentrations from Pacific and riverine influence: $\delta^{30}Si(OH)_4$ of Pacific water is ≅ +1.4 ± 0.2‰ (Reynolds et al. 2006) and the isotopically light source of DSi is traced through the Bering strait and into the upper halocline waters of the Arctic Ocean (Giesbrecht et al., 2022). Pacific $\delta^{30}Si(OH)_4$ is lighter than North Atlantic signatures ($\delta^{30}Si(OH)_4$ ≥ +1.7‰) which are enriched to a greater extent from the Southern Ocean source signal as DSi is depleted through partial uptake and subsequent burial of DSi in the North Atlantic (Brzezinski and Jones, 2015; De Souza et al., 2012). Siberian rivers have high seasonal and regional variability in their isotopic signatures, which are isotopically light from weathering processes in Arctic rivers, leading to fractionation of the isotope from the local bedrock (Pokrovsky et al., 2013; Sun et al., 2018). The mean $\delta^{30}Si(OH)_4$ of DSi from major rivers to the Arctic Ocean is estimated at +1.3 ± 0.3‰ (Sun et al., 2018). In addition to these sources, lithogenic benthic supply of DSi to Arctic shelves was recently documented in the Barents Sea which adds light isotopes to shelf waters (Ward et al., 2022a, 2022b), although the magnitude of this flux on a basin-wide scale is currently unknown.

While Arctic sources of DSi are isotopically light, Arctic polar surface waters are isotopically heavy ($\delta^{30}Si(OH)_4 \cong +1.8 \pm 0.1‰$) with isotopically heavy deep basins (Brzezinski et al., 2021; Giesbrecht et al., 2022; Varela et al., 2016). This heavy isotopic enrichment is attributed to physical processes (Liguori et al., 2020) and biological modification within surface waters (Giesbrecht et al., 2022; Varela et al., 2016). A recent study however highlights the importance of biological productivity and biogenic Si burial of riverine DSi in generating these enriched Arctic signatures (Brzezinski et al., 2021). Although isotopic signatures have been measured up to 60˚N in the Atlantic Ocean (De Souza et al., 2012; Sutton et al., 2018b), no direct measurements of $\delta^{30}Si(OH)_4$ are available from Atlantic-Arctic Gateways such as the Fram Strait. Therefore, $\delta^{30}Si(OH)_4$ signatures of modified inflowing AW in the Arctic ocean and outflowing PSW and the contributions from East Greenland shelves are unknown.

This study fills this crucial gap in the Arctic silicon isoscape, documenting isotope signatures and nutrient cycling processes in Fram Strait, focussing on the upper water masses. We use a combination of geochemical parameters ($\delta^{30}Si(OH)_4$, $\delta^{15}N\text{-}NO_3$, $\delta^{18}O\text{-}NO_3$, Δ(15-18), N* & Si*) alongside hydrographic data (salinity, temperature, mixed layer depth) to explore the sources and internal cycling of DSi in the water masses exported through the Fram Strait. We then proceed to put these in the context of pan-Arctic isotope datasets and evaluate the implications of Arctic nutrient cycling on how nutrient export is likely to change in the future with ongoing climate change.

3.2 Method

3.2.1 Sample collection

Samples were collected from two CTD sections across the Fram Strait (JR17005 & FS2018) and from CTD profiles near the Ile-de-France between 2017-2019 (Table 3.1). The CTD package was equipped with a SBE911plus CTD system recording multiple parameters (conductivity, temperature, pressure & salinity). Salinity was calibrated on-board using an Autosal 8400B salinometer (JR17005) and a Guildline Portasal salinometer (FS2017-2019). Samples for dissolved inorganic nutrient

analysis were collected from Niskin bottles and stored in pre-cleaned HDPE bottles which were frozen at -20 °C immediately after collection. Samples for isotopic analysis were filtered inline using Nuclepor polycarbonate membranes (0.4µm pore size) into acid-cleaned polypropylene bottles and stored at -20˚C (nitrate isotopes) or acidified at 0.1% v/v with 12M HCl and stored at 4°C (silicon isotopes).

Table 3.1: Summary of sections along which samples were collected

Year	Cruise	Dates	Vessel	Section
2018	JR17005	9 May - 9 June	RRS James Clark Ross	Fram Strait (79˚N)
2018	FS2018	25 August – 11 September	RV Kronprins Haakon	Fram Strait (78° 50'N) Ile de France
2017	FS2017	24 August -13 September	RV Lance	Ile de France
2019	FS2019	1 September – 16 September	RV Kronprins Haakon	Ile de France

3.2.2 Dissolved inorganic nutrient measurements

Dissolved inorganic nutrient concentrations for JR17005 were determined from frozen samples on autoanalysers following standard colorimetric methods on a Bran and Luebbe QuAAtro 5-channel autoanalyser at the National Oceanographic Centre UK (Brand et al., 2020). Detection limit for nutrient analysis was 0.1µM and 0.03µM for DSi and nitrate respectively with accuracy with respect to CRMS of 2.75% and 0.91% (Brand et al., 2020). For FS2018, nutrients were analysed following methods from Hansen and Koroleff, (1999) & Schnetger and Lehners, (2014) on a SmartChem 200 discrete analyser at the Technical University of Denmark (FS2017-19) and calibrated using OSIL nutrient standards. Analytical precision is of 2% and the detection limit was of 0.4µM for nitrate and 0.1µM for DSi. While measurement from frozen is suboptimal for silicic acid concentrations, separate non-frozen samples could not be collected for nutrients due to sampling and shipping restrictions. DSi concentrations were independently checked at the University of Edinburgh from the silicon isotope samples (acid preserved) during analysis with the HACH reagent method. Both datasets from frozen and acidified were in very good agreement and frozen samples were not found to have lower DSi concentrations. DSi concentrations from FS2018 also closely align with concentrations measured in the

same water masses in JR17005 below the seasonal layer in the upper 500m of the water column, and align with published concentrations in the literature.

3.2.3 Nitrate isotope analysis

$\delta^{15}N\text{-}NO_3$ & $\delta^{18}O\text{-}NO_3$ were measured using the bacterial strain of *P. aureofaciens* following the Denitrifier Method (Casciotti et al., 2002; Sigman et al., 2001). Measurements were corrected using international reference standards IAEA-N3 and USGS-34 in each run, as well as an internal standard of North Atlantic Deep Water ($\delta^{15}N\text{-}NO_3$ = 4.92 ± 0.12 ‰, $\delta^{18}O\text{-}NO_3$ = 1.88 ± 0.45‰) for inter-run comparability, with standard reproducibility across runs of ±0.1‰ and ±0.4‰ for $\delta^{15}N\text{-}NO_3$ & $\delta^{18}O\text{-}NO_3$ respectively. Final values were corrected using the correction scheme described in Weigand et al. (2016) and following Tuerena et al. (2021a, 2021b) for inter-comparability of datasets in the Atlantic-Arctic region.

3.2.3.1 $\delta^{15}N$-PN

Seawater samples were collected from the underway system or niskin bottles into acid-cleaned carboys and filtered through combusted GF/F filters (0.7µm pore size) within 2h of collection on a filtration system. The filters were stored at -80°C until analysis. Prior to analysis the filters were freeze-dried, wrapped in tin foil cones (OEA Laboratories) and pelletised. $\delta^{15}N$-PN was determined by EA-IRMS using *a* Costech Instruments Elemental Analyser coupled to Thermo Scientific Delta V Advantage mass spectrometer fitted with Conflo IV gas handling system by Louisa Norman (NOC). The instrumentation was operated using ISODAT 3.0 isotope ratio MS software. L-glutamic acid standards USGS 40 and USGS 41a (US Geological Survey, Reston Stable Isotope Laboratory) were run alongside the samples and were used both for data processing and to assess the performance of the instrumentation.

3.2.4 Silicon isotope analysis

DSi concentrations are very low in the Arctic ocean (<10µM), as such, previous protocols from Brzezinski et al. (2003) and Reynolds et al. (2006), originally based on the Magnesium Induced Coprecipitation (MAGIC) method described in Karl and

Tien (1992), were adapted to allow measurements at concentrations below 10µM, following the procedure described in Section 2.3.2.

The isotopic composition of the prepared solution was determined by MC-ICP-MS on a Nu Plasma II instrument at the University of Edinburgh using standard-sample bracketing and calculated from the permil deviation from isotopic reference material NBS28 (Georg et al., 2006b), calculated as:

$$\delta\,{}^{x}\mathrm{Si} = \left(\frac{\left(\frac{{}^{x}\mathrm{Si}}{{}^{28}\mathrm{Si}}\right)_{\mathrm{sample}}}{\left(\frac{{}^{x}\mathrm{Si}}{{}^{28}\mathrm{Si}}\right)_{\mathrm{NBS28}}} - 1 \right) \times 1000[‰] \qquad \textit{Eq. 3.1}$$

Where δ^{x}Si is either δ^{29}Si or δ^{30}Si. As per Fripiat et al. (2011a, 2011b) and Liguori et al. (2021), δ^{29}Si were converted to δ^{30}Si to improve reliability and global comparability of datasets (Cardinal et al., 2003, 2005), using the theoretical conversion factor of 1.96, calculated from the kinetic fractionation law (Young et al., 2002). (Figure S1, see supporting information S1).

Inter-run comparability & method reproducibility of measurements was checked with the international solid standard Big Batch & both high and low concentration seawater standards Aloha$_{1000}$ & Aloha$_{300}$. Average standard measurements for the period of this study is Aloha$_{1000}$= +0.67 ± 0.03‰, +1.32 ± 0.06‰ (n=16), BigBatch = -5.33 ± 0.02‰, -10.50 ± 0.04‰ (n=7) for δ^{29}Si(OH)$_4$ and δ^{30}Si(OH)$_4$ respectively (uncertainties of 1SD). Long-term reproducibility of converted δ^{30}Si(OH)$_4$ is BigBatch = -10.49 ± 0.09‰ (n=58), Aloha$_{1000}$= +1.29 ± 0.08‰ (n=58) and Aloha$_{300}$= +1.70 ± 0.05‰ (n=30) compared to inter-laboratory measurements of BigBatch = -10.48 ± 0.2‰, Aloha$_{1000}$= +1.25 ± 0.2‰, Aloha$_{300}$= +1.66± 0.35‰ (Grasse et al., 2017; Reynolds et al., 2007). The reproducibility of the full chemical and analytical procedure, including chemical preparation and analytical measurements in separate MC-ICP-MS sessions, was additionally estimated on a subset of duplicate seawater samples (*n* = 8). The mean absolute difference between duplicate samples analysed was ± 0.04‰ (1 SD).

3.2.4.1 δ^{30}Si-PSi

Seawater samples were collected from the underway system or niskin bottles into acid-cleaned polyethylene bottles and immediately filtered through nuclepore filters (0.8μm pore size) on a filtration system. The filters were stored at -20°C until analysis. Cleaning and dissolution of particulate silica was adapted from Morley et al. (2004). Filters were rinsed with MQ and collected particles were dried in digestion vials. 0.5ml of 10% HCl was added to dissolve carbonates overnight and evaporated at 100˚C. 0.2ml of concentrated H_2O_2 was added to dissolve organic compounds overnight and fully evaporated at 120˚C. 1ml of 0.1M NaOH was added to dissolve the particulate silica overnight. Solution was neutralized with HCl and eluted to 5ppm Si. The solution was subsequently processed through resin columns and analysed for δ^{30}Si on MC-ICP-MS as per the method of analysis of $\delta^{30}Si(OH)_4$ described in section 3.2.4 for $\delta^{30}Si(OH)_4$.

3.2.5 Derived parameters

Mixed-Layer Depth (MLD) is identified as the maximum depth at which the potential density was within 0.1kgm^{-3} of the shallowest measurement (Peralta-Ferriz and Woodgate, 2015). MLD governs the depth for which nutrients resupply surface waters and to which planktons are mixed (Yool et al., 2015). In this study, PSW is defined as potential temperature (θ) <0 °C and potential density (σ_θ) <27.7 kgm^{-3}, and AW is defined as θ>2°C and 27.7<σ_θ<27.97 kgm^{-3} or σ_θ <27.7 kgm^{-3} and salinity >34.92 psu, as per Richter, Von Appen and Wekerle (2018).

The semi-conservative tracers N* & Si* were calculated from inorganic nutrient concentrations where N* = NO_x – PO_4^- x 16, adapted from Gruber & Sarmiento (1997), and Si* = DSi – NO_x (Sarmiento et al., 2004). Both tracers are indicative of nutrient deviation from typical Redfield ratio, and highlight additional sources or processes through which nutrient become deficit (i.e Negative N* shows nitrate deficit in comparison to phosphate). The isotopic parameter Δ(15-18) is calculated as Δ(15-18) = $\delta^{15}N\text{-}NO_3$ - $\delta^{18}O\text{-}NO_3$. Δ(15-18) captures variation in both isotopes, tracing sources and modification of nitrate (Rafter et al., 2013).

3.3 Results

3.3.1 Hydrography & mixed layer depth

Figure 3.2 shows temperature and salinity across Fram Strait in July-August 2018. The hydrographic situation is typical of the late summer season. Warm inflowing and recirculating sub-tropical originating AW is found primarily between 2.5W and the Eastern end of the section at 10°E, in the upper 500 m. Its core flows northward within the West Spitsbergen Current at 6-8˚E. Over the East Greenland Shelf, PSW dominates the upper 150m, extending from the western end of the section to the AW/PSW interface at about 3 ˚W. Re-circulating Atlantic Waters (RAW), underlays PSW on the East Greenland shelf, while Arctic Atlantic Water (AAW) is also found below AW at the foot of the East Greenland Shelf. We refer the reader to Rudels et al. (2002) for an overview of the properties of water masses found in Fram Strait.

The MLD did not exceed 100m for FS2018. Late-season MLD was deeper in AW than in PSW, occurring between 30-60m. MLD is significantly shallower over the East Greenland shelf, occuring at 5-10m. Hydrography and nutrient distribution of JR17005 follow roughly similar patterns as FS2018 apart from seasonal variations, and are previously described in Tuerena et al. (2021).

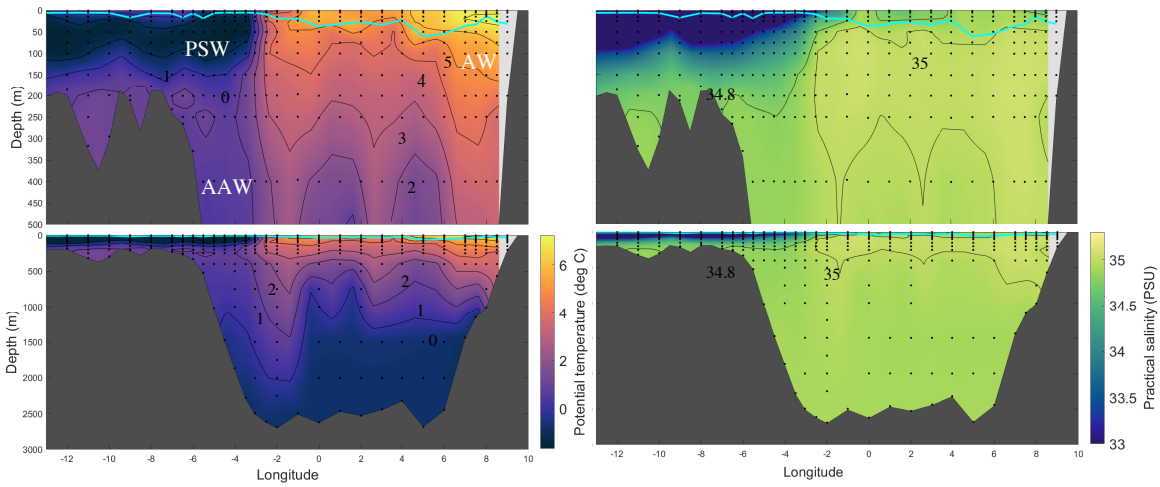

Figure 3.2: Hydrography of Fram Strait cruise FS2018 from August-September 2018 presented for full depth (bottom panel) and upper water column (top panel) for temperature (left) and salinity (right). The mixed-layer depth is shown by a cyan line (calculation of MLD is described in method section below). Isotherms (left) & isohalines (right) are also displayed. Atlantic Water (AW), Polar Surface Water (PSW) & Arctic Atlantic Water (AAW) are marked.

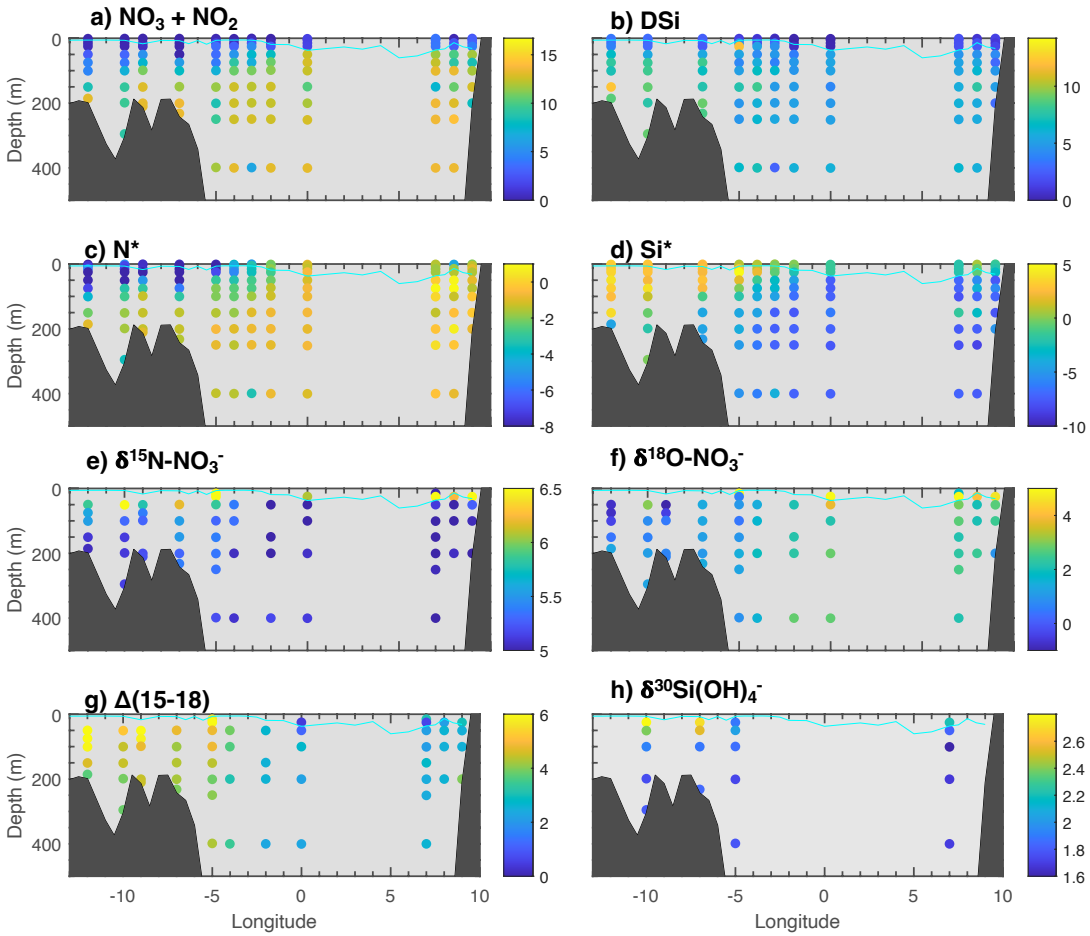

Figure 1.3: Nutrients and isotopes across Fram Strait section of late summer 2018 a) NOx (where NOx= nitrate + nitrite), b) DSi, c) N* (where N*= NOx – 16*PO_4^-), d) Si* (where Si* = $Si(OH)_4$ - NOx), e) $\delta^{15}N$-NO_3, f) $\delta^{18}O$-NO3, g) Δ(15-18) (where Δ(15-18) = $\delta_{15}N$-NO_3 - $\delta^{18}O$-NO_3), h) $\delta^{30}Si(OH)_4$. Cyan line displays MLD for the section (calculation described in method section).

3.3.2 Nutrient concentrations

Panels a and b of Figure 3.3 show the nitrate and DSi concentrations in the upper 400m of the water column along the late-summer 2018 Fram Strait section. P-values reported are for t-tests between AW and PSW water masses. Nitrate concentrations were low across the section in the upper 50m of the water column from phytoplankton utilisation and dilution by low-nitrate freshwater sources. Below the mixed-layer depth, NO_x is higher in AW (12.10 ± 0.98 μM) than in PSW (8.08 ± 2.19 μM, p <0.01), consistent with export of low nitrate waters from the Central Arctic.

Negative N* reflecting a deficit of nitrate are evident on the East Greenland Shelf in panel c of Figure 3.3. In constrast, N* reaches near positive values in AW with an average of -0.55 ± 0.38 below the MLD (Table 3.2). This highlights that nitrate is more depleted in PSW relative to dissolved phosphate, becoming potentially limiting to primary production towards the end of the biological growth season as nitrate concentrations approach 0μM.

DSi concentrations were low across the section above the MLD with stronger depletion at shallower depths and further West (Figure 3.3b). Comparison of DSi concentrations measured during May-June 2018 and August-September 2018 (Table 3.2) reveals that DSi concentrations were similarly higher in PSW (4.28 ± 2.93 μM) and in AW (3.19 ± 1.20 μM) in the mixed layer at the start of the season, and fell to similarly depleted concentrations by the end of the summer (1.03 ± 0.98 μM and 1.26 ± 1.11 μM for AW and PSW respectively).

Below the mixed layer, DSi is low in AW (5.42 ± 0.71 μM) from DSi poor Atlantic waters of sub-tropical origins. DSi in PSW is higher than in AW (6.64 ± 1.71 μM, p <0.01), potentially reflecting Arctic sources of DSi to PSW. In the deep Fram Strait, DSi concentrations vary locally, but generally increase with depth up to a concentration of 9.45 ± 2.48 μM in deep waters (Figure 3.4). On Figure 3.3d, strongly negative Si* in AW reflect the strong DSi deficit relative to nitrate in Atlantic-originating waters, while Si* closer to phytoplankton requirement in PSW illustrate excess DSi in PSW.

3.3.3 Isotopic measurements

Measured profiles of $\delta^{30}Si(OH)_4$ across Fram Strait are shown in panel h of Figure 3.3 (late summer data, spring data is displayed on Figure 3.12 in Appendix section 3.7.1) and Figure 3.4. Positive signatures of $\delta^{30}Si(OH)_4$ were measured throughout the water column, ranging from +1.34‰ to +3.16‰ for the entire section (Figure 3.3, panel h). The heaviest $\delta^{30}Si(OH)_4$ signatures were measured in the upper 100m of the section (Figure 3.4), consistent with fractionation from diatom uptake during growth. Below the MLD, mean $\delta^{30}Si(OH)_4$ for AW was +1.74 ± 0.06‰ (Table 3.2), which aligns closely with measurements of waters from North Atlantic origin

(Brzezinski and Jones, 2015; De Souza et al., 2012). Conversely, DSi in PSW was isotopically heavier than DSi in AW ($p < 0.02$), the mean $\delta^{30}Si(OH)_4$ value for PSW was +1.85 ± 0.09‰. This is comparable to measurements of the upper halocline layer in the Canadian basin ($\delta^{30}Si(OH)_4$= +1.84‰) from Varela et al. (2016), and outflowing surface measurements from Brzezinski et al. (2021) in the TPD where $\delta^{30}Si(OH)_4$= +1.92‰, and aligns with the heavy signatures of Arctic-originating waters in the North Atlantic (De Souza et al., 2012; Sutton et al., 2018b).

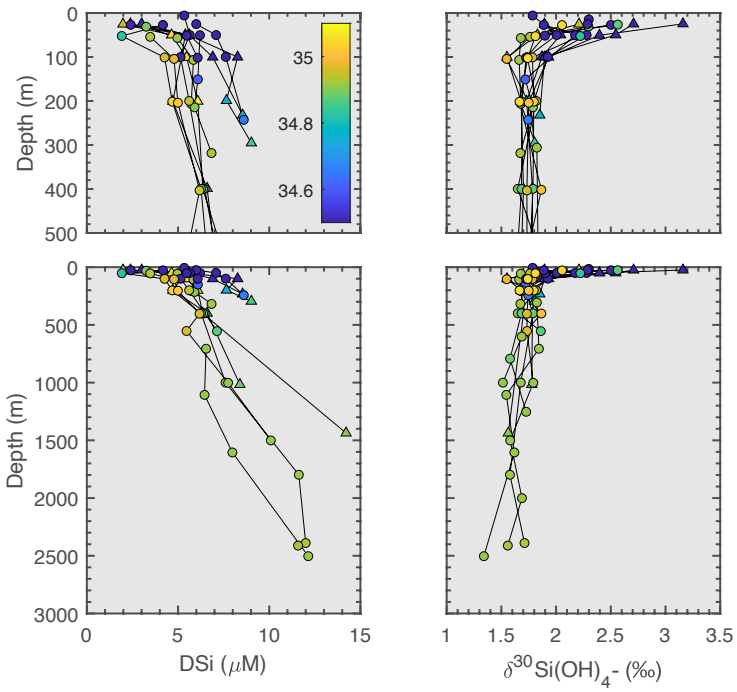

Figure 3.4: DSi concentrations (left) and dissolved silicon isotope profiles (right) for spring (JR17005, circles) and late summer (FS2018, triangles) of the 2018 growth season in Fram Strait. Colour scale represents salinity (psu).

In the deep waters of Fram Strait, $\delta^{30}Si(OH)_4$ are lighter than PSW (Figure 3.4), aligning with the gradient decrease of -0.15‰ over the full depth profile reported in Brzezinski et al. (2021). The measured signatures also align with measurements in the North Atlantic of Nordic originating endmembers (DW-$\delta^{30}Si(OH)_4$.= +1.65 ± 0.13‰ & DSOW-$\delta^{30}Si(OH)_4$.= +1.75 ± 0.08‰, De Souza et al., 2012). Light $\delta^{30}Si(OH)_4$ values were measured at the sediment interface of deep basins (Figure 3.4), showing potential interaction of benthic efflux of DSi from isotopically light pore-waters (Ehlert et al., 2016; Ward et al., 2022a, 2022b), and remineralisation of

isotopically lighter biogenic Si in the deep. This is also observed in Brzezinski et al. (2021) and Liguori et al. (2020) who found isotopically light measurements in the deep Nansen & Amundsen basins. Low sampling resolution within our dataset and the strong influence of local circulation precludes quantification of such local recycling processes from advective signals in Fram Strait with certainty.

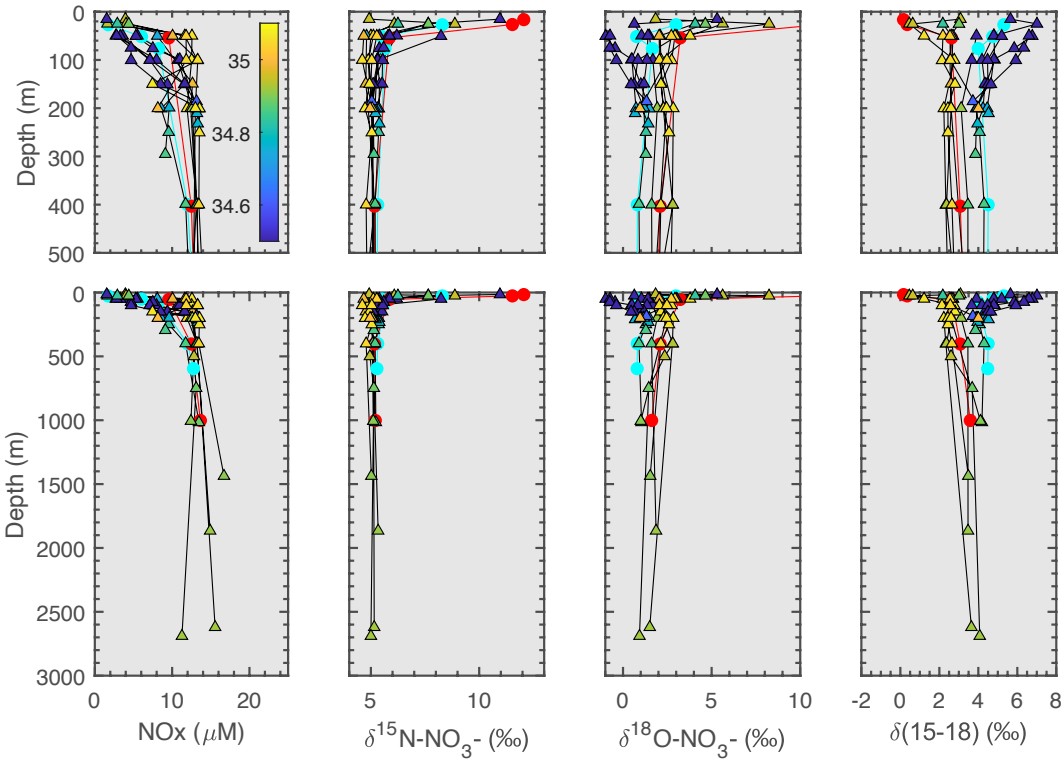

Figure 3.5. Nitrate concentrations (left), δ^{15}N-NO_3 (middle-left), δ^{18}O-NO_3 (middle-right) and Δ(15-18) profiles (right) for FS2018 (triangles) in Fram Strait. Typical profiles for PSW (cyan) and AW (red) from JR17005 are shown in circles for comparison between studies (Tuerena et al., 2021). Colourscale represents salinity (psu).

Figure 3.5 displays the full water column profiles of nitrate isotopes measured along the spring (JR17005) and late-summer (FS2018) sections. δ^{15}N-NO_3 is enriched in PSW (5.44‰) compared to AW (5.18‰, p <0.01) while the δ^{18}O-NO_3 is lighter in PSW (1.22‰) than in AW (2.33‰, $p < 0.01$, Table 3.2) following trends identified in Tuerena et al. (2021a). Panel g of figure 3.3 illustrates the decoupling of both isotopes reflected in diverging Δ(15-18), indicative of CPND. A high confidence in accuracy and reproducibility of nitrate isotopes measurements in this study is

obtained as the dataset aligns and follow the same trends as profiles reported in Tuerena et al. (2021a).

In surface waters, $\delta^{15}N\text{-}NO_3$ increase with reducing nitrate concentrations, which is consistent with biological uptake (Figure 3.5). This is also observed in most $\delta^{18}O\text{-}NO_3$ profiles apart from PSW profiles measured far onto the East Greenland shelf in FS2018 (Figure 3.3), where signals of denitrification dominates over biological uptake signals, even in the upper water column. As shown in Figure 3.3, and summarised in Table 3.2, isotopic signatures of both dissolved silicon and nitrate isotopes closely follow the hydrography of water masses in spring and summer. In Fram Strait, a key area of exchange with the North Atlantic where inflowing & outflowing water masses show strong differences in their physical properties, dissolved nitrate & silicon isotopes measurements provide insights into nutrient sources and cycling within the Arctic ocean and the pathways through which nutrient modification and exchange occurs.

Table 3.2: Averaged water mass signatures of the Fram Strait (a) excluding the mixed layer depth and (b) within the mixed layer in spring (JR17005) and summer (FS2018). Water mass definitions based on (Richter et al., 2018)**. AW = Atlantic Water, PSW = Polar Surface Water, wPSW = warm PSW, AAW = Arctic Atlantic Water, DW = Deep Water, DSOW = Denmark Strait Overflow Water. N* is defined as N*= NOx – 16*PO_4^-) and Si* is defined as Si* = $Si(OH)_4$ - NO_x).**

	Nitrate (µM)	N*	Si*	δ^{15}N-NO3 (‰)	δ^{18}O-NO3 (‰)	Δ(15-18) (‰)	DSi (µM)	$\delta^{30}Si(OH)_4$ (‰)
AW	12.10 ± 0.98	-0.55 ± 0.38	-6.73 ± 0.95	5.18 ± 0.21	2.33 ± 0.51	2.85 ± 0.46	5.42 ± 0.71	+1.74 ± 0.06
PSW	8.08 ± 2.19	-2.36 ± 0.70	-1.37 ± 2.43	5.44 ± 0.15	1.22 ± 0.92	4.22 ± 0.89	6.64 ± 1.71	+1.85 ± 0.09
wPSW	11.52 ± 1.59	-0.50 ± 1.14	-5.00 ± 2.61	5.09 ± 0.34	2.12 ± 0.78	2.97 ± 0.84	6.53 ± 1.52	
AAW	11.94 ± 1.40	-1.19 ± 0.59	-5.26 ± 1.37	5.31 ± 0.33	1.93 ± 0.77	3.38 ± 0.61	6.63 ± 1.31	+1.74 ± 0.06
DW	14.02 ± 1.11	-0.98 ± 0.47	-4.58 ± 1.66	5.28 ± 0.17	1.60 ± 0.33	3.68 ± 0.30	9.45 ± 2.48	+1.65 ± 0.13
DSOW	12.33 ± 1.18	-0.90 ± 0.55	-6.20 ± 1.08	5.24 ± 0.20	1.91 ± 0.69	3.33 ± 0.65	6.15 ± 1.00	+1.75 ± 0.08
	Nitrate (µM)	**N***	Si*	**δ^{15}N-NO3** (‰)	**δ^{18}O-NO3** (‰)	**Δ(15-18)** (‰)	**DSi (µM)**	**$\delta^{30}Si(OH)_4$** (‰)
AW spring	3.83 ± 4.49	-2.06 ± 0.76	-0.73 ± 3.57	8.48 ± 2.34	6.70 ± 3.29	1.78 ± 1.19	3.19 ± 1.20	+2.04 ± 0.37
AW summer	2.71 ± 1.24	-1.27 ± 0.41	-1.76 ± 0.31	6.63 ± 2.02	5.23 ± 3.22	1.39 ± 1.48	1.03 ± 0.98	
PSW spring	1.50 ± 1.18	-5.52 ± 2.70	2.73 ± 2.73	8.80 ± 1.06	4.63 ± 1.49	4.17 ± 1.62	4.28 ± 2.93	+2.12 ± 0.29
PSW summer	0.19 ± 0.12	-6.03 ± 2.21	1.06 ± 1.14				1.26 ± 1.11	

3.4 Discussion

3.4.1 Using nutrient isotopes to examine Arctic nutrient cycling

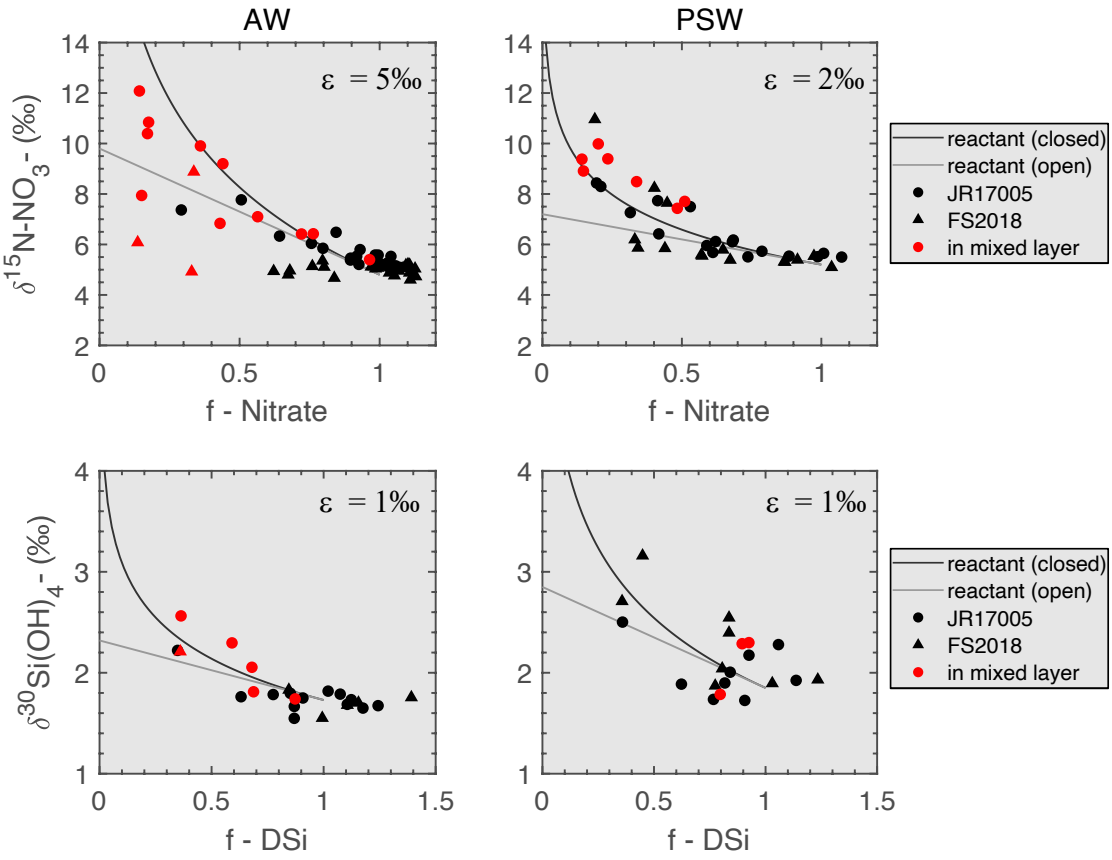

Figure 3.6: Nitrate utilisation vs δ^{15}N-NO$_3$ for AW (left, depth <600m) and PSW (right, depth < 150m). Bottom panels: DSi utilisation vs δ^{30}Si(OH)$_4$ for AW (left, depth <600m) and PSW (right, depth < 150m).” (3) Also added to figure caption: “f is the fraction of nutrient remaining, calculated from the nutrient concentrations of water masses AW and PSW below the MLD (Table 2).

3.4.1.1 Trends between δ^{15}N-NO$_3$, δ^{30}Si(OH)$_4$ and nutrient utilisation

In this section we compare δ^{15}N-NO$_3$ and δ^{30}Si(OH)$_4$ measurements with the fraction of nitrate and DSi remaining (f) in PSW and AW in Fram Strait (Figure 3.6, panels a and b). We define f as the fraction of nutrient remaining in the surface layer relative to concentrations below the MLD (Table 3.2). f=1 indicates no nitrate or DSi has been used, f=0 indicates complete depletion of the nutrient inventory.

The fractionation of nitrate and DSi during phytoplankton uptake can be modelled by Rayleigh systematics described in Section 1.4 (Altabet and Francois, 2001; Mariotti et al., 1981), and is often linked to local hydrography. Rayleigh systematics assume a closed system: i.e there is no import/export of the nutrient from the euphotic zone while it is being utilised by phytoplankton. In late spring and summer, the PSW layer in Fram Strait is largely a closed system as it is highly stratified. Nitrate and DSi are mainly replenished during winter destratification (Altabet and Francois, 2001). In this environment, $\delta^{15}N\text{-}NO_3$ and $\delta^{30}Si(OH)_4$ can be expected to fall on a trend based on their isotopic effect (~2-6‰ for nitrate and ~1‰ for DSi globally), and are described by exponential trendlines in the Rayleigh field on Figure 3.6 (Varela et al., 2004). In areas of upwelling, or in a case where the resupply of nutrients to the euphotic zone occurs due to multiple stratification and destratification events throughout growth season, conditions are better modelled as open system, described by a linear trendline in the Rayleigh field. However, in low-nutrient zones such as the PSW layer in Fram Strait, nutrient uptake stoichiometry can be dictated by nutrient-limitation itself rather than by the physical re-supply of nutrients (Hutchins and Bruland, 1998; Moore et al., 2013), which in turn can lead to a shift from open to closed system dynamics as the source of nutrients switches from new to remineralised.

During the growth season of 2018, nitrate in AW and PSW is enriched in $\delta^{15}N\text{-}NO_3$ at lower nitrate concentrations, consistent with fractionation associated with nutrient uptake by phytoplankton (Figure 3.6). AW follows the traditional isotopic effect of 5‰ and PSW follows the particularly low isotopic effect of 2‰ observed in Tuerena et al. (2021a). Nitrate fractionation in AW behaves between closed and open system kinetics, with a shift from more closed conditions in spring towards more open conditions in summer. This corroborates with the relatively weak stratification of AW (Rudels et al., 2005), facilitating re-supply of nitrate and other nutrients over the spring and summer growth season through destratification events such as those described by Tuerena et al. (2021a). In PSW, $\delta^{15}N\text{-}NO_3$ fractionation follows an exponential trend and behaves as a closed system in spring, indicative of the strong salinity stratification of PSW. A shift towards a mostly linear trend in summer is

observed, suggesting open system kinetics in the mixed layer. While a shift from open to closed system could be expected due to strengthening of stratification over the summer season, we observe a shift from closed to open systems instead. This is unlikely to reflect a change in hydrographic conditions. Instead, it indicates a shift towards the consumption of regenerated N with lighter $\delta^{15}N$ in nitrate depleted waters, thereby lowering ambient $\delta^{15}N\text{-}NO_3$ from expected trends. This is further supported by the equivalent trends observed in $\delta^{15}N$-PN (Figure 3.13, see Appendix section 3.7.2).

The relationship between apparent DSi and $\delta^{30}Si(OH)_4$ in AW is weaker than for N, but follows closed system kinetics during the growth season (Figure 3.6) after DSi was drawn down to 1μM in AW in summer 2018 (Figure 3.4). DSi is strongly depleted in surface AW in summer, preventing direct $\delta^{30}Si(OH)_4$ measurements within the MLD and observation of shifts within the isotopic system. Our observations remain consistent with other studies which find that DSi is one of the limiting nutrients to diatom growth in AW in the Eastern Fram Strait along with Fe (Krisch et al., 2020). In contrast to nitrate, biogenic silica is recycled less within the upper water column, preventing a switch to recycled nutrient sources later in the seasons. As DSi becomes fully utilised and ambiant conditions become unfavourable to diatom growth, a shift towards non-siliceous species is expected in late summer along with a shift towards open system kinetics.

$\delta^{30}Si(OH)_4$ in PSW does not show a good fit with either of the fractionation models and measurements from within the MLD aren't consistent with fractionation associated with nutrient uptake by phytoplankton at lower nutrient concentrations. Trends of $\delta^{30}Si$-PSi are also inconsistent with any model (Figure 3.13, see appendix Section 3.7.2). This suggests that unlike nitrate, DSi in PSW is not primarily controlled by biological processes as it does not fit a fractionation model, and its variations are more likely to be driven by physical mixing and dilutive effects instead. The decoupling of N & DSi isotopic systems is indicative that N is strongly limiting in the highly stratified PSW and prevents extensive DSi utilisation locally.

Nutrient uptake in surface AW is constrained by low DSi concentrations in limiting conditions for diatom growth, while uptake in PSW is constrained by strong nitrate limitation and DSi is only partially utilised. This indicates that the extent to which DSi is taken up is regulated by nitrate availability in PSW at Fram Strait. $\delta^{15}N\text{-}NO_3$ and $\delta^{30}Si(OH)_4$ show a link between the silicon and nitrogen cycles in Fram Strait as they regulate uptake through availability, contributing to the asymmetry observed in nutrient exports across the strait (Torres-Valdés et al., 2013).

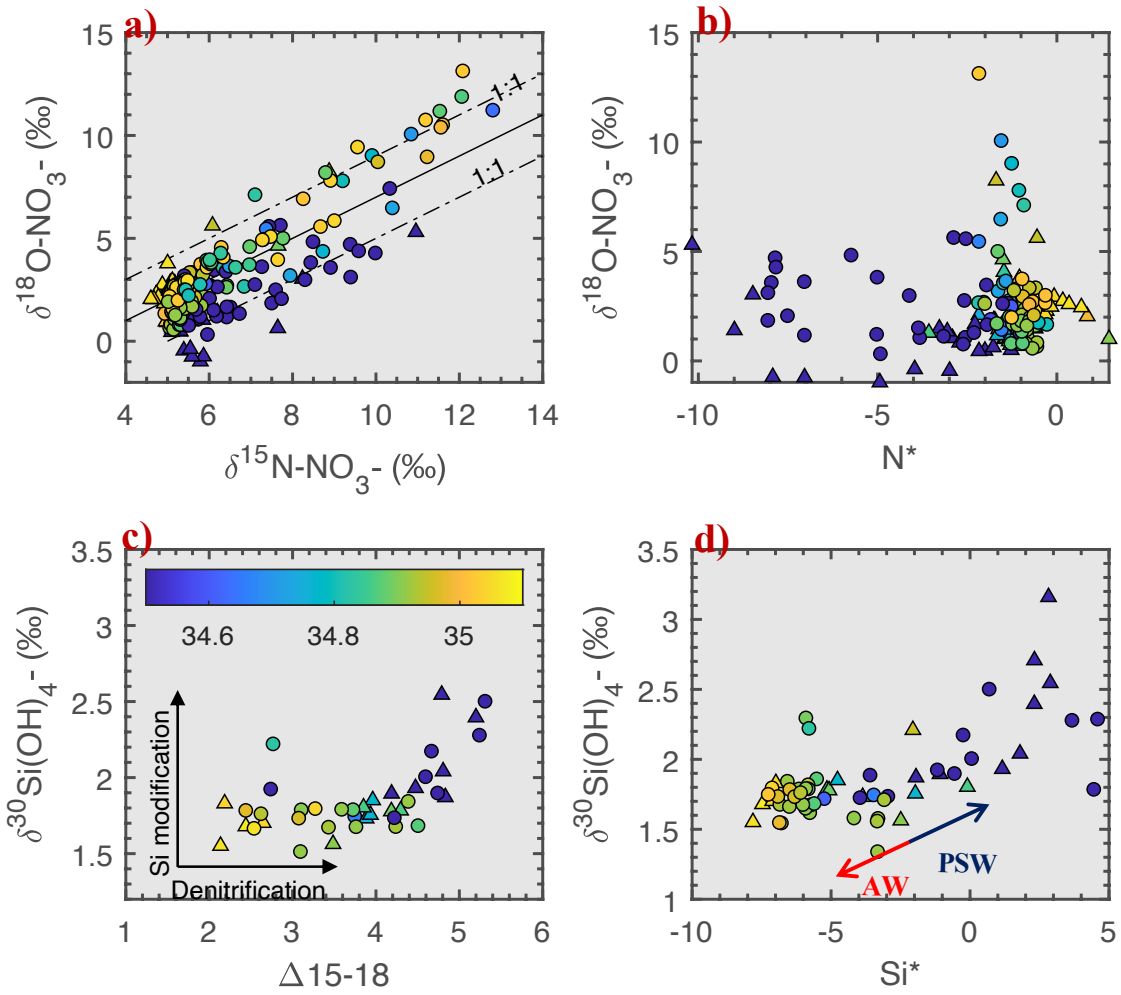

Figure 3.7: Fram Strait measurements of a) δ15N-NO3 vs δ18O-NO3 (solid and dotted lines show 1:1 fractionation lines). b) δ18O-NO3 vs N*. c) Δ(15-18) vs δ30Si(OH)4 excluding samples from within the mid-layer depth to remove seasonal variation. d) Si* vs δ30Si(OH)4. In all figures, circles represent spring (JR17005) and triangles show late summer (FS2018). Colorscale for all plots show salinity (psu).

3.4.1.2 Upstream transformation of nitrate and DSi in PSW and AW in Fram Strait

The nutrient composition of PSW exported through Fram Strait reflect the nutrient cycling history through altered DSi:N ratio and isotopic signatures in the Arctic Ocean. Figure 3.7a shows trends for $\delta^{15}N\text{-}NO_3$ vs $\delta^{18}O\text{-}NO_3$, displaying that fractionation due to uptake by phytoplankton assimilation follows the established fractionation ratio of 1:1 (Granger et al., 2004; Sigman et al., 2005) but on separate fractionation lines. $\delta^{15}N\text{-}NO_3$ and $\delta^{18}O\text{-}NO_3$ of PSW plots on a trend consistent with isotopically lighter sources of $\delta^{18}O\text{-}NO_3$, while $\delta^{15}N\text{-}NO_3$ and $\delta^{18}O\text{-}NO_3$ measured in surface AW follow a line consistent with isotopically heavier sources, suggesting different nutrient sources in AW and PSW.

The modification of nitrate in the Arctic ocean is readily apparent when plotting N* against $\delta^{18}O\text{-}NO_3$ (Figure 3.7b); as salinity decreases and the influence of Polar-originating waters increases, N* decreases, indicating a nitrogen deficit in relation to phosphate in PSW. Water samples with lower N* are accompanied by lighter $\delta^{18}O\text{-}NO_3$ signatures. This relationship is attributed to CPND in the Arctic ocean (Granger et al., 2011): settling PON from coastal productivity degrades at the sediment interface of the extensive shallow shelves and produces large sources of sedimentary ammonium. In anoxic shelves where sedimentary denitrification preferentially consumes isotopically light NO_3, the NH_4^+ thus released into the water column is isotopically heavy in $\delta^{15}N$. Subsequently, during partial nitrification, this benthic efflux of isotopically heavy NH_4^+ is combined with light oxygen isotopes nearing local $\delta^{18}O\text{-}H_2O$ into the nitrate pool. This decouples the two isotopes by decreasing the $\delta^{18}O\text{-}NO_3$ of nitrate overall whilst increasing $\delta^{15}N\text{-}NO_3$.

CPND is a widespread process in Arctic shelves and has been observed in the Chukchi Sea (Brown et al., 2015; Granger et al., 2018) and the East Siberian Sea (Fripiat et al., 2018) and contributes to the observed Arctic-wide nitrogen deficit in relation to phosphate (Torres-Valdés et al., 2013; Yamamoto-Kawai et al., 2006). This shelf-derived signal is exported into the Arctic halocline (Granger et al., 2018) through the TPD, and can be traced in the outflowing water-masses in Fram Strait (Tuerena et al., 2021a), reflecting the impact of shelf processes on PSW nutrient

ratios. Thus, the low N*, light $\delta^{18}O\text{-}H_2O$ and heavy Δ(15-18) signal exported in the PSW is the signature of N loss on Eurasian shelves and the Chukchi Sea.

DSi concentrations in outflowing PSW are 1.2μM higher and $\delta^{30}Si(OH)_4$ is isotopically heavier by +0.11‰ relative to inflowing AW (Table 3.2). Documented Pacific and meteoric sources of DSi are isotopically light (Hawkings et al., 2017; Pokrovsky et al., 2013; Reynolds et al., 2006; Sun et al., 2018) but DSi behaves non-conservatively across the Arctic ocean. DSi uptake by phytoplankton in the Arctic ocean and loss due to biogenic Si burial fractionate the upper water column $\delta^{30}Si(OH)_4$ towards heavier signatures (Brzezinski et al., 2021; Liguori et al., 2020; Varela et al., 2016).

Varela et al. (2016) suggest the heavy signal observed in the deep Arctic is sourced from intermediate Atlantic-originating waters but we observe no significant enrichment of $\delta^{30}Si(OH)_4$ in the intermediate water masses of Fram Strait (Figure 3.3, Figure 3.4). Given that the inflowing AWs are already too poor in DSi to contribute to isotopic enrichment, the observed increase in DSi concentrations may point to riverine DSi sources subject to enrichment due to biogenic si production and burial instead (Brzezinski et al., 2021) .

As seawater is undersaturated with respect to biogenic Si at all depths in the ocean (Archer et al., 1993), biogenic Si dissolution occurs in the water column and at the sediment-water interface. Upon burial, biogenic Si will continue to dissolve until pore-waters are saturated (Kamatani, 1982; Nelson et al., 1995). Arctic shelves are characterized by a shallow water column with relatively high sedimentation rates influenced by river and biogenic fluxes, conditions favourable to reduced biogenic Si exposure to dissolution, and rapid burial. Therefore, it is expected that Arctic shelf seas are particularly efficient at removing biogenic Si through opal burial.

Recent work from the Barents Sea shelf found low opal burial rates and rapid recycling within the seafloor (Ward et al., 2022a, 2022b), but the low rate of opal burial in the Barents Sea may not be observed on shallower Eurasian shelves with stronger riverine influence (Kara Sea, Laptev Sea & East Siberian Sea) as geochemical cycling strongly varies from one Eurasian shelf to another (Macdonald

et al., 2010). In areas of low nitrate concentrations such as the Eurasian sector of the Arctic Ocean, DSi is only partially utilised in the surface as productivity is limited by N deficit, leading to fractionation of the DSi pool. The isotopically lighter biogenic Si is preferentially buried enriching water column $\delta^{30}Si(OH)_4$ overall. This contrasts with deep Arctic basins with low productivity and long water residence times which provide opportunity for dissolution in the deep water column and at the water-sediment interface, leading to a relatively small modification in the water-column $\delta^{30}Si(OH)_4$ (Brzezinski et al., 2021; Liguori et al., 2020). The heavy $\delta^{30}Si(OH)_4$ signatures of PSW thus records the partial utilisation and the loss of lighter Si through burial in the Arctic shelves.

Figure 3.7c shows the relationship between Δ(15-18) and $\delta^{30}Si(OH)_4$ in samples below the MLD which should not be affected by seasonal biological fractionation. A gradient is observed between AW and PSW, with a gradual increase in Δ(15-18) from 2‰ to 4‰ as salinity decreases, and an increase in $\delta^{30}Si(OH)_4$ from +1.7‰ to +2‰, linking the processes of denitrification (Fripiat et al., 2018; Granger et al., 2011, 2018) and removal of isotopically light DSi sources through biogenic Si burial in the shelves (Brzezinski et al., 2021; Liguori et al., 2020) contributing to the evolution of the dual isotope signal of PSW. The combination of both CPND and biogenic Si burial indicated by the isotopic signatures of N and DSi can only occur in areas which receive a direct high influx of terrestrial DSi and hosts CPND, namely, the Bering Sea and Eurasian shelves.

AW entering the Arctic is poor in DSi which limits biological uptake in AW (Agustí et al., 2018; Krause et al., 2018, 2019). Any excess DSi (e.g from Pacific and shelf waters supplied to AW) will be consumed during the growth season until nitrate is exhausted. The enrichment of $\delta^{30}Si(OH)_4$ in Arctic waters exported out of Fram Strait points towards partial utilisation of DSi, constrained by the availability of nitrate within the TPD (Brzezinski et al., 2021; Liguori et al., 2021). The combination of supply and use of these nutrients is reflected in panel d of Figure 3.7, where PSW is distinct from AW with positive Si* (DSi sources from terrestrial runoff and Pacific influence where nitrate is in deficit relative to phytoplankton requirements) and heavy $\delta^{30}Si(OH)_4$ signatures whereas the relationship with salinity

reflects the mixing of these distinct water mass signatures. While AW signals remain clustered, large variability in PSW Si* and isotopic signature highlight the regional variation and complexity of the Si budget around the Arctic ocean (Table 3.2).

In summary, low availability of nitrogen in the Eurasian sector of the Arctic Ocean appears to regulate the extent to which DSi is utilised and subsequently exported through PSW. At Fram Strait, PSW carries the isotopic signals of DSi and N modification within Eurasian shelves through processes such as CPND and partial utilisation of DSi.

3.4.2 Si cycling in the Arctic ocean and sources of dissolved silicon exported through Fram Strait

The Arctic exports significant amounts of DSi but not N through Fram Strait (Torres-Valdés et al., 2013). Modification of PSW as a result of shelf processes can be traced across the Arctic simultaneously using N & DSi isotopes (Figure 3.7c). Here we use $\delta^{30}Si(OH)_4$ against ln[DSi] plots to examine the pathway of this transformation from DSi sources to Fram strait (Figure 3.8). Broad negative trendlines are observed in Figure 3.8, but on separate trendlines for AW and the pan-Arctic, with PSW in-between. Decreasing DSi and heavier $\delta^{30}Si(OH)_4$ are not linked to uptake as they do not fit fractionation models, suggesting instead that mixed riverine and Pacific sources of DSi are transported across the Arctic towards Fram Strait through PSW.

3.4.2.1 The Bering Strait inflow

$\delta^{30}Si(OH)_4$ in the upper 100m of the water column in the North Pacific is relatively light (~ +1.5‰), with high DSi concentrations (~40μM) (Reynolds et al., 2006). Pacific-originating nutrients are strongly modified in the Bering Strait by riverine input with high Si:N ratio from the Yukon river, by benthic denitrification, and significant biological consumption over the broad shallow shelves in the Bering & Chuchki seas. The combined processes lead to increasing $\delta^{30}Si(OH)_4$ following biological uptake and fractionation (Brzezinski et al., 2021; Giesbrecht et al., 2022). Thus the Pacific endmember measured in the Bering Strait is heavily modified by biogeochemical cycling on shelves, and Arctic inflow here has lower DSi concentrations relative to the Pacific Ocean (Giesbrecht et al., 2022). At lower

ln(DSi) on the Pan-Arctic trendline, riverine and pacific sources become indistinguinshable in surface water masses of the Arctic Ocean and the TPD, reflecting that mixing and biogeochemical cycling in the high Arctic homogenises both nutrient sources prior to export in PSW.

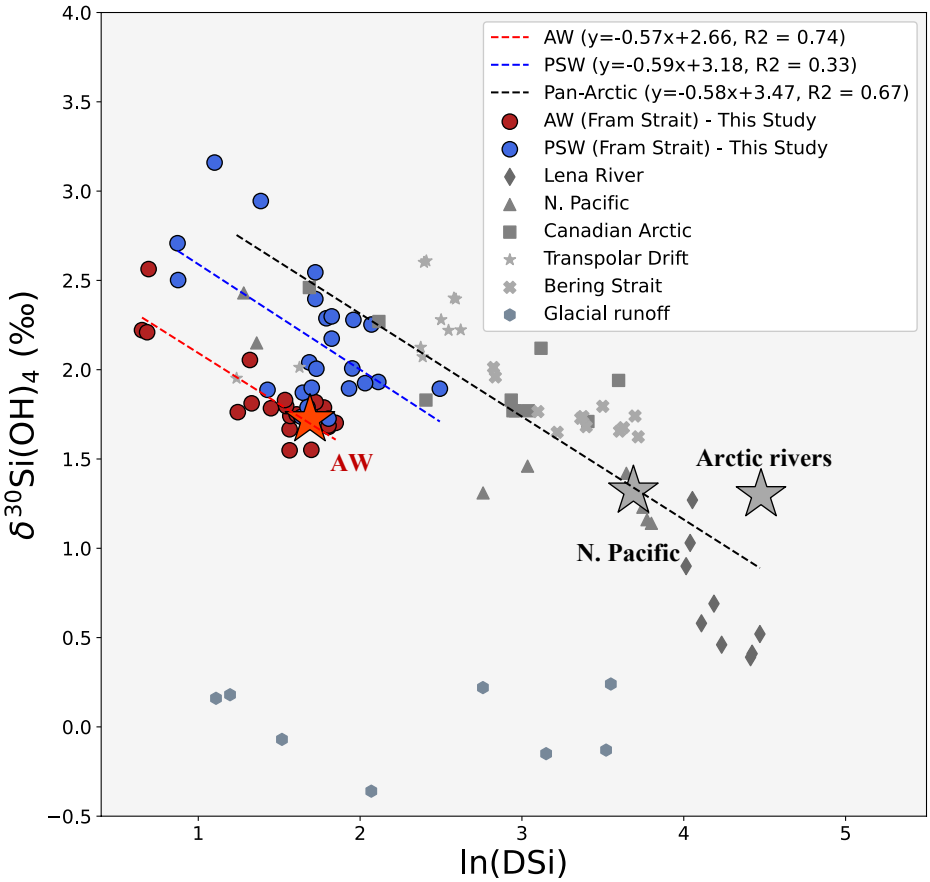

Figure 3.8: Pan-Arctic trends of $\delta^{30}Si(OH)_4$ against ln(DSi). Colored dots show measurements from within AW (red, max. depth = 600m) and PSW water masses (blue, max.depth = 150m) from this study based on water mass definitions in Table 3.2. Grey symbol sets are published $\delta^{30}Si(OH)_4$ from major DSi sources to the surface Arctic domain and surface water masses. Triangles: N.Pacific (<100m, stations 1-6); Stars: Transpolar drift (<60m, stations 30-38 from Brzezinski et al., 2021). Crosses: Bering Strait (max. depth = 60m, stations 4-6 from Brzezinski et al., 2021). Squares: Canadian Arctic (surface and intermediate water mass signatures of the Canadian Arctic sector, from Table 2 in Giesbrecht et al., 2022). Octogones: Glacial runoff from Greenland and Svalbard glaciers (Hatton et al., 2019). Diamonds: Lena river (Sun et al., 2018). Stars show average endmember composition of AW (red) and Pacific and riverine sources (Grey). Red dotted trendline is the least-squared regression for $\delta^{30}Si(OH)_4$ vs the natural logarithm of DSi within AW, blue and grey dotted trendlines are the equivalent for PSW and pan-Arctic (excluding Fram Strait) respectively. These trendlines show fractionation from partial utilisation of DSi consistent with fractionation models.

3.4.2.2 The Eurasian shelf signal

Siberian rivers have isotopically light $\delta^{30}Si(OH)_4$ from clay mineral weathering (Mavromatis et al., 2016; Pokrovsky et al., 2013; Sun et al., 2018). However, terrestrial DSi input and biological consumption occurs simultaneously on shallow Eurasian shelves. Riverine inputs support one third of the net primary productivity of the Arctic ocean (Terhaar et al., 2021), most of which occurs on the Eurasian shelves (MacDonald et al,. 2010). Phytoplankton uptake further reduces DSi concentrations and leads to isotopically heavier $\delta^{30}Si(OH)_4$. This inference follows Brzezinski et al. (2021), as it is also reflected in the TPD. Thus, in Figure 3.8, the broad negative trendline from riverine and Pacific sources across the TPD to Fram Strait reflects the progressive depletion of DSi through biological uptake and biogenic Si burial resulting in isotopic enrichment as it travels through the Arctic. Partial DSi utilisation modifies both the Si budget and its isotopic composition. DSi transported from Eurasian shelves through the TPD towards Fram Strait is reflected in isotopically heavy $\delta^{30}Si(OH)_4$ in PSW which aligns with the broad Rayleigh field in Figure 3.8.

In Fram Strait, $\delta^{30}Si(OH)_4$ fractionation involves separate trendlines for AW and PSW. The trend for AW is statistically significant at Fram strait (R^2>0.7) but shifted downwards indicating distinct DSi pools, lighter for AW. In contrast, the PSW trendline is shifted towards heavier isotopic values and higher DSi concentrations, following more closely the broader Arctic trend. In addition, larger variability in Si isotope signatures of PSW (R^2>0.3) reflects the combined effects of local biological uptake and mixing between Arctic and Atlantic source signatures around Fram Strait.

3.4.2.3 Glacial influence on $\delta^{30}Si(OH)_4$ exported from the Arctic Ocean via Fram Strait

Glacial and sea ice inputs have been suggested to significantly impact Arctic Si budgets (Fripiat et al., 2014; Hawkings et al., 2017), this is evaluated further in Figure 3.8. Isotopic studies in Greenland and Svalbard glaciers have shown isotopically light signatures with low DSi concentrations (Hatton et al., 2019). Benthic studies in SW Greenland fjords found a significant diffusive flux of isotopically light Si into overlying shelf waters (Ng et al., 2020) although export

from fjords remains to be characterised. Si inputs from Greenland and Svalbard have been suggested as significant contributors to the Arctic Si budget which is exported through PSW to the North Atlantic (Hatton et al., 2019; Hawkings et al., 2017, 2018), though the glacial freshwater content of PSW at 79˚N is relatively small (<13%, Stedmon et al., 2015).

In Figure 3.8, we show that light $\delta^{30}Si(OH)_4$ signatures from Greenland and Svalbard glacial sources also have low DSi concentrations and do not align in the Rayleigh field with the Arctic trend observed. This suggests Greenland and Svalbard glaciers are not significantly impacting the Si budget of outflowing PSW at Fram Strait. This implies in-situ studies of glacial streams in Greenland may overestimate glacial contribution of Si to Eurasian Arctic nutrient budgets. A possible explanation for this is amorphous phases of Si represent >95% of the total Si flux (Hawkings et al., 2017) and a large fraction of this may be buried in the sediments of Arctic Fjords prior to dissolution, reducing the impact of glacially-sourced DSi. Additionally, cycling of DSi in Arctic fjords can remove large fluxes of DSi both through intense diatom blooms & burial and reverse weathering (Hopwood et al., 2020).

3.4.2.4 $\delta^{30}Si(OH)_4$ of sea ice

The particularly low apparent isotopic effect of the Arctic Ocean has been attributed to the influence of sea ice and sea ice diatoms drawing down DSi (Giesbrecht et al., 2022; Varela et al., 2016). Sea ice brine is heavier or equal to surrounding waters $\delta^{30}Si(OH)_4$ (Fripiat et al., 2007, 2014) and may contribute to the isotopically heavy signature of polar waters (Liguori et al., 2020; Varela et al., 2016). A recent study from Brzezinski et al. (2021) did not find direct evidence of such an impact on a basin-wide scale. Here we evaluate the role of sea-ice in influencing Arctic $\delta^{30}Si(OH)_4$ signatures in a region influenced by brine rejection. On Figure 3.9, we present hydrography and late-summer profiles of DSi and $\delta^{30}Si(OH)_4$ collected from the Ile-de-France section between 2017-2019 (section location is shown in Figure 3.1). This area is characterized by perennial sea ice cover (Schneider and Budeus, 1995). A PSW layer extends down to 125m of the water column and is influenced by brine released during winter sea ice formation (Budeus and Schneider, 1995). In the

freshwater layer, a small peak in DSi concentration (2-3 µM) is observed at ~40m. The small increase in DSi concentration at this depth suggests a DSi source from sea ice processes. However, there is no distinct isotopic enrichment (Figure 3.9) associated with this source. Thus DSi inputs from sea ice appear to have a negligle effect on PSW $\delta^{30}Si(OH)_4$. This is consistent with studies suggesting that sea ice and sea ice brine tend to be relatively low in DSi (Fripiat et al., 2017), with no significant impact on pan-Arctic isotope signatures (Brzezinski et al., 2021).

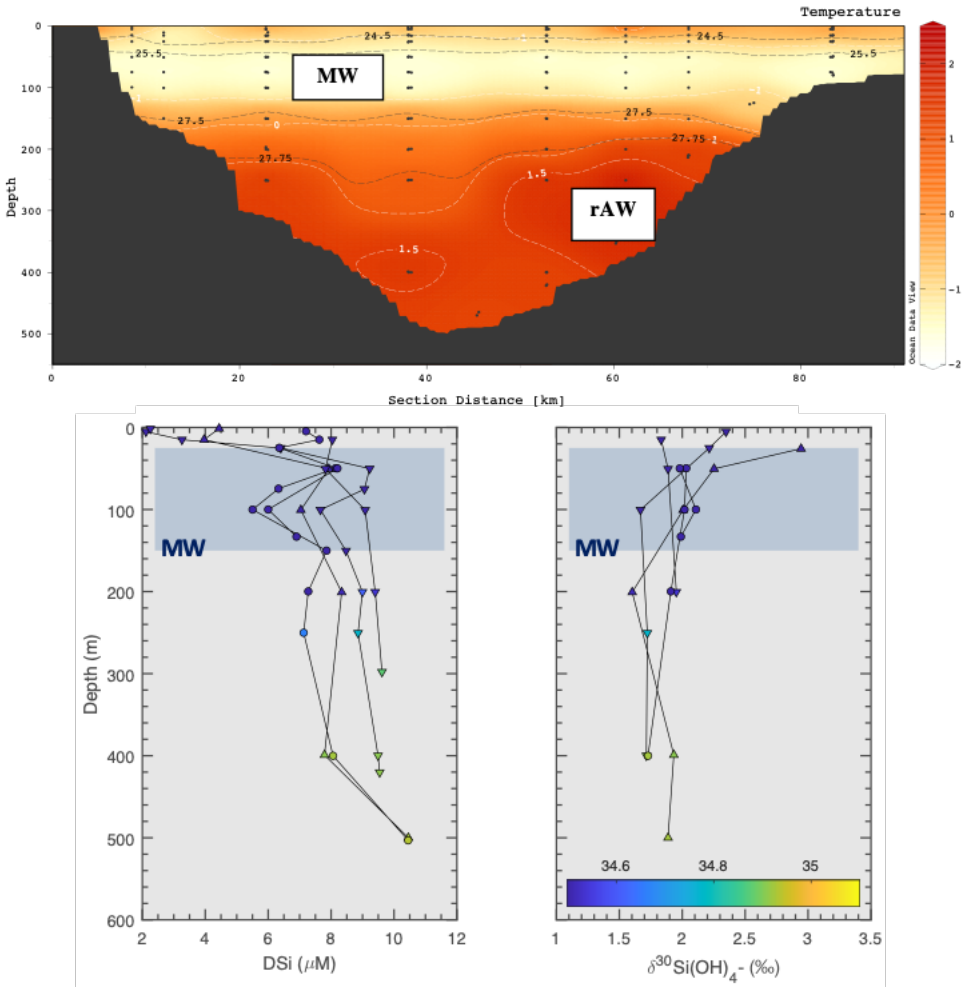

Figure 3.9: Top: Integrated hydrography of the Ile-de-France section for 2017-2019. Isotherms are shown in white and isopycnals in black. MW = meteoric water, rAW = recirculated Atlantic Water. Bottom panels: DSi concentrations (left) and δ30Si(OH)4 (right) for late summer 2017 (circle), 2018 (upwards triangle) & 2019 (downwards triangle) of the Ile-de-France section. Colourscale represents salinity (psu).

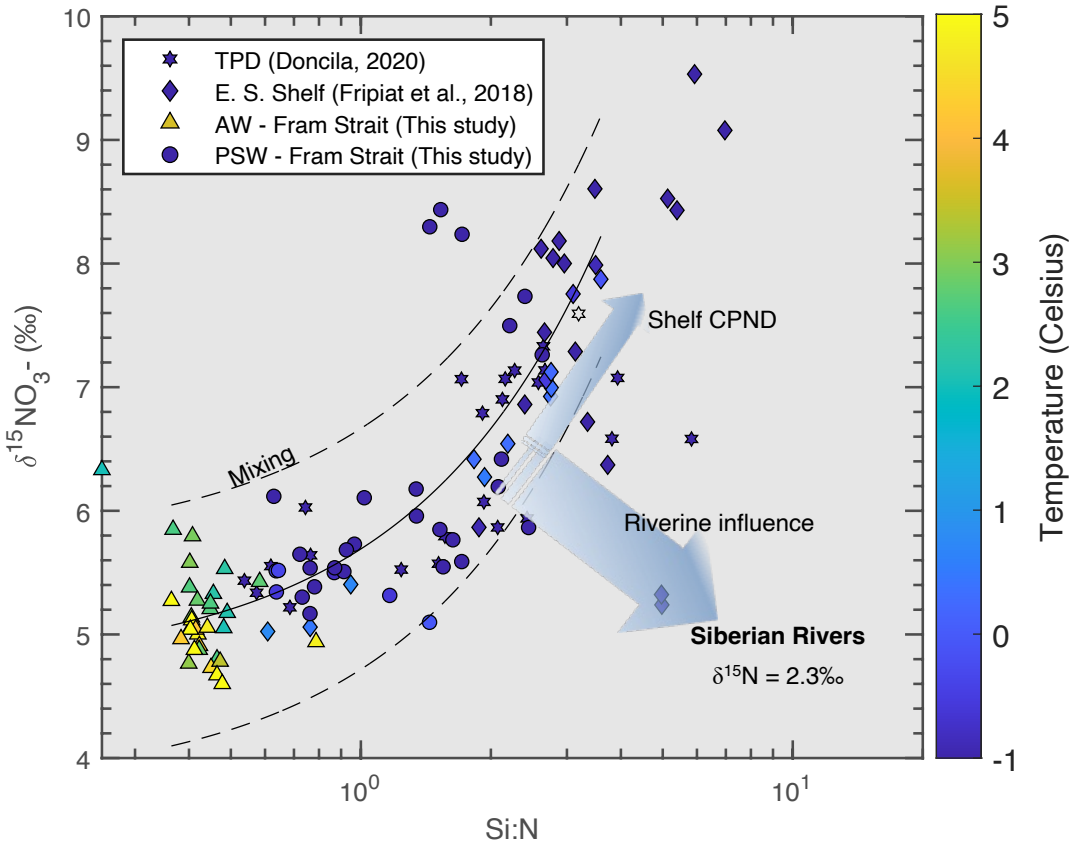

Figure 3.10: Pan-Arctic trends of δ15N-NO3 against Si:N ratio. Triangles = Atlantic water at Fram Strait; Circles = Polar surface water at Fram Strait (this study). Stars = Transpolar drift (Doncila, 2020); Diamonds = East Siberian shelf (Fripiat et al., 2018). Dotted lines shows the regression line between AW and shelf endembers, dotted lines are for 1SD. Data is plotted below the mid-layer depth in Fram Strait to remove seasonal variation. This could not be applied to the transpolar drift and East Siberian shelf due to the shallowness of the water masses. Colorscale shows temperature. δ15N-NO3 endmember for summertime Siberian rivers is obtained from Francis, 2019, from ArcticGRO measurements.

3.4.2.5 Processes affecting the export of Arctic DSi to the Atlantic Ocean

Figure 3.8 reveals that DSi exported to the Atlantic in PSW in 2018 was sourced from incomplete utilisation of DSi on Eurasian shelves. This leads to the question as to what limits the complete utilisation of DSi in the Arctic. In Figure 3.10, we plot $\delta^{15}N\text{-}NO_3$ versus DSi:N ratios, excluding measurements within the MLD at Fram Strait to remove seasonal uptake trends (this was not applied to measurements in the TPD and shelf seas due to the shallow nature of the water masses). The figure reveals the three mixing components of the Arctic N budget, namely, the very heavy $\delta^{15}N$-

NO_3 values generated on the the shelves with high DSi:N ratios due to removal of light nitrate by CPND; The input of terrestrial riverine N with relatively light $\delta^{15}N$-NO_3 signatures ($\delta^{15}N$-NO_3 = 2.3‰, Francis, 2019) with variable but high DSi:N ratios; and Atlantic sources ($\delta^{15}N$-NO_3 = 4.8 ± 0.2‰, Tuerena et al., 2015, and DSi:N = 0.6, World Ocean Database, 2013). AW sources become important in Fram strait and contribute to nitrate by mixing across the halocline in basins where AAW underlies below PSW. Pan-Arctic N isotopic trends, shown in Figure 3.10, are dominated by mixing of sources rather than fractionation by biological uptake; a striking constrast to the $\delta^{30}Si(OH)_4$ trend (Figure 3.8). This is arguably caused by the near-complete utlisation of nitrate on Eurasian shelves and above the halocline, leading to limited overall fractionation from source signatures. This widespread nitrate limitation in the Arctic is attributed to fixed N loss from benthic denitrification on the shallow shelves which constitute approximately 50% of the Arctic ocean area. A significant portion of N loss from denitrification is derived from organic matter from the overlying water column (Mctigue et al., 2016; Tuerena et al., 2021c); leading to a net deficit of N exported out of the Arctic (Torres-Valdés et al., 2013; Yamamoto-Kawai et al., 2006).

Furthermore, Arctic rivers are a larger source of DSi than N (Holmes et al., 2012) and the N supplied is quickly removed in river deltas (Tuerena et al., 2021c). For example, on the Laptev sea shelves, it is estimated that 62-76% of riverine dissolved organic nitrogen is removed within a couple of months by denitrification and biolgical utilisation (Thibodeau et al., 2017a). This is evident from the very low nitrate concentrations in the TPD and high DSi:N ratios (~5µM and 1.8 respectively, Doncila, 2020) which is heavily influenced by riverine inputs and modification over the Eurasian shelves. The near-absence of nitrate in surface waters overall contributes to the higher DSi:N output observed in PSW in Fram Strait. We conclude that incomplete utilisation of DSi in the Arctic ocean and its subsequent export through the Fram Strait is governed largely by widespread N limitation due to the rapid removal of nitrate in the Arctic ocean, namely on Eurasian shelves.

3.4.3 Evaluating contribution of DSi sources at Fram Strait

With decreasing ln(DSi) in Figure 3.8, riverine and pacific sources of $\delta^{30}Si(OH)_4$ form a homogenous Pan-Arctic trendline driven by partial utilisation of DSi, separate from AW in the Rayleigh field. The $\delta^{30}Si(OH)_4$ of PSW plots between these two trendlines, as a mixture of AW and Arctic-sourced nutrients instead (figure 3.6 & figure 3.8).

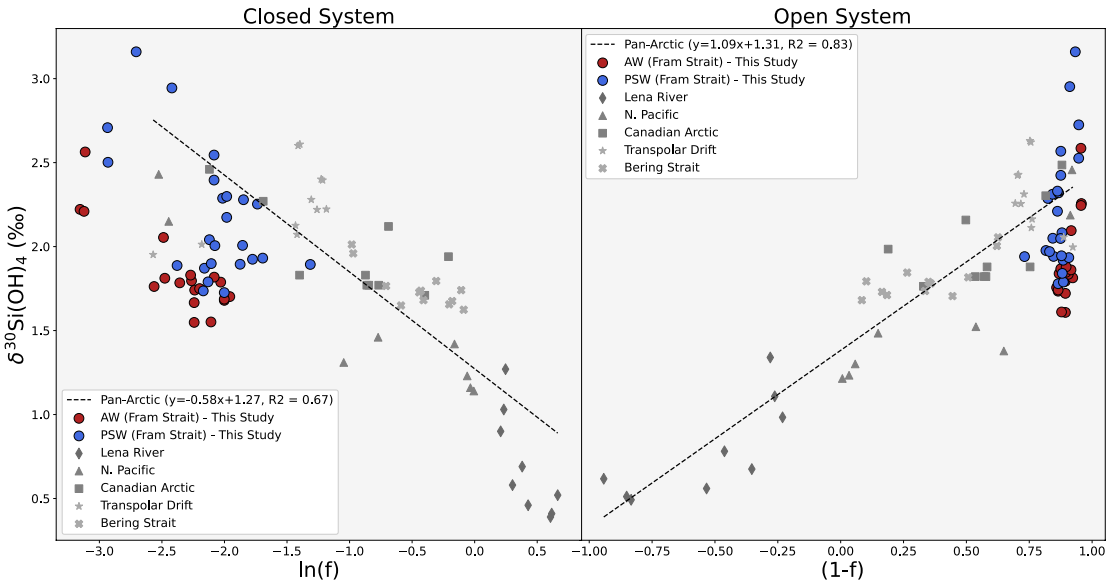

Figure 3.11. Estimate of the apparent $\delta^{30}Si$ isotopic effect across the Arctic Ocean from source to export to Fram Strait through the transpolar drift. The lines and equations are the result of linear regression of $\delta^{30}Si(OH)_4$ vs the natural logarithm of f (where f = measured DSi/ DSi source prior to any biological consumption), representative of closed system dynamics (left) and $\delta^{30}Si(OH)_4$ vs 1-f, representative of open system dynamics. AW & PSW are not included in this regression as it is assumed they originate from different nutrient sources. Colored dots show measurements from within AW (red, max. depth = 600m) and PSW water masses (blue, max.depth = 150m) from this study based on water mass definitions in Table 3.2. Grey symbol sets are published $\delta^{30}Si(OH)_4$ from major DSi sources to the surface Arctic domain and surface water masses. Triangles: N.Pacific (<100m, stations 1-6); Stars: Transpolar drift (<60m, stations 30-38 from Brzezinski et al., 2021). Crosses: Bering Strait (max. depth = 60m, stations 4-6 from Brzezinski et al., 2021). Squares: Canadian Arctic (surface and intermediate water mass signatures of the Canadian Arctic sector, from Table 2 in Giesbrecht et al., 2022). Octogones: Glacial runoff from Greenland and Svalbard glaciers (Hatton et al., 2019). Diamonds: Lena river (Sun et al., 2018). The y-intercept of both trendlines provide a $\delta^{30}Si(OH)_4$ estimate of DSi sources in the Arctic Ocean ranging from 1.27 – 1.31‰.

As the pan-Arctic relationship is strong (R^2=0.67), the extent of utilisation of DSi sources and their relative contribution to PSW can be estimated from the apparent pan-Arctic isotopic effect $^{30}\varepsilon$ (regression of trendline in the Rayleigh field). Using this dataset we estimate $^{30}\varepsilon$ = -0.58‰ for closed system fractionation and $^{30}\varepsilon$ = -1.09‰ for open system fractionation (Figure 3.11). Considering the multiple nutrient pathways and physical mixing as waters are transported from Arctic shelves to the Fram Strait in the Arctic Ocean, it is expected that the pan-Arctic dataset fits an open system. This is what is observed on Figure 11, with a stronger R^2 for the open system model (R^2 = 0.83) than for a closed system (R^2 = 0.67). Additionally, the open model is more coherent with a $^{30}\varepsilon$ close to global estimates of -1‰ and a both models are in close agreement with measured isotopic effects in the Canadian Arctic sector (-0.59‰ and -1.19‰ for closed and open systems respectively, Giesbrecht et al., 2022).

Assuming 43% of riverine DSi is removed on shelves prior to transport into the TPD (Charette et al., 2020) and using the PSW signature calculated in Table 3.2 (1.84 ± 0.09‰), the apparent remaining nutrient fraction (f_{PSW}) within PSW can be estimated from the isotopic effects calculated above. We estimate f_{PSW} = 0.37 ± 0.06 and f_{PSW} = 0.51 ± 0.08 for closed and open systems respectively. This calculation shows that the PSW DSi inventory is extensively consumed by biological activities, and up to 50% of the pre-formed PSW DSi stock is used up in the Arctic Ocean. Considering the large-scale patterns of transport, circulation and mixing within the Arctic Ocean, we can assume the system is open as nutrients are likely to be frequently resupplied and closed system assumptions would lead to an overestimation of nutrient consumption. Assuming utilisation of 51% of the PSW pre-formed DSi stock, modelled DSi and $\delta^{30}Si(OH)_4$ would thus be 7.8 ± 0.6 µM and 1.89 ± 0.02‰ respectively, which reproduces well what we measure in Fram Strait.

This calculation assumes Arctic shelf DSi concentration of 45 µM, an average between Pacific-originating shelf waters (30-40µM Brzezinski et al., 2021; Giesbrecht et al., 2022) and the concentration of DSi exported from rivers into the TPD after burial in estuaries and shelves (47µM, Charette et al., 2020). The

differences in predicted nutrient utilisation between open and closed system nonetheless highlights that care needs to be applied when choosing models and initial conditions in the Arctic Ocean as this could lead to important bias in calculations.

Additionally, the parameters used in the calculation to model PSW signature based on utilisation are as follow: riverine DSi = 83µM and $\delta^{30}Si(OH)_4$ = 1.3‰ (Charette et al., 2020; Sun et al., 2018) and upper halocline waters of Pacific influence DSi = 30.6µM and $\delta^{30}Si(OH)_4$ = 1.71‰ (Giesbrecht et al., 2022). A PSW hydrological composition of 13% meteoric water, 4% Pacific water and 8% sea ice melt is assumed, with the remaining composition of seawater being AW (Dodd et al., 2012).

Based on the calculation above, riverine sources contribute to 40 ± 4% of the total DSi inventory at Fram Strait, with Pacific sources contributing to 8 ± 1%. This basic calculation reproduces DSi concentrations and isotopic signatures measured within PSW, albeit slightly overestimates them. It is a rough estimate, as it assumes sea ice only dilutes ambient DSi concentrations and has no net isotopic effect, in accordance with our observation locally (section 4.2.4), although sea ice has been proved to play an important role for DSi cycling in other parts of the Arctic Ocean (Giesbrecht et al., 2022; Liguori et al., 2021). Nonetheless this exercise illustrates that a mixture of heavily utilised riverine DSi and partially utilised Pacific-originating nutrients modify the nutrient inventory in PSW from its AW baseline. The PSW DSi inventory is highly sensitive to the extent of utilisation of riverine DSi on Arctic shelves due to the high initial concentration. This calculation highlights that modification of riverine nutrient sources and removal on Arctic shelves is likely to have a large influence to exported concentrations and isotopic budgets. To improve the above estimate, accurate understanding of DSi consumption on shelves prior to export in the central Arctic Ocean is required, with improved isotopic signature determination of riverine sources and shelf water masses.

3.5 Future implications

Our results highlight some important connections between nutrient cycling and the control on the exchange of nutrients between the Arctic and the Atlantic Ocean. This study has identified a link between the Arctic N and Si cycles: low Nitrogen

availability regulates the extent of DSi drawdown in exported PSW and is traced to Arctic shelf processes. The nitrogen deficit is generated by biological Arctic processes such as CPND. This along with the extent of utilisation of DSi sources controls the excess DSi exported out of the Arctic ocean through gateways such as the Fram Strait. In the changing Arctic Ocean, this has far-reaching implications to ecosystems and nutrient budgets as discussed below.

Using $\delta^{30}Si(OH)_4$ signatures, we have estimated that >40% of DSi exported out through Fram Strait is of riverine origin. Freshwater inputs to the Arctic ocean from the Eurasian sector are expected to increase in response to climate change (Mcclelland et al., 2006; Rawlins et al., 2010). Increasing riverine discharge and permafrost degradation is accelerating the transport of terrestrial material to Eurasian shelves and likely increasing the export of major nutrients (Zhang et al., 2021). As NO_3^- delivery from rivers is low, riverine sources of DSi are increasing faster than N inputs.

Light, DSi and NO_3^- availability all play an important role in dictating the complex patterns of diatom production around the Arctic Ocean (Giesbrecht et al., 2019; Krause et al., 2019). Our study illustrates that NO_3^- availability plays an important role for opal production in the Eurasian Arctic. Nitrogen is quickly removed in Siberian rivers at low salinities (Sanders et al., 2021; Tuerena et al., 2021c) through benthic denitrification, with roughly 70% of terrestrial N removed before reaching the seawater endmember (Letscher et al., 2013) depleting N in relation to DSi in the deeper water column. Such rapid N removal implies additional terrestrial NO_3^- inputs are not likely to significantly impact N-availability.

Nitrogen deficiency on Arctic shelves is currently limiting DSi consumption to only 14.3% of its net riverine input (Le Fouest et al., 2013). This implies that as terrestrial DSi inputs increase, a larger proportion of terrestrial DSi will remain unutilised and ultimately get transported through the TPD out to Fram Strait. This will increase the export of DSi to the North Atlantic, but also alter the $\delta^{30}Si(OH)_4$ of PSW which is derived from the partial biological utilisation of DSi. Terrestrial DSi inputs increasing in the future combined with increased N-limitation will reduce the

percentage of DSi consumption in the Arctic ocean, leading to lighter isotopic signatures of DSi exported towards the North Atlantic.

Locally, the larger export of DSi through the TPD has implications for nutrient dynamics in Fram Strait. N-limitation is strong in PSW and is predicted to increase in AW (Tuerena et al., 2021a). Increasing primary production in the Arctic shelves as sea ice melts and light availability increases (Arrigo et al., 2008; Arrigo and van Dijken, 2015) will increase N-demand, and further N losses through denitrification which could reduce DSi uptake further and limit net productivity from silicifying species and impact carbon drawdown in Fram Strait. A decline in diatoms and a shift towards smaller phytoplankton assemblages is already observed with warming in Fram Strait (Lalande et al., 2013). Such changes will be accentuated further with N-limitation.

We also recognize there are competing influences on the future nutrient status of the Fram Strait. The higher export of DSi can compensate for decreasing DSi supply through AW to the Arctic ocean resulting from Atlantification (Arthun et al., 2012; Lind et al., 2018) which leads to decreasing DSi concentrations in AW (Hátún et al., 2017). While terrestrial increase in DSi input and reduced utilisation in the Arctic will supersede this signal in PSW over time, this can potentially lead to a decrease in the DSi inventory of intermediate and deep waters of the Arctic ocean influenced by AW, while increasing DSi export out of the Arctic through the PSW.

The far-reaching consequences of the predicted future increases in Arctic DSi export to the North Atlantic imply changes to primary production patterns and DSi concentrations in deep water masses formed here. Waters in the North Atlantic are richer in nitrate than DSi, and available evidence indicate DSi limitation of diatom spring blooms due to limiting concentrations of silicic acid in the region (Henson et al., 2006; Leblanc et al., 2005). This envisioned additional supply of DSi can impact the duration of diatom blooms in the sub-Arctic North Atlantic (Allen et al., 2005), and possibly enhance diatom production with subsequent implications for carbon export to the deep ocean. In longer time scales, this can also increase the preformed

DSi inventories in the North Atlantic deep waters, with an impact on the nutrient status of the deep water masses worldwide.

3.6 Conclusions

Previous understanding of the importance of physical (water-mass mixing) vs biological (production and dissolution) controls in setting $\delta^{30}Si(OH)_4$ distribution across the Arctic was limited by the lack of direct measurements at major gateways (Brzezinski et al., 2021). This study provides the first full depth profiles of $\delta^{30}Si(OH)_4$ in Fram Strait, in combination with $\delta^{15}N\text{-}NO_3$ and $\delta^{18}O\text{-}NO_3$, closing gaps in the Arctic isoscape and confirming mechanisms of transformation.

Isotopic measurements document the transformation of PSW outflowing through Fram Strait, with isotopic signatures $\Delta(15\text{-}18) = 4.22 \pm 0.89‰$ and $\delta^{30}Si(OH)_4 = +1.85 \pm 0.09‰$. $\delta^{30}Si(OH)_4$ is enriched by +0.11‰ in PSW compared to inflowing AW, while $\Delta(15\text{-}18)$ is enriched by 1.37‰, showing significant source modification of the nutrients between the inflow and outflow waters.

Further examination of DSi & N isotopes trace nutrient sources and modification processes in PSW primarily to Eurasian shelves: The increase in DSi concentration and enrichment of $\delta^{30}Si(OH)_4$ is traced to biological uptake of DSi and burial of opal on the shelves, sustained by the high DSi load from Eurasian rivers. Export of DSi out of the Arctic through Fram Strait is ultimately regulated by N-limitation resulting from N-poor input from terrestrial sources combined with efficient removal of N through denitrification on shelves. This is documented in PSW through de-coupling of the oxygen and nitrogen isotopes of nitrate from traditional 1:1 relationship. Glacial influence from Greenland and Svalbard glaciers and Pacific inflow appeared of smaller influence at Fram Strait in PSW, with riverine sources contributing to ~40% of the DSi exported out of Fram Strait.

The measurement of DSi & N isotopes provides the first insights into the coupling of the N and Si cycle in the Arctic Ocean. Nitrate limitation during primary production generates excess DSi which is subsequently exported to the North Atlantic. As riverine nutrient sources of DSi are expected to increase faster than N with climate

warming, this can enhance N limitation within the Eurasian Arctic ocean and increase the export of DSi to the North Atlantic ocean.

3.7 Appendix

3.7.1 Section of $\delta^{30}Si(OH)_4$ (JR17005)

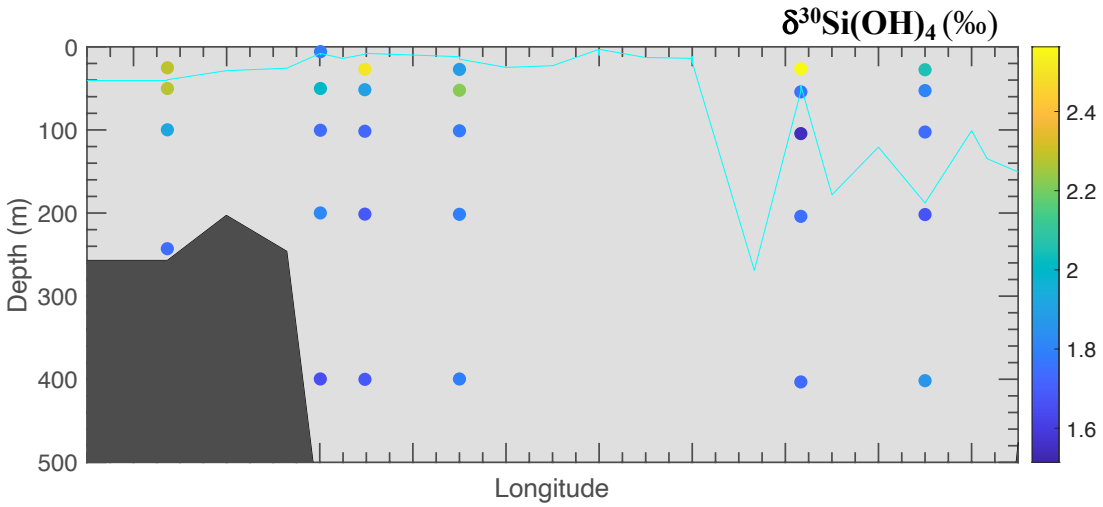

Figure 3.12. $\delta^{30}Si(OH)_4$ (‰) across the Fram Strait section of spring 2018 (JR17005). Cyan line displays MLD for the section (calculation described in main method section).

3.7.2 Isotopic trends in PN and PSi

The nitrogen isotopic composition of particulate nitrogen (δ^{15}N-PN) and the silicon isotopic composition of particulate silicon (δ^{30}Si-PSi) was measured alongside nitrate and $\delta^{30}Si(OH)_4$ for FS2018 and JR17005 cruises. The methods of collection and analysis is briefly described below. Measurements of δ^{15}N-PN and δ^{30}Si-PSi are shown in the Rayleigh field on Figure S3 and briefly discussed here.

δ^{15}N-PN is very variable but generally high throughout the spring and summer in AW and PSW, highlighting N limitation to local phytoplankton and the shift towards consumption of regenerated nitrogen.

δ^{30}Si-PSi in AW is consistent with the isotopic trends of closed system products and $\delta^{30}Si(OH)_4$ observations that DSi is not resupplied in AW and becomes progressively depleted. δ^{30}Si-PSi in PSW does not follow any fractionation model, consistent with

$\delta^{30}Si(OH)_4$ trends which indicate that DSi trends in PSW are driven by mixing rather than biological uptake locally.

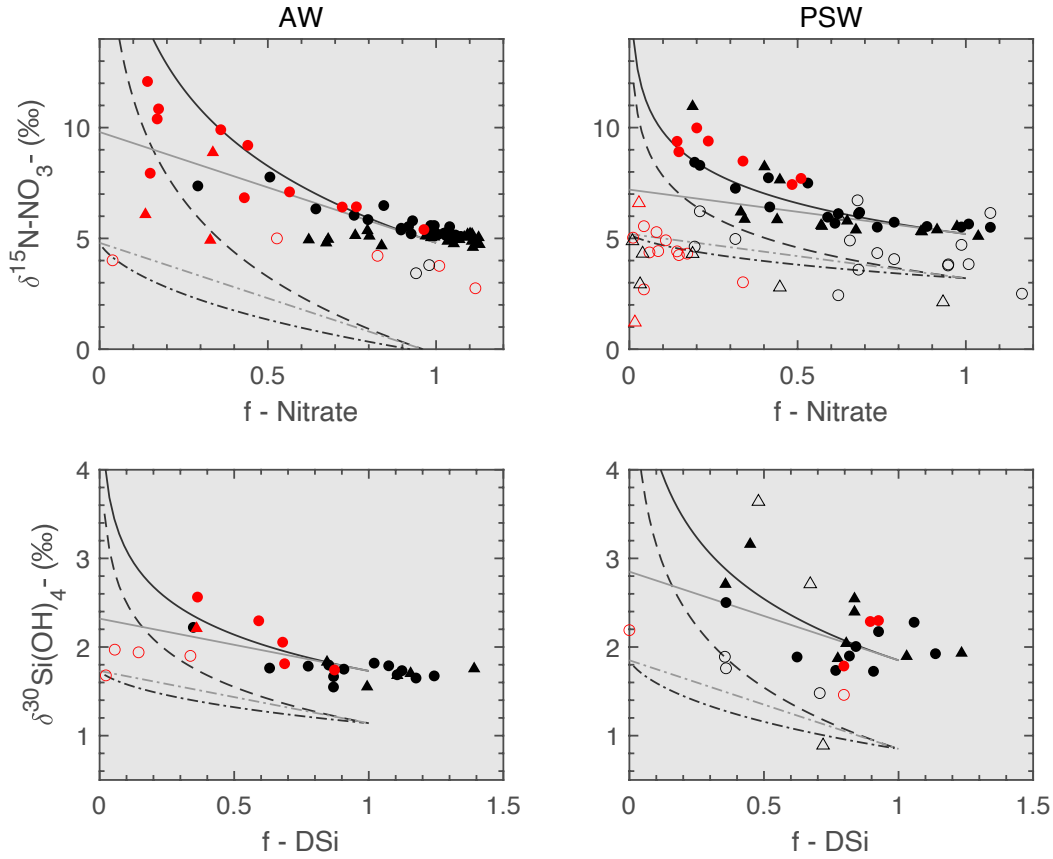

Figure 3.13. Top panels: nitrate utilisation vs $\delta^{15}N\text{-}NO_3$ for AW (left) and PSW (right). Bottom panels: DSi utilisation vs $\delta^{30}Si(OH)_4$ for AW (left) and PSW (right). Circles are denote measurements from JR17005 (spring) and triangles from FS2018 (summer). Red symbols show measurements within the MLD. Black line follows the closed fractionation model and grey line an open fractionation model. Full symbols are seawater measurements, open symbols are for $\delta^{15}N$-PN (above) and $\delta^{30}Si$-PSi (below).

4. Importance of riverine nutrient supply for the marine Si pump of Arctic shelves: Evidence from the Laptev Sea

This chapter is based on a manuscript intended for submission to the journal *Global Biogeochemical Cycles*. Supplementary N isotope data not included in the manuscript is presented in an appendix.

M. C. F. Debyser[1], L. Pichevin[1], R.E Tuerena[2], A. Doncila[1], I. Semiletov[3], and R.S. Ganeshram[1]

Affiliations

[1]School of Geosciences, University of Edinburgh, Edinburgh, EH9 3FE, United Kingdom

[2]Scottish Association for Marine Science, Dunstaffnage, PA37 1QA, United Kingdom

[3]V.I. Il'ichev Pacific Oceanological Institute (POI), Far East Division of the Russian Academy of Science, Vladivostok, Russia

Contribution

Author – M.C.F. Debyser

Research Design – R.S. Ganeshram, M.C.F Debyser, I. Semiletov, L. Pichevin

Data collection – I. Semiletov

Method development – M.C.F Debyser

Sample analysis – M.C.F Debyser, A. Doncila

Scientific interpretation and manuscript implementation – M.C.F Debyser, L. Pichevin, R.E. Tuerena, R.S. Ganeshram, I. Semiletov

Abstract

Arctic shelves receive a disproportionate amount of nutrients from Arctic rivers and play a major role in the biogeochemical cycles of the Arctic Ocean. In this study we present the first direct measurements of dissolved silicon isotopes ($\delta^{30}Si(OH)_4$) around the Lena Delta and the Laptev Sea collected in October 2018. The aim of this work is to understand and document terrestrial DSi modifications on shelves and their contribution to the Arctic basin.

Modification of inflowing nutrient stoichiometry is observed on the Eurasian shelf, owing to nutrient input from rivers, and partial utilisation of DSi and subsequent burial of opal in the shelf sediments. Nitrogen was found to be depleted in surface waters and the limiting nutrient to primary production in the Laptev Sea, allowing excess DSi export to the central Arctic Ocean.

Heavy $\delta^{30}Si(OH)_4$ in the water column were linked to strong biological removal of DSi on shelves, enabled by vigorous N recycling. Through heavy silicon isotopic signatures, we trace enriched shelf waters feeding into the Transpolar Drift. From isotopically-constrained processes, we estimate that >40% of the DSi from riverine inputs is removed within the Lena River delta and on the Laptev Sea shelf. Extrapolating this to major Siberian rivers, this leads to an export of 3.10 ± 0.71 kmol/s of riverine DSi through the transpolar drift.

An updated isotopic budget of the Arctic Ocean based on updated opal burial rates reproduces the observed $\delta^{30}Si(OH)_4$ signatures out of the Arctic Ocean and underlines the importance of biological processes in modulating DSi export. Given that opal burial fluxes on Artic shelves are controlled by denitrification and N-limitation, these processes are sensitive to ongoing climate change. As a consequence of higher riverine DSi inputs and shelf denitrification responding to productivity, it is inferred that DSi export from the Arctic Ocean could increase in the future, accompanied by lighter $\delta^{30}Si(OH)_4$ signatures.

4.1 Introduction

The Arctic Ocean is a shelf sea and receives the highest input of freshwater and organic matter relative to its volume globally (Dittmar and Kattner, 2003). Shallow shelves primarily ranging between 0-50m depth cover >50% of its total area (Jakobsson, 2002). It represents around 1% of the volume of the world's oceans, yet receives >10% of global riverine discharge (Aagaard and Carmack, 1989; McClelland et al., 2012) which supply essential terrestrial material to the Arctic Ocean. Nitrate and Dissolved Silicon (DSi) are key inorganic nutrients required for diatom bloom development, which are important primary producer in polar ecosystems, contributing to around 50% of primary production in the Arctic Ocean (Krause et al., 2019; Sakshaug, 2004). Around three quarters of primary productivity of the Arctic Ocean occurs on Arctic shelves, which also account for >90% of opal production (Macdonald et al., 2010). This makes nutrient cycling in shelf ecosystems disproportionately important for regulating the export of inorganic nutrients to the central Arctic Ocean and the North Atlantic.

The Eurasian margin constitutes half of the Arctic Ocean's total shelf area (Jakobsson, 2002), and is important to the Si budget of the Arctic Ocean. While the extensive Barents Sea shelf has a relatively low riverine influence (200 km^3/yr), the Kara, Laptev and East Siberian Seas receive freshwater input from four major rivers, the Ob, Yenisey, Lena & Kolyma rivers, which contribute to >1700 km^3/yr of freshwater to the surrounding shallow shelf seas. These major rivers provide large supplies of carbon and DSi to the Arctic Ocean (Holmes et al., 2012). On the Laptev Sea shelf, diatoms are the predominant form of marine primary producers and support large settling flux of organic carbon and nutrients to the seafloor (Cremer, 1999; Fahl et al., 1999).

Stable isotope measurements of DSi ($\delta^{30}Si(OH)_4$) provide useful insights into DSi sources, drawdown and export to surface waters within the Arctic Ocean (Brzezinski et al., 2021; Liguori et al., 2021; Varela et al., 2016). Previous preliminary Si budget and isotopic mass balance for the Arctic Ocean have struggled to reconcile the net export of DSi from the Arctic to the Atlantic Ocean (Torres-Valdés et al., 2013) with

the heavy $\delta^{30}Si(OH)_4$ of polar waters compared to the global ocean (Brzezinski et al., 2021; Giesbrecht et al., 2022; Liguori et al., 2020, 2021; Varela et al., 2016). A hypothesis to reconcile this discrepancy is the partial utilisation of terrestrial DSi and implies burial of isotopically light opal over Arctic shelves (Section 3.4.2, Brzezinski et al., 2021). This mechanism can explain the export of residual DSi with heavy $\delta^{30}Si(OH)_4$ as diatoms fractionate the isotope load during uptake (De La Rocha et al., 2000), originating from isotopically light Arctic riverine sources of DSi (Mavromatis et al., 2016; Pokrovsky et al., 2013; Sun et al., 2018). This mechanism requires large-scale burial of Si in the shallow shelves with large terrestrial DSi inputs. However, this process remains to be documented and quantified. Other hypotheses include mixing with isotopically light water masses (Varela et al., 2016), although these have not been documented around the Arctic Ocean.

Understanding the removal of DSi over Eurasian shelves and near major river deltas is important as it ultimately controls DSi fluxes and cycling in the central Arctic Ocean through its transport via the TPD (Charette et al., 2020; Liguori et al., 2021), and its net export to the North Atlantic. In this study we present the first full depth profiles of $\delta^{30}Si(OH)_4$ along a transect in the Laptev Sea, as well as surface measurements from the Eurasian shelves. The isotope dataset combined with hydrographic data allows us to examine the importance of riverine nutrient supply in the Arctic Ocean, to evaluate the role of 'Arctic shelf Si pump' and to develop an isotope constrained budget of Si in the Arctic Ocean.

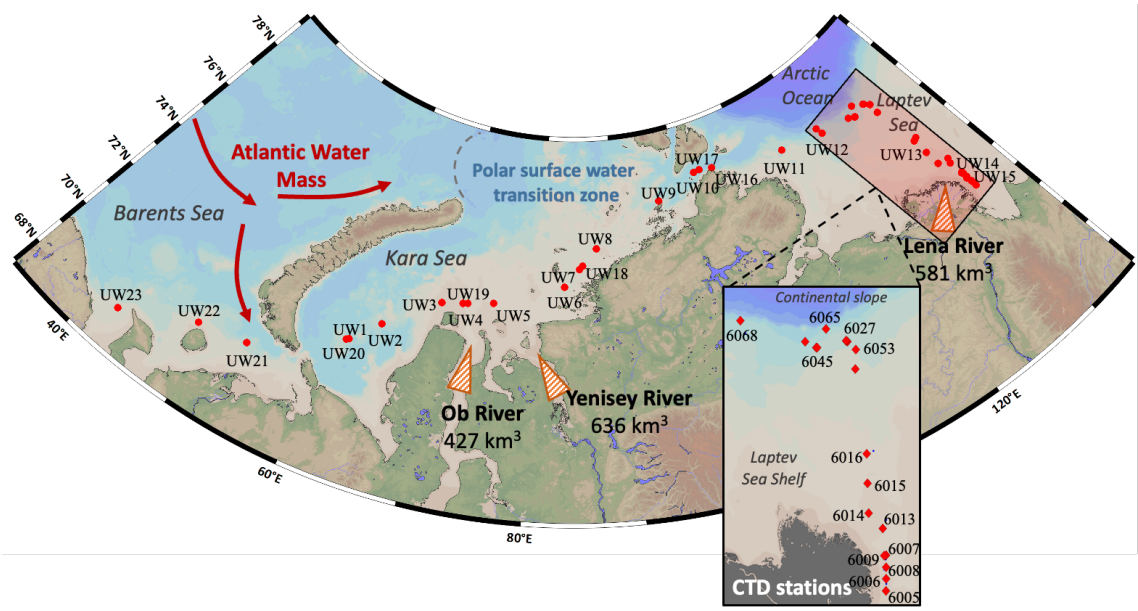

Figure 4.1. Map showing the study area of this research and general surface circulation patterns of the Eurasian shelves. Red arrows represent warm, saline current of Atlantic water. Orange triangles show the delta of major rivers within the study area which constitute the largest freshwater source to the Eurasian Arctic sector: the Ob, the Yenisey and the Lena rivers. Discharge is in km^3/yr. AMK73 CTD and underway sample locations are shown with red dots. Shaded red area highlights the CTD section. Stations numbers are labelled UW for underway samples and numbered for CTD stations. Map modified from Ocean Data View.

4.2 Materials and Methods

4.2.1 Study Area

Samples were collected in October 2018 during the 73rd expedition of R/V *Akademik Mstislav Keldysh* (AMK73). The main transect is located in the Laptev Sea along the Lena estuary, shelf area and the upper part of the continental slope. Underway samples were also collected during transit covering the Eurasian shelf (see Figure 4.1). The stations were free of sea ice at the time of sampling.

On Eurasian shelves, the surface waters of the Barents Sea are dominated by warm, saline Atlantic Waters (AW) inflowing from the North Atlantic through the Barents Sea Opening (Årthun et al., 2011; Rudels et al., 2004). The discharge from major rivers form freshwater plumes and freshened surface layers over wide areas of the Kara & Laptev seas (Spivak et al., 2021), leading to buoyant, eastward-travelling boundary currents (Osadchiev et al., 2020). Much of this plume enters the TPD

within 1-2 years and reaches Fram Strait in 2-3 years (Semiletov et al., 2000), undergoing periodic mixing with underlying AW and vigorous cycling of nutrients on the shelves prior to transport (Thibodeau et al., 2017a), before eventually getting exported to the North Atlantic through the TPD (Karcher and Oberhuber, 2002) along with terrigenous nutrients (Charette et al., 2020).

The Laptev Sea receives discharge from one of the largest river on earth, the Lena river, which supplies large amounts of organic and inorganic nutrients to the surrounding shelf (Holmes et al., 2012; Stedmon et al., 2011). Because of the influence of the Lena river, the hydrography of the Laptev Sea is characterized by large gradients in physical and chemical properties within the water column (Kostyleva et al., 2020; Spivak et al., 2021). As discharge from the Lena river enters the sea, the Lena Freshwater Plume (LFP) is formed. The buoyant fresh water mass at the surface of the water column overlays saline waters, setting up a strong salinity gradient which restricts mixing. These shelf waters gradually become more saline as they extend out towards the continental slope where LFP meets advected AW. The discharge of the Lena river varies strongly with seasonality as the lower reaches of the catchment freeze in winter contracting the extent of the plume on the shelf, and subsequently expands in spring-summer as the Lena discharge increases (Kostyleva et al., 2020; Pavlov et al., 1996). Variations from the Lena discharge also affect the chemical and physical properties of the Lena plume in the Laptev Sea. Underneath the plume, near-bottom stagnant waters are found, constrained by local bathymetry (Kostyleva et al., 2020; Létolle et al., 1993).

4.2.2 Physical parameters

Seawater samples were collected from rosette-mounted Niskin bottles also equipped with sensors recording physical parameters (conductivity, temperature, pressure & salinity). Apparent Oxygen Utilisation (AOU) is used in this study as a tracer of biological activity and nutrient sources in the water column (Tremblay et al., 2015). AOU was calculated as

$$\mathrm{AOU}\ (\mu\mathrm{mol/kg}) = [\mathrm{O_2\ sat}] - [\mathrm{O_2\ obs}] \qquad \textit{Eq. 4.1}$$

Where [O_2 sat] is the theoretical equilibrium saturation concentration in water at the same physical properties and [O_2 obs] is the dissolved oxygen concentration measured.

The oxygen isotope of seawater ($\delta^{18}O$-H_2O) samples within the inner-plume was calculated based on salinity, using the combined datasets from Hölemann et al. (2021) & Létolle et al. (1993) displayed on Figure 4.2. $\delta^{18}O$-H_2O was calculated as

$$\partial^{18}O - H_2O = 0.4897 * S - 19.964 \qquad \textit{Eq. 4.2}$$

following the linear regression observed between salinity & $\delta^{18}O$-H_2O in both datasets. The correlation is very strong ($R^2 = 0.98$) in the salinity range of 0-29psu, and does not appear to significantly change seasonally.

As no trend is observed in marine samples (S>29 psu), an average endmember value was calculated instead for samples from the outer-plume, within the range of 29-31 psu ($\delta^{18}O$-H_2O = -4.10‰ ± 0.11‰). $\delta^{18}O$-H_2O for the AW endmember at the Laptev Sea (S>31 psu) was defined as $\delta^{18}O$-H_2O = 0.3‰ as reported in Bauch et al. (2010).

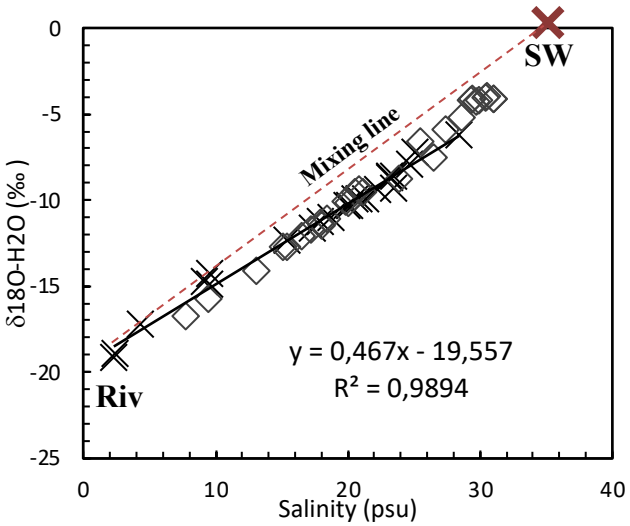

Figure 4.2. Relationship between salinity & $\delta^{18}O$-H_2O in the combined datasets of Hölemann et al. (2021) & Létolle et al. (1993). This relationship is used to predict $\delta^{18}O$-H_2O of samples for AMK73 samples. Equation displays least squares regression between the two parameters.

4.2.2.1 Determination of freshwater fraction

The contribution of freshwater to each individual sample was quantified using mass balance equations of salinity and $\delta^{18}O\text{-}H_2O$ based on the three major endembers of the Arctic Ocean: marine (AW), riverine water and sea-ice melt following the method described in Bauch et al. (1995).

$$f_{sw} + f_{riv} + f_{sim} = 1 \qquad \textit{Eq. 4.3}$$

$$S_{measured} = f_{sw} * S_{sw} + f_{riv} * S_{riv} + f_{sim} * S_{sim} \qquad \textit{Eq. 4.4}$$

$$\partial^{18}O_{corrected} = f_{sw} * \partial^{18}O_{sw} + f_{riv} * \partial^{18}O_{riv} + f_{sim} * \partial^{18}O_{sim} \qquad \textit{Eq. 4.5}$$

Where f_{sw}, f_{riv} and f_{sim} are the fractions of seawater, riverine water and sea-ice melt respectively. S_{sw}, S_{riv} and S_{sim} are the endmember salinities for seawater, riverine water and sea-ice melt respectively. $\delta^{18}O_{sw}$, $\delta^{18}O_{riv}$ and $\delta^{18}O_{sim}$ are the respective $\delta^{18}O\text{-}H_2O$ for these endmembers. Endmember values were defined for the Laptev Sea and the Lena Delta following work from Bauch et al. (2010) and Thibodeau et al. (2017). These are shown in Table 4.1 below.

Table 4.1. Parameters used in mass balance equations to calculate freshwater fractions of AMK73 samples.

Endmember	Salinity (PSU)	$\delta^{18}O\text{-}H_2O$ (‰)
Seawater	34.92	0.3
Riverine	0	-20
Sea-ice	4	2.6

4.2.3 Dissolved nutrient concentrations

Dissolved inorganic nutrient concentrations were determined live onboard using an autoanalyzer following standard colorimetric methods. The underway samples are immediately frozen onc collection and subsequently analyzed for nutrient concentrations, DOCz and TDN at the Scottish Association for Marine Science using

a Shimadzu TOC-V analyser and reference materials from the University of Miami (Hansell lab) were run within each batch. The semi-conservative tracers N* & Si* were calculated from inorganic nutrient concentrations where $N^* = NO_x - PO_4^- * 16$, adapted from Gruber & Sarmiento (1997), and $Si^* = SiOH_4 - NO_x$ (Sarmiento et al., 2004). Both tracers are indicative of deviation from typical Redfield ratio and average DSi:N ratios of marine dissolved nutrient ratios respectively.

4.2.4 Silicon isotopes

Water samples were collected from Niskin bottles onboard and from the ship's underway system and filtered inline using Nuclepore polycarbonate membranes (0.4μm pore size). These were immediately acidified with 0.1% v/v 12M HCl for preservation and stored at 4°C until analysis. $\delta^{30}Si$ was determined following the protocol described in Chapter 2.3.2 for low concentration determination (<10μM), following the Magnesium Induced Coprecipitation (MAGIC) method described in Karl and Tien (1992) and Brzezinski et al. (2003) and Reynolds et al. (2006).

Resulting solutions were analysed on a Nu Plasma II MC-ICP-MS at the University of Edinburgh, using standard-sample bracketing protocol (Georg et al., 2006b) and the primary isotopic standard NBS28. Following corrections described in section 2.4, $\delta^{29}Si$ was converted to $\delta^{30}Si$ using a theoretical conversion factor of 1.96, as calculated from the kinetic fractionation law (Young et al., 2002). This correction was applied to avoid interference on $\delta^{30}Si$ measurements from the low concentrations (Fripiat et al., 2011a, 2011b; Liguori et al., 2021).

The international solid standard Big Batch and both high and low concentration seawater standards $Aloha_{1000}$ and $Aloha_{300}$ were used as reference materials for measurement precision and method reproducibility at low concentrations. Standards were measured with each sample batch. Average standard measurements for the period of this study are: BigBatch = -5.35 ± 0.04‰ (n=8), $Aloha_{1000}$= 0.63 ± 0.05‰ (n=8) and $Aloha_{300}$= 0.84 ± 0.02‰ (n=7) for $\delta^{29}Si(OH)_4$, with converted $\delta^{30}Si(OH)_4$ as follow: BigBatch = -10.51 ± 0.08‰, $Aloha_{1000}$= 1.25 ± 0.10‰ and $Aloha_{300}$= 1.66 ± 0.05‰. This aligns extremely well with $\delta^{30}Si(OH)_4$ inter-laboratory

measurements of BigBatch = -10.48 ± 0.2‰, $Aloha_{1000}$= 1.25 ± 0.2‰, $Aloha_{300}$= 1.66± 0.35‰ (Grasse et al., 2017; Reynolds et al., 2007).

4.3 Result

4.3.1 Eurasian shelf transect

Displayed on Figure 4.3 is the riverine fraction of shelf waters increases from West to East (from <10% in the Barents Sea to 30-40% in the Laptev Sea). This illustrates the freshening of eastward-travelling surface boundary currents (Osadchiev et al., 2020) as it gradually picks up riverine discharge. Along the Ob & Yenisey river mouth, riverine fractions reach >60%, and >90% near the Lena Delta, indicative of the riverine freshwater plumes that form from major Siberian rivers in the Kara and Laptev Sea (Spivak et al., 2021).

Peaks in DSi are observed at the inflows of the Ob & Yenisey (>20 μM) and the Lena Delta (>30 μM), with a general increase in DSi from West to East, with concentrations of ~5 μM in the Barents Sea increasing to >10 μM in the East Kara Sea & the Laptev Sea, showing riverine discharge is increasing the DSi content as well as modifying nutrient stoichiometry of surface shelf waters from DSi:N <10 to >15.

Positive $\delta^{30}Si(OH)_4$ are measured and range from 0.74 – 2.41‰ across the transect. The isotopically lowest measurements are found in the Lena Delta plume in samples that have the highest riverine fraction (0.74 – 1.44‰), which aligns well with estimations of 0.86 ± 0.3‰ from Sun et al., (2018) for the average signature of the annual Lena Delta $\delta^{30}Si(OH)_4$ influx. Lighter $\delta^{30}Si(OH)_4$ are also measured in the Ob & Yenisey plume (1.78 – 1.95‰), in agreement with findings in Mavromatis et al. (2016) that the $\delta^{30}Si(OH)_4$ of the Yenisey is isotopically heavier than other Eurasian rivers due to deep underground flow through permafrost. Away from the freshwater plumes, a general increase in $\delta^{30}Si(OH)_4$ is observed from lower longitudes of the East Kara Sea to the East of the Laptev Sea, increasing from ~1.8‰ to ~2.4‰ while DSi concentrations remain ~12 μM.

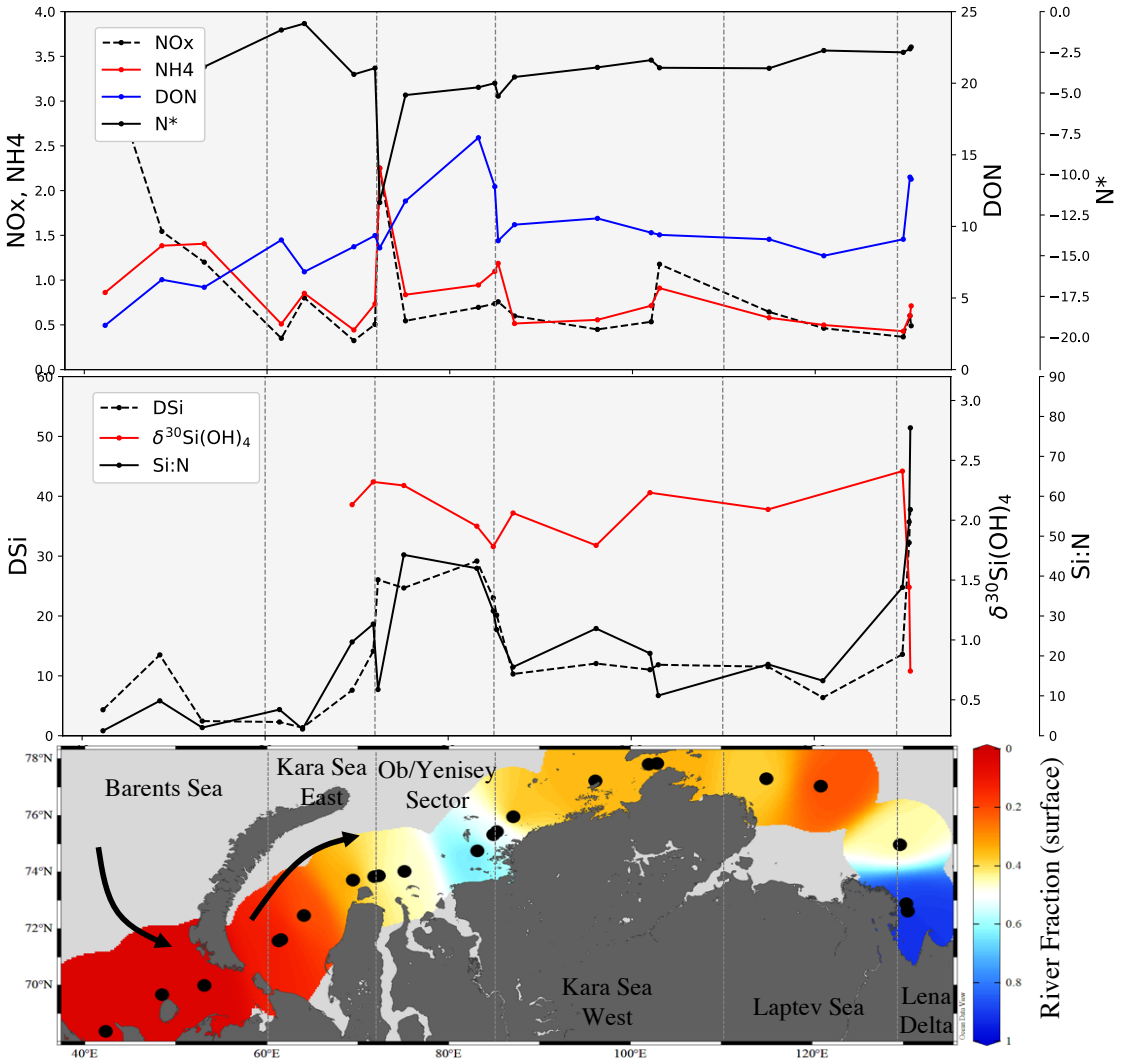

Figure 4.3. Longitudinal transect of nutrient concentrations and isotopic measurements of underway samples of AMK73. Top panel: Dotted black lines display surface concentrations of NO_x (nitrate + nitrite, µM) concentrations, red line is ammonia (µM), blue line is Dissolved Organic Nitrogen (DON, µM), and black line is N* (= NO_x – 16*PO_4) with longitude along the Eurasian shelf. Middle panel: Displayed are surface concentrations of DSi (black dotted line, µM), $\delta^{30}Si(OH)_4$ (red line, ‰) and Si:N (black line) with longitude along the Eurasian shelf. Bottom panel: Calculated riverine contribution to underway measurements along the transect. BS = Barents Sea, KS = Kara Sea, OB/YN = Ob & Yenisey river inflow, LS = Laptev Sea, LD = Lena Delta inflows.

4.3.2 Laptev Sea transect

4.3.2.1 Hydrographic structure

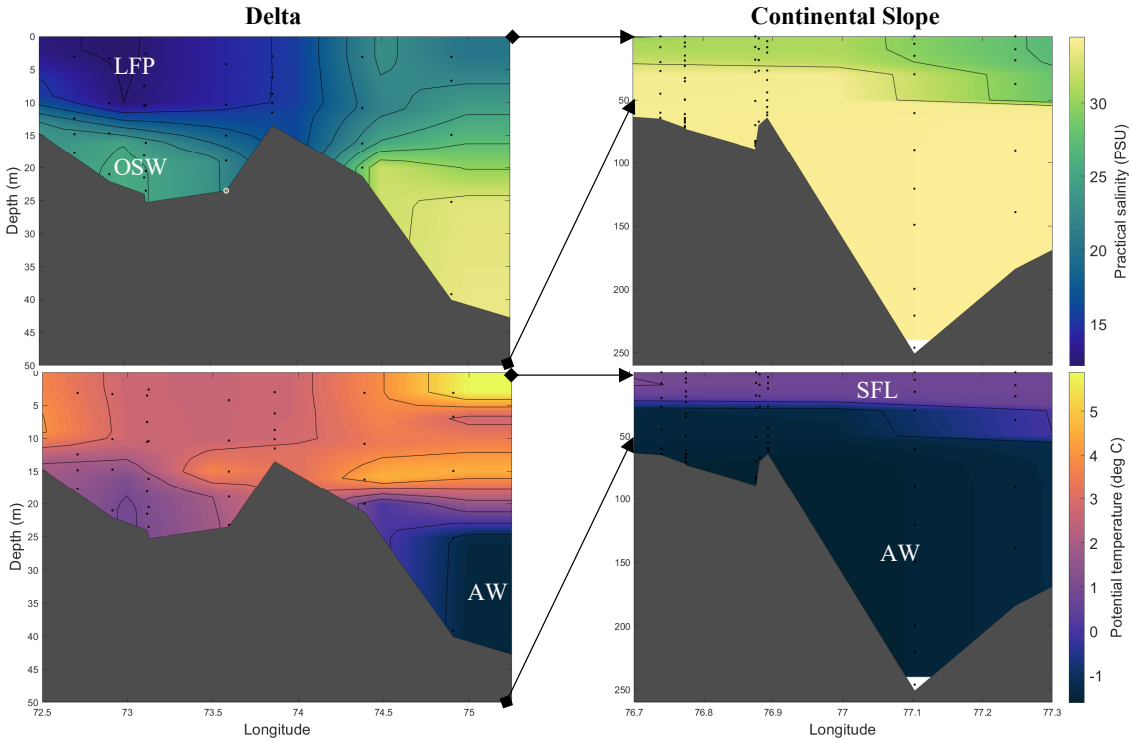

Figure 4.4. Hydrography of the Laptev Sea in October 2018 along the CTD transect of AMK73. Left pannels: Lena Delta. Right pannels: Laptev shelf and continental slope. Top pannels show salinity (PSU) and bottom pannels show temperature (˚C). LFP = Lena Freshwater Plume, OSW = Old Shelf Water, AW = Advected Atlantic Water, SFL = Surface Freshwater Layer.

As shown on Figure 4.4, large salinity and temperature gradients are observed in the estuarine region across the Lena delta and the continental slope of the Laptev Sea. Salinity varies from <10 psu in the upper 10m of the water column near the Lena Delta to >34 psu over the continental slope. Temperatures vary from 2-5˚C around the Lena Delta to 1˚C in the upper 30m of the continental slope, overlaying cold (-1˚C), saline waters.

The fresh, colder plume of water in the upper 15m of the Lena Delta region (at latitudes of 72.5˚- 74.5˚) characterizes the core of LFP. During the expedition of AMK73 in October 2018, this extends out northward and contributes to a Surface Freshwater Layer (SFL) in the upper 20m of the water column, overriding denser, more saline advected and modified Atlantic Waters (AW). Under the LFP, colder,

more saline (<1˚C, >25 psu) waters are found, characteristic of Older Shelf Water (OSW) constrained locally by hydrography (Kostyleva et al., 2020; Létolle et al., 1993). The LFP and SFL are strongly stratified in the summer months from the surrounding waters by steep salinity gradients, restricting the exchange of nutrients, before mixing in the winter (Janout et al., 2020).

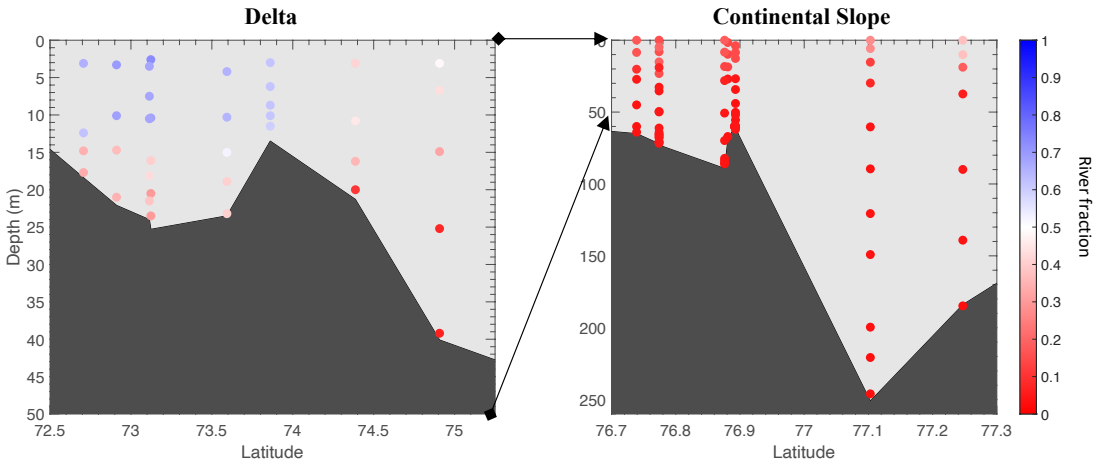

Figure 4.5. Calculated riverine fraction of samples along the CTD transect of AMK73 for the shallow Lena Delta (left) and continental slope (right).

Figure 4.5 displays the calculated riverine fraction of samples for the transect. The LFP has the highest riverine content with >70% of freshwater. The influence of riverine freshwater decreases in the SFL but is still high, with a riverine content between 20-50%. OSW have >30% of riverine fraction, indicating a strong influence from the overlaying river plume. Over the continental shelf, AW has relatively small freshwater content (<10%) as stratification restricts mixing.

4.3.2.2 Nitrogen concentrations & distribution

Figure 4.6 displays the distribution of NO_x, DON and the derived parameter N*. Overall, nutrient distribution largely follows the major hydrographic structure of the transect. In the LFP, NO_x is depleted (<1 µM), but DON concentrations are high (>10 µM), confirming N supplied by the Lena river is mostly in organic form in the summer (Holmes et al., 2012; Thibodeau et al., 2017a). DON concentrations rapidly decrease in the SFL while NO_x remains low. In the advecting AW, NO_x concentrations are high (>10 µM) sourced from the Atlantic Ocean. In the OSW,

NO_x is varying locally but generally the concentrations are higher near the bottom, potentially reflecting benthic remineralisation of nitrogen and subsequent sedimentary supply to the water column (Sun et al., 2021). N*, where positive values reflect the relative enrichment of nitrate in comparison to phosphate (Sarmiento et al., 2004), are highly variable over the section (bottom panels of Figure 4.6). In the LFP and the SFL, N* is negative, ranging from -2 to -4, reflective of N-limitation during uptake and denitrification on Arctic shelves. Negative N* values are observed down to the sediments and decrease offshore of the Lena Delta, indicating N removal is not limited to the euphotic zone. Positive N* is observed in AW advecting over the Laptev Sea shelf, indicative of N-enrichment from Atlantic origins, while N* remains negative in the upper fresh water layer of the continental slope.

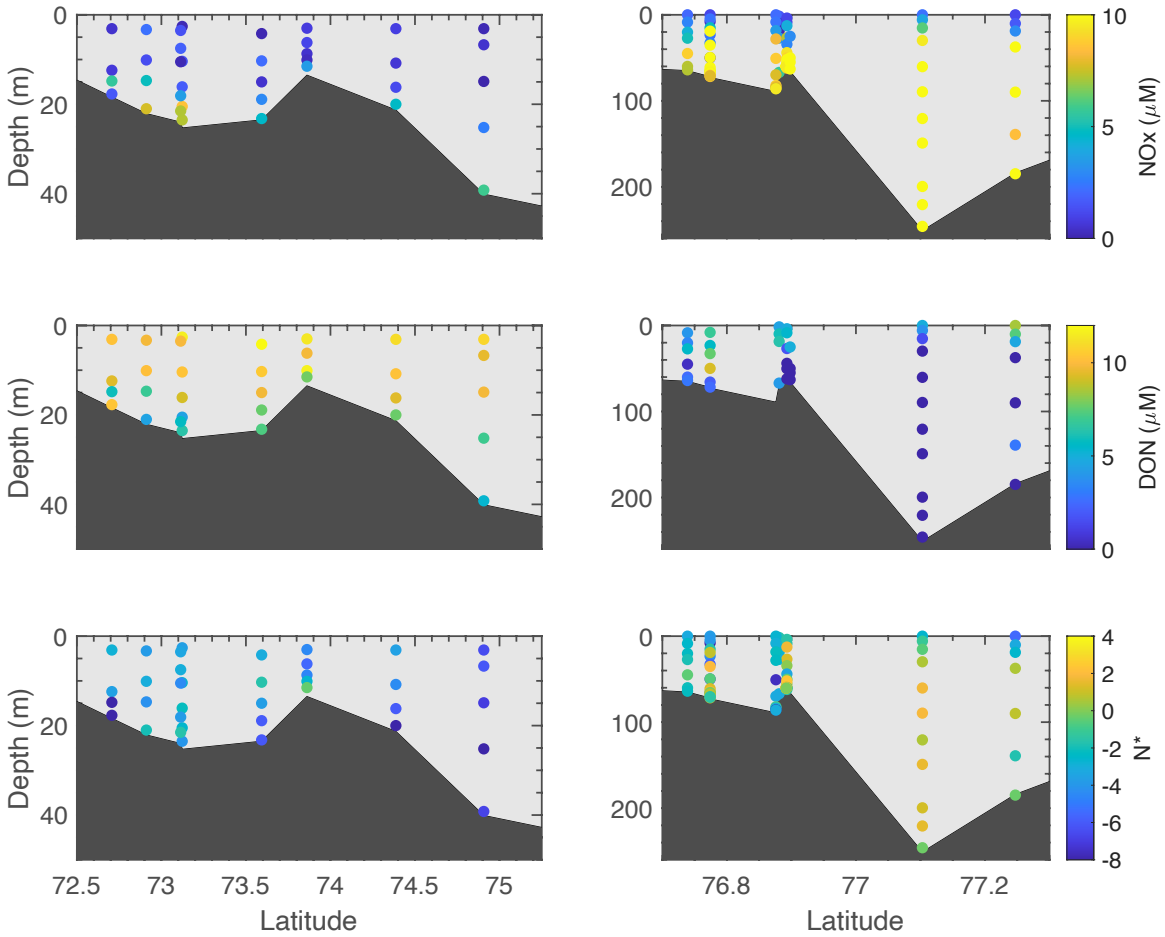

Figure 4.6. NO_x (= NO_3 + NO_2, top panels), Dissolved Organic Nitrogen (DON, middle panels), and N* (= NO_3 – 16*PO_4, Sarmiento et al., 2004, bottom panels) along the Lena Delta (left panels) and over the continental slope (right panels) for AMK73.

4.3.2.3 Silicon concentrations & isotope distribution

DSi concentrations, the derived parameter Si* and $\delta^{30}Si(OH)_4$ for the Laptev Sea transect are shown on Figure 4.7. DSi concentrations follow the riverine fraction shown on Figure 4.5, with high concentrations (>30 µM) in the LFP which subsequently decrease in the SFL. This follows previous findings that with exception to OSW, DSi is well corelated with riverine influence from the Lena river (Kostyleva et al., 2020; Létolle et al., 1993). Over the continental slope, low DSi concentrations are generally observed, reflective of DSi-poor AW owing to its origins in the North Atlantic. A gradient is observed in Si* from South to North along the transect. Positive Si* (>20) are observed close to the Lena Delta, reflecting the high DSi:N stoichiometry of terrestrially supplied nutrients, with values gradually decreasing to reach negative (<0) over the continental slope.

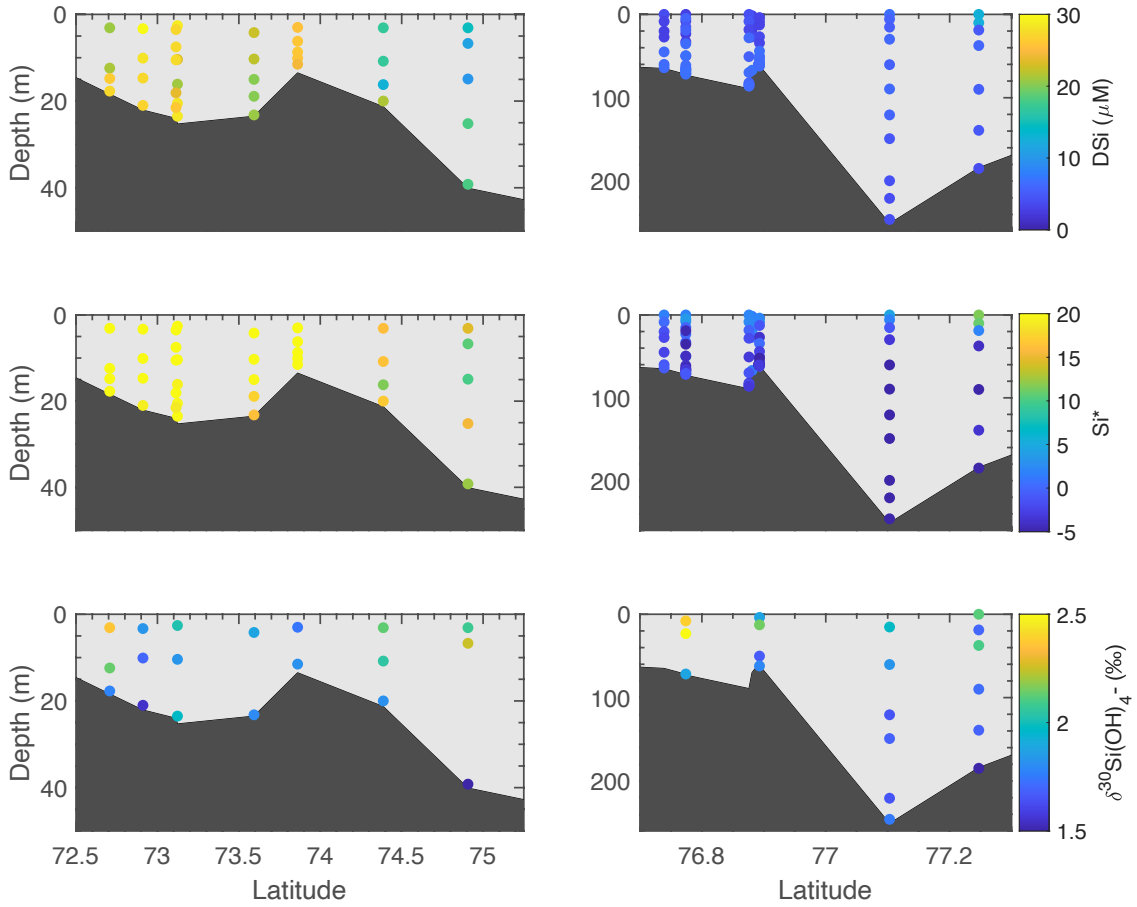

Figure 4.7. DSi (top panels), Si* (= DSi – NO_3, middle panels) and $\delta^{30}Si(OH)_4$ (bottom panels) along the Lena Delta (left panels) and over the continental slope (right panels) for AMK73.

Positive $\delta^{30}Si(OH)_4$ values are measured and range from 1.43 – 2.55‰ along the transect. Generally, isotopically higher values are measured towards the surface in the LFP and FSL, with decreased DSi concentrations, consistent with fractionation from biological uptake by silicifying species (i.e diatoms) during growth. The average $\delta^{30}Si(OH)_4$ for AW is 1.72 ± 0.16‰, which aligns with measurements of $\delta^{30}Si(OH)_4$ of AW at Fram Strait (see Chapter 2) and aligns closely with measurements of waters from North Atlantic origin (Brzezinski and Jones, 2015; De Souza et al., 2012), confirming the DSi in AW is of Atlantic origins. In the LSP, $\delta^{30}Si(OH)_4$ is variable but generally high (1.95 ± 0.2‰) with high DSi concentrations (25 ± 2 μM).

4.4 Discussion

DSi concentrations & nutrient stoichiometry along the Eurasian shelf are strongly linked to the local hydrography and displays a particularly strong relationship with riverine influence (Figure 4.3, Figure 4.5 & Figure 4.7), highlighting the role of Eurasian rivers in modifying freshwater and nutrient budgets of Arctic shelves. Here we focus on the processes that transform riverine inputs, as well as the controls on DSi removal and export to the central Arctic Ocean.

4.4.1 Transformation of DSi along the Eurasian shelf

Waters of Arctic origins are isotopically heavy. The origins of this enrichment were initially associated with physical mixing processes (Liguori et al., 2020; Varela et al., 2016), although findings from Chapter 3 point towards the partial utilisation of DSi on Arctic shelves instead (Brzezinski et al., 2021; Liguori et al., 2021). Surface measurements from the Eurasian shelf in this study (Figure 4.3) show that rivers supply high DSi loads through large peaks in concentrations which rapidly decrease away from river mouths. We observe a gradual modification of $\delta^{30}Si(OH)_4$ in surface waters (+ 0.6‰) with an increase of ~1 μM of DSi. Terrestrial sources of DSi to the Arctic Ocean are isotopically light (Mavromatis et al., 2016; Pokrovsky et al., 2013; Sun et al., 2018) from weathering of bedrock with low $\delta^{30}Si(OH)_4$.

Sea ice brine, a potential source of DSi, has a $\delta^{30}Si(OH)_4$ equal or heavier than surrounding waters (Fripiat et al., 2007, 2014) although evidence of this influence in the Arctic Ocean remains limited (Section 3.4.2, Brzezinski et al., 2021) and no statistically significant increase in the sea-ice melt fraction of underway samples was measured in this study. The small increase in DSi concentrations coupled with increasing $\delta^{30}Si(OH)_4$ of surface waters reflects the addition of terrestrial DSi coupled with biological consumption of DSi simultaneously occurring on the shallow Eurasian shelves, thereby enriching $\delta^{30}Si(OH)_4$. DSi is only partially utilised, as NO_x concentrations are depleted (<1 μM), preventing further biological uptake of DSi and thereby fractionating $\delta^{30}Si(OH)_4$ away from light source values. A significant fraction of biological Si must be trapped in the sediments for ambient water signatures to remain enriched, as sedimentary dissolution of biological Si would otherwise return $\delta^{30}Si(OH)_4$ towards source values. A study of porewater nutrient concentrations from Sun et al. (2021) highlights this regionally, with high DSi concentrations in the sediments of the Laptev and East Siberian shelf (100-250 μM) indicating significant sedimentary burial of DSi.

We find in section 4.1 that rivers supply a high DSi load which is removed to a large extent away from riverine sources while N concentrations remain low (Figure 4.3 & 4.6). In the next section, we explore the cycling processes which can enable substantial DSi removal in N-limited conditions.

4.4.2 Nitrogen dynamics in the Laptev Sea

Generally in the Arctic Ocean, primary production is N-limited (Le Fouest et al., 2013; Tuerena et al., 2021c) and is exacerbated locally around river mouths from terrestrial inputs with high DSi:N ratio and through benthic denitrification which removes excess N (Chang and Devol, 2009). Substantial benthic N loss due to denitrification has been documented in the Laptev Sea (Sun et al., 2021). Additionally, diatoms have a large nitrate requirement relative to P (Glibert et al., 2016), which may further exacerbate N-deficiency. Thus, diatom production and biological DSi drawdown can be limited by the availability of N-locally, and controls the proportion of terrestrial DSi which is removed on Eurasian shelves.

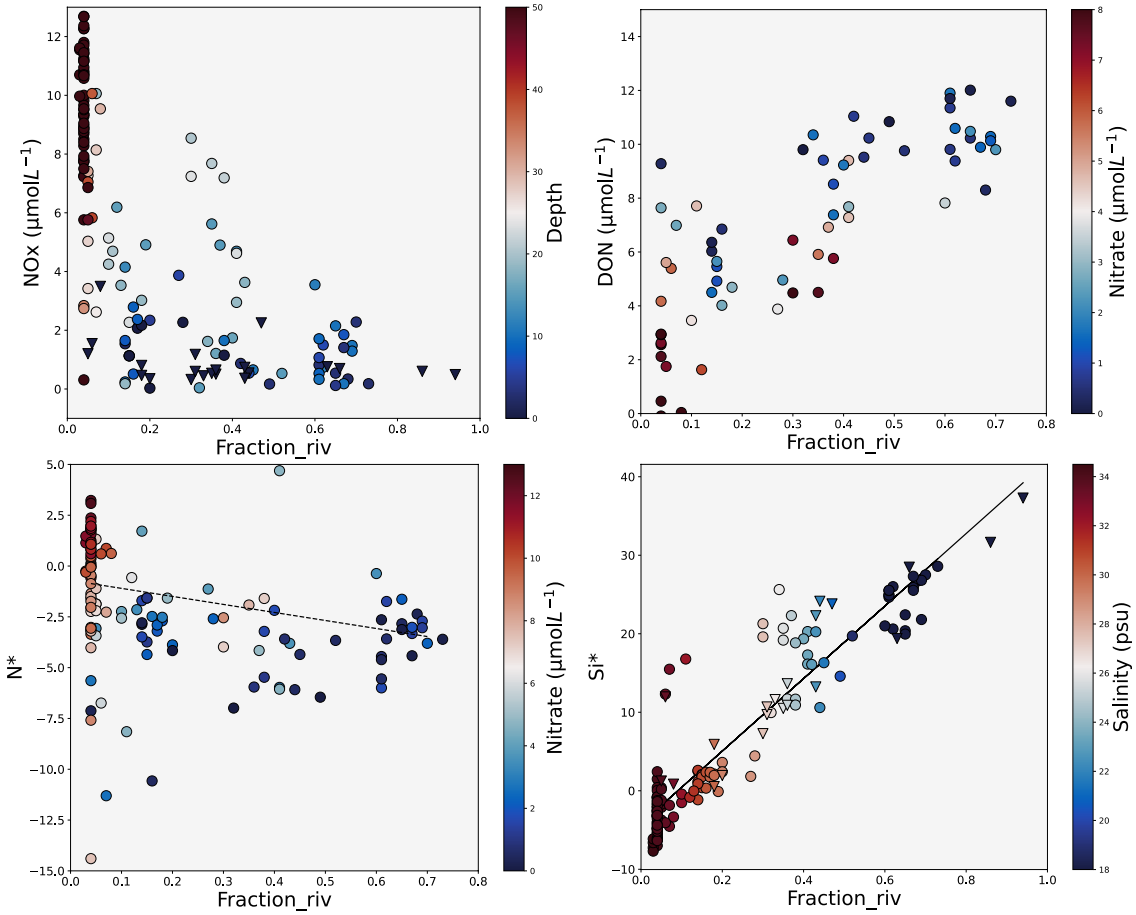

Figure 4.8: Nitrogen species and their derived parameters with relation to riverine content of samples on AMK73. Top left: NO_x (= NO_3 + NO_2, µmolL^{-1}) against riverine fraction, color scale is depth (m). Top right: Dissolved Organic Nitrogen (DON, µmolL^{-1}) against riverine fraction, color scale is nitrate (µmolL^{-1}). Bottom left: N* (= NO_3 – 16*PO_4) against riverine fraction, color scale is nitrate (µmolL^{-1}). Dotted black line shows least square regression. Bottom right: Si* (= DSi – NO_3) against riverine fraction, color scale is salinity (psu). Black line shows least square regression. Circles show measurements from CTD casts, triangles are from the ship's underway system.

Riverine input of nutrients from Eurasian rivers typically have low DSi:N ratio (Holmes et al., 2012), and thereby modify nutrient stoichiometry as well as the inventory of shelf waters, leading to a N-deficit with respect to DSi compared to traditional Redfield ratio (Tuerena et al., 2021c). This is seen through the increase of DSi:N ratio across the Eurasian shelf on Figure 4.3 and is also observed in the Lena Delta, where DSi concentrations are high within the LFP and well in excess with respect to N (middle panel of Figure 4.7). Additionally to low DSi:N terrestrial input,

N is actively removed on Eurasian shelves through strong processes of denitrification (Le Fouest et al., 2013; Fripiat et al., 2018; Sun et al., 2021). As nitrogen availability regulates DSi drawdown and DSi uptake in the TPD was found to be limited by N (Liguori et al., 2021), here we examine the availability and cycling of N in the Laptev Sea and evaluate the implications on DSi distribution.

Nitrogen from Eurasian rivers is primarily supplied in the form of DON, particularly over the summer months where nitrate represents only 20% of the total DON flux (Holmes et al., 2012). This trend is observed within our study (Figure 4.6), with high (>10 $\mu molL^{-1}$) DON concentrations within the LFP, while nitrate concentrations are low (<2 $\mu molL^{-1}$). While DON is not directly available to phytoplankton for uptake, it is quickly remineralised to nitrate on the Laptev Sea shelf (62-76% of DON released from the Lena river is removed within 2 months, Thibodeau et al., 2017). Residence time of waters on Eurasian shelves is estimated to be 1-2 years prior to export through the TPD (Semiletov et al., 2000), and 70% of terrestrial DON is consumed within a couple of years before reaching the marine endmember (Letscher et al., 2013). We observe the conversion of DON to nitrate locally within our study, where samples with lower DON at riverine fractions <0.5 are characterized with higher nitrate, increasing availability of N for primary production.

Despite the local supply of DON, NO_x (= NO_3 + NO_2) concentrations in the study area remain very low overall. In the LFP, NO_x concentrations are depleted (<1 $\mu molL^{-1}$), with concentrations varying between 0-8 $\mu molL^{-1}$ over the shelf. The average nitrate concentration of Eurasian rivers is 4.2 $\mu molL^{-1}$ (Holmes et al., 2019 from Charette et al., 2020), depletion of NO_x to the concentrations observed in the shelf area imply significant fast removal in the estuary or on the shelf through biological uptake and/or denitrification (Le Fouest et al., 2013; Thibodeau et al., 2017a). Supply of additional N through DON cycling appears to be rapidly utilized, with nitrate concentrations quickly returning to near-complete depletion. The non-linear relationship between nitrate concentrations and N* with river fraction confirms N-deficit is not governed by dilution but is actively removed from surface waters via N-removal processes, with an excess of terrestrial-originating phosphate exported. As per previous studies, the left panel of Fig 4.9 shows that DSi behaves quasi-

conservatively when oceanic and riverine waters mix in the coastal zone (Létolle et al., 1993), and excess export of DSi from riverine sources is also observed, as highlighted by the linear trend between Si* and riverine fraction, with DSi excess of up to 30 $\mu molL^{-1}$ in relation to NO_x.

The DSi:N requirement for diatom consumption on Arctic shelves is estimated between 1.8-2.1 (Macdonald et al., 2010; Simpson et al., 2008; Tremblay et al., 2008). This is lower than DSi:N ratio observed along the Eurasian shelves owing to depleted nitrate concentrations (Figure 4.3). Instead, DSi:N covaries with DSi concentrations, and is thus dictated by DSi variability. The extremely low NO_x concentrations and higher concentrations of phosphate and DSi confirm nitrate is the limiting nutrient of primary production, limiting DSi drawdown and modulating its export to the TPD (Chapter 3.4.2, Doncila et al., 2019).

Significant benthic efflux of nutrients is present on the Laptev shelf. Benthic DSi fluxes for the Laptev Sea were estimated at 15% of the total riverine input, and 29% for NO_x (Sun et al., 2021). This implies that terrestrial NO_x is recycled twice as much as DSi, fueling "new" DSi utilisation and potentially increasing net opal burial. Evidence for nutrient regeneration is observed in the OSW of the section, with increased DSi and NO_x concentrations (Figure 4.6, 4.7) and isotopically lower $\delta^{30}Si(OH)_4$ by ~0.4‰ (Figure 4.6), indicative of dissolution of biogenic Si towards the sediment interface, and lower ambient water $\delta^{30}Si(OH)_4$ locally.

These benthic fluxes illustrate that geochemical cycling of N is vigorous on the shallow Laptev sea shelf, where N is recycled at least twice as much as DSi. The differential recycling of N & DSi allows for additional uptake of DSi by diatoms. Considering the processes of recycling and removal of nutrients illustrated above on Arctic shelves, in the following section we aim to quantify the burial of terrestrial DSi on shelves through isotopic constraints. Later we evaluate whether shelf processes characterized within this study allow us to close the gap in the Arctic Ocean's isotope budget.

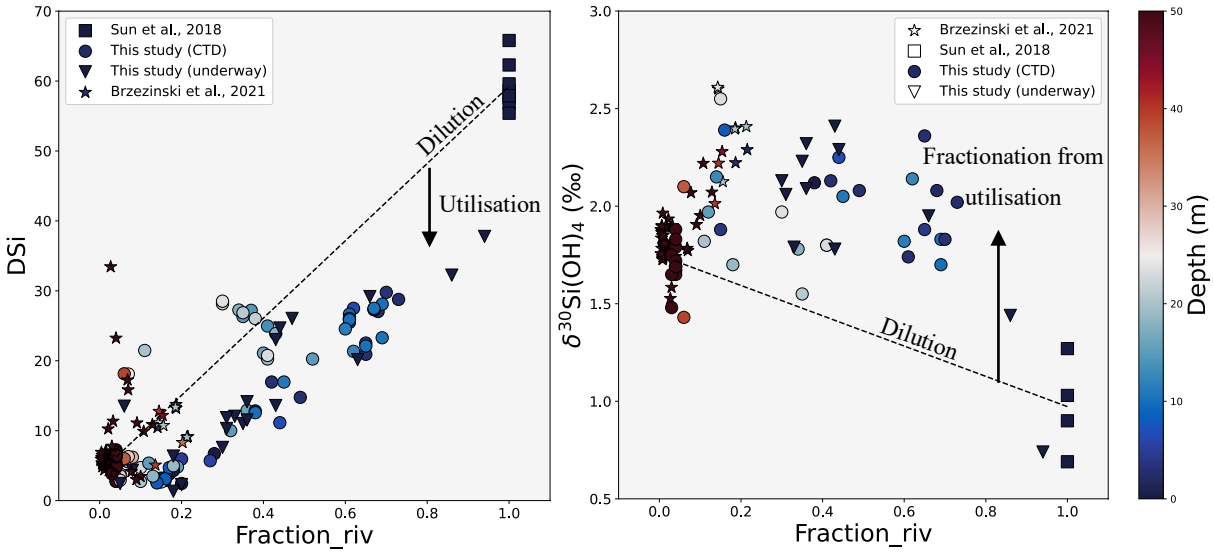

Figure 4.9: DSi (left) and $\delta^{30}Si(OH)_4$ (right) against riverine fraction. Circles show measurements from CTD casts of this study, (AMK73), triangles are from the ship's underway system. Black squares are measurements from the Lena river (Sun et al., 2018), and stars are from transpolar drift stations (stations 30, 32, 38 & 43, depths < 500m) in the central Arctic Ocean (Brzezinski et al., 2021). Color scale is depth (m). Dotted lines show the theoretical conservative mixing line between the Atlantic Water (AW) endmember (defined here as riverine fraction <0.1) and the Lena river freshwater endmember at the main river outflow below the three main tributaries (from Sun et al., 2018).

4.4.3 Calculating DSi removal on the Laptev shelf

We have established that N is the limiting nutrient to primary productivity in the Laptev Sea, and modulates the fraction of DSi which is removed on Arctic shelves. Figure 4.9 shows the $\delta^{30}Si(OH)_4$ of waters in the Laptev Sea from this study in comparison with TPD $\delta^{30}Si(OH)_4$ from Brzezinski et al. (2021). Surface waters of the TPD with high riverine influence (>0.1) meet the trend of increasing $\delta^{30}Si(OH)_4$ as DSi is utilised on the Laptev shelf and over the continental slope in our study. $\delta^{30}Si(OH)_4$ signatures show mixing between AW-sourced DSi and isotopically-enriched DSi sourced from Eurasian rivers and partially utilised on the Eurasian shelves, illustrating that DSi from Eurasian shelves directly feeds into the export of inorganic nutrients to the central Arctic Ocean, namely through the TPD. Findings from Liguori et al. (2021) concur with direct evidence of isotopically heavy Eurasian

shelf-derived DSi in the TPD. As geochemical cycling of nutrients on the Arctic shelves directly controls export and nutrient cycles in the central Arctic Ocean, next we attempt to quantify the proportion of DSi which is removed in the shelf area using $\delta^{30}Si(OH)_4$ and simple mixing models.

Figure 4.9 displays the trend between the fraction of riverine water in each sample and their respective $\delta^{30}Si(OH)_4$ isotopic signature. The dotted black line shows the theoretical conservative mixing line between the Lena river riverine endmember (main river outflow below main tributaries, Sun et al., 2018) and the AW endmember measured on the Laptev Shelf in this study ($\delta^{30}Si(OH)_4$ = 1.72‰). This trendline assumes the $\delta^{30}Si(OH)_4$ is only controlled by physical mixing between the two endmembers, and no modification via biological processes are occurring. All samples with a riverine fraction >0.1 fall above this mixing line by up to 1.1‰. As there is a net deficit of DSi compared to the theoretical mixing line, the enrichment of $\delta^{30}Si(OH)_4$ can be attributed to significant biological fractionation by phytoplankton growth and implies removal of a significant proportion of riverine DSi through subsequent burial in the shelf sediments.

We evaluate the percentage of riverine DSi removal on the Laptev shelf using $\delta^{30}Si(OH)_4$ through two simple models, described by Eq. 4.6 and 4.7. The first model is described by the Rayleigh distillation equation:

$$\delta^{30}\mathrm{Si(OH)}_{4-\mathrm{observed}} = \delta^{30}\mathrm{Si(OH)}_{4-\mathrm{source}} + {}^{30}\varepsilon \ln(f) \qquad \textit{Eq. 4.6}$$

And assumes a closed system where nutrient consumption at the surface is not replenished by external sources of nutrients. As the Lena freshwater plume is strongly stratified by salinity, we expect replenishment of nutrients to the surface via mixing with underlying waters to be limited and estimate that the equation for a closed system is a good approximation of the physical conditions on the Laptev Sea shelf in late summer 2018. To encapsulate potential nutrient replenishment to the plume, a second open model is used which assumes nutrient inputs to the plume are equal to nutrient outputs, where:

$$\delta^{30}\mathrm{Si(OH)}_{4-\mathrm{observed}} = \delta^{30}\mathrm{Si(OH)}_{4-\mathrm{source}} + {}^{30}\varepsilon\,(1-f) \qquad \textit{Eq. 4.7}$$

For both systems, $\delta^{30}Si(OH)_{4\,-\,observed}$ is the measured $\delta^{30}Si(OH)_4$ of a sample, $\delta^{30}Si(OH)_{4\,-\,source}$ is the $\delta^{30}Si(OH)_4$ in surface water prior to biological utilization. f is the fraction of DSi remaining and is described as:

$$f = \frac{[\mathrm{Si(OH)}_{4-\mathrm{observed}}]}{\mathrm{Si(OH)}_{4-\mathrm{source}}} \qquad \textit{Eq. 4.8}$$

And $^{30}\varepsilon$ is the biological fractionation factor of $\delta^{30}Si(OH)_4$ in surface water. For this study, we used a fractionation factor of $^{30}\varepsilon$ = -1.07‰, an average $^{30}\varepsilon$ estimation from modern studies in the global ocean for closed-system kinematics (Giesbrecht et al., 2022 and references herein). A range of $^{30}\varepsilon$ was also used to encompass for the average $^{30}\varepsilon$ of open-system in the global ocean ($^{30}\varepsilon$ = -1.14), and for in-field measurements of closed-system fractionation in the Canadian Arctic sector ($^{30}\varepsilon$ = -0.59, from Giesbrecht et al., 2022).

Due to the large salinity gradient across the shelf and the significant importance of dilution to measured DSi concentrations, the $\delta^{30}Si(OH)_{4\,-\,source}$ of surface waters is composed of a mixture between the AW and the Lena river endmember ($\delta^{30}Si(OH)_4$ = 0.97‰, Sun et al., 2018), and is varying. Therefore, the $\delta^{30}Si(OH)_{4\,-\,source}$ for an individual sample was adjusted for dilution through its riverine fraction (F_{riv}) through the following relationship to account for physical mixing:

$$\delta^{30}\mathrm{Si(OH)}_{4-\mathrm{source}} = -0.776 * \mathrm{F_{riv}} + 1.749 \qquad \textit{Eq. 4.9}$$

Where the gradient and intercept were calculated from the mixing line on Figure 4.9.

Using a closed-system model for $^{30}\varepsilon$ = -1.07‰, the estimated mean shelf DSi removal from riverine input along the sector is 43 ± 13% when taking the average of all $\delta^{30}Si(OH)_4$ measurements from this study at F_{riv}>0.1 on Fig. 4.9. This aligns with findings from Charette et al., (2020) who found that 43% of DSi is removed in estuaries or over the shelf prior to transport in the TPD. This is significantly higher than a similar estimation based on DSi alone for this study (33 ± 23%) and previous

findings that 9-24% of the riverine supply of DSi does not get consumed by phytoplankton due to nitrogen limitation (Le Fouest et al., 2013). This suggests that nutrient concentrations from the shelf alone underestimate siliceous primary productivity on the Laptev Sea Shelf, and highlights the role of recycled nitrate within the water column to sustain further drawdown of DSi. Isotopically-based calculations are significantly more accurate compared to deduction from concentration data. Different estimations of removal are 54 ± 20% for open system model where $^{30}\varepsilon$ = -1.14‰ (Global Ocean), and 62 ± 16% for closed system model where $^{30}\varepsilon$= -0.59‰ (Canadian Arctic). Significant removal is observed over the large range of $^{30}\varepsilon$ even though open system and Canadian Arctic $^{30}\varepsilon$ are less likely to describe the hydrographic conditions of the transect, leading to overestimation of removal of DSi compared to the export observed through the TPD.

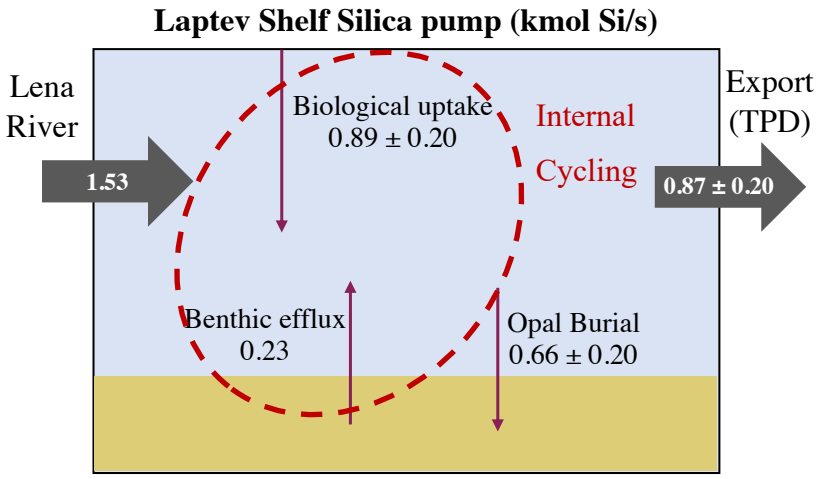

Figure 4.10. Schematic of the Laptev shelf Si pump with riverine supply of DSi (Holmes et al., 2012), export out of the continental shelf, opal burial and the internal cycling processes of biological uptake and benthic efflux (Sun et al., 2021). In this budget, riverine inputs = export to TPD + opal burial. Inside the dotted red circle shows internal cycling processes. Water column dissolution of opal is assumed to be negligible due to small water column depths (<50m) and continuous riverine supply of DSi. All fluxes are shown in kmolSi/s.

The biological pump of the Laptev Sea sequesters a significant amount of opal. On an annual basis, 1.53 kmolSi/s is supplied from the Lena river (Holmes et al., 2012), and assuming an integrated 43% removal as per above, 0.87 ± 0.20 kmolSi/s is exported from the shelf area. As much as 0.23 kmolSi/s is resupplied from sediments through benthic efflux on the Laptev shelf (Sun et al., 2021), leading to fluxes of

biological uptake of 0.89 ± 0.20 kmolSi/s and burial of 0.66 ± 0.20 kmolSi/s. This leads to an isotopically-constrained estimate of burial of 74 ± 22% of the total opal production in the Laptev Sea into the benthic sediments, as illustrated on Figure 4.10.

Combined, the four major Eurasian rivers deliver 4816 x 10^9 g DSi/yr (Holmes et al., 2012). Extrapolating the removal observed on the Laptev Sea shelf to the Eurasian shelf, this leads to an estimate of total terrestrial export of 3.1 ± 0.71 kmol Si/s, or 7.35 ± 1.68 kmolSi /s if all pan-Arctic rivers are considered. Isotopic evidence that DSi directly feeds into the TPD allows to estimate the proportion of DSi from rivers transported within the TPD. Estimated DSi concentrations in the TPD at 20% meteoric water are 12.5µmol/L and the transport core rate of the TPD is 0.9 ± 0.4 Sv (Charette et al., 2020). This leads to a total flux of DSi of 11.25 ± 5 kmolSi /s, which would indicate around 72 ± 6 % of DSi transported within the TPD is of preformed marine origins. This estimation is likely an underestimate of terrestrial DSi export as it only accounts for the four major Siberian rivers and assumes the same intense biological removal for all riverine input on less productive shelves such as the Barents Sea. This approximation however is of the same magnitude as the export of excess DSi from the Arctic Ocean (15.7 ± 3.2 kmol/s, Torres-Valdes et al., 2013) although it can not fully account for it.

The use of isotopic tools allows for more accurate determination of DSi export, and highlights the importance of Eurasian rivers as source of DSi to the Arctic Ocean and the importance of shelf cycling in controlling the export of inorganic nutrients. Nonetheless, we observe large variability in the range of DSi export calculated, which is primarily associated with uncertainty in the transport rate of the TPD (standard error is 44% of total rate, Charette et al., 2020), and is sensitive to the annual DSi flux from rivers. It is assumed that exported $\delta^{30}Si(OH)_4$ into the TPD is not largely affected by seasonality, as shelves homogenise the input from terrestrial sources over 1-2 years (Semiletov et al., 2000). Nonetheless, additional uncertainty arises from riverine endmember $\delta^{30}Si(OH)_4$ (Sun et al., 2018) and $^{30}\varepsilon$ variability, as affected by silicification and phytoplankton assemblages.

4.4.4 Constraining the Arctic Ocean Silicon isotope budget

Previous attempts of isotopic mass balance struggled to reconcile the heavy isotopic signature of DSi observed in the Arctic Ocean with the net export of DSi (Brzezinski et al., 2021; Torres-Valdés et al., 2013). Gaps in the isotopic composition of key gateways such as Fram Strait and the Barents Sea Opening increased the overall uncertainty, but early estimates indicate that biological uptake and opal recycling are dominant processes in the DSi budget of the Arctic Ocean (Brzezinski et al., 2021), and that shelf production is needed to balance the isotopic budget of the Arctic Ocean.

We use the first direct measurements of $\delta^{30}Si(OH)_4$ on the Eurasian shelves presented in this study to create an updated DSi isotopic mass balance of the Arctic Ocean. This budget combines the recent datasets describing the $\delta^{30}Si(OH)_4$ of Fram Strait (Chapter 3), the Barents Sea Opening (Appendix 2 – Section 4.7) and recent advances in describing DSi cycling processes (Brzezinski et al., 2021; Giesbrecht et al., 2022; Liguori et al., 2020, 2021; Varela et al., 2016; Ward et al., 2022b, 2022a) and is described in Table 4.2.

Table 4.2. Synthesis of the silicic acid and modelled DSi isotopic budget for the Arctic Ocean compared to measured $\delta^{30}Si(OH)_4$ input and outflux through the David and Fram Strait. This model accounts for additional removal of riverine DSi on Arctic shelves.

		Tmol Si/yr	Range	$d^{30}Si(OH)_4$	Range	Isotopic data source
Influx	Bering Strait	0.66[a]		1.72	1.67 - 1.79	Giesbrecht et al., 2022; Brzezinski et al., 2021
	Barents Sea Opening	0.42[a]		1.67	1.47 - 1.87	**This study (Appendix 2)**
	Fram Strait	0.66[a]		1.74	1.68 - 1.80	**This study (Chapter 3)**
	Rivers	0.44[b]	-0.41 - -0.45	1.27	1.00 - 1.60	Sun et al., 2018
Measured Input		**2.37**		**1.61**		
Outflux	Davis Strait	-1.35[a]		1.75		Giesbrecht et al., 2022
	Fram Strait	-1.08[a]		1.85	1.76 - 1.94	**This study (Chapter 3)**
Measured Outflux		**2.43**		**1.79**		
Add. Output	Removal - Ocean	-.20[c]	-0.26 - -0.14	1.16	1.16 - 1.5	Brzezinski et al., 2021
	Removal - Shelf	-0.19	-0.33 - -0.19	0.65	0.42 - 0.92	**This study (Chapter 4)**
Modelled Outflux		**1.98**		**1.78**		**This study (Chapter 4)**

a - Torres-Valdes et al., 2013
b - Holmes et al., 2012
c - Brzezinski et al., 2021

The DSi budget presented in Table 2 uses the DSi fluxes across Arctic gateways from Torres-Valdés et al. (2013) and pan-Arctic annual riverine DSi fluxes measured

over a decade in Holmes et al. (2012) of 0.41 TmolSi/yr, with an additional input of 0.01 – 0.04 TmolSi/yr from riverine opal leading to a total of 0.44 TmolSi/yr, assuming around half of opal material dissolves within the water column (Carey et al., 2020; Tréguer et al., 2021). In the Bering Strait, $\delta^{30}Si(OH)_4$ was measured between 1.67 – 1.79‰ (Brzezinski et al., 2021; Giesbrecht, 2019), leading to an average of 1.72‰. Fram Strait and the Barents Sea opening have inflow signatures of 1.74 ± 0.06‰ (Table 3.2) and 1.67‰ (Depth > 100m, data in Appendix 2 – Section 4.7) respectively. Outflowing polar waters have signatures of 1.75‰ (Giesbrecht, 2019) and 1.85 ± 0.09‰ (Table 3.2) for the Davis Strait and Fram Strait respectively.

Using DSi isotopes, we have evidence that a significant proportion of DSi is removed on the Laptev Sea shelf, implying strong biological control over the Si budget and significant burial on the shallow Eurasian shelves. There is large associated uncertainties with opal burial. Previous estimates of opal burial for the Arctic Ocean are of 0.16 – 0.30 TmolSi / yr (Brzezinski et al., 2021; März et al., 2015), based on opal content of 2% weight averaged for the Arctic Ocean. This however does not encapsulate opal content from shallow Arctic shelves. Recently in the Barents Sea, opal content was documented to be particularly low (0.26-0.52% weight), and to be rapidly recycled near the surface of the seafloor (Ward et al., 2022b). Nonetheless, the average of 2% weight can underestimate sedimentary opal content on Eurasian shelves around river deltas, where opal content >3% and up to 13% have been measured in the regions of the Laptev and East Siberian Seas (Mammone, 1998; Nürnberg et al., 1997). In Table 4.2, we characterize a separate removal term for Eurasian shelves based on estimates from the Laptev Sea. Productive Eurasian shelves (defined here as the White Sea, Kara Sea, Laptev Sea & East Siberian Sea) account for 12% of the total Arctic Ocean area (Jakobsson, 2002), leading to adjusted fluxes of 0.14 – 0.26 TmolSi/yr for opal burial for the rest of the Arctic Ocean. The Barents Sea was not included in the Eurasian shelf removal estimate due to evidence of different nutrient cycling from Siberian shelves and low burial opal rates (Tuerena et al., 2021b; Ward et al., 2022b).

Still, most of the Arctic's opal production occurs on shelves, with the Laptev & Kara seas particularly favourable for diatom production (Macdonald et al., 2010). Regional highs in productivity and zones of intense burial can significantly affect exported $\delta^{30}Si(OH)_4$ on a basin-wide scale. Significant differences in nutrient cycling between the Barents Sea shelf and other Eurasian shelves may also be observed as the Barents Sea Opening experiences strong mixing from tidal and frontal currents, and experiences deep winter convection through its entire water column (Sundfjord et al., 2007), leading to low burial rates of opal in the Barents Sea Opening (Ward et al., 2022b). This is not necessarily representative of nutrient cycling on other Eurasian shelves (Tuerena et al., 2021b).

On shallow shelves, the burial of Si can be approximated from removal only as opal dissolution within the water column on shallow shelves is small, although dissolution is an important mechanism to vertically redistribute DSi and isotopic signatures in deep Arctic basins (Giesbrecht et al., 2022; Liguori et al., 2020). We estimated above that 43 ± 13% of DSi from riverine origins is removed on the Laptev Sea shelf. Extrapolating this to pan-Arctic river fluxes, an additional term for net shelf removal of DSi js estimated at 0.19 TmolSi/yr.

As the source of DSi from rivers is isotopically lighter than marine-sourced DSi (Frings et al., 2016), the isotopic signature of opal buried on shelves ($\delta^{30}Si\text{-}BSiO_2$) from terrestrial origins can be estimated using the fractionation model fractionation for opal described in Varela et al. (2004):

$$\delta^{30}\mathrm{Si} - \mathrm{bSiO_2} = \delta^{30}\mathrm{Si(OH)_{4-initial}} - {}^{30}\varepsilon((f\ln f)/(1-f)) \qquad \textit{Eq. 4.10}$$

Where $\delta^{30}Si(OH)_{4\ -\ initial}$ is the $\delta^{30}Si(OH)_4$ in surface waters prior to utilisation, here 1.30‰ for riverine-sourced DSi (Sun et al., 2018). Using a range of biological fractionation factors (-1.14 to -0.59 as per section 4.3) and a range of fraction of DSi remaining (0.38 – 0.57 as per section 4.3), we calculate a mean $\delta^{30}Si\text{-}BSiO_2$ of 0.65‰ (ranges 0.42 – 0.92‰). This is substantially lighter than the $\delta^{30}Si\text{-}BSiO_2$ measured in other Arctic basins, ranging from 1.5-2.5‰ (Giesbrecht et al., 2022; Varela et al., 2016), reflecting the isotopically lighter source of terrestrial DSi onto

shelves in this study. Following this, the isotopic signature of riverine-sourced DSi (1.30‰, Sun et al., 2018) was adjusted for the dissolution of isotopically light riverine opal, giving a mass-weighted riverine source $\delta^{30}Si(OH)_4$ of 1.27‰.

From the inflow and removal terms described above, the $\delta^{30}Si(OH)_4$ of outflowing waters from the Arctic Ocean is estimated using isotopic mass-balance and assuming steady-state:

$$DSi_{inflow} = DSi_{removed} + DSi_{outflow} \qquad Eq.\ 4.11$$

$$\delta^{30}Si(OH)_{4-\,inflow} = f_{removed}\ \delta^{30}Si(OH)_{4\,-removed} + (1 - f_{removed})\ \delta^{30}Si(OH)_{4\,-outflow} \qquad Eq.\ 4.12$$

Where f is the fraction of Si removed compared to total inflow, $\delta^{30}Si(OH)_{4\,-\,inflow}$ is the mass-balanced isotopic signatures of inputs (inflow + rivers) and $\delta^{30}Si_{removed}$ is the mass-balanced isotopic signature of Si removal processes (shelf + open ocean). Using the mean $\delta^{30}Si\text{-}BSiO_2$ of 0.65‰ calculated with eq. 4.10, modelled shelf burial of isotopically light opal contributes to an isotopic shift of +0.10‰.

Extrapolating the net removal of nutrients to productive Eurasian shelves helps to close the isotope mass balance of the Arctic Ocean and reproduces well the observed outflowing isotopic signature of the Arctic Ocean (mass-weighted modelled $\delta^{30}Si(OH)_4$ = 1.78‰). Our modelled budget simplifies internal cycling processes and does not account for the entire DSi outflow flux observed, though the discrepancy is not large in absolute terms. This could be consistent with potential additional sources of isotopically light DSi from hydrothermal vents (Edmonds et al., 2003; Liguori et al., 2020), lithogenic sources (Ward et al., 2022b) and submarine groundwater discharge on shelfs unaffected by permafrost, which can all contribute to closing this gap. Although the magnitude of these inputs are likely to be small they are currently unknown.

The findings from the budget in 4.2 are summarised on Fig.4.11. If unaccounted for, the exported DSi observed would be isotopically similar to inflow from AW (bottom

panels from Fig .4.11). Thus, this model illustrates the need of a intense shelf removal term to account for the heavy isotopic enrichment observed in the TPD.

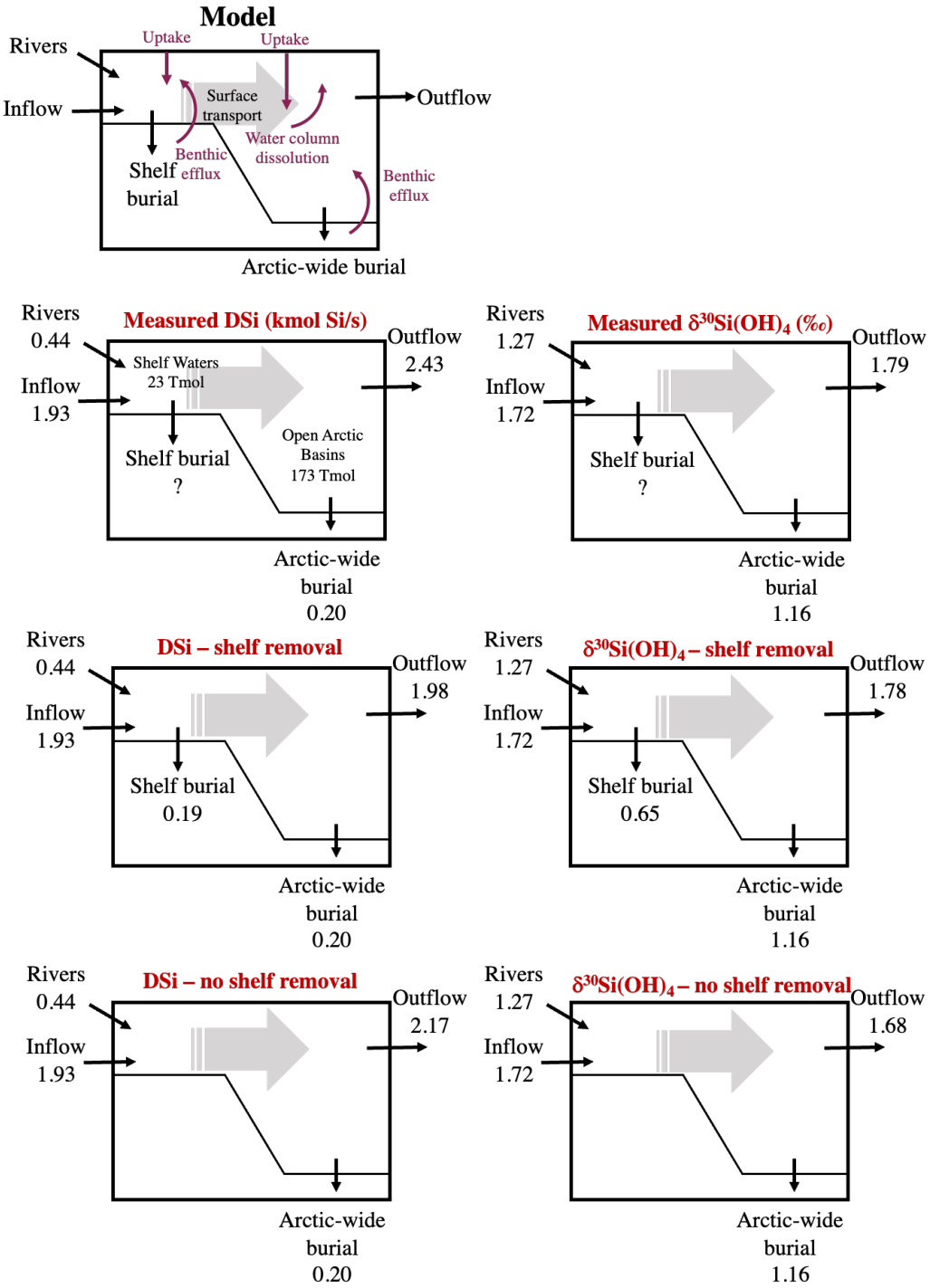

Figure 4.11. Schematic of fluxes, burial and export of DSi in the Arctic Ocean, with observed and modelled DSi and $\delta^{30}Si(OH)_4$ under various scenarios: Actual (top panels), including shelf removal (middle panels) and without accounting for shelf removal (bottom panels) . These scenarios illustrate the importance of shelf removal in balancing the Arctic isotope budget. Red

arrows show internal cycling proccesses of opal dissolution and benthic efflux of DSi. DSi fluxes are in TmolSi/yr and $\delta^{30}Si(OH)_4$ is in permil (‰).

This simple model highlights the role of the Arctic shelf Si pump in enriching the isotopic signature of Arctic DSi and regulating export out to the Atlantic Ocean, while illustrating the sensitivity of the Arctic DSi budget to biological processes.

4.4.5 Future implications & limitations

Climate change is significantly affecting the Arctic Ocean and its shallow coastal shelves. Considering its connection to the surrounding land, the Arctic Ocean is particularly sensitive to change in its freshwater budget and terrigenous supply of nutrients (Macdonald et al., 2015). Discharge from Eurasian rivers is increasing (Mcclelland et al., 2006), permafrost thaw and degradation is increasing nutrient fluxes to the coast (Frey et al., 2007; Frey and McClelland, 2009; Zhang et al., 2021), sea-ice cover is decreasing (Notz and Stroeve, 2016) and primary productivity in the Eurasian Arctic is increasing (Frey et al., 2018). These changes have been increasing primary productivity in the Arctic Ocean from enhanced nutrient supply (Ardyna and Arrigo, 2020) and the prevalence of diatoms is changing (Blais et al., 2017). Changes in the flux and stoichiometry of nutrients delivered to Arctic shelves will impact nutrient demand, primary productivity locally but also change nutrient budgets and the export of DSi out of the Arctic Ocean (Torres-Valdés et al., 2013).

We still observe a discrepancy between predicted and measured DSi at outflow gateways. This can be partially linked to uncertainty within measurement of fluxes or missing sources of DSi to the Arctic Ocean. Amongst these suggested sources are hydrothermal vents and lithogenic Si from the benthos (Edmonds et al., 2003; Liguori et al., 2020, Ward et al., 2022b). Kipp et al. (2018) have observed increased fluxes of shelf-derived materials from sediment-water exchange which can significantly change the supply and balance of nutrients on Arctic shelves and impact burial of DSi. Lithogenic supply of DSi could become increasingly important in the future Arctic Ocean, highlighting the importance of further constraining this flux on a basin-wide scale (Ward et al., 2022b).

The DSi and $\delta^{30}Si(OH)_4$ isotope budget of the Arctic Ocean shows that biological cycling plays a key role for the burial of opal and export of DSi in the Arctic Ocean. The Arctic shelf Si pump is currently limited by nitrogen. Increasing riverine discharge and permafrost degradation is likely increasing the export of major nutrients (Zhang et al., 2021). As riverine discharge is rich in DSi but poor in nitrogen, the DSi:N ratio of riverine delivery can increase in the future. Further to this, nitrogen is quickly removed in Siberian rivers and shelves, with 70% of terrestrial N removed before reaching the seawater endmember (Letscher et al., 2013). As DSi inputs increase and removal processes of nitrogen strengthen (Tuerena et al., 2021c, 2021a), a smaller proportion of DSi may end up buried on Eurasian shelves. Due to the strong biological controls on the shelf Si pump, this could in turn lead to an increase in DSi export and lower isotopic signatures. Our mass-balanced isotope budget also shows that the $\delta^{30}Si(OH)_4$ of exported DSi is extremely sensitive to the $\delta^{30}Si$ of biogenic Si removed. To further constrain the DSi budget of the Arctic Ocean, better characterization of $\delta^{30}Si$ of biogenic Si and $^{30}\varepsilon$ is needed, particularly within rivers and on Eurasian shelves. Characterisation of removal in the East Siberian Sea would also confirm the suitability of extrapolating removal in the Laptev Sea to the Eurasian shelf.

4.5 Conclusions

This study presents the first direct measurements of $\delta^{30}Si(OH)_4$ along the Lena Delta & the Laptev Sea, as well as providing surface measurements along a transect on the Eurasian shelves. A gradual increase in DSi, DSi:N ratio and enrichment is found from West to East in the surface waters of the Eurasian shelf. This is attributed to nutrient input from rivers, and partial utilisation of DSi and subsequent burial of isotopically light $\delta^{30}Si$ in the shelf sediments.

Nitrogen was found to be strongly depleted on the Laptev sea shelf, limiting uptake of DSi. Through heavy silicon isotopic signatures, we trace the partial uptake signal of shelf waters feeding over the continental slope to the TPD, documenting the export of excess riverine DSi to the Arctic Ocean. From isotopic measurements, it is estimated that >40% of DSi from riverine inputs is removed within the Lena River

delta and on the Laptev Sea shelf, leading to an export of 3.10 ± 0.71 kmol/s of riverine DSi through the transpolar drift. This highlights the role of Eurasian rivers in supplying nutrients to the Arctic Ocean and the importance of shelves which modify nutrient stoichiometry on Arctic shelves.

An updated isotopic budget of the Arctic Ocean displays the importance of biological processes in controlling DSi export and enriching the $\delta^{30}Si(OH)_4$ of outflowing water masses from the Arctic Ocean. The study highlights the role of nitrogen limitation in the shallow Arctic shelves in determining the DSi fluxes which are highly sensitive to ongoing climate change. As a consequence of changing biogeochemical cycles in the Arctic Ocean, it is envisioned that changes to the DSi export out of the Arctic will increase and a lighter $\delta^{30}Si(OH)_4$ signatures of the Arctic Ocean are expected in the near-future.

4.6 Appendix 1 – Supplementary N isotope dataset

Here, supplementary data of stable isotopes from N species (nitrate, DON, PON) measured for the Eurasian shelf and Laptev Sea transects is presented and briefly described. As discussed in Section 4.4.2, N is vigorously cycled on the Eurasian Arctic shelves as it receives riverine N, mostly in the form of DON (>90%), while also undergoing full assimilation to depletion of nitrate and benthic denitrification. As isotopic measurements of $\delta^{15}N\text{-}NO_3$ only characterises a minor component of the total N inventory, both the inorganic and organic pools of N isotopes were measured along the transect, These measurements are used to determine how riverine N is cycled as it enters the Eurasian shelf, prior to export through the TPD. Isotopic signatures and key findings from this dataset are briefly outlined below.

4.6.1 Analysis

4.6.1.1 N isotopes

Seawater samples for nitrate isotope analysis were collected following GEOTRACES protocols (Schlitzer et al., 2018) and analysed using the Denitrifier Method (Casciotti et al., 2002; Sigman et al., 2001). Samples with very low concentrations (<2μM) were analysed at 5nmol instead on an Elementar Isoprime precision mass sprectrometer coupled with an Elementar greenhouse gas device. Measurements were corrected using international reference standards IAEA-N3 and USGS-34 in each run with standard reproducibility of ±0.2‰ and ±0.4‰ for $\delta^{15}N\text{-}NO_3$ & $\delta^{18}O\text{-}NO_3$ respectively. This follows corrections in described in Section 2.4 for inter-comparability of datasets across the Eurasian Arctic. The isotopic parameter Δ(15-18) is calculated as $\Delta(15\text{-}18) = \delta^{15}N\text{-}NO_3 - \delta^{18}O\text{-}NO_3$.

The $\delta^{15}N$ of total dissolved N ($\delta^{15}N$-TDN) was measured in nitrate isotope samples by peroxidation of TDN to NO_3 and subsequent N isotope analysis through the Denitrifier Method. This follows the method described in Knapp et al. (2005) and used for the Bering Sea shelf in Granger et al. (2011). Measurement accuracy and reproducibility was checked with the international organic standards U40 and internal laboratory standard, Glycine in each run. Average measurements for the duration of this study were -4.3 ± 0.2‰ (n=5) and 0.8 ± 0.3‰ (n=7) for U40 and

Glycine respectively, within error of published standards (δ^{15}N-TDN = -4.5‰ and δ^{15}N-TDN = 1.1‰ respectively).

4.6.1.2 Particulate Nitrogen

Seawater samples were collected from the underway system into acid-cleaned carboys and filtered through combusted GF/F filters (0.7µm pore size) within 2h of collection. The filters were stored at -80°C until analysis. Prior to analysis the filters were freeze-dried, wrapped in tin foil cones (OEA Laboratories) and pelletised.

δ^{15}N-PN was determined by EA-IRMS using a Costech Instruments Elemental Analyser coupled to Thermo Scientific Delta V Advantage mass spectrometer fitted with Conflo IV gas handling system. The instrumentation was operated using ISODAT 3.0 isotope ratio MS software. L-glutamic acid standards USGS 40 and USGS 41a (US Geological Survey, Reston Stable Isotope Laboratory) were run alongside the samples and were used both for data processing and to assess the performance of the instrumentation. An internal standard consisting of freeze-dried, finely powdered prawn was also used as a further 'check standard'. A 10-point calibration using standard USGS 40 was measured to provide the linear regression equation which was used to derive PON concentrations from the respective peak areas. µg/L concentrations were then then calculated using the concentration obtained from the whole filter and volume of seawater filtered. The detection limit for PON was 10µg.

4.6.2 Dataset

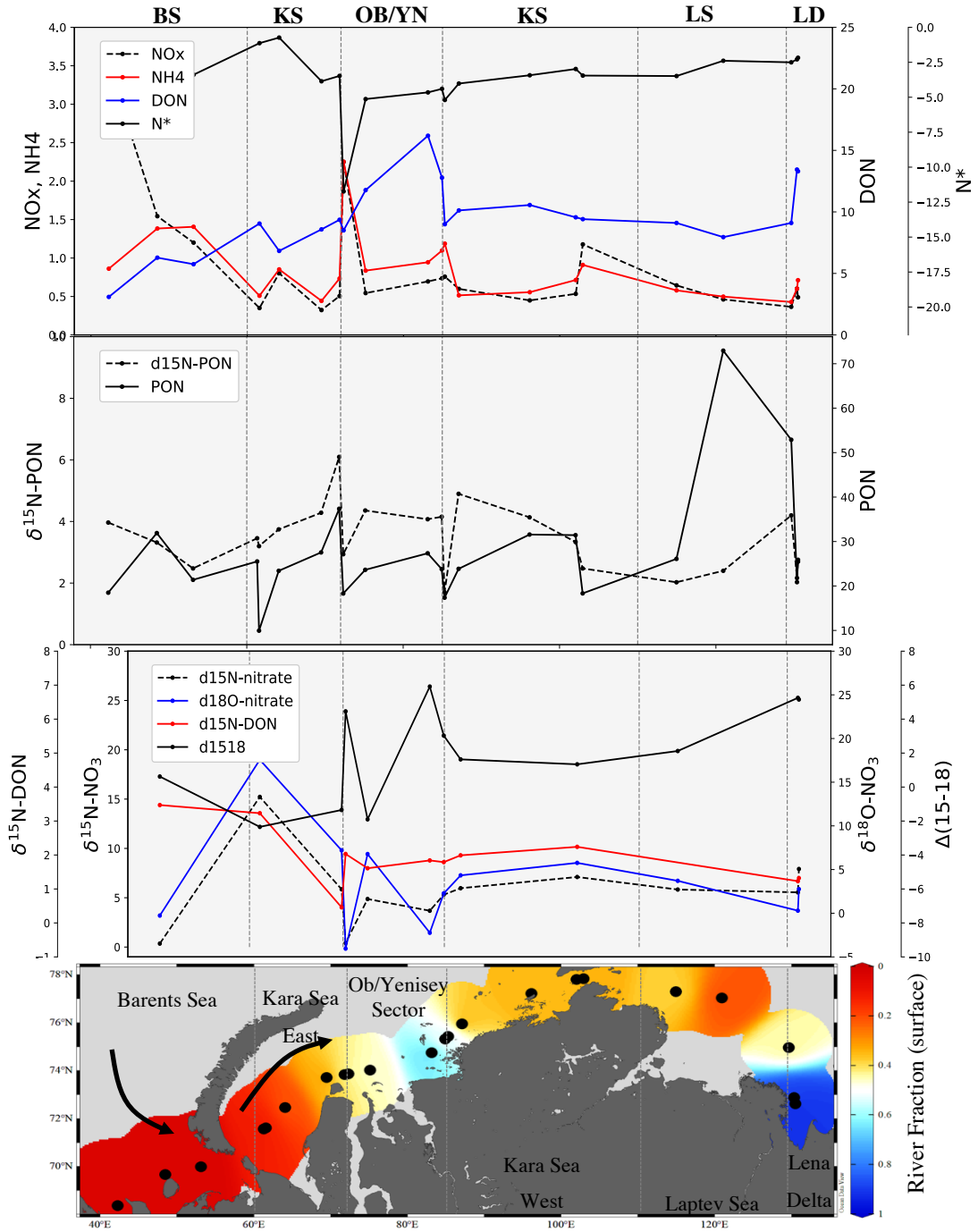

Figure 4.12. Longitudinal transect of nutrient concentrations and isotopic measurements of underway samples of AMK73. Top panel: Dotted black lines display surface concentrations of NO_x (nitrate + nitrite, µM) concentrations, red line is ammonia (µM), blue line is Dissolved Organic Nitrogen (DON, µM), and black line is N* (= NO_x – 16*PO_4) with longitude along the Eurasian shelf. Middle top panel: Particulate Organic Nitrogen (PON, black line, µM) and δ^{15}N-PON (black dotted line, ‰). Middle bottom panel: Displayed are δ^{15}N-NO_3 (black dotted line,

‰), $\delta^{18}O\text{-}NO_3$ (blue line, ‰), $\delta^{15}N$-TDN (red line, ‰) and Δ(15-18) (black line, ‰) with longitude along the Eurasian shelf. Bottom panel: Calculated riverine contribution to underway measurements along the transect. BS = Barents Sea, KS = Kara Sea, OB/YN = Ob & Yenisey river inflow, LS = Laptev Sea, LD = Lena Delta inflows.

4.6.2.1 Key observations

-Figure 4.12 shows underway measurements along the Eurasian shelf during October 2018. In the Barents Sea sector, all N concentrations are low (<4 μM), but N is principally present in the inorganic form.

-Over the rest of the Eurasian shelf, N is primarily present as DON, with peaks >10 μM near the Ob, Lena and Yenisey deltas which is quickly removed. Nitrate and nitrite (NO_x) and ammonium concentrations are low throughout the transect (<3 μM aparts from the Barents Sea).

-The strong DON peaks observed near the major rivers are consistent with the addition of terrestrial N to the Eurasian shelf. The gradual addition of terrestrial N is observed through an overall increase in N from W-E.

-PON and $\delta^{15}N$-PON are variable throughout the section, and generally show both high concentrations and isotopic enrichment west of river deltas. Generally, $\delta^{15}N\text{-}PON \approx \delta^{15}N\text{-}NO_3$, showing nitrate is nearly fully consumed by primary production on the Eurasian shelves.

-$\delta^{15}N$-DON is low in the Kara and Laptev Seas (<3‰), reflecting the addition of isotopically light terrestrial N through Arctic rivers (Francis, 2019). $\delta^{15}N\text{-}NO_3$ lowers near river mouths, which reflects the cycling from DON to nitrate and potential regeneration from PN dissolution in riverine waters.

- As $\delta^{15}N\text{-}NO_3$ becomes lighter eastward of the Eurasian shelf, Δ(15-18) increases from the low AW influence from nitrate regeneration (<2‰) to >5‰. This is reflective of increased N regeneration in fully depleted N environment, coupled with benthic denitrification on the Eurasian shelf (CPND).

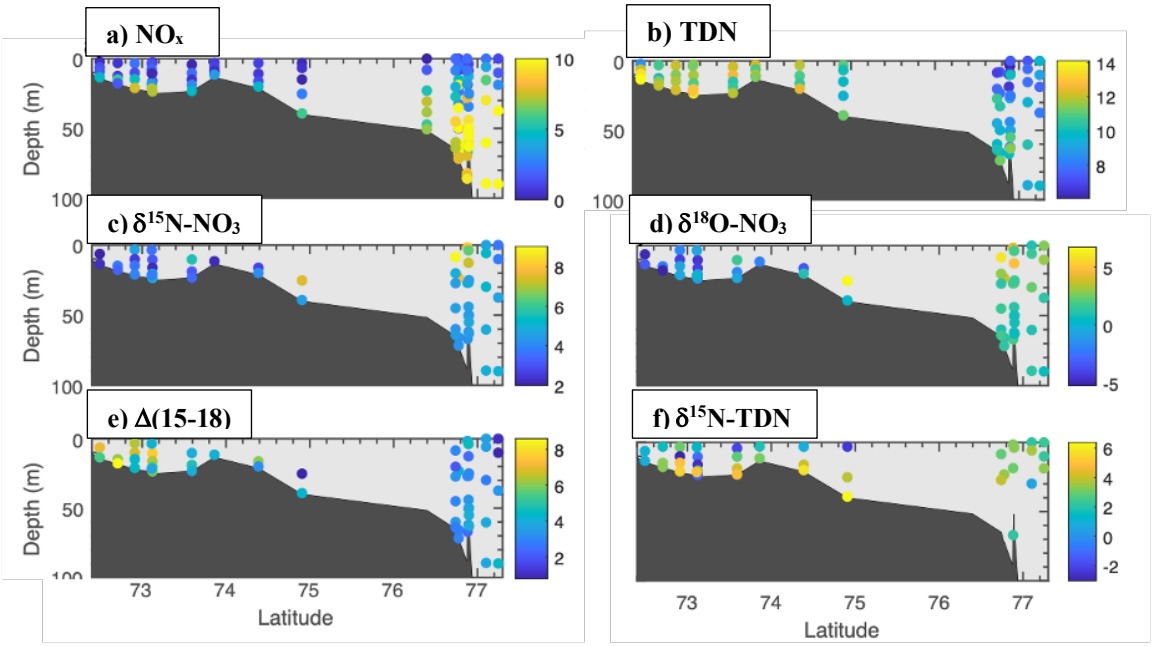

Figure 4.13. NO_x (top left) and TDN (top right) concentrations, and isotopic N measurements for $\delta^{15}N\text{-}NO_3$ (middle left), $\delta^{18}O\text{-}NO_3$ (middle right), Δ(15-18) (bottom left) and $\delta^{15}N$-TDN (bottom right) along the Lena Delta and continental slope for AMK73.

-Figure 4.13 shows the distribution of N concentrations and isotopes from the CTD transect from the Lena delta to the continental slope. N input from the river plume is primarily as DON, as nitrate concentrations are near 0 µM. The isotopic signature of $\delta^{15}N$-DON is very light in surface waters, and increases at depths.

-DON is quickly cycled to nitrate, as DON concentrations decrease before reaching the saline endmember over the continental slope (Sanders et al., 2021; Tuerena et al., 2021c).

-$\delta^{15}N\text{-}NO_3$ is generally heavier towards the surface, associated with assimilation, although this signal is erased in the river plume, where $\delta^{15}N\text{-}NO_3$ is low, reflective of the terrestrial origins of N, from permafrost thaw and vegetation (Francis, 2019).

-$\delta^{18}O\text{-}NO_3$ is also low and near-negative in the river plume with a slight increase in surface waters. This is indicative of nitrate remineralisation in the low $\delta^{18}O\text{-}H_2O$ (as low as -19‰) freshwater of the Lena river (Létolle et al., 1993), along with significant nitrate assimilation.

-Waters over the continental slope of the Laptev Sea do not host widespread CPND. The Laptev Sea shelf is generally well oxygenated and currents are fast moving (Pavlov et al., 1996), which are unfavorable conditions for benthic denitrification, which only occurs to a smaller extent in the Laptev Sea compared to the East Siberian Sea (Sun et al., 2021). Water flow below the LFP is restricted by bathymetry, forming near-stagnant OSW. In OSW, significant AOU, higher N concentrations and heavier $\delta^{15}N$ is observed below the LFP, which indicates CPND occurring on a local scale.

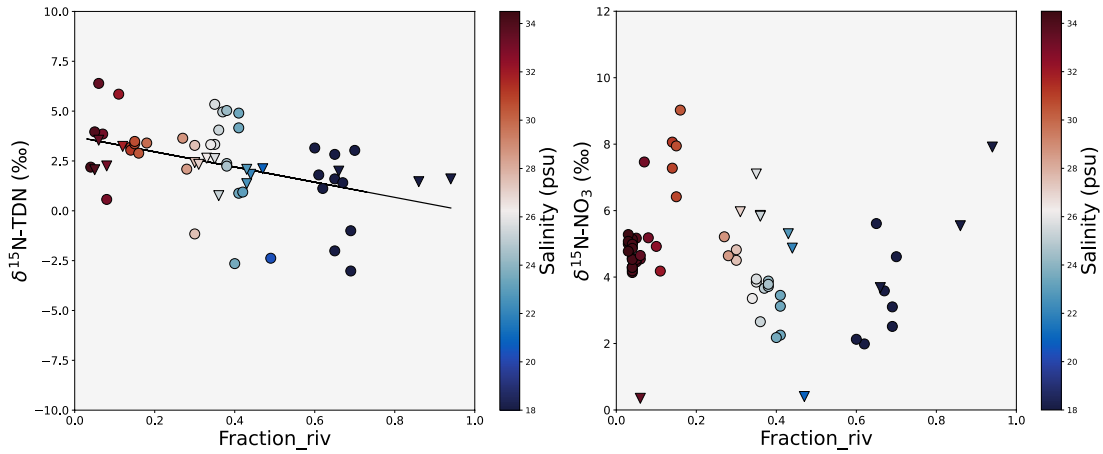

Figure 4.14: $\delta^{15}N$-TDN (left) and $\delta^{15}N$-NO_3 (right) against riverine fraction. Circles show measurements from CTD casts of this study, (AMK73), triangles are from the ship's underway system. Line shows least square regression.

-Figure 4.14 shows the relationship between N isotopes and the riverine fraction. Generally speaking, $\delta^{15}N$-TDN is variable but behaves semi-conservatively between the fresh and marine endmember. $\delta^{15}N$-NO_3 displays some very low signatures (<1‰) regionally in nutrient-deplete regions, indicative of strong nitrate remineralisation. Elevated $\delta^{15}N$-NO_3 values are found in the OSW, the Kara Sea and in the Lena river mouth, displaying local regions of denitrification.

-As can be observed on Figure 4.14, the isotopic composition of N species is highly variable spatially and temporally (Thibodeau et al., 2017a), and appears closely tied to local bathymetry and complex current circulation over the shelf, as well as riverine supply of N and oxygenation of the benthos. Figure 4.12 however

shows that this signal gets integrated during its transport along the Eurasian shelf as it undergoes winter mixing, leading to an outflow signal of shelf waters with high Δ(15-18) as they get increasingly modified through CPND.

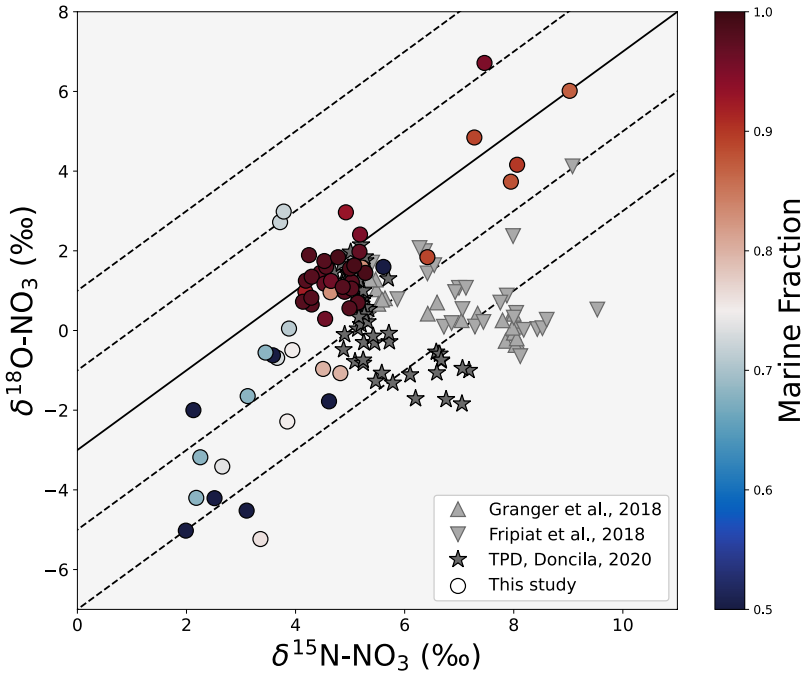

Figure 4.15. Tracking the origins of N in the Transpolar Drift through δ15N-NO3 against δ18O-NO3. Circles show dataset from the Laptev Sea (this study). Upward triangles are from the Canada basin (Granger et al., 2018), downward pointing triangles are from the East Siberian Sea (Fripiat et al., 2018) and stars show measurements from within the Transpolar Drift (Doncila, 2020).

-Assimilation of isotopically light terrestrial N remains the dominant process impacting δ^{15}N-NO$_3$ distribution in the waters advected over the continental slope. Shelf waters are eventually transported into the TPD, along with entrained AW. Figure 4.15 shows measurements from the Laptev Sea in comparaison to shelves hosting CPND, in the context of the TPD, to determine the origins of N it transports.

-δ^{15}N-NO$_3$ in the TPD is lighter than in AW and waters which hosts CPND. This shows that riverine N significantly contributes to the N inventory of the TPD. This is consistent with estimates from Doncila (2020), who estimated riverine N contribution to the TPD at 14-21%, primarily supplied through DON remineralisation, which subsequently fuels additional N loss in the TPD, with a

limited impact on central Arctic productivity (Doncila, 2020), and is nearly fully removed in PSW at Fram Strait.

4.7 Appendix 2 – Barents Sea Opening $\delta^{30}Si(OH)_4$

Table 4.3 $\delta^{30}Si(OH)_4$ measurements from the Barents Sea Opening (JR16006, August 2017, Changing Arctic Ocean program) measured following the method described in Section 4.2.4. Physical and nutrient data is also presented (doi:10.5285/aed2abbb-9814-4a1b-e053-6c86abc04d55).

Cruise	Station	Latitude	Longitude	Depth (m)	T (˚C)	S (psu)	NO3 (µM)	DSi (µM)	Si* (µM)	δ30Si(OH)4 (‰)	Stdv (‰)
JR16006	B01	70.77	20.00	182.75	6.7	35.03	12.76	6.07	-6.75	**1.74**	**0.02**
JR16006	B01	70.77	20.00	140.57	6.8	35.03	12.63	5.51	-7.19	**1.97**	**0.04**
JR16006	B03	72.63	19.25	159.69	5.9	35.10	11.82	5.60	-6.27	**1.29**	**0.04**
JR16006	B03	72.63	19.25	339.71	4.2	35.06	12.83	6.42	-6.49	**1.52**	**0.03**
JR16006	B03	72.63	19.25	359.55	3.9	35.05	12.67	6.25	-6.49	**1.60**	**0.06**
JR16006	B03	72.63	19.25	70.16	6.1	35.08				**1.63**	**0.05**
JR16006	B03	72.63	19.25	40.19	6.4	35.07				**1.92**	**0.06**
JR16006	B03	72.63	19.25	24.80	8.4	35.01				**2.08**	**0.05**
JR16006	B03	72.63	19.25	10.13	8.8	34.99				**2.70**	**0.04**
JR16006	B07	76.00	16.83	249.29	4.0	35.05	11.92	5.15	-6.83	**1.69**	**0.06**
JR16006	B07	76.00	16.83	139.69	5.0	35.09	11.46	4.83	-6.79	**1.73**	**0.02**
JR16006	B07	76.00	16.83	308.47	2.9	35.01	11.73	5.19	-6.60	**1.80**	**0.02**
JR16006	B07	76.00	16.83	99.56	5.3	35.06	10.33	4.93	-5.58	**2.18**	**0.07**
JR16006	B07	76.00	16.83	49.45	5.9	34.95	5.14	3.39	-1.91	**2.26**	**0.05**
JR16006	B07	76.00	16.83	27.94	6.4	34.91	2.77	1.59	-1.26	**2.53**	**0.05**
JR16006	B07	76.00	16.83	5.47	7.0	34.85	0.67	1.19	0.47	**3.07**	**0.04**

5. Recent changes in nutrient supply routes and internal cycling of the subpolar North Atlantic

Abstract

The subpolar North Atlantic is an important region of primary productivity and deep nutrient export through the formation of North Atlantic Deep Waters (NADW). In this study, we present nitrate and dissolved silicon (DSi) stable isotope data in the subpolar North Atlantic, to understand the mechanisms of low-latitude and high-latitude nutrient supply and the processes which eventually control the NADW nutrient inventory.

In the upper 1000m of the subpolar North Atlantic, Δ(15-18) decreases from 3.1‰ to 2.5‰ towards increasingly North Atlantic Water (NAW) influenced waters, associated with biological assimilation and nitrate regeneration which dominates isotopic gradients in the upper water column. In the Labrador Basin, the polar origins of surface currents are traced through the remote signal of coupled-partial nitrification and denitrification on Arctic shelves. Through the temporal examination of $\delta^{18}O\text{-}NO_3$ trends in the Iceland basin, a shift in the nitrate isotope pool is observed as a result of the extreme freshening event of the subpolar North Atlantic. The lowering of $\delta^{18}O\text{-}NO_3$ is consistent with a deviation from the Labrador Current eastwards. The freshening is associated with decreased assimilation and regeneration, linked to increased stratification and lower preformed N:DSi stoichiometry.

In the global context, we find that deep water masses of the subpolar North Atlantic have heavy $\delta^{30}Si(OH)_4$ (1.6 – 1.7‰). This is primarily linked to the fractionation from Southern Ocean-sourced DSi as it travel in the upper water column of the North Atlantic. We measure relatively light $\delta^{30}Si(OH)_4$ in the surface waters of the North Atlantic (NAW) considering its DSi-deplete nature, which we hypothesize to originate from Mediterranean outflow waters with low DSi and low $\delta^{30}Si(OH)_4$ due to an abnormally large lithogenic control on the DSi budget of the Mediterranean

Sea. Direct measurements of this key region to the nutrient inventory and stoichiometry of the North Atlantic are however required to confirm this hypothesis. This finding leads us to conclude that the isotopic signal and concentration of DSi in the North Atlantic is primarily sourced from the SO and transformed in the Atlantic Ocean by fractionation, with the contribution of a small isotopic enrichment is linked to high-latitude Arctic processes (~0.1‰). Further dilutive effects from freshwater sources diverge these water masses from the trends. Thus, the isotopic signature of NAW highlights the dilutive effect of subsurface waters in the North Atlantic which undergo deep winter convection, dampening the heavy isotopic enrichment linked to high-latitude Arctic processes and its contribution to NADW.

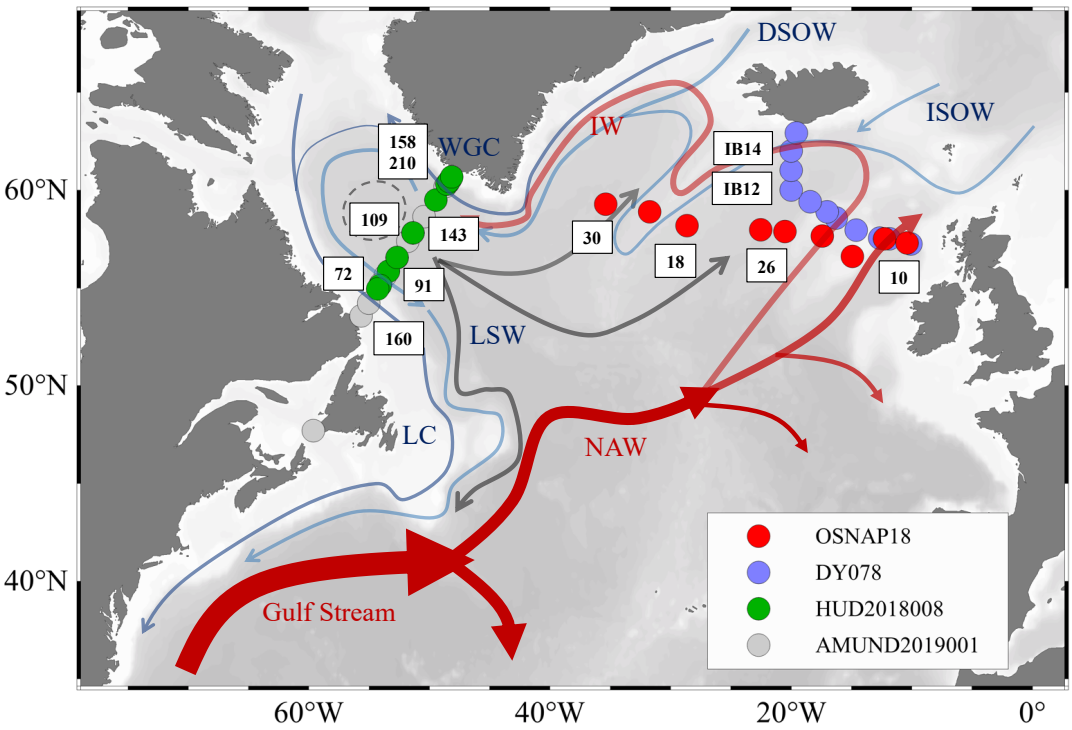

Figure 5.1: Map showing the sampling region of this study and schematic of the general circulation within the subpolar North Atlantic. Red arrows represent currents of Atlantic origins, blue arrows show currents and water masses from polar origins. Grey arrows show the pathways of Labrador Sea Water (LSW) after formation in the Labrador basin. NAW = North Atlantic Water, ISOW = Iceland-Scotland Overflow Water, DSOW = Denmark Strait Overflow Water, IW = Irminger Water, WGC = West Greenland Current, LC = Labrador Current. Colored dots show CTD station location for nitrate isotope profiles. Stations numbers highlight location of stations with silicon isotope profiles.

5.1 Introduction

The Meridional Overturning Circulation (MOC) is a major current system within the Atlantic Ocean and a key component of the Earth's climate system. Northward-flowing currents bring heat and salt to the subpolar regions of the Atlantic and to parts of the Arctic Ocean. The cooling of these currents at Northern latitudes in the subpolar North Atlantic form dense waters at intermediate and deep depths in the Labrador Sea and Nordic Seas, which eventually feed into North Atlantic Deep Water (NADW), the southward flowing, returning branch of the MOC.

The MOC regulates climate over the Northwest European continent through the northward transport of heat from the tropics (shown on Figure 5.1), on both modern and palaeoceanographic timescales (Pohlmann et al., 2006; Srokosz et al., 2012; Zhang et al., 2019). The MOC also dictates nutrient distribution across the Atlantic Ocean, with nutrient characteristics reflecting the origins of water mass formation (further details in section 1.3.2 and Figure 1.5), as well as regions of primary productivity which are stimulated by the upwelling of nutrient-rich deep waters (Allen et al., 2005; Sarmiento et al., 2004).

The hydrography of the North Atlantic is characterised by two gyre systems, the subtropical and subpolar gyres, with contrasting biogeochemical features. The subtropical gyre is oligotrophic and N-limited, with year-round stratification, and is an important area of N_2 fixation (Marconi et al., 2015; Moore et al., 2008, 2013). By contrast, the subpolar gyre is eutrophic: Deep winter convection seasonally supplies nutrients to the surface of the gyre, which sustains a strong phytoplankton and diatom spring bloom and a significant carbon flux to the deep ocean (Allen et al., 2005; Martin et al., 2011). Additionally, fresh and cold polar outflow currents from the Baffin Bay and the Fram Strait circulate around the Irminger and Labrador Seas, bringing in the remote signal of Arctic nutrient processes to the surface subpolar regions.

The MOC plays a key role in the cycling and storing of carbon and nutrients as it traps sinking carbon and nutrients into the deep ocean (Frajka-Williams et al., 2019; Muglia et al., 2018), particularly in the North Atlantic. From the intense spring

diatom blooms and the sequestration of carbon-rich cold waters into the deep ocean, the subpolar North Atlantic is one of the most efficient oceanic sink of atmospheric CO_2. (Olafsson et al., 2021; Takahashi et al., 2009), accounting for >40% of the global flux of CO_2 to the oceans (Takahashi et al., 2002).

Processes in the subpolar north Atlantic impacts both NADW and Arctic water masses. The inflow of North Atlantic Water (NAW) from the North Atlantic current, plays a key role to the Eurasian Arctic Ocean as it brings both heat (Lundrigan and Demirov, 2012; Rudels et al., 2004) and nutrients (Hátún et al., 2017; Torres-Valdés et al., 2013) to the shelves and deep basins, supporting productivity on Eurasian shelves (Tuerena et al., 2021b, 2021c) and feeding Arctic nutrient stocks. The inflow of Atlantic Waters (AW) in the Arctic Ocean originates in the subpolar North Atlantic and its hydrographic and nutrient properties are a function of the contribution from subpolar and subtropical waters (Hátún et al., 2005; Holliday et al., 2008). As the subpolar gyre contracts, the NAW path migrates westward (schematic pathway shown on Figure 5.1), allowing warm, saline oligotrophic AW to enter the Nordic Seas and Arctic Ocean and thereby reducing DSi stocks. The nutrient inventory of the subpolar regions fluctuates naturally through time (Hátún et al., 2017), as it is regulated by climate and the relative strength of both gyres (Foukal and Lozier, 2017; Spivak et al., 2021).

From the 1990ies to 2010, decreasing DSi concentrations have been observed in the subpolar regions and the Nordic seas, due to the increasing influence of oligotrophic subtropical waters (Hátún et al., 2017). The influence of increasing heat and oligotrophic water transport to the Eurasian Arctic Ocean has led to “Atlantification” of the Arctic Ocean. Increasing heat stocks and weakened stratification accelerates sea ice melt (Lind et al., 2018; Polyakov et al., 2017) and limits winter sea ice expansion (Barton et al., 2018). This in turn has led to the northward expansion of Atlantic phytoplankton, increasing DSi limitation and N demand and reduction of polar ecosystems associated to sea ice in the Eurasian Arctic Ocean (Hátún et al., 2017; Ingvaldsen et al., 2021; Krause et al., 2019; Randelhoff et al., 2018; Tuerena et al., 2021c).

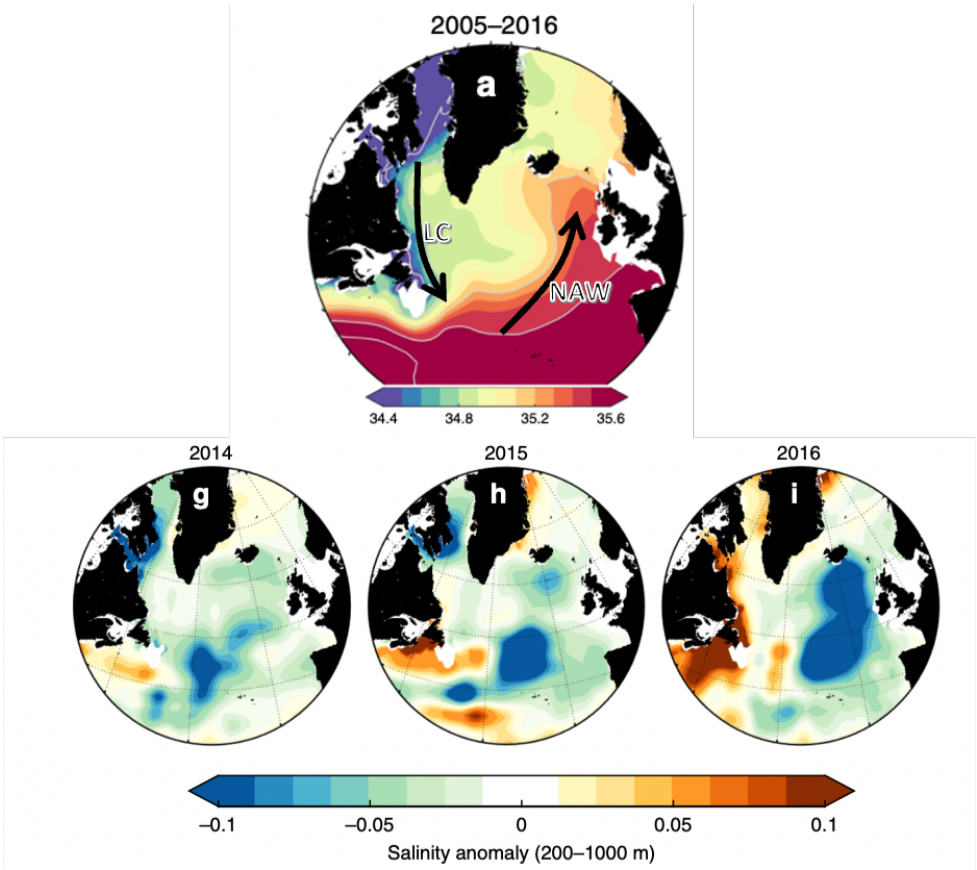

Figure 5.2. Recent freshening of the subpolar North Atlantic. Top shows average salinity (psu) from 2005-2016 and bottom panels show the northward spreading of the salinity anomaly between 2014-2016 for depths of 200-1000m. Warm colors represent high salinity waters from the subtropical North Atlantic Current, while cold colors show low salinity waters from polar and subpolar regions. LC = Labrador Current, NAW = North Atlantic Waters. Adapted from Holliday et al. (2020).

More recently, over the last decade, the subpolar North Atlantic has experienced an extreme freshening and cooling event of its upper water column, with the lowest salinities recorded for 120 years (Holliday et al., 2020). It has been observed from 2012 onwards, reaching its peak in 2016 over the Iceland basin and Rockall Trough. The transport of the anomalous freshwater plume is shown on Figure 5.2. The origin of this freshening is still uncertain and debated. Current theories of the driving mechanisms include (1) a shift in the pathways of the Labrador Current and Arctic freshwater driven by wind patterns (Holliday et al., 2020), (2) reduced heat transport from the subtropics leading to cooling of the eastern subpolar North Atlantic (Bryden et al., 2020), or (3) increased recirculation of the subpolar gyre (Fox et al., 2022).

Pulses of subpolar waters rich in nutrients have been shown to increase productivity in the past and stimulate ecosystems (Hátún et al., 2017). This demonstrates that the origins of freshening can have large implications for the biogeochemistry of the Iceland basin, as it will affect both stratification (and nutrient resupply) and nutrient inventory of the subsurface.

Considering the importance of the subpolar North Atlantic in controlling nutrient distribution both in the Arctic and the deep via NADW, and the large variability of surface currents in the region, it is important to understand the processes which control nutrient cycling within the region. The isotopic composition of DSi and nitrate are powerful tools for this purpose as they have the potential to link physical transport and internal nutrient cycling together on basin-wide scale.

The nitrogen isoscape is becoming increasingly well mapped out in the North Atlantic (Marconi et al., 2015, 2019), with fewer studies in the subpolar North Atlantic (Deman et al., 2021; Van Oostende et al., 2017; Peng et al., 2018). A few studies have provided the first measurements of $\delta^{30}Si(OH)_4$ in the subtropical and subpolar North Atlantic (De Souza et al., 2012; Sutton et al., 2018b), although coverage remains sparse in the subpolar regions, particularly in the upper 1000m of the water column and on shelves of the Labrador basin due to low DSi concentrations. Through these combined efforts, some advances have been made to understand the nutrient origins and processes which control the nutrient stoichiometry in the NADW at its point of formation, although lack of clarity on the relative importance of low-latitude and high-latitude processes remains.

It is well established that the Southern Ocean-sourced water masses strongly control nutrient distribution across the Atlantic (Sarmiento et al., 2004; De Souza et al., 2015). Under GEOTRACES and the UK Changing Arctic Ocean programs, outflow currents from the Arctic Ocean and their cycling history have now been documented (Giesbrecht et al., 2022; Lehmann et al., 2019, 2022; Tuerena et al., 2021a), which are also thought of importance in setting the heavy isotopic signatures of convective water masses of the subpolar North Atlantic (Brzezinski and Jones, 2015; Sutton et al., 2018b). It however remains unclear how important the contribution of preformed

nutrients from Pacific and Arctic origins are to the convective water masses of the subpolar North Atlantic, and what processes drive the modification of DSi and N in NAW locally in the subpolar regions.

In the light of recent changes to the surface North Atlantic (Hátún et al., 2017; Holliday et al., 2020), it is important to approach nutrient cycling in the subpolar regions with a global outlook. This study uses a dual isotope method to characterise the importance of local versus remote processes in the subpolar North Atlantic with the aim to better understand how climatic changes will affect nutrient inflow pathways to the Arctic Ocean in the future. The use of both isotopes provides the information to constrain remote and internal cycling processes to predict the impact that such fluctuation in nutrient origins will have on North Atlantic spring blooms and downstream ecosystems. The improved understanding of nutrient cycling in the subpolar North Atlantic is put in the global context, tying into NADW nutrient contribution and downstream ecosystems.

5.2 Methods

5.2.1 Sampling and hydrographic parameters

Samples were collected onboard four oceanographic cruises: in the Labrador Basin from HUD2018008 (25th April – 22nd May 2018) and AMUND2019001 (30th May – 23rd June 2019), two cruises along the AR7W transect under the Atlantic Zone Monitoring Program (AZOMP). On the Eastern side of the transect, samples were collected from DY078 (6th – 28th May 2017) and OSNAP18-E (1-29th July 2018) along the Extended Ellett Line and OSNAP transects respectively. All four transects combined cover the Labrador, Irminger and Iceland basins, the three convective areas in the subpolar North Atlantic, as well as the Rockall Trough, a region of Atlantic water inflow to the Nordic and Arctic Seas.

Seawater samples were collected from 24 rosette-mounted Niskin bottles also equipped with sensors recording physical parameters (conductivity, temperature, pressure & salinity). Dissolved O_2 was determined using a Seabird SBE 43 sensor and calibrated onboard using a photometric Winkler titration system (Carritt and Carpenter, 1966). Biogeochemical characterization of water mass and surface layers

within the region was done based on potential density (σ, kg m^{-3}) isopycnals which separates and tracks convective water masses across the OSNAP array, as well as separating out the seasonally warmed surface layer and the permanent thermocline/pycnocline of the North Atlantic (Holliday et al., 2015; Li et al., 2021; Lozier et al., 2019; Yashayaev and Loder, 2009).

5.2.2 Nutrient concentrations

Concentrations of dissolved inorganic nutrients (NO_x, $Si(OH)_4$) were measured following standard colorimetric methods and best practice measures (Becker et al., 2020; Grasshoff et al., 1983). Accuracy of the nutrient dataset with respect of CRMS is of 0.8% and 1.2% respectively for AZOMP cruises and 0.9% and 0.9% respectively for OSNAP18-E and DY078 cruises. The wate**r** mass tracer parameter N* was not calculated in this study due to suspected low phosphate data quality, and the phosphate dataset was discarded as unsuitable for stoichiometric work. The nutrient tracer Si* was used instead, defined as $Si^* = SiOH_4 – NO_x$ (Sarmiento et al., 2004). This tracer is indicative of deviation from typical DSi:N ratios of marine dissolved nutrient ratios.

5.2.3 Stable Isotope analysis

Water samples were collected from Niskin bottles onboard and filtered inline using Nuclepore polycarbonate membranes (0.4μm pore size). These were immediately acidified with 0.1% v/v 12M HCl for preservation and stored at 4°C until analysis for $\delta^{30}Si(OH)_4$. For nitrate isotope analysis, samples were frozen upon collection and stored at -20˚C.

Nitrate isotope samples were prepared according to the Denitrifier Method (Casciotti et al., 2002; Sigman et al., 2001) at the University of Edinburgh, and analysed on a GC-IRMS. The dataset was corrected using international reference standards IAEA-N3 and USGS-34 (further details in method chapter, section 2.2.4). Data reproducibility is ±0.2‰ for $\delta^{15}N\text{-}NO_3$ and ±0.3‰ for $\delta^{18}O\text{-}NO_3$. For DY078, the dataset presented also includes the partial ancillary $\delta^{15}N\text{-}NO_3$ and $\delta^{18}O\text{-}NO_3$ dataset from Doncila (2020), analysed and corrected using the same methods as described in method chapter, section 2.2.4. The isotopic parameter Δ(15-18) is calculated as Δ(15-

18) = $\delta^{15}N\text{-}NO_3$ - $\delta^{18}O\text{-}NO_3$. Δ(15-18) captures variation in both isotopes, tracing sources and modification of nitrate in open ocean regions (Rafter et al., 2013).

DSi isotope samples were pre-concentrated using the MAGIC method (Karl and Tien, 1992; Reynolds et al., 2006) and purified using 1.8ml Biorad AG50W-X8 cation-exchange resin columns (Georg et al., 2006b). All three isotopes of Si were measured on a Nu Plasma II MC-ICP-MS at the University of Edinburgh using standard-sample bracketing and calculated from the permil deviation from international isotopic reference material NBS28. To avoid potential interferences on the δ30Si, measured $\delta^{29}Si$ was converted to $\delta^{30}Si$ instead using the theoretical conversion factor of 1.96 (Young et al., 2002). This method and data quality checked is explained in further details in method chapter section 2.2.3. Long-term measurement accuracy was checked with the international solid standard Big Batch ($\delta^{29}Si$ = -5.35 ± 0.03‰, n=65) & both high and low concentration seawater standards $Aloha_{1000}$ ($\delta^{29}Si$ = 0.66 ± 0.02‰, n = 59) & $Aloha_{300}$ ($\delta^{29}Si$ = 0.86 ± 0.03‰, n=30). This is in close agreement and within analytical error of accepted published measurements of Big Batch ($\delta^{29}Si$ = -5.34 ± 0.15‰, Reynolds et al., 2007), $Aloha_{1000}$ ($\delta^{29}Si$ = 0.65 ± 0.10‰) and Aloha300 ($\delta^{29}Si$ = 0.85 ± 0.10‰, Grasse et al., 2017).

Table 5.1. Definition of water column structure based on potential density ranges, adapted from definitions in Holliday et al. (2015), Li et al. (2021) and Lozier et al. (2019).

Layer	σ (kg m^{-3})
Seasonally warmed surface layer/ currents	< 27.20
Upper Ocean (WNAW, NAW)	27.20 – 27.50
Permanent thermocline/pycnocline	27.50 – 26.70
Intermediate water (LSW)	27.70 – 27.80
Deep waters (NEADW)	27.80 – 27.88
Overflow water (ISOW, DSOW, WTOW)	>27.88

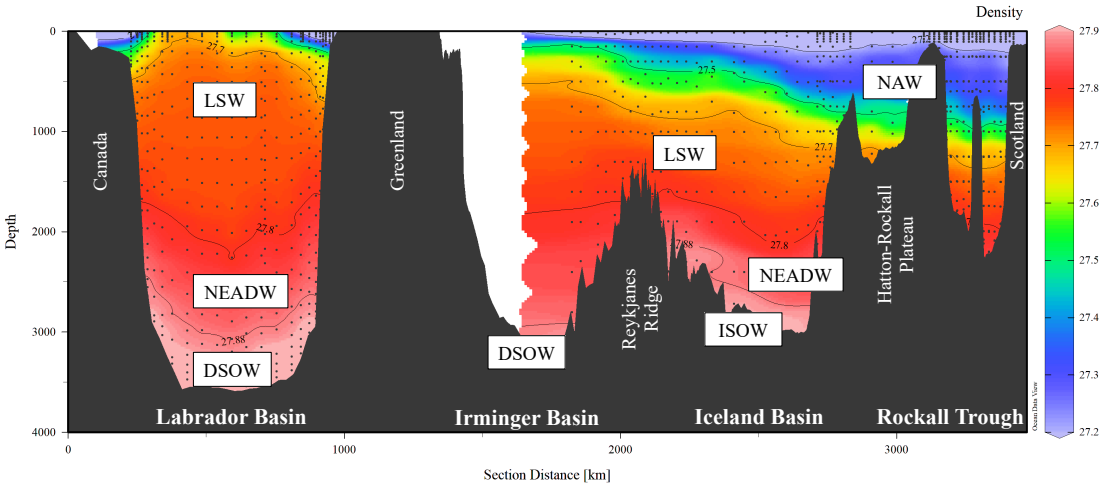

Figure 5.3. Full depth section of potential density along the AR7W and OSNAP-East transect in 2018. Black lines show key isopycnals. LSW = Labrador Sea Water, NEADW = Northeast Atlantic Deep Water, DSOW = Denmark Strait Overflow Water, ISOW = Iceland-Scotland Overflow Water, NAW = North Atlantic Water.

5.3 Results

5.3.1 Hydrography

The structure of water masses and surface properties along the subpolar North Atlantic transect is identified through the density layers defined in Table 5.1.

On the Eastern side of the transect shown in Figure 5.3, the hydrography of the upper water column (<1000m) is dominated by branches of the NAW flow path, which is itself controlled by the relative strength of the subpolar and subtropical gyres (Hátún et al., 2005, 2017). On the Western side, fresh polar currents with low density, LC and WGC ($\sigma < 27.5$ kg m^{-3}), dominate the Western and Eastern shelves respectively, flowing anticlockwise around the Labrador Basin (Han et al., 2010). Isopycnals deepen on the Eastern side of the transect over the Greenland slope between 200 – 1000m depth. This is the Irminger current Water (IW), remnant of the NAW originating current which forms in the Irminger Sea and enters the Labrador Sea off the Southern tip of Greenland. It flows anticlockwise around the basin and exits on the Western side, visible to a smaller extent over the Labrador slope (Yashayaev and Loder, 2009).

Below the permanent thermocline/pycnocline, convective LSW overlays NEADW, spreading to the Rockall Trough at its easternmost reach, following the circulation pathways highlighted in Figure 5.1. Very dense overflow waters ISOW and DSOW underlay NEADW, circulating cyclonically along ridges and troughs of the seafloor after their formation further north. The core of NAW over the Rockall Trough cools and becomes increasingly fresh as it circulates around the Iceland and Irminger basin. LSW becomes saltier from its formation in the Labrador Basin to the Rockall Trough as it is increasingly modified by Atlantic originating waters, and is also pushed downward by the core of NAW. The combined modification of surface and intermediate currents are reflected in the shoaling of isopycnals of the upper and intermediate layers of the water column from east to west (Figure 5.3).

5.3.2 Nutrient & Isotopic distribution

Nutrient distribution across the section is shown in Figure 5.4 and reflects the different origins of water masses. Nitrate and DSi are low (2.5 μM and <5 μM respectively) in surface NAW, reflective of the oligotrophic surface waters of the subtropical gyre, where year-round stratification prevents nutrient replenishment from deep waters (Moore et al., 2008, 2013). The polar origins of LC and WGC are reflected through their positive Si*, showing the relative enrichment of DSi in relation to nitrate due to nitrate removal processes in the Arctic Ocean (shelf denitrification). In intermediate waters, the highest nitrate concentrations are observed at the permanent pycnocline, associated with remineralisation of PON in the Oxygen Minimum Zone (OMZ). In the deep, the high DSi influence of AABW is reflected in NEADW and overflow waters through elevated DSi concentrations (>15 μM) and positive Si*. This Southern-sourced DSi influence is traced into NEADW in the Labrador basin between layers of subpolar originating water masses with lower DSi concentrations and negative Si*.

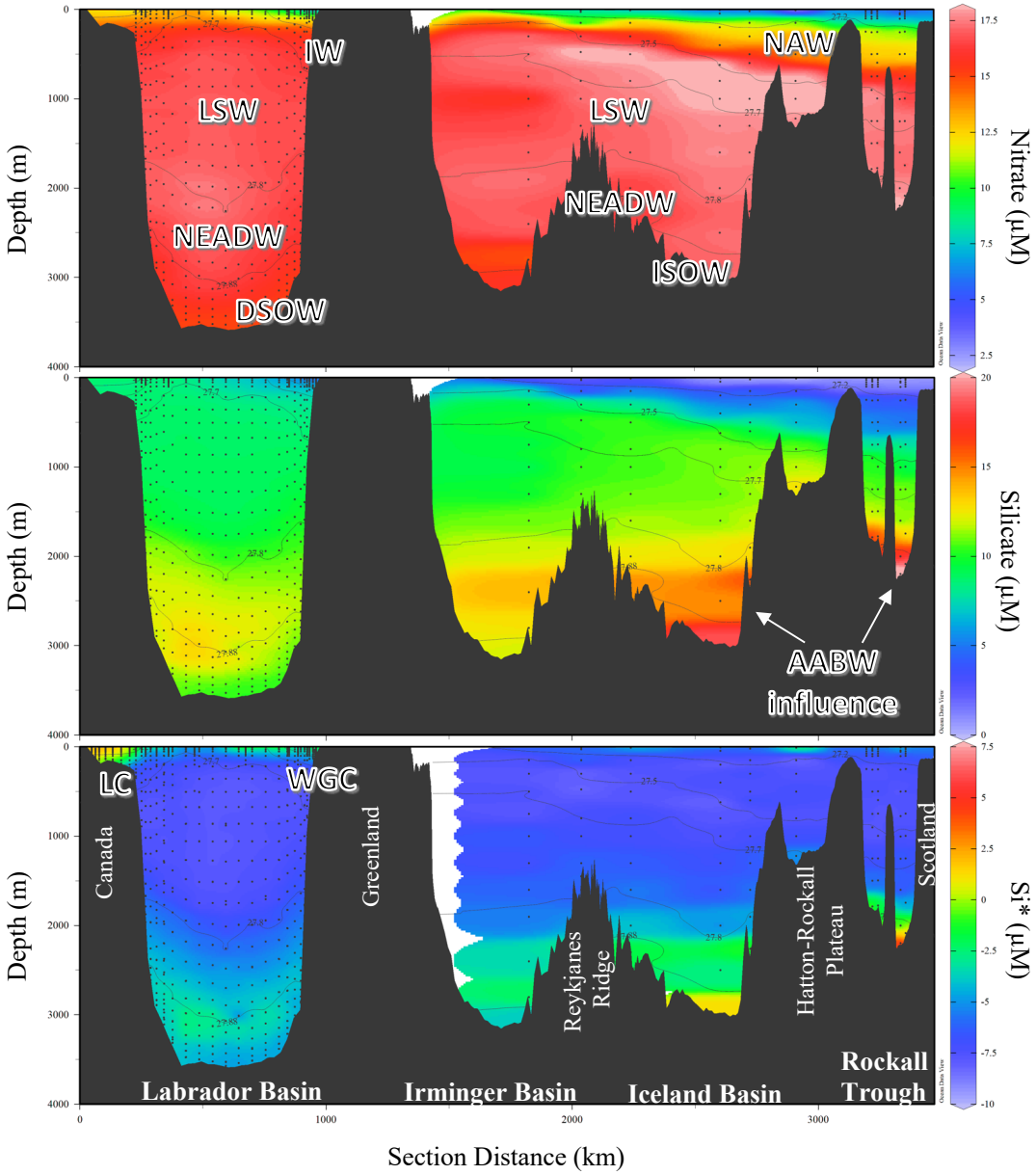

Figure 5.4. Full depth section of nutrient concentrations and derived parameters in the subpolar North Atlantic in 2018. Nitrate (top), DSi (middle) and Si* (bottom) are shown (unit for all parameters is µM). Black lines show key isopycnals defined in Table 5.1.

5.3.2.1 Isotopic signatures of convective basins

Figure 5.5 shows the isotopic profiles of δ^{15}N-NO_3, δ^{18}O-NO_3 and the derived parameter Δ(15-18) for each of the four basins in the subpolar North Atlantic. Water mass nutrient and isotopic properties measured along the transect are summarised in Table 5.2. In surface waters, δ^{15}N-NO_3 and δ^{18}O-NO_3 increase with decreasing

nitrate concentrations, consistent with fractionation during biological nitrogen assimilation (Sigman et al., 2009a). $\delta^{15}N\text{-}NO_3$ values are relatively constant over the Rockall, Iceland and Irminger basins below the surface signal of assimilation. Variations are however observed in $\delta^{18}O\text{-}NO_3$ down to 1000m of the upper water column. NAW $\Delta(15\text{-}18)$ is low (2.11 – 2.48‰), falling below the mean ocean average of 3‰.

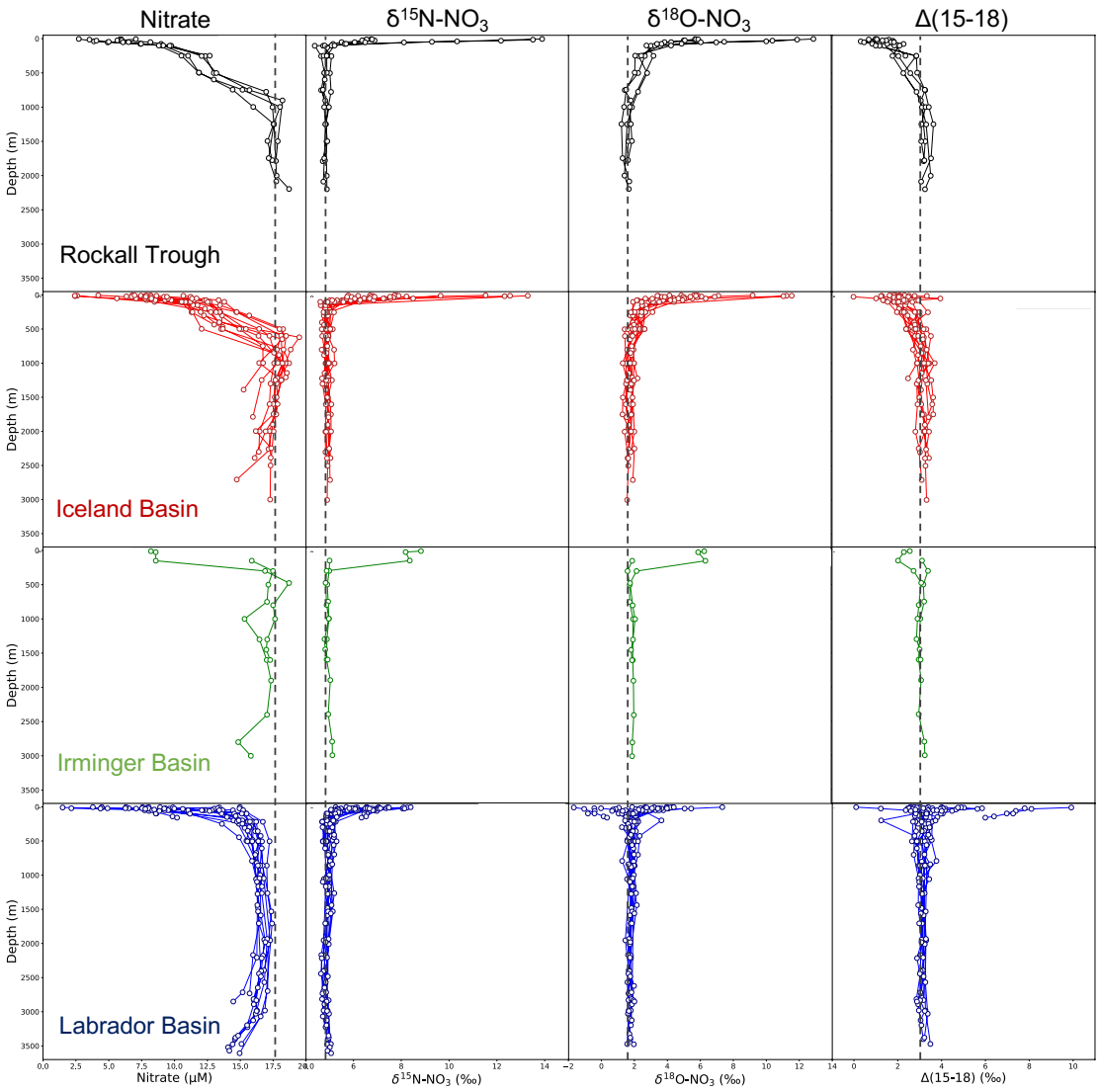

Figure 5.5. Nitrate concentrations (left), $\delta^{15}N\text{-}NO_3$ (middle-left), $\delta^{18}O\text{-}NO_3$ (middle-right) and $\Delta(15\text{-}18)$ profiles (right) within the subpolar North Atlantic, separated by convective basin (2017-2019).

As can be seen on Figure 5.5, nitrate is only partially assimilated in the eastern basins (>2.5μM) and nitrate regeneration occurs in NAW, as seen from elevated nitrate concentrations in the thermocline. Nitrification increases the $\delta^{18}O\text{-}NO_3$ of regenerated nitrate from partially assimilated PON, while $\delta^{15}N\text{-}NO_3$ remains relatively similar to $\delta^{15}N\text{-}PN$ (Deman et al., 2021; Peng et al., 2018; Sigman et al., 2009a). Thus, when partial assimilation and nitrification are co-occuring in the water column, Δ(15-18) decreases (further detailed in Section 1.4.3), and the low Δ(15-18) observed in NAW is reflective of regeneration coupled to partial assimilation of N.

Small variations are observed in $\delta^{15}N\text{-}NO_3$ in the deep Labrador basin, with a slight enrichment in $\delta^{15}N\text{-}NO_3$ in LSW (4.96 ± 0.15‰) compared to NEADW (4.79 ± 0.09‰, $p < 0.01$). $\delta^{18}O\text{-}NO_3$ of LSW is slightly higher (1.85 ± 0.20‰) than in NEADW (1.74 ± 0.13‰, $p < 0.05$), albeit within analytical error, linked to heavily utilised nutrient pools in the subarctic regions. This closely aligns with previously measured endmember values in the Labrador Basin (Deman et al., 2021; Lehmann et al., 2019) and NEADW in the Labrador basin is close to measured deep ocean values in the North Atlantic ($\delta^{15}N\text{-}NO_3$ = 4.83 ± 0.01‰, $\delta^{18}O\text{-}NO_3$ = 1.76 ± 0.13‰, Marconi et al., 2019). In the deep Labrador Basin, DSOW has a $\delta^{15}N\text{-}NO_3$ = 4.92 ± 0.09‰ and $\delta^{18}O\text{-}NO_3$ = 1.76 ± 0.12‰.

As LSW spreads eastward, a gradual decrease from 4.96 ± 0.15‰ to 4.86 ± 0.06‰ is observed across the basins. This is accompanied by a 0.24‰ decrease in $\delta^{18}O\text{-}NO_3$, along with increasing salinity. In the Iceland basin, LSW & NEADW nitrate isotopic properties are virtually indistinguishable, indicating modification through mixing and nitrate regeneration from subtropical sources via the raining down of PON.

Figure 5.6 displays the isotopic profiles of $\delta^{30}Si(OH)_4$ for the study region. Positive values are measured across the dataset, ranging from 1.41 – 3.01‰. The steepest gradients are observed at depths <200m, along with decreasing DSi concentrations, consistent with fractionation during biological uptake by diatoms (Cardinal et al., 2005; De La Rocha et al., 2000). Below this, deep ocean $\delta^{30}Si(OH)_4$ varies between

1.60 – 1.80‰, aligning with other published measurements of water masses in the subpolar North Atlantic (Giesbrecht et al., 2022; De Souza et al., 2012).

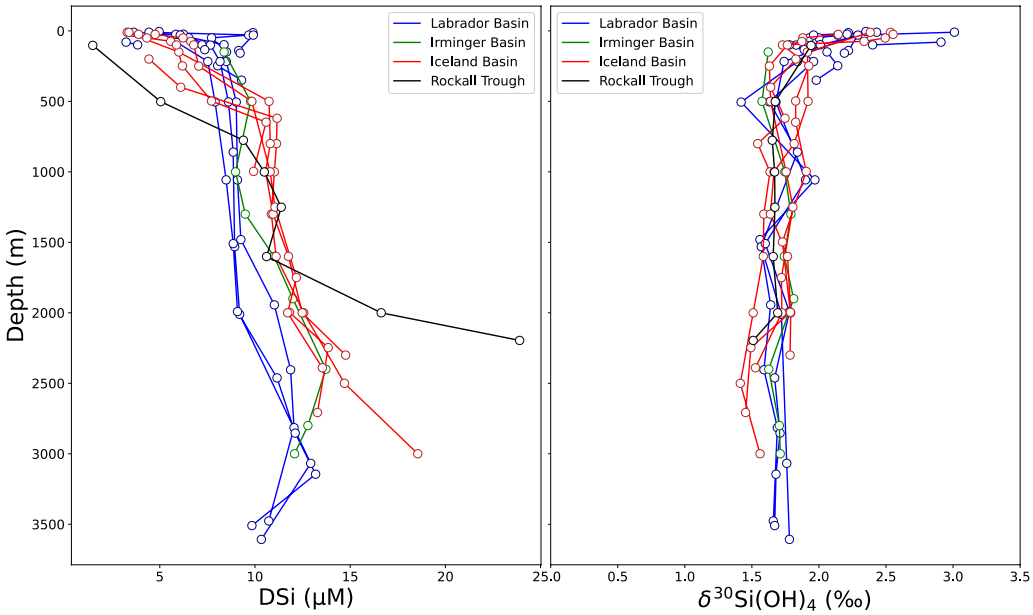

Figure 5.6. DSi concentrations (left) and $\delta^{30}Si(OH)_4$ (right) profiles within the subpolar North Atlantic, separated by convective basins (2017-2019).

Relatively small variability is observed down the water column in the Labrador basin, with LSW $\delta^{30}Si(OH)_4$ = 1.69 ± 0.16‰, NEADW $\delta^{30}Si(OH)_4$ = 1.68 ± 0.05‰ and DSOW $\delta^{30}Si(OH)_4$ = 1.70 ± 0.05‰. NEADW aligns perfectly with the $\delta^{30}Si(OH)_4$ of the water mass in Giesbrecht et al. (2022) (1.68 ± 0.14‰). A large range of $\delta^{30}Si(OH)_4$ has been documented for LSW in previous studies (1.56 – 1.79‰, (Giesbrecht et al., 2022; De Souza et al., 2012; Sutton et al., 2018b). The variability has been attributed to the convective nature of the water mass (Giesbrecht et al., 2022), where the relative contribution of polar-sourced DSi (heavy $\delta^{30}Si(OH)_4$) and Atlantic-sourced DSi (lighter $\delta^{30}Si(OH)_4$) leads to gradients between the two isotopic endmembers, varying both locally along the transect and interannually. This variability is reflected within our measurements with a standard deviation three times as large as for any other deep water mass and a gradient between newly-convected and older LSW.

NAW is isotopically moderately heavy ($\delta^{30}Si(OH)_4$ = 1.76 ± 0.13‰) from extensive utilisation in an oligotrophic environment. Below the seasonally warmed surface

layer, NAW carries an increasingly heavy $\delta^{30}Si(OH)_4$ signature (1.84 ± 0.18‰ over the Iceland Basin, 1.95 ± 0.18‰ in the IW of the Labrador basin), with increasing DSi (6.0 ± 2.0µM and 8.1 ± 2.5µM respectively), reflecting the gradual addition of isotopically heavy, polar-sourced DSi westward of the tropically influenced NAW core, and is consistent with the addition of biogenic opal dissolution from the Labrador Basin Eastward.

Table 5.2. Nutrient and isotope signatures for water masses in each basin along the transect measured in this study.

Basin	Water mass	NO_3	$\delta^{15}N\text{-}NO_3$	$\delta^{18}O\text{-}NO_3$	Δ(15-18)	DSi	$\delta^{30}Si(OH)_4$
Rockall	NAW	12.9 ± 1.9	4.87 ± 0.13	2.38 ± 0.60	2.50 ± 0.59	5.4 ± 1.9	1.76 ± 0.13
	LSW	17.5 ± 0.3	4.86 ± 0.06	1.61 ± 0.18	3.26 ± 0.14	12.7 ± 2.2	1.67 ± 0.01
	NEADW	18.1 ± 0.5	4.88 ± 0.07	1.61 ± 0.13	3.27 ± 0.18	19.8 ± 3.0	1.60 ± 0.09
Iceland	NAW	13.1 ± 2.2	5.11 ± 0.44	2.64 ± 0.80	2.48 ± 0.53	6.1 ± 2.0	1.84 ± 0.18
	LSW	17.5 ± 0.7	4.93 ± 0.12	1.75 ± 0.22	3.18 ± 0.28	11.5 ± 1.1	1.69 ± 0.09
	NEADW	17.1 ± 0.3	4.94 ± 0.07	1.75 ± 0.20	3.19 ± 0.22	13.9 ± 1.6	1.60 ± 0.16
	ISOW	16.1 ± 0.8	4.92 ± 0.07	1.71 ± 0.14	3.21 ± 0.14	14.0 ± 2.7	1.58 ± 0.12
Irminger	LSW	16.9 ± 0.6	4.90 ± 0.06	1.89 ± 0.10	3.01 ± 0.11	10.3 ± 0.1	1.71 ± 0.08
	NEADW	16.4 ± 1.1	5.03 ± 0.07	1.95 ± 0.04	3.08 ± 0.11	12.8 ± 0.7	1.71 ± 0.08
	DSOW	15.8	5.12	1.89	3.23	12.1	1.71
Labrador	LC	7.7 ± 2.8	6.55 ± 0.75	0.63 ± 1.58	5.93 ± 2.10	7.9 ± 3.0	2.27 ± 0.29
	WGC	5.3 ± 3.8	5.92 ± 0.64	2.48 ± 1.35	3.44 ± 0.95	3.7 ± 2.1	2.43 ± 0.34
	IW	16.4 ± 2.2	4.94 ± 0.14	1.87 ± 0.33	3.07 ± 0.33	9.8 ± 4.1	1.89 ± 0.16
	LSW	16.3 ± 0.9	4.96 ± 0.15	1.85 ± 0.20	3.11 ± 0.18	9.0 ± 0.6	1.69 ± 0.16
	NEADW	16.5 ± 0.5	4.79 ± 0.09	1.74 ± 0.13	3.07 ± 0.13	11.8 ± 0.9	1.68 ± 0.05
	DSOW	15.3 ± 0.7	4.92 ± 0.09	1.76 ± 0.12	3.14 ± 0.17	11.4 ± 1.3	1.70 ± 0.05

In the Iceland basin, a difference is observed between the $\delta^{30}Si(OH)_4$ of polar-influenced LSW (1.69 ± 0.09‰) and Southern Ocean controlled NEADW (1.60 ± 0.16‰, $p < 0.03$) and ISOW (1.58 ± 0.12‰, $p < 0.02$). This highlights the difference

in DSi origins of the water masses. The isotopic signature of LSW is not strongly modified laterally, while DSi concentrations increase by ~20%, suggesting it is somewhat influenced by water-column dissolution of biogenic opal, while density gradients prevent homogenisation with underlying deep waters. On the other hand, the NEADW $\delta^{30}Si(OH)_4$ is modified eastward to match the isotopic signature of overlaying LSW, with decreasing DSi concentrations, indicative of mixing and dilution with the isotopically heavy polar-influenced water mass as it travels west. The LC in the Labrador basin is lighter than upstream measurements from the polar mixed layer in the Canadian Arctic Archipelago (5.4 ± 2.0 μM, 2.46 ± 0.26‰, Giesbrecht et al., 2022) and exhibits both higher DSi concentrations and lighter isotopic signatures than upstream. This is perhaps unsurprising considering the complex hydrography and various water pathways of the Canadian Arctic Archipelago, and indicates the branching of nutrient-rich Pacific-originating nutrients rejoining the main LC further downstream.

5.4 Discussion

5.4.1 Polar-sourced nutrients in currents of the Labrador Basin

An exception to the dual enrichment of $\delta^{15}N\text{-}NO_3$ and $\delta^{18}O\text{-}NO_3$ associated with assimilation in surface waters is observed in the LC and WGC. Elevated $\delta^{15}N\text{-}NO_3$ is associated with low $\delta^{18}O\text{-}NO_3$ (<1.8‰), carrying the remnant signal of nitrogen removal processes on Arctic shelves, namely through benthic Coupled-Partial Nitrification Denitrification (CPND) at high latitudes (Doncila, 2020; Fripiat et al., 2018; Granger et al., 2011, 2018). This signal is subsequently exported out of the Arctic in PSW (Tuerena et al., 2021a). This is the first time this signal is documented in the Labrador basin (Deman et al., 2021; Lehmann et al., 2022), and appears to be contained within the core of LC over the Labrador shelf and slope.

The polar-sourced LC has isotopically very heavy DSi (2.27 ± 0.30‰, Table 5.2) with relatively high DSi concentrations (7.9 ± 3.0 μM). LC has similar $\delta^{30}Si(OH)_4$ to WGC with nearly doubled DSi concentrations (Table 5.2). This is indicative of a difference in DSi nutrient sources between Polar waters from the Canadian Arctic

and the Eurasian Arctic sectors, and Pacific-sourced DSi is tracked into the LC. For nitrate, this difference in sources between sectors is largely erased by vigorous N-removal on Arctic shelves.

5.4.2 Evolution of DSi from Fram Strait to the Labrador Sea

The Greenland Ice sheet has been previously suggested to be an isotopically important source of DSi to the Atlantic & Arctic regions (Hatton et al., 2019; Hawkings et al., 2017, 2018), allegedly bringing in isotopically light glacial DSi to the Arctic and Atlantic. No evidence of this isotopic impact was found in PSW at Fram Strait (see Section 3.4.2.3). As PSW travels along the Greenland shelf to reach the Labrador Basin as WGC, it cumulatively picks up Greenland glacial melt, and could potentially show a greater glacial influence further south. In the Labrador basin, WGC is isotopically heavy (2.58 ± 0.23‰) with very low DSi in the WGC (3.5 ± 2.1 μM). WGC is significantly more enriched than in PSW at Fram Strait (6.6 ± 1.7 μM, 1.85 ± 0.09‰, Table 3.2). The shift towards heavier signature follows the expected trend of isotopic enrichment during partial DSi uptake as the waters travel along the Greenland shelf and move towards the Labrador Basin. The addition of isotopically light DSi from the Greenland ice sheet to Greenland shelf waters is not readily apparent. This is also supported by concurrent measurements of $\delta^{30}Si(OH)_4$ on the East Greenland shelf (Laukert, pers.comm.).

The DSi and amorphous Si contribution from the Greenland Ice Sheet in Hawkings et al. (2017) and Meire et al. (2016) has led to an additional calculated flux of 0.29 (±0.22) Tmol $Siyr^{-1}$ to the global Si budget (Tréguer et al., 2021). Our isotopic measurements however suggest that this is an overestimate. Estimates from Hawkings et al. (2017) are based on glacial meltwaters Si concentrations prior to entering coastal ecosystems. While biogeochemical cycling of Si in fjords is complex, meltwaters are strongly diluted, and it is expected that a significant portion of DSi will be quickly removed and trapped within fjordic systems prior to reaching the marine endmember (Hopwood et al., 2020) through assimilation and burial and/or reverse weathering. Further to this, DSi constitutes only <15% of the total Si flux from the Greenland Ice Sheet (Tréguer et al., 2021), with the remaining 0.25

Tmol $Siyr^{-1}$ in the form of amorphous Si. As previously discussed in Section 3, the solubility of amorphous Si in estuarine environments is poorly documented, and a large fraction of it may be buried in the sediments of Arctic before it can be dissolved, thereby largely reducing the calculated impact of glacially-sourced Si to the subpolar environment.

To recap, local processes of assimilation dominate the upper 1000m of the Subpolar North Atlantic with regeneration of N in the OMZ, while lateral transport of remote N & Si cycling is tracked in both polar (LC & WGC) and subtropical (NAW) waters. In light of the recent changes to the water regimes of the Subpolar North Atlantic, we use stable isotopes to detangle the importance of local vs far-field processes to Atlantic nutrient inventories and productivity.

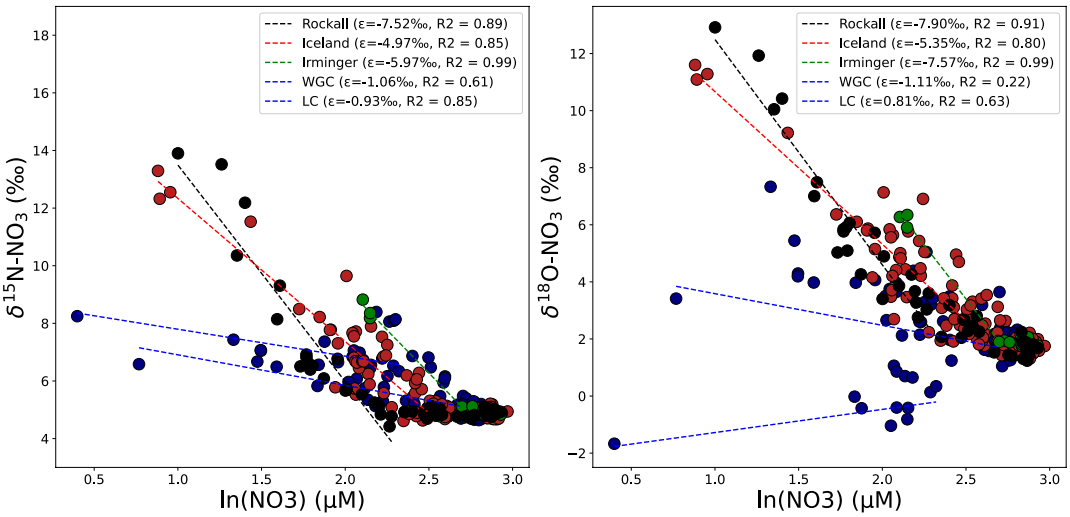

Figure 5.7. Plot of $\delta^{15}N\text{-}NO_3$ vs ln(nitrate) for all profiles within the transect for the Labrador basin (blue), Irminger basin (green), Iceland basin (red) and Rockall Trough (black). The isotope effect from subsurface nitrate pools is calculated for each basin.

5.4.3 Upper subpolar North Atlantic: local vs remote processes

In the upper 200m of the water column, based on linear regression in the Rayleigh space, nitrate isotopes are negatively correlated with nitrate concentrations, indicating they are kinetically fractionated by assimilation (Figure 5.5). Nitrate is strongly depleted, but not fully consumed, as concentrations remain above 2.5 µM.

The seasonal uptake of nitrate fractionates $\delta^{15}N\text{-}NO_3$ and $\delta^{18}O\text{-}NO_3$ with an isotope effect (ε) close to 5‰ (Sigman et al., 2009b). ε > 5‰ has been observed in the North Atlantic regions, as a result of simultaneous assimilation and nitrification co-occuring in the euphotic zone (Deman et al., 2021; Difiore et al., 2010). Meanwhile, in Arctic polar surface waters, ε is muted from dilution with nitrate depleted freshwater, reaching ε as low as 1.8‰ (Tuerena et al., 2021b).

Figure 5.7 shows the isotopic effect for each basin, with data following a Rayleigh fractionation (Mariotti et al., 1981). Observed ε for the subpolar North Atlantic range between 4.97 – 7.52‰, reflecting that the characteristics of subsurface nitrate pools in the subpolar North Atlantic differ between basins (Deman et al., 2021). The eastward increase is reflective of co-occurring partial assimilation and nitrification in surface waters, as described by Difiore et al. (2010). The two polar currents have much lower ε, and lower than measured in the Barents Sea, indicating that the currents are further diluted during their southward transport, picking up glacial and riverine freshwater.

The nitrate isotopic signature of outflow polar currents (high $\delta^{15}N\text{-}NO_3$, low $\delta^{18}O\text{-}NO_3$) is characteristic of CPND which occurs on shallow Arctic shelves, strongly modified from its Pacific and Atlantic origins. This is consistent with findings from Lehmann et al. (2019, 2022) which find a strong influence from remineralisation in the Canadian Arctic Archipelago, and that much of the Pacific-originating nitrate is trapped in the deep Baffin Bay, similar to Pacific-originating DSi (Giesbrecht et al., 2022).

The trends of uptake observed in the subpolar region are plotted in the $\delta^{15}N\text{-}NO_3$ vs $\delta^{18}O\text{-}NO_3$ space on Figure 5.8. In general, they follow 1:1 fractionation of both isotopes, as expected from assimilation and denitrification, but on separate Δ(15-18) contours. An Eastward gradient towards lighter Δ(15-18) is measured, with lightest Δ(15-18) (< 2‰) in the Iceland and Rockall basins. Where the surface nitrate pool is not fully consumed, co-occurring nitrification increases the $\delta^{18}O$ of regenerated NO_3 (+1.1‰ from $\delta^{18}O\text{-}H_2O$) while $\delta^{15}N\text{-}NO_3$ remains the same as that of $\delta^{15}N\text{-}PN$

(Marconi et al., 2019; Peng et al., 2018; Sigman et al., 2009a). This leads to an overall decrease Δ(15-18). Thus, the separation of trends on Figure 5.8 clearly displays the increasing influence of the subpolar N pool (Deman et al., 2021), with increasing importance of nitrate regeneration through nitrification in NAW. The decreasing influence of subpolar sourced nitrate westward is traced through increasing Δ(15-18) towards the Labrador basin (Deman et al., 2021), where Arctic nitrate pools with the isotopic imprint of CPND may further increase Δ(15-18) above the mean ocean Δ(15-18) = 3‰.

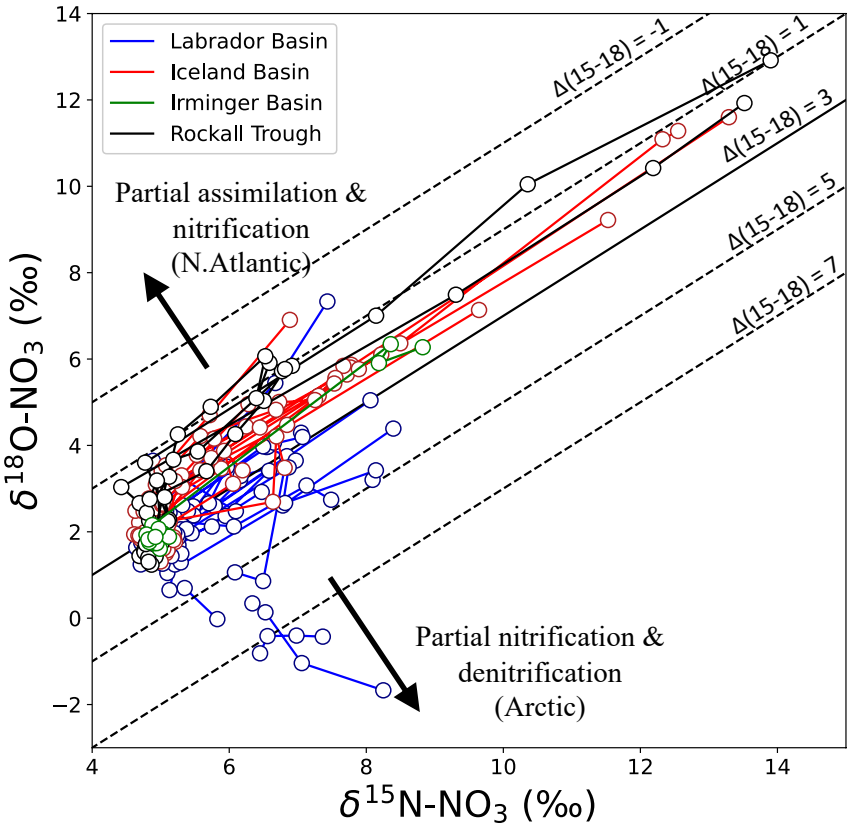

Figure 5.8. Plot of δ^{15}N-NO_3 vs δ^{18}O-NO_3 for all profiles within the transect for the Labrador basin (blue), Irminger basin (green), Iceland basin (red) and Rockall Trough (black). Dotted lines show 1:1 fractionation lines between the two isotopes (expected during assimilation/remineralisation) at separate Δ(15-18) contours.

A similar analysis of $\delta^{30}Si(OH)_4$ variation in the subsurface of the subpolar North Atlantic has not been possible in the past due to lack of measurements in the upper water column (<500m, (De Souza et al., 2012; Sutton et al., 2018b). NAW contributes to halocline and intermediate waters of the Arctic Ocean and Arctic DSi

stocks (Rudels et al., 1994), and DSi can be limiting to primary production in the Eurasian Arctic (Krause et al., 2018, 2019; Randelhoff et al., 2018). Therefore, processes tied to the origins and signature of NAW have a basin-wide impact on the Arctic Ocean.

This study thus provides the first measurements of $\delta^{30}Si(OH)_4$ in the subsurface, completing the isoscape of the subpolar North Atlantic. We measure low DSi in the upper ocean (5-6 μM), with slightly heavier isotopic signatures (1.76 – 1.84‰) from oligotrophic tropical origins albeit much lighter than in heavily utilised polar currents LC and WGC (Table 5.2). The $\delta^{30}Si(OH)_4$ of inflow of NAW through the Rockall Trough (1.76 ± 0.13‰) is identical to AW and AAW in Fram Strait (DSi = 5.4 – 6.6 μM, $\delta^{30}Si(OH)_4$ = 1.74 ± 0.06‰, see Section 3, Table 3.2). This demonstrates that the bulk of the signature of AW in the Arctic Ocean is tied to subtropical and subpolar processes, with little further modification as it travels northward through the Nordic Seas.

Globally, N limits primary production in much of the low-latitude regions where nutrient resupply from the subsurface is slow (Moore et al., 2008, 2013). Nitrate is drawn down to 0 μM in the subtropical gyre, thus the exported isotopic signature of PN is the same as that of the surface nitrogen pool, leading to relatively uniform profiles of $\delta^{15}N\text{-}NO_3$ through the Atlantic (Marconi et al., 2015, 2019). On the other hand, DSi in the low-latitudes of the Atlantic is also strongly depleted, but is not fully utilised, leading to a difference in isotopic signatures of exported PSi compared to $\delta^{30}Si$ of seawater. This leads to increasingly heavy $\delta^{30}Si(OH)_4$ signatures as the Sub-Antarctic Mode Waters and Antarctic Intermediate Waters provide DSi to the Northward-travelling North Atlantic surface currents via upwelling and diapycnal mixing (Brzezinski and Jones, 2015; De Souza et al., 2012). Thus, the characteristics of the NAW inflow to the Arctic Ocean are made increasingly isotopically heavy with the extent of utilisation of this southern-sourced DSi pool as it moves northwards. This links $\delta^{30}Si(OH)_4$ of the Arctic DSi pool both to Fe limitation in the Southern Ocean during the formation of mode and intermediate waters, and N-availability in the low latitudes of the North Atlantic as nutrient upwells.

The evolution of assimilation and regeneration of nitrate in AW is examined on Figure 5.9 through integrated profiles covering the subtropics to the Fram Strait. In the subpolar regions, nitrate regeneration in the upper 600m increases $\delta^{18}O\text{-}NO_3$. This signal of assimilation and regeneration is integrated into the water column down to 1000m in the subtropics (Deman et al., 2021). Additionally, N_2 fixation at low-latitude regions lowers $\delta^{15}N\text{-}NO_3$ further below the global average, supporting further assimilation and regeneration within the water column and further decreasing Δ(15-18) from its convected sub-polar signal.

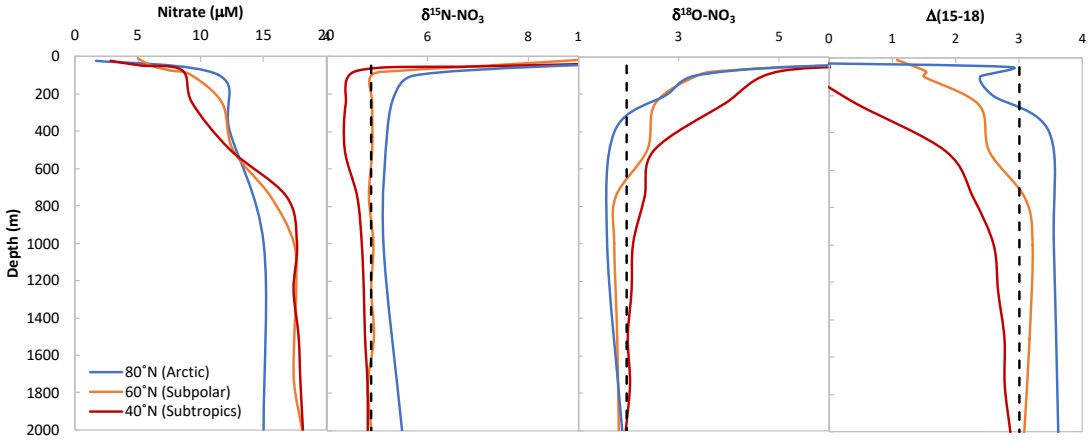

Figure 5.9. Integrated profiles of nitrate concentrations (left), $\delta^{15}N\text{-}NO_3$ (middle-left), $\delta^{18}O\text{-}NO_3$ (middle-right) and Δ(15-18) profiles (right) as during northward transport of AW through the subtropics regions (Deman et al., 2021), subpolar regions (this study) and polar regions (section 3). Dotted black line shows global mean deep ocean values for each parameter.

Cycling in Atlantic waters shifts significantly from the subpolar to polar regions.. Both shoaling and muting of the low Δ(15-18) signal is observed in Fram Strait compared to the subpolar North Atlantic. Subsurface $\delta^{15}N\text{-}NO_3$ is higher in AW than in NAW. This indicates more complete utilisation of the N pool in the Arctic Ocean, which acts to increase $\delta^{15}N\text{-}PN$ and thus the $\delta^{15}N\text{-}NO_3$ of regenerated nitrate, increasing Δ(15-18) towards 3.0‰ in the upper 400m. Thus in subsurface waters of the Atlantic, Δ(15-18) can act as an indicator of N depletion. The muted effect of regeneration on $\delta^{18}O\text{-}NO_3$ is also reflective of nitrate regeneration in lower ambient $\delta^{18}O\text{-}H_2O$ of AW in the Arctic Ocean ($\delta^{18}O\text{-}H_2O$ = ~0.3 ‰, Schlitzer et al., 2018) where nitrification ($\delta^{18}O\text{-}H_2O$ +1.1 ‰, Sigman et al., 2009a) leads to lower

regenerated $\delta^{18}O\text{-}NO_3$ (=1.4 ‰), compared to 1.9 ‰ for regenerated nitrate in AW ($\delta^{18}O\text{-}H_2O$ = ~0.8 ‰, Schlitzer et al., 2018).

Higher Δ(15-18) in AW reflects more complete assimilation of nitrate and increased pressure on the N inventory to support primary production towards the pole. Atlantification of AW has enhanced primary production, leading to a decrease of 0.09 μM /yr in NO_x concentrations of surface waters from 1990 until today (Tuerena et al., 2021c). This is a 3% loss per year of the late summer NO_3 inventory of AW (Table 3.2, Section 3). Following the current trend, summer NO_x stocks will be drawn down to 0μM by 2050, making N the limiting nutrient to phytoplankton growth in AW instead of DSi and reversing the current trends of increased primary productivity linked to global warming (Arrigo and van Dijken, 2015).

To summarise, assimilation is the primary process controlling N and DSi concentrations in the upper waters of the subpolar North Atlantic, with significant regeneration of N in NAW. Polar currents LC & WGC advect the signal of denitrification from the Arctic Ocean, which removes the isotopic signal of pre-formed N in the Arctic Ocean, while DSi sources are further modified during their southward transport, and Pacific DSi in LC remains distinct. Figure 5.9 highlights that the pool of N available to sustain primary productivity in the Arctic Ocean directly depends on the extent of assimilation of N in NAW in the subpolar regions. As pressures on nitrate continue to increase to sustain increasing primary productivity linked to global warming, it is important to understand how the recent freshening event of the subpolar regions has affected regional nitrate assimilation. Next, we use these insights of N-cycling in the subpolar North Atlantic to investigate the origins of the recent freshening of the region, and evaluate its impact on assimilation and regeneration locally, and explore potential implications to the Eurasian Arctic Ocean.

5.4.4 Origins of nitrate during the freshening of the subpolar North Atlantic

The upper water column of the subpolar North Atlantic has recently undergone large-scale freshening, with a salinity anomaly of -0.1 psu at depths of 200-1000m

(Holliday et al., 2020). This has been observed to modify nutrient inventories and impact biogeochemical cycling in situ (Holliday, pers. comm) and in the Eurasian Arctic. To understand the impact of this freshening on productivity of the subpolar region and implications to the nutrient stoichiometry of convective water masses over the next decades, it is important to constrain the origins of the nutrients associated with the freshening event.

The cause of the freshening, and thus its nutrient origins, is highly debated. Currently, proposed mechanisms to explain its origins are

1) Deviation of the Labrador Current to the East (Holliday et al., 2020)
2) Cooling of subtropical waters (Bryden et al., 2020).
3) Recirculation of the subpolar gyre (Fox et al., 2022)

As highlighted in Table 5.2, nutrient isotopic differences between water masses of the subpolar region are subtle, however, as discussed in section 5.4.1, $\delta^{18}O\text{-}NO_3$ and $\Delta(15\text{-}18)$ strongly differentiate between sub-tropical and sub-polar influenced nutrient regimes (high $\delta^{18}O\text{-}NO_3$, low $\Delta(15\text{-}18)$) and polar nutrient regimes (low $\delta^{18}O\text{-}NO_3$, high $\Delta(15\text{-}18)$). These differences stem from the relative importance of nitrate regeneration. Here we examine temporal trends in $\delta^{18}O\text{-}NO_3$ in the Iceland basin to elucidate the nutrient origins of the freshening event.

The extreme freshening event has spread northward from 2012 onwards, reaching its peak over the Iceland basin in 2016. Figure 5.10 displays the $\delta^{18}O\text{-}NO_3$ against the natural logarithm of nitrate at 200-1000m in the Iceland basin from prior to the freshening event reaching the Iceland basin in 2013-2014 (Deman et al., 2021; Peng et al., 2018) compared to after in 2017-2018 (this study, DY078, OSNAP18-E). From Figure 5.10, two general trends emerge: (1) a shift towards lighter $\delta^{18}O\text{-}NO_3$ and decreasing ε, and (2) a decrease in the correlation of isotopes with $\ln(NO_3)$ over time.

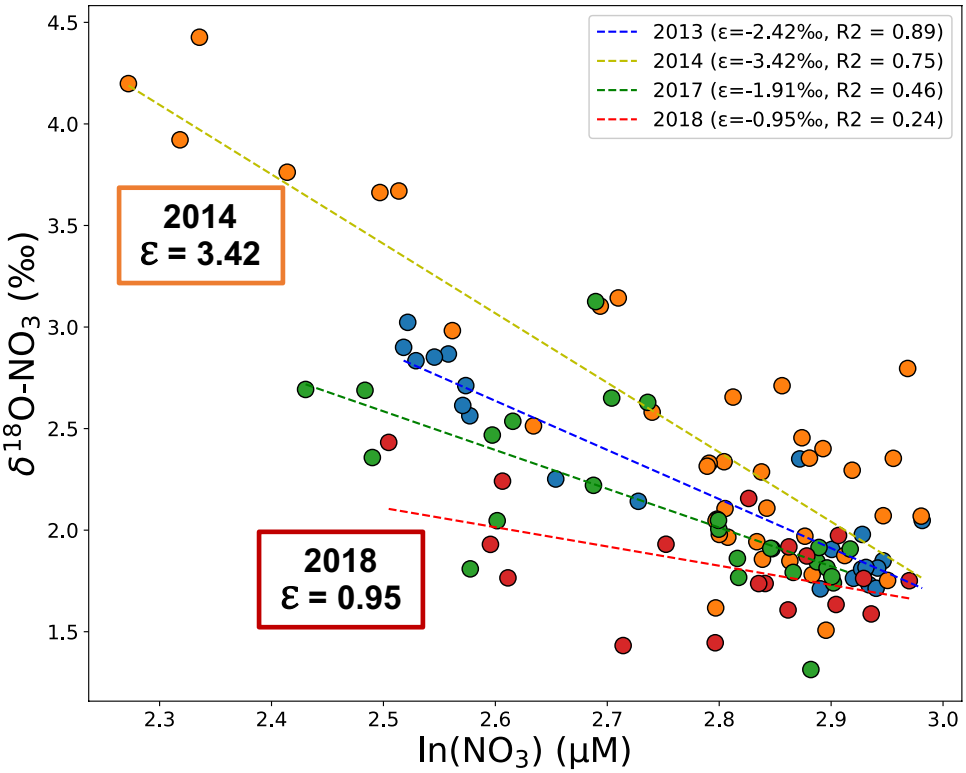

Figure 5.10. Temporal trends of δ^{18}O-NO_3 against ln(NO_3) in the Iceland Basin between 200-1000m depth between 2013 – 2018. Datasets are from Peng et al. (2018, blue circles), Deman et al. (2021, orange circles), DY078 (this study, green circles) and OSNAP18-E (this study, red circles). Dotted lines are the least square regression for each dataset. Standard deviation of the linear regressions (RMSE) are: 2013 = 0.64‰, 2014 = 0.50‰, 2017 = 0.43‰ , 2018 = 0.25‰.

The high correlation between δ^{18}O-NO_3 and ln(NO_3) prior to the freshening event (2013-2014) indicates a tight biological control of processes fractionating isotopes locally. Over time, the correlation between nitrate concentration and isotopes weakens, which reflects the increased influence of physical transport and mixing of remote water masses, rather than in situ biological processes. The decrease in ε observed in Figure 5.10 over time is consistent with increased influence of subpolar/polar water masses over the central Iceland basin and decreasing nitrification. This is consistent with hypothesis 1 and 3 from Holliday et al. (2020) and Fox et al. (2022) respectively.

A shift towards lighter δ^{18}O-NO_3 in the Iceland basin is observed over time (Figure 5.10). Two processes can explain this trend: reduced assimilation within the water column, and/or with remineralisation in lower ambient δ^{18}O-H_2O. During

interglacials in the subpolar North Atlantic, enhanced stratification from meltwater was linked to near complete N-utilisation from the shallower mixed layer (Thibodeau et al., 2017b). It is expected that stratification increased from 2012-2016 as the fresh water propagated over the Iceland basin. Increased stratification inhibits nutrient resupply to surface waters in the Iceland basin, thereby lowering assimilation and thus biological productivity over the growth season, while leading to nitrate depletion within the mixed layer. The LC is associated with particularly low $\delta^{18}O$-H_2O (<-1.0‰, Schlitzer et al., 2018) due to its high fresh water influence. Thus the shift towards lighter $\delta^{18}O$-NO_3 could also be indicative of nitrate regeneration in lighter $\delta^{18}O$-H_2O waters, and is likely to be a combination of both processes described above.

Therefore, our findings are inconsistent with theory 2 from Bryden et al (2020), as no such shift in $\delta^{18}O$-NO_3 would be expected if the new nitrate pool accompanying the freshening remained of subtropical origins. No equivalent trend is observed in the $\delta^{15}N$-NO_3, with only a slight shift towards heavier $\delta^{15}N$-NO_3 (~0.1‰) after the freshening event. Although the isotopic increase of $\delta^{15}N$ is within analytical error, the increase in $\delta^{15}N$-NO_3 is consistent with isotopically heavy LC nitrate carrying the remote signal of CPND. Considering the nitrate content of the LC and a 0.1psu increase in salinity, its heavy isotopic signature would increase $\delta^{15}N$-NO_3 and decrease $\delta^{18}O$-NO_3, both in the order of ~0.1‰. If subpolar sources of nitrate are considered instead, they are isotopically similar across much of the subsurface in the basins (Table 5.2), and therefore could not contribute to both the $\delta^{15}N$-NO_3 enrichment and the lowering of $\delta^{18}O$-NO_3. Our findings are therefore inconsistent with the mechanism suggested by Fox et al., 2022 (hypothesis 3). Thus, the shift in N cycling observed in 2017-2018 is consistent with nutrient originating from the polar LC (hypothesis 1).

As discussed above, dilution alone can not fully explain the observed decrease in $\delta^{18}O\text{-}NO_3$ observed in the Iceland basin, despite the very low $\delta^{18}O\text{-}NO_3$ signature of LC. This implies that the shifting nutrient regimes accompanied by the freshening event have also impacted the extent of assimilation occurring locally in the Iceland basin, the conditions in with nitrate is regenerated and the subsequent integration of its isotopic signature into the upper 1000m of the water column during deep gyre-scale winter convection (Piron et al., 2017; Yashayaev, 2007). Figure 5.11 shows the changes in concentrations of DSi against NO_3 over time. Prior to the freshening event, higher NO_3 concentrations are observed with respect to DSi, which is consistent with the nitrate regeneration within the upper water column and sinking of biogenic Si. This is also consistent with the elevated $\delta^{18}O\text{-}NO_3$ linked to NO_3 regeneration in situ in 2013-2014.

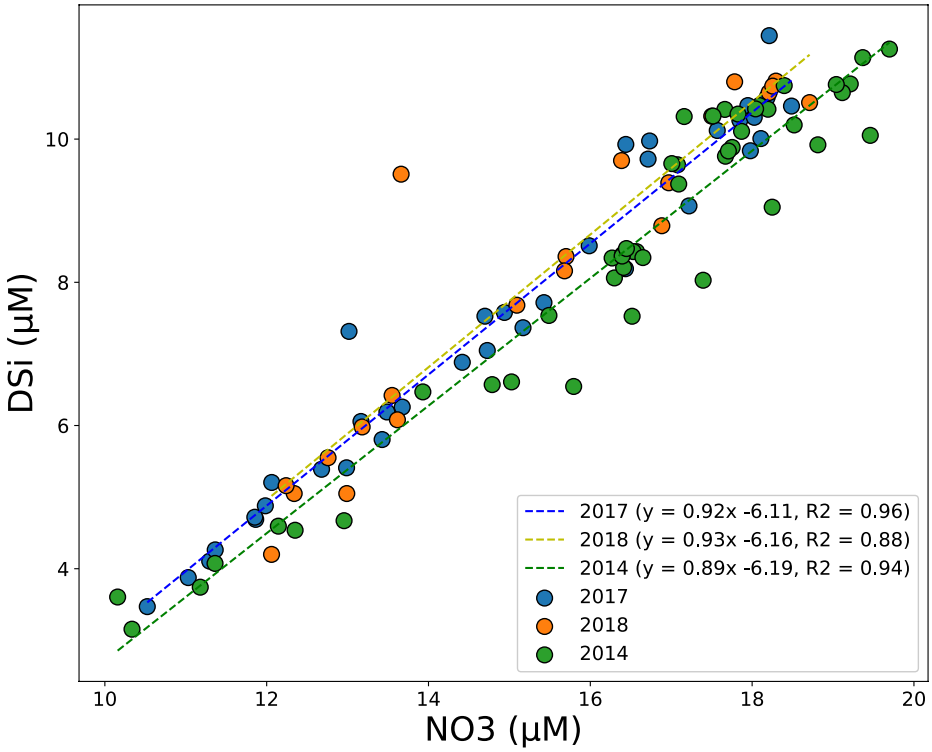

Figure 5.11. Temporal trends of DSi against NO_3 in the Iceland Basin between 200-1000m depth between 2014– 2018. Datasets are from Deman et al. (2021, green circles), DY078 (this study, blue circles) and OSNAP18-E (this study, orange circles). Dotted lines are the least square regression for each dataset.

The shift towards lower nitrate concentrations in relation to DSi after the freshening event indicates lower preformed N:DSi, linked to shelf denitrification in the Arctic Ocean, or decoupling of regeneration and assimilation in-situ, linked to the freshwater lens and stratification.

To conclude, nutrient stoichiometry and isotopic measurements in the Iceland basin in 2017-2018 suggest that the nutrient origins of the freshening event originates from an eastward deviation of the LC, consistent with findings from Holliday et al. (2020). The freshening is associated with reduced assimilation in the years following the event, and decreasing primary productivity and of the N inventory in relation to DSi.

The freshwater content of the subpolar North Atlantic has been increasing, linked to climate warming induced melting and export of ice and freshwater from the Arctic and the Nordic Seas (Dukhovskoy et al., 2019), thereby weakening the Atlantic MOC (Thornalley et al., 2018). Increased stratification linked to meltwater has led to N-depletion in the subpolar North Atlantic during past interglacial events (Thibodeau et al., 2017b), limiting primary production locally. Models predict a decrease in the primary production of the Atlantic Ocean of 1.3 PgC/yr as Greenland Ice sheet melt increases stratification and shoals mixed layer depth, thereby reducing nutrient resupply and availability (Kwiatkowski et al., 2019; Mathis and Mikolajewicz, 2020). The impact of increased stratification in the Atlantic ocean on primary productivity largely supersedes potential increases from glacial upwelling and DSi and N supply (Hopwood et al., 2020). This work provides direct evidence of these predicted changes in the subpolar North Atlantic, and offers insight of how primary productivity may decline as the upper water column becomes increasingly fresher. Due to the interconnectedness of the region, the impact of freshwater on primary production is not contained to the subpolar North Atlantic, and primary production is predicted to reduce in both the subpolar and subtropical gyres (Kwiatkowski et al., 2019). The freshening event observed in the Iceland basin will have widespread impacts on nutrient assimilation as it is now propagating into the Labrador Sea, Irminger Sea and the Nordic Seas.

5.4.5 Atlantic meridional $\delta^{30}Si(OH)_4$ gradients

In this final section, $\delta^{30}Si(OH)_4$ datasets from this study and the literature are used to examine the contribution of polar-sourced DSi to convective waters of the subpolar North Atlantic and eventually NADW.

The MOC drives meridional DSi distribution globally, through upwelling, assimilation and mixing. During glacial and interglacial events, changes in oceanic circulation and ventilation of deep waters have led to large-scale shifts in biological production and carbon-trapping efficiency of diatoms, with repercussions on carbon sequestration and thus atmospheric CO_2 concentrations (Anderson et al., 2002; Hendry et al., 2016; Tagliabue et al., 2009). Diatoms thrive in nutrient-rich turbulent conditions, and thus are prevalent at high latitudes and coastal upwelling regions (Nelson et al., 1995; Tréguer et al., 2018). Thus, the mechanisms that lead to the DSi inventory of NADW impacts DSi distribution and cycling globally.

The Southern Ocean has highly concentrated DSi and the highest concentrations of the deep ocean globally (>125µM, Olsen et al., 2016). This is because the Southern Ocean acts as a Si trap from high biological assimilation in surface waters and deep dissolution, as well as a significant supply from upwelling waters (DeMaster, 2002; Tréguer, 2014). This leads to the export of high DSi concentrations and low $\delta^{30}Si(OH)_4$ in Southern-sourced waters (Fripiat et al., 2011a, 2011b). In the modern ocean, the gradient of seawater $\delta^{30}Si(OH)_4$ between the Southern Ocean (~1.2‰) and NADW (~1.6-1.7‰) is a well-documented feature of the Atlantic, and behaves quasi-conservatively (Brzezinski and Jones, 2015; De Souza et al., 2012; Sutton et al., 2018b). De Souza et al. (2012,2015) attributes this gradient primarily to isotopically fractionated DSi from Antarctic Intermediate Waters (AAIW) and Sub-Antarctic Mode Waters (SAMW) as they travel northwards at the surface of the meridional overturning circulation, implying a Southern Ocean control of DSi distribution in the Atlantic Ocean. Meanwhile, Brzezinski and Jones (2015) and Sutton et al. (2018) attribute a significant part of the gradient to enrichment from isotopically heavy DSi from Arctic origins instead, introducing the concept of a bipole from mixing between the two polar DSi sources.

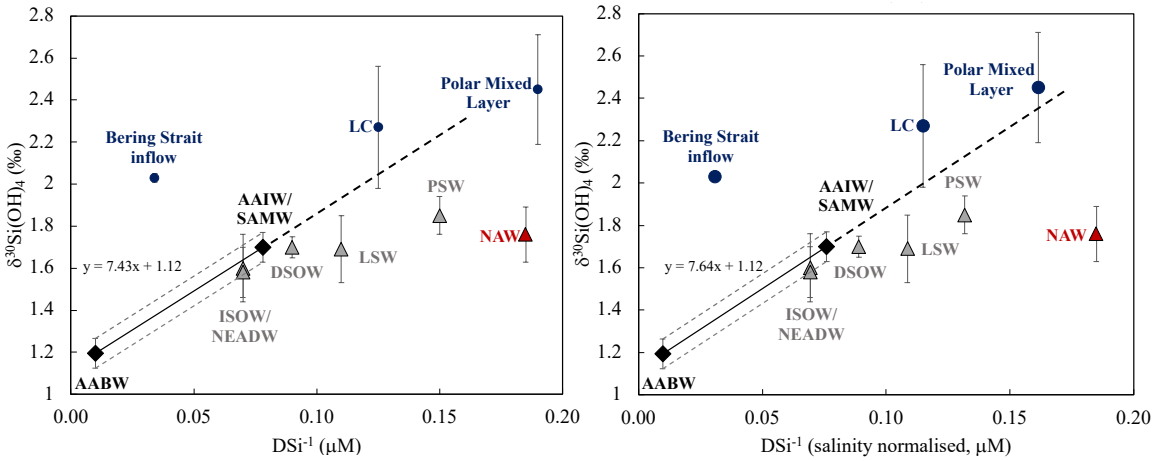

Figure 5.12. Endmember characteristics of water masses in the subpolar North Atlantic and Arctic in context of the Atlantic silicon isotope gradient. Bottom panel shows the same DSi^{-1} concentrations as shown on the top panel, but normalised to salinity to account for the large dilution factor associated with Arctic currents. The Atlantic gradient (black symbols and line) shows the quasi-conservative behaviour in De Souza et al. (2012) between Southern Ocean water masses (AABW, AAIW, SAMW) and water masses of the Atlantic (NEADW). Dotted lines are 1SD of the correlation between AABW and AAIW/SAMW (0.07‰). Triangles are endmember measurements from this study. Blue circles are endmember measurements from Giesbrecht et al. (2022). Error bars shown are 1SD. LC = Labrador Current, AABW = Antarctic Bottom Water, AAIW = Antarctic Intermediate Water, SAMW = SubAntarctic Mode Water, ISOW = Iceland-Scotland Overflow Water, NEADW = NorthEast Atlantic Deep Water, DSOW = Denmark Strait Overflow Water, LSW = Labrador Sea Water, PSW = Polar Surface Water, NAW = North Atlantic Water.

Since these studies, considerable advances have been made in mapping out the outflow of $\delta^{30}Si(OH)_4$ from the Arctic Ocean (Giesbrecht et al., 2022, section 3), and the dataset presented here fills in the gaps of North Atlantic Water evolution from the subtropics to the Arctic Ocean. Here we combine datasets of $\delta^{30}Si(OH)_4$ to understand the exact mechanisms that lead to the DSi inventory of NADW and its isotopic enrichment.

The $\delta^{30}Si(OH)_4$ of key water masses in the North Atlantic against DSi^{-1} are shown on Figure 5.12. All convective water masses, LSW, ISOW, DSOW and NEADW fall at the heavy end of the isotopic trend of the Atlantic, although subtle differences are measured between the water masses. DSOW and LSW fall away from the quasi-conservative line due to low DSi concentrations, while their $\delta^{30}Si(OH)_4$ is not

significantly higher than North Atlantic endmembers. The subpolar and polar regions have isotopic signatures which diverge away from this gradient. In the Arctic Ocean, Pacific-originating DSi from the Bering Strait inflow leads to isotopically heavy and high DSi waters on a separate trend from the Atlantic-influenced PSW. The Pacific nutrient influence is reflected in the signal of outflowing LC, which is isotopically very distinct from convective water masses and its signal does not significantly imprint on the Subpolar regions. This is consistent with findings from de Souza et al. (2015), who estimated contribution of Pacific-sourced DSi to the North Atlantic at <10%.

A key outlier from the Atlantic isotopic gradient measured within this study is NAW, particularly when normalized to salinity to account for the heavy dilution with polar currents (right panel, Figure 5.12). It bears low DSi concentrations (<6 μM) with a $\delta^{30}Si(OH)_4$ of ~1.7‰ in the subpolar regions and in the Arctic AW inflow. Following theoretical fractionation models would predict the isotopic signature of NAW from Southern-sourced DSi to be = 2.5 ± 0.4 ‰ for a closed system or 2.3 ± 0.3 ‰ for an open system (using NAW DSi concentrations from Table 5.2 and fractionation model equations in Section 1.4, and $^{30}\varepsilon$ = -1.07‰ and -1.14‰ respectively, from Giesbrecht et al., 2022. AAIW concentrations and $\delta^{30}Si(OH)_4$ are taken from Brzezinski & Jones, 2015). The $\delta^{30}Si(OH)_4$ of NAW measured within this work is 0.7-1.0‰ lower than expected from the Atlantic isotopic fractionation trend, as it shows very low DSi concentrations with only a moderate $\delta^{30}Si(OH)_4$ enrichment.

Higher isotopic signatures are expected from utilisation in oligotrophic gyres alone (Brzezinski and Jones, 2015; Grasse et al., 2020), with evaporation increasing salinity. To explain deviation from the quasi-conservative trend, significant dilution of ambient North Atlantic DSi with particularly low DSi concentration waters and relatively low $\delta^{30}Si(OH)_4$ are required in the regions between the subtropics and subpolar regions.

We consider a pathway overlooked in previous studies: the mixing of Mediterranean Outflow Water (MOW) in the upper waters of the North Atlantic has the potential to

lead to both dilution and mixing from lighter source $\delta^{30}Si(OH)_4$, leading to the NAW signature observed. While it could be assumed that the isotopic signature of MOW is high as its DSi concentration is low (<10 μM), the Si budget of the Medditerranean Sea significantly differs from other basins. No isotopic measurements are available for the Mediterranean Sea, and its outflow signature is currently unknown, but De Souza et al., (2012) find much lower $\delta^{30}Si(OH)_4$ associated with MOW (~1.4 – 1.5‰) in the Eastern North Atlantic. Radium isotope studies have found that submarine groundwater discharge supply 110 x 10^9 mol of DSi to the Mediterranean Sea annually, which is the same order of magnitude as riverine supply (Rodellas et al., 2015; Tamborski et al., 2018). Generally speaking, submarine groundwater discharge has very light $\delta^{30}Si(OH)_4$ owing to dissolution of secondary clay minerals (Georg et al., 2009a, 2009b). Additionally, the Mediterranean Sea hosts large DSi fluxes from lithogenic sediment weathering and from dust dissolution, primarily from Saharan origins with a large clay content (Krom et al., 2014). All three of these proccesses can lead to lighter $\delta^{30}Si(OH)_4$ with respect to DSi, distinct from riverine sources. In Brzezinski & Jones (2015), the distribution of lighter $\delta^{30}Si(OH)_4$ in NAW correlates with the influence MOW (20-40%, Jenkins et al., 2015).

Alternative sources of light $\delta^{30}Si(OH)_4$ to NAW could originate from submarine groundwater discharge from the European continent, although geochemical or radioactive tracers such as radium isotopes are required to characterise this source accurately (Garcia-Orellana et al., 2021). Another potential contributor of DSi with light $\delta^{30}Si(OH)_4$ is dust dissolution, although its influence to the North Atlantic is largely unconstrained (Tréguer et al., 2021) and very unlikely to have such a basin-wide effect.

The dilutive effect of DSi deplete waters mixing in the surface of the Subpolar North Atlantic is potentially reflected in particularly low $^{30}\varepsilon$ (-0.13 to - 0.53‰) in the Iceland basin and Rockall Trough (Figure 5.13), which falls much below the global average of -1.07‰ (Giesbrecht et al., 2022 and references therein). As per the isotope effect of nitrate, $^{30}\varepsilon$ can artificially be shifted towards lower isotope effects as the DSi pool mixes with waters of lower DSi concentrations or lower $\delta^{30}Si(OH)_4$.

MOW has characteristically low DSi concentrations from its oligotrophic origins in the Mediterranean Sea, and is distinguished by very low Si* (<10 µM). As it enters the Atlantic Ocean, it significantly impacts the nutrient concentrations and stoichiometry of the subtropical and subpolar North Atlantic (van Aken, 2000).

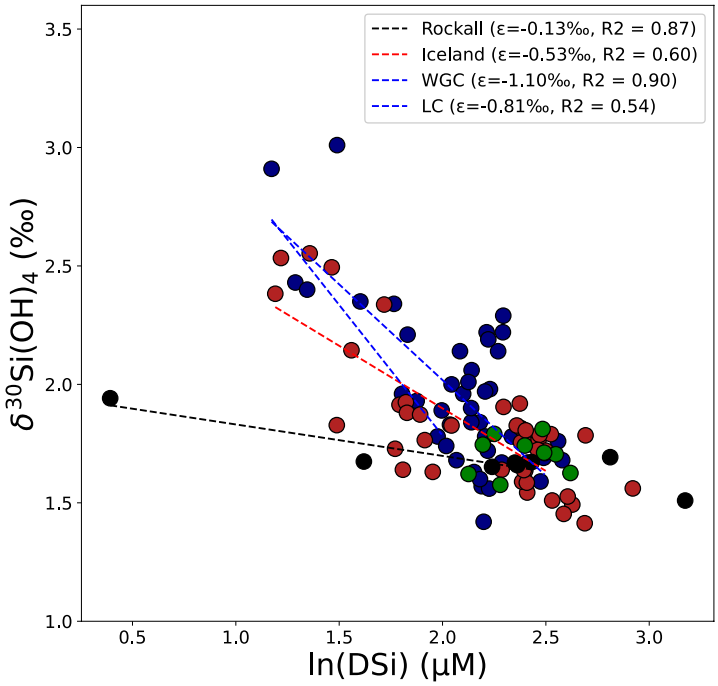

Figure 5.13. Plot of $\delta^{30}Si(OH)_4$ vs ln(DSi) for all profiles within the transect for the Labrador basin (blue), Irminger basin (green), Iceland basin (red) and Rockall Trough (black). The $^{30}\varepsilon$ from subsurface DSi pools is calculated for each basin.

In the subpolar North Atlantic, NAW branch off from the Atlantic gradient driven by fractionation of Southern Ocean sources, and display heavier isotopic signatures due to a diluted isotopic effect potentially associated with MOW and to a smaller extent, polar DSi sources (Pacific, riverine). NAW is a key feature of the subpolar North Atlantic, where it dominates the upper 1000m of the water column, and its signal is integrated into convective water masses through deep winter convection across the North Atlantic (Piron et al., 2017; Yashayaev and Loder, 2009). Furthermore, it provides much of the baseline for Arctic nutrient stocks. The isotopically lighter, diluted sources of DSi play a dampening role on the heavy isotopic enrichment expected from nutrient utilisation alone in the subpolar and Arctic regions. This is clearly observed in the $\delta^{30}Si(OH)_4$ of Eurasian Arctic outflow waters (PSW) which

are heavily influenced by pre-formed nutrients from the Atlantic, compared to Canadian Arctic outflow waters (LC), with Pacific and riverine nutrient origins (Figure 5.13). PSW falls close to Atlantic water masses and NAW, albeit heavier (0.09‰) and slightly richer in DSi primarily from Arctic riverine influence, while the LC falls in line with isotopic enrichment from fractionation associated with uptake.

Thus, convective water masses in the subpolar North Atlantic are isotopically heavy, primarily from fractionation from Southern-sourced DSi transported in SAIW/AAIW. A small enrichment (<0.1‰, Chapter 3) is associated with high-latitude processes in the Arctic Ocean, with much lower DSi concentrations than expected from the quasi-conservative behaviour of the Atlantic Ocean. We highlight the role of NAW in dampening much of the heavy isotopic fractionation associated with high-latitude processes, and hypothesize the origins of this dilution to arise from low DSi, low $\delta^{30}Si(OH)_4$ originating from MOW, although in situ measurements are required to confirm this. Thus, while high latitudes drive the DSi inventory of upper water masses of the North Atlantic, $\delta^{30}Si(OH)_4$ are significantly modified by low latitude mixing and dilution.

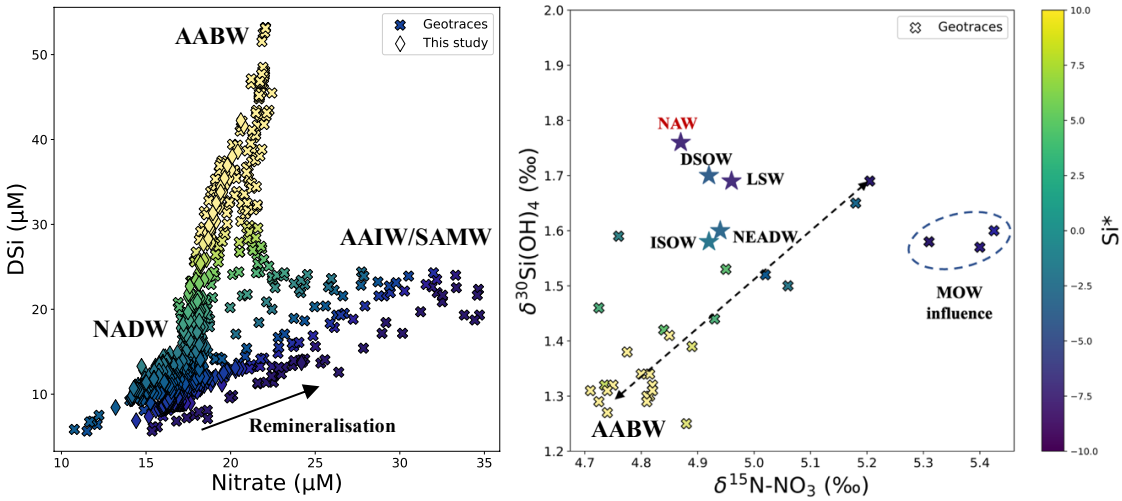

Figure 5.14. The relationship between DSi and nitrate (>600m, left panel) and $\delta^{30}Si(OH)_4$ and $\delta^{15}N\text{-}NO_3$ (>600m, right panel) in the deep North Atlantic from datasets presented in this study and GA03 (GEOTRACES). Star symbols show the isotopic signature of convective water masses in the subpolar regions measured in this study.

5.5 Global synthesis

Due to the differences in DSi and N cycles, namely from the greater depth and lower sensitivity of water-column DSi dissolution compared to N in one hand, and widespread N-limitation in the North Atlantic on the other hand (Moore et al., 2013), the isotope cycling of the two nutrients diverge. DSi is increasingly modified from its Southern Ocean source by biological utilisation, while N cycling is dictated by assimilation and regeneration across the Atlantic. A comparison of DSi and N concentrations and their isotope systems of the deep North Atlantic is shown in Figure 5.14.

The separate branches of Southern-sourced nutrients are clearly differentiated between the high DSi, lower N deep AABW and the lower DSi, high N intermediate SAMW/AAIW, where N_2 fixation and regeneration increases nitrate concentrations with respect to DSi (Sarmiento et al., 2004). The right panel of Figure 5.14 shows that the heavy $\delta^{30}Si(OH)_4$ coincides with waters with heavy $\delta^{15}N\text{-}NO_3$. Unlike the Indo-Pacific Oceans, the Atlantic ocean does not sustain significant water-column denitrification, thus the elevated $\delta^{15}N\text{-}NO_3$ in intermediate waters of the Atlantic are linked to Southern-sourced nitrate (Marconi et al., 2015; Sigman et al., 2003) with elevated $\delta^{15}N\text{-}NO_3$ from partial assimilation as shown on Figure 5.15. This confirms that the $\delta^{30}Si(OH)_4$ enrichment across the Atlantic stems from the strong DSi uptake in surface Atlantic waters sourced from AAIW/SAMW at low latitudes.

The isotopic signatures of convective water masses in the subpolar North Atlantic and NAW fall off this gradient, and a clear outlier from this trend are waters influenced by lighter $\delta^{30}Si$, with enriched $\delta^{15}N\text{-}NO_3$ (>5.3‰) indicated introduction of a different nutrient pool. Convective water masses of the subpolar North Atlantic appear to be largely controlled by the relative mixture of NAW and deep nutrient stocks during their formation.

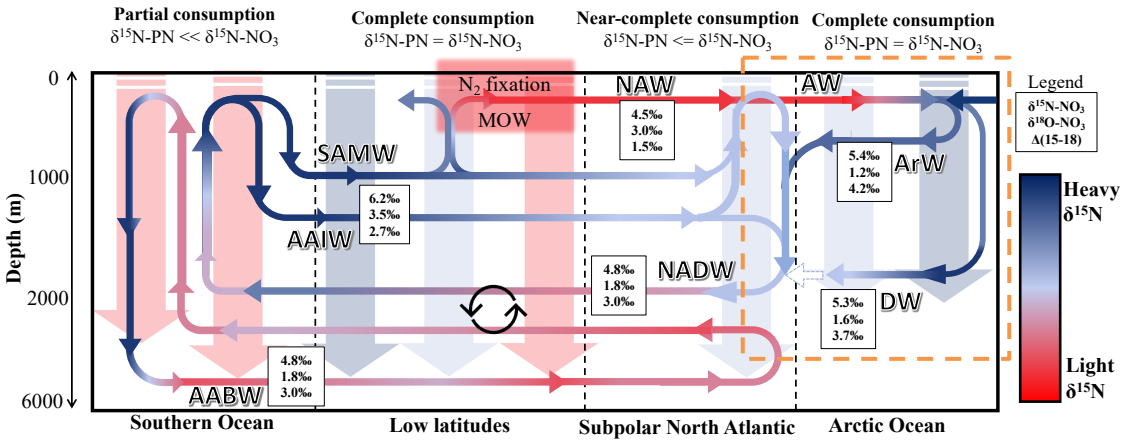

Figure 5.15. Updated (orange dotted box) version of Figure 1.11 (Chapter 1) to include cycling of N in the Arctic Ocean and subpolar regions in the context of the meridional overturning circulation.

A summary of the biological processes and physical transport leading to the isotopic gradients observed for both systems through the Atlantic and Arctic Ocean through this study is shown on Figure 5.15 & Figure 5.16. It illustrates the complex interactions of nutrients with both physical and biological processes, and their susceptibility to change with physical forcings and changes to nutrient sources. Biological utilisation of nutrients from the South Atlantic and subtropics dictates nutrient depletion in NADW. The interconnection of the Arctic basin with the Atlantic Ocean through advection of nutrients implies that changes to the subpolar North Atlantic will directly impact Arctic ecosystems. The observed decrease in N regeneration associated with the 2016 freshening event will lead to the decrease of N inventory of AW in the Arctic Ocean, with further pressures on N-demand and Arctic ecosystems.

Major gaps still exist for understanding DSi cycling and its isotopic fractionation in the Atlantic Ocean, namely from the under-characterisation of low-latitudes processes and key water masses such as MOW. Direct measurements of this key region to the nutrient inventory and stoichiometry of the North Atlantic are however required to confirm this hypothesis.

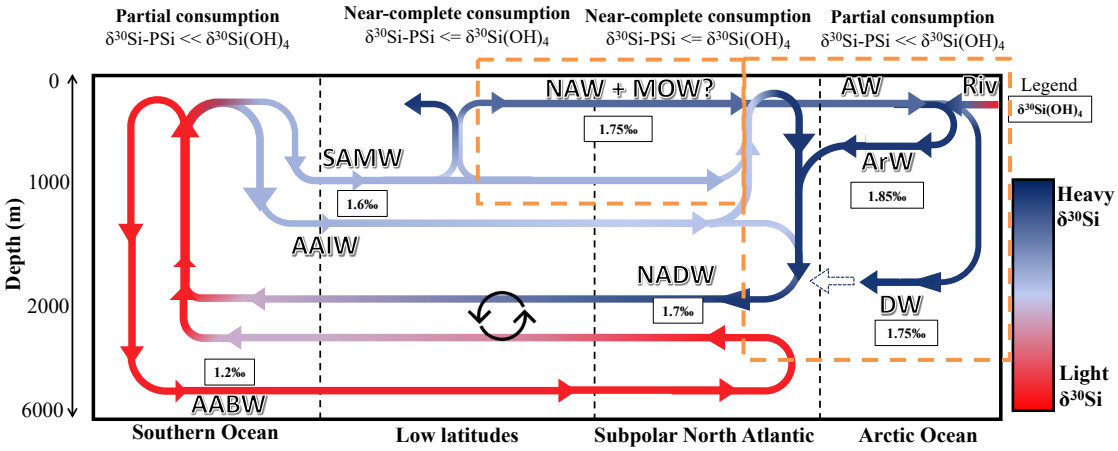

Figure 5.16. Updated (orange dotted box) version of Figure 1.13 (Chapter 1) to include cycling of DSi in the Arctic Ocean and subpolar regions in the context of the meridional overturning circulation.

Nitrogen, oxygen and silicon isotopic data in the Arctic Ocean contribute to closing the loop of the global nutrient budget (Figure 5.15, 5.16). The Arctic Ocean influences NADW primarily through dilutive effects, and as a small source of isotopically heavy DSi. Nonetheless, nitrate and DSi in NADW remain primarily controlled by the extent of biological utilisation in surface waters at both high and low latitudes in the Atlantic Ocean.

6. Concluding Remarks

The research presented in this thesis provides a comprehensive assessment of N and Si cycling in the Arctic Ocean and the Subpolar regions. This work provides the first measurements of the stable isotope of dissolved silicon in Fram Strait and the Eurasian shelf. It is the first study of combined dissolved silicon and nitrate isotopes in the Arctic Ocean and provides an understanding of the processes which control biogeochemical cycling. This knowledge allows better prediction of future nutrient inventory and primary productivity in regions that are heavily impacted by climate change.

6.1 Key Findings

1. Nitrogen is depleted in shelf waters of the Eurasian Arctic due to 3 mechanisms: N-poor freshwater sources, intense utilisation and denitrification on shallow shelves. This leads to N-limited primary production in the Eurasian sector of the Arctic Ocean, which modulates the extent of DSi utilisation in surface waters and thus its isotopic signature within the Arctic Ocean.

2. Eurasian shelves sustain extensive DSi uptake and opal burial. Through the biological shelf pump of the Laptev Sea, 43 ± 13% of the DSi supplied by the Lena river is removed within the Laptev Sea. Vigorous recycling of N on the shelf enables stronger DSi depletion than predicted from nutrient concentrations alone. As N is limiting to primary productivity, DSi is only partially utilised. The excess DSi (>60%) is directly exported from the continental shelf via the Transpolar Drift.

3. The Si isotopic budget of the Arctic Ocean is controlled by biological processes rather than physical transport. The extent of DSi utilisation and subsequent burial of opal on Arctic shelves controls the DSi inventory of outflow Arctic waters, enriching the $\delta^{30}Si(OH)_4$ of outflowing water masses by the 0.1‰ compared to the Atlantic inflow (1.7‰).

4. Eurasian rivers provide 40 ± 4% of the DSi concentrations exported in polar surface waters. By comparison, Pacific sources only contribute to 8 ± 1% of the

total DSi and glacial influence from the Greenland Ice sheet is negligible at Fram Strait.

5. Climate change will affect the DSi inventory and isotopic signature of Arctic outflow polar waters. Due to global warming, riverine inputs of DSi are increasing faster than N. The flux of DSi exported through the TPD is dependent on N-availability. Thus, the outflow waters of the Arctic are predicted to transport a larger flux of DSi in the future, with a lower isotopic signature.

6. Biological assimilation and regeneration at high and low latitudes control the nutrient inventory of North Atlantic Deep Waters. Surface waters are integrated into the deep waters of the Atlantic. Important processes at low latitudes dilute DSi concentrations of Atlantic surface waters and dampen their isotopic signature. Convective water masses integrate this signal with the one of heavily utilised, low nutrients surface waters from the subpolar regions and the Nordic Seas.

7. Deviation of the fresh Labrador Current to the subpolar North Atlantic has reduced N assimilation in recent years. The freshwater content of the subpolar North Atlantic is predicted to increase from increased Greenland melt due to global warming. Increased stratification can decrease the primary production of the region in the future.

6.2 Impact and use of research

This work has significantly increased the global dataset of dissolved silicon isotopes and nitrate isotopes measurements, particularly addressing gaps in nutrient-depleted waters. This data can be used in future modelling studies to understand nutrient cycling, and interactions between N and DSi cycles.

Global warming is affecting nutrient supply and the foodweb in the Arctic and subpolar regions. An increasing number of modelling studies attempt to predict the future of primary productivity linked to anthropogenic climate change. Models often overlook the interaction of nutrient cycles with each other. This project shows the strong interconnection between Si and N cyclin in the Arctic Ocean, with mechanisms affecting N availability/remineralisation, in turn controlling the fate of

Si assimilation close to its source or export. It also casts doubt on the importance of glaciers as a source of DSi to the marine budget. The effect of polar freshwater fluxes appear to primarily be a dilutive one affecting stratification rather than significantly impacting nutrient budgets as they are often deplete of nutrients.

Key processes such as shelf denitrification in the Arctic Ocean or the increasing demand on N-stock from primary producers are often overlooked by models. Stable isotopes can be used as additional constraints to stoichiometric parameters to ensure future patterns of primary productivity are realistically predicted from a geochemical perspective.

6.3 Critical evaluation of work

This work uses stable isotopes to constrain biogeochemical processes. High precision is critical, particularly as $\delta^{30}Si(OH)_4$ isotopic gradients in the deep ocean are relatively small (0.5‰) compared to the accepted inter-laboratory accuracy (0.2‰). A substantial amount of work under this project has gone into developing a method of analysis that has the ability to measure the isotopic signal of samples with very low DSi concentrations while keeping measurement error low. Integrating routine measurements of international seawater standards with each sample run has allowed to monitor laboratory reproducibility and measurement accuracy over the course of the entire project.

Further work is required to improve the analysis of DSi isotopes in seawater. Characterising the effect of anion matrix interferences on both $\delta^{29}Si$ and $\delta^{30}Si$ when lower concentrations are analysed remains a priority for the research field, particularly as the limit of the method are pushed further to fill in gaps of the modern ocean's isoscape to ensure datasets are comparable to each other.

Considering the recent work which has been undertaken around Arctic surface waters and glacial melt, there is also a need for an international seawater standard with DSi concentrations and isotopic signatures which encapsulate the signature of heavily fractionated waters. This can ensure inter-laboratory calibration around the full range of isotopic measurement.

6.4 Future direction of research

Eurasian Arctic shelves are regions of vigorous nutrient cycling which control the nutrient inventory of the surface Arctic Ocean and outflow waters. This study provides the first documentation of opal burial on Eurasian shelves from the Lena river. Each river of the Arctic Ocean has differing nutrient properties and cycling as they drain large areas of land with varying permafrost extent. To further constrain the DSi budget of the Arctic Ocean, evidence-based estimates of opal burial in the East Siberian Seas and from the Ob and Yenisey rivers are required.

There is currently little understanding on how the rates of benthic denitrification on Arctic shelves will react to climate change. Changing rates of denitrification can have widespread impact on Arctic biogeochemistry as N-limitation controls primary productivity and nutrient export in large regions of the Arctic Ocean. Thus, predicting future rates of benthic denitrification in the Arctic Ocean are a research priority, as it will impact the future availability of N.

Chapter 5 highlights some crucial gaps in our understanding of the Atlantic DSi distribution at low latitudes. Characterisation of Mediterranean-sourced waters and other DSi pathways such as submarine groundwater discharge are required to understand the origins of dilution in North Atlantic surface and intermediate waters which contribute to the low nutrient inventory of NADW.

7. References

Aagaard, K. and Carmack, E. C.: The role of sea ice and other fresh water in the Arctic circulation, J. Geophys. Res., 94(C10), 14485, doi:10.1029/jc094ic10p14485, 1989.

Agustí, S., Assmy, P., Duarte, C. M., Wiedmann, I., Marquez, I. A., Fernández-Méndez, M., Kristiansen, S., Krause, J. W. and Wassmann, P.: Biogenic silica production and diatom dynamics in the Svalbard region during spring, Biogeosciences, 15(21), 6503–6517, doi:10.5194/bg-15-6503-2018, 2018.

van Aken, H. M.: The hydrography of the mid-latitude Northeast Atlantic Ocean., 2000.

Albarède, F., Telouk, P., Blichert-Toft, J., Boyet, M., Agranier, A. and Nelson, B.: Precise and accurate isotopic measurements using multiple-collector ICPMS, Geochim. Cosmochim. Acta, 68(12), 2725–2744, doi:10.1016/j.gca.2003.11.024, 2004.

Allen, J. T., Brown, L., Sanders, R., Moore, C. M., Mustard, A., Fielding, S., Lucas, M., Rixen, M., Savidge, G., Henson, S. and Mayor, D.: Diatom carbon export enhanced by silicate upwelling in the northeast Atlantic, Nature, 437(7059), 728–732, doi:10.1038/nature03948, 2005.

Altabet, M. A. and Francois, R.: Nitrogen isotope biogeochemistry of the Antarctic polar frontal zone at 170°W, Deep. Res. Part II Top. Stud. Oceanogr., 48(19–20), 4247–4273, doi:10.1016/S0967-0645(01)00088-1, 2001.

Altabet, M. A., Pilskaln, C., Thunell, R., Pride, C., Sigman, D., Chavez, F. and Francois, R.: The nitrogen isotope biogeochemistry of sinking particles from the margin of the eastern North Pacific, Deep. Res. Part I Oceanogr. Res. Pap., 46(4), 655–679, doi:10.1016/S0967-0637(98)00084-3, 1999.

Anderson, R. F., Chase, Z., Fleisher, M. Q. and Sachs, J.: The Southern Ocean's biological pump during the Last Glacial Maximum, Deep. Res. Part II Top. Stud.

Oceanogr., 49(9–10), 1909–1938, doi:10.1016/S0967-0645(02)00018-8, 2002.

Archer, D., Lyle, M., Rodgers, K. and Froelich, P.: What controls opal preservation in tropical deep-sea sediments?, Paleoceanography, 8(1), 7–21, 1993.

Ardyna, M. and Arrigo, K. R.: Phytoplankton dynamics in a changing Arctic Ocean, Nat. Clim. Chang., 10(10), 892–903, doi:10.1038/s41558-020-0905-y, 2020.

Arrigo, K. R. and van Dijken, G. L.: Continued increases in Arctic Ocean primary production, Prog. Oceanogr., 136, 60–70, doi:10.1016/j.pocean.2015.05.002, 2015.

Arrigo, K. R., van Dijken, G. and Pabi, S.: Impact of a shrinking Arctic ice cover on marine primary production, Geophys. Res. Lett., 35(19), 1–6, doi:10.1029/2008GL035028, 2008.

Arthun, M., Eldevik, T., Smedsrud, L. ., Skagseth, Ø. and Ingvaldsen, R. .: Quantifying the Influence of Atlantic Heat on Barents Sea Ice Variability and Retreat *, J. Clim., 25, 4736–4743, doi:10.1175/JCLI-D-11-00466.1, 2012.

Årthun, M., Ingvaldsen, R. B., Smedsrud, L. H. and Schrum, C.: Dense water formation and circulation in the Barents Sea, Deep. Res. Part I Oceanogr. Res. Pap., 58(8), 801–817, doi:10.1016/j.dsr.2011.06.001, 2011.

Barnes, I. L., Moore, L. J., Machlan, L. A., Murphy, T. J. and Shields, W. R.: Absolute Isotopic Abundance Ratios and the Atomic Weight of a Reference Sample of Silicon, J. Res. Natl. Bur. Stand. - Anal. Phys. Chem., 79(December), 727–735, 1975.

Barton, B. I., Lenn, Y. D. and Lique, C.: Observed atlantification of the Barents Sea causes the Polar Front to limit the expansion of winter sea ice, J. Phys. Oceanogr., 48(8), 1849–1866, doi:10.1175/JPO-D-18-0003.1, 2018.

Bauch, D., Schlosser, P. and fairbanks, richard g.: The distribution of d18O in the Arctic Ocean: implications for the freshwater balance of the halocline and the sources of deep and bottom waters, Reports Polar Res., 159(95), 5–143, 1995.

Bauch, D., Hölemann, J., Willmes, S., Gröger, M., Novikhin, A., Nikulina, A., Kassens, H. and Timokhov, L.: Changes in distribution of brine waters on the Laptev Sea shelf in 2007, J. Geophys. Res. Ocean., 115(11), 1–11, doi:10.1029/2010JC006249, 2010.

Becker, S., Aoyama, M., Woodward, E. M. S., Bakker, K., Coverly, S., Mahaffey, C. and Tanhua, T.: GO-SHIP Repeat Hydrography Nutrient Manual: The Precise and Accurate Determination of Dissolved Inorganic Nutrients in Seawater, Using Continuous Flow Analysis Methods, Front. Mar. Sci., 7(October), doi:10.3389/fmars.2020.581790, 2020.

Bekryaev, R. V., Polyakov, I. V. and Alexeev, V. A.: Role of polar amplification in long-term surface air temperature variations and modern arctic warming, J. Clim., 23(14), 3888–3906, doi:10.1175/2010JCLI3297.1, 2010.

Benoiston, A. S., Ibarbalz, F. M., Bittner, L., Guidi, L., Jahn, O., Dutkiewicz, S. and Bowler, C.: The evolution of diatoms and their biogeochemical functions, Philos. Trans. R. Soc. B Biol. Sci., 372(1728), doi:10.1098/rstb.2016.0397, 2017.

Blais, M., Ardyna, M., Gosselin, M., Dumont, D., Bélanger, S., Tremblay, J. É., Gratton, Y., Marchese, C. and Poulin, M.: Contrasting interannual changes in phytoplankton productivity and community structure in the coastal Canadian Arctic Ocean, Limnol. Oceanogr., 62(6), 2480–2497, doi:10.1002/lno.10581, 2017.

Van Den Boorn, S. H. J. M., Vroon, P. Z. and Van Bergen, M. J.: Sulfur-induced offsets in MC-ICP-MS silicon-isotope measurements, J. Anal. At. Spectrom., 24(8), 1111–1114, doi:10.1039/b816804k, 2009.

Boyd, P. W. and Law, C. S.: The Southern Ocean Iron RElease Experiment (SOIREE) - Introduction and summary, Deep. Res. Part II Top. Stud. Oceanogr., 48(11–12), 2425–2438, doi:10.1016/S0967-0645(01)00002-9, 2001.

Boyd, P. W., Jickells, T., Law, C. S., Blain, S., Boyle, E. A., Buesseler, K. O., Coale, K. H., Cullen, J. J., Baar, H. J. W. De, Follows, M., Harvey, M., Lancelot, C. and Levasseur, M.: Mesoscale Iron Enrichment Experiments 1993 – 2005: Synthesis and

Future Directions, Science (80-.)., 315(February), 612–618, 2007.

Brand, T., Norman, L., Mahaffey, C., Tuerena, R., Crocket, K. and Henley, S.: Dissolved nutrient samples collected in the Fram Strait as part of the Changing Arctic Ocean programme during cruise JR17005, May-June 2018., , doi:doi:10.5285/b61d58df-b8e8-11c4-e053-6c86abc0246c, 2020.

Brandes, J. A. and Devol, A. H.: A global marine-fixed nitrogen isotopic budget: Implications for Holocene nitrogen cycling, Global Biogeochem. Cycles, 16(4), 67-1-67–14, doi:10.1029/2001gb001856, 2002.

Broecker, W. and Peng, T.: Tracers in the sea, Geochim. Cosmochim. Acta, 47(7), 1336, doi:10.1016/0016-7037(83)90075-3, 1983.

Brown, Z. W., Casciotti, K. L., Pickart, R. S., Swift, J. H. and Arrigo, K. R.: Aspects of the marine nitrogen cycle of the Chukchi Sea shelf and Canada Basin, Deep. Res. Part II Top. Stud. Oceanogr., 118, 73–87, doi:10.1016/j.dsr2.2015.02.009, 2015.

Bryden, H. L., Johns, W. E., King, B. A., McCarthy, G., McDonagh, E. L., Moat, B. I. and Smeed, D. A.: Reduction in ocean heat transport at 26°N since 2008 cools the eastern subpolar gyre of the North Atlantic Ocean, J. Clim., 33(5), 1677–1689, doi:10.1175/JCLI-D-19-0323.1, 2020.

Brzezinski, M. A. and Jones, J. L.: Coupling of the distribution of silicon isotopes to the meridional overturning circulation of the North Atlantic Ocean, Deep. Res. Part II Top. Stud. Oceanogr., 116, 79–88, doi:10.1016/j.dsr2.2014.11.015, 2015.

Brzezinski, M. A., Jones, J. L., Barbara, S., Bidle, K. D. and Azam, F.: The balance between silica production and silica dissolution in the sea : Insights from Monterey Bay , California , applied to the global data set, Limnol. Oceanogr., 48(5), 1846–1854, 2003.

Brzezinski, M. A., Jones, J. L., Beucher, C. P., Demarest, M. S. and Berg, H. L.: Automated determination of silicon isotope natural abundance by the acid decomposition of cesium hexafluosilicate, Anal. Chem., 78(17), 6109–6114,

doi:10.1021/ac0606406, 2006.

Brzezinski, M. A., Closset, I., Jones, J. L., de Souza, G. F. and Maden, C.: New Constraints on the Physical and Biological Controls on the Silicon Isotopic Composition of the Arctic Ocean, Front. Mar. Sci., 8(August), doi:10.3389/fmars.2021.699762, 2021.

Buchwald, C., Santoro, A. E., McIlvin, M. R. and Casciotti, K. L.: Oxygen isotopic composition of nitrate and nitrite produced by nitrifying cocultures and natural marine assemblages, Limnol. Oceanogr., 57(5), 1361–1375, doi:10.4319/lo.2012.57.5.1361, 2012.

Budeus, G. and Schneider, W.: On the hydrography of the Northeast Water Polynya, J. Geophys. Res., 100(C3), 4269–4286, doi:10.1029/94JC02349, 1995.

Cardinal, D., Alleman, L. Y., De Jong, J., Ziegler, K. and André, L.: Isotopic composition of silicon measured by multicollector plasma source mass spectrometry in dry plasma mode, J. Anal. At. Spectrom., 18(3), 213–218, doi:10.1039/b210109b, 2003.

Cardinal, D., Alleman, L. Y., Dehairs, F., Savoye, N., Trull, T. W. and André, L.: Relevance of silicon isotopes to Si-nutrient utilization and Si-source assessment in Antarctic waters, Global Biogeochem. Cycles, 19(2), 1–13, doi:10.1029/2004GB002364, 2005.

Carey, J. C., Gewirtzman, J., Johnston, S. E., Kurtz, A., Tang, J., Vieillard, A. M. and Spencer, R. G. M.: Arctic River Dissolved and Biogenic Silicon Exports—Current Conditions and Future Changes With Warming, Global Biogeochem. Cycles, 34(3), no, doi:10.1029/2019GB006308, 2020.

Carpenter, E. J., Harvey, H. R., Brian, F. and Capone, D. G.: Biogeochemical tracers of the marine cyanobacterium Trichodesmium, Deep. Res. Part I Oceanogr. Res. Pap., 44(1), 27–38, doi:10.1016/S0967-0637(96)00091-X, 1997.

Carritt, D. E. and Carpenter, J. H.: Comparison and Evaluation of Currently

Employed Modifications of the Winkler Method for Determining Dissolved Oxygen in Seawater; A NASCO Report, J. Mar. Res., (24,3), 1966.

Casciotti, K. L., Sigman, D. M., Hastings, M. G., Bo, J. K. and Hilkert, A.: Measurement of the Oxygen Isotopic Composition of Nitrate in Seawater and Freshwater Using the Denitrifier Method, Anal. Chem., 74(19), 4905–4912, doi:10.1021/ac020113w, 2002.

Chang, B. X. and Devol, A. H.: Seasonal and spatial patterns of sedimentary denitrification rates in the Chukchi sea, Deep. Res. Part II Top. Stud. Oceanogr., 56(17), 1339–1350, doi:10.1016/j.dsr2.2008.10.024, 2009.

Charette, M. A., Kipp, L. E., Jensen, L. T., Dabrowski, J. S., Whitmore, L. M., Fitzsimmons, J. N., Williford, T., Ulfsbo, A., Jones, E., Bundy, R. M., Vivancos, S. M., Pahnke, K., John, S. G., Xiang, Y., Hatta, M., Petrova, M. V., Heimbürger-Boavida, L. E., Bauch, D., Newton, R., Pasqualini, A., Agather, A. M., Amon, R. M. W., Anderson, R. F., Andersson, P. S., Benner, R., Bowman, K. L., Edwards, R. L., Gdaniec, S., Gerringa, L. J. A., González, A. G., Granskog, M., Haley, B., Hammerschmidt, C. R., Hansell, D. A., Henderson, P. B., Kadko, D. C., Kaiser, K., Laan, P., Lam, P. J., Lamborg, C. H., Levier, M., Li, X., Margolin, A. R., Measures, C., Middag, R., Millero, F. J., Moore, W. S., Paffrath, R., Planquette, H., Rabe, B., Reader, H., Rember, R., Rijkenberg, M. J. A., Roy-Barman, M., Rutgers van der Loeff, M., Saito, M., Schauer, U., Schlosser, P., Sherrell, R. M., Shiller, A. M., Slagter, H., Sonke, J. E., Stedmon, C., Woosley, R. J., Valk, O., van Ooijen, J. and Zhang, R.: The Transpolar Drift as a Source of Riverine and Shelf-Derived Trace Elements to the Central Arctic Ocean, J. Geophys. Res. Ocean., 125(5), 1–34, doi:10.1029/2019JC015920, 2020.

Codispoti, L. A., Brandes, J. A., Christensen, J. P., Devol, A. H., Naqvi, S. W. A., Paerl, H. W. and Yoshinari, T.: The oceanic fixed nitrogen and nitrous oxide budgets: Moving targets as we enter the anthropocene?, Sci. Mar., 65.2, 85–105, doi:10.1109/TWC.2009.081524, 2001.

Codispoti, L. A., Kelly, V., Thessen, A., Matrai, P., Suttles, S., Hill, V., Steele, M.

and Light, B.: Synthesis of primary production in the Arctic Ocean: III. Nitrate and phosphate based estimates of net community production, Prog. Oceanogr., 110, 126–150, doi:10.1016/j.pocean.2012.11.006, 2013.

Cremer, H.: Distribution patterns of diatom surface sediment assemblages in the Laptev Sea (Arctic Ocean), Mar. Micropaleontol., 38(1), 39–67, doi:10.1016/S0377-8398(99)00037-7, 1999.

Curry, R. and Mauritzen, C.: Ocean Science: Dilution of the Northern North Atlantic Ocean in recent decades, Science (80-.)., 308(5729), 1772–1774, doi:10.1126/science.1109477, 2005.

Deman, F., Fonseca-Batista, D., Roukaerts, A., García-Ibáñez, M. I., Le Roy, E., Thilakarathne, E. P. D. N., Elskens, M., Dehairs, F. and Fripiat, F.: Nitrate Supply Routes and Impact of Internal Cycling in the North Atlantic Ocean Inferred From Nitrate Isotopic Composition, Global Biogeochem. Cycles, 35(4), 1–15, doi:10.1029/2020GB006887, 2021.

Demarest, M. S., Brzezinski, M. A. and Beucher, C. P.: Fractionation of silicon isotopes during biogenic silica dissolution, Geochim. Cosmochim. Acta, 73(19), 5572–5583, doi:10.1016/j.gca.2009.06.019, 2009.

DeMaster, D. J.: The accumulation and cycling of biogenic silica in the Southern Ocean: Revisiting the marine silica budget, Deep. Res. Part II Top. Stud. Oceanogr., 49(16), 3155–3167, doi:10.1016/S0967-0645(02)00076-0, 2002.

Difiore, P. J., Sigman, D. M., Karsh, K. L., Trull, T. W., Dunbar, R. B. and Robinson, R. S.: Poleward decrease in the isotope effect of nitrate assimilation across the Southern Ocean, Geophys. Res. Lett., 37(17), 1–5, doi:10.1029/2010GL044090, 2010.

Dittmar, T. and Kattner, G.: The biogeochemistry of the river and shelf ecosystem of the Arctic Ocean: A review, Mar. Chem., 83(3–4), 103–120, doi:10.1016/S0304-4203(03)00105-1, 2003.

Dodd, P. A., Rabe, B., Hansen, E., Falck, E., MacKensen, A., Rohling, E., Stedmon, C. and Kristiansen, S.: The freshwater composition of the Fram Strait outflow derived from a decade of tracer measurements, J. Geophys. Res. Ocean., 117(11), 1–26, doi:10.1029/2012JC008011, 2012.

Doncila, A.: Nitrogen Cycling in the Warming Arctic Ocean, PhD thesis, Univ. Edinburgh, 2020.

Dukhovskoy, D. S., Yashayaev, I., Proshutinsky, A., Bamber, J. L., Bashmachnikov, I. L., Chassignet, E. P., Lee, C. M. and Tedstone, A. J.: Role of Greenland Freshwater Anomaly in the Recent Freshening of the Subpolar North Atlantic, J. Geophys. Res. Ocean., 1992, 3333–3360, doi:10.1029/2018JC014686, 2019.

Edmonds, H. N., Michael, P. J., Baker, E. T., Connelly, D. P., Snow, J. E., Langmuir, C. H., Dick, H. J. B., Mühe, R., German, C. R. and Graham, D. W.: Discovery of abundant hydrothermal venting on the ultraslow-spreading Gakkel ridge in the Arctic Ocean, Nature, 421(6920), 252–256, doi:10.1038/nature01351, 2003.

Egan, K. E., Rickaby, R. E. M., Leng, M. J., Hendry, K. R., Hermoso, M., Sloane, H. J., Bostock, H. and Halliday, A. N.: Diatom silicon isotopes as a proxy for silicic acid utilisation: A Southern Ocean core top calibration, Geochim. Cosmochim. Acta, 96, 174–192, doi:10.1016/j.gca.2012.08.002, 2012.

Ehlert, C., Doering, K., Wallmann, K., Scholz, F., Sommer, S., Grasse, P., Geilert, S. and Frank, M.: Stable silicon isotope signatures of marine pore waters – Biogenic opal dissolution versus authigenic clay mineral formation, Geochim. Cosmochim. Acta, 191, 102–117, doi:10.1016/j.gca.2016.07.022, 2016.

Fahl, K., Cremer, H., Erlenkeuser, H., Hanssen, H., Hölemann, J., Kassens, H., Knickmeier, K., Kosobokova, K., Kunz-Pirrung, M., Lindemann, F., Markhaseva, E., Lischka, S., Petryashov, V., Piepenburg, D., Schmid, M., Spindler, M., Stein, R. and Tuschling, K.: Sources and pathways of organic carbon in the modern Laptev Sea (Arctic Ocean): Implications from biological, geochemical and geological data, Polarforschung, 69(1–3), 193–205, 1999.

Field, C. B., Behrenfeld, M. J., Randerson, J. T. and Falkowski, P.: Primary production of the biosphere: Integrating terrestrial and oceanic components, Science (80-.)., 281(5374), 237–240, doi:10.1126/science.281.5374.237, 1998.

Le Fouest, V., Babin, M. and Tremblay, J. E.: The fate of riverine nutrients on Arctic shelves, Biogeosciences, 10(6), 3661–3677, doi:10.5194/bg-10-3661-2013, 2013.

Foukal, N. P. and Lozier, M. S.: Assessing variability in the size and strength of the North Atlantic subpolar gyre, J. Geophys. Res. Ocean., 122(8), 6295–6308, doi:10.1002/2017JC012798, 2017.

Fowler, D., Coyle, M., Skiba, U., Sutton, M. A., Cape, J. N., Reis, S., Sheppard, L. J., Jenkins, A., Grizzetti, B., Galloway, J. N., Vitousek, P., Leach, A., Bouwman, A. F., Butterbach-Bahl, K., Dentener, F., Stevenson, D., Amann, M. and Voss, M.: The global nitrogen cycle in the Twentyfirst century, Philos. Trans. R. Soc. B Biol. Sci., 368(1621), doi:10.1098/rstb.2013.0164, 2013.

Fox, A. D., Biastoch, A., Cunningham, S. A., Gary, S. F., Handmann, P., Penny, N., Johnson, C., Martin, T., Rath, W., Rühs, S. and Schmidt, C.: How reduced Labrador Sea surface heat loss caused exceptional freshening and cooling in the eastern subpolar North Atlantic, Ocean Sci., in prep.(April), 1–35, 2022.

Frajka-Williams, E., Ansorge, I. J., Baehr, J., Bryden, H. L., Chidichimo, M. P., Cunningham, S. A., Danabasoglu, G., Dong, S., Donohue, K. A., Elipot, S., Heimbach, P., Holliday, N. P., Hummels, R., Jackson, L. C., Karstensen, J., Lankhorst, M., Le Bras, I. A., Susan Lozier, M., McDonagh, E. L., Meinen, C. S., Mercier, H., Moat, B. I., Perez, R. C., Piecuch, C. G., Rhein, M., Srokosz, M. A., Trenberth, K. E., Bacon, S., Forget, G., Goni, G., Kieke, D., Koelling, J., Lamont, T., McCarthy, G. D., Mertens, C., Send, U., Smeed, D. A., Speich, S., van den Berg, M., Volkov, D. and Wilson, C.: Atlantic meridional overturning circulation: Observed transport and variability, Front. Mar. Sci., 6(JUN), 1–18, doi:10.3389/fmars.2019.00260, 2019.

Francis, A.: Stable Isotope Tracing of Dissolved Nitrogen from Permafrost

Degradation in Arctic Rivers, University of Edinburgh., 2019.

Frey, K. E. and McClelland, J. W.: Impacts of permafrost degradation on arctic river biogeochemistry, Hydrol. Process., 23(1), 169–182, doi:10.1002/hyp.7196, 2009.

Frey, K. E., McClelland, J. W., Holmes, R. M. and Smith, L. G.: Impacts of climate warming and permafrost thaw on the riverine transport of nitrogen and phosphorus to the Kara Sea, J. Geophys. Res. Biogeosciences, 112(4), 1–10, doi:10.1029/2006JG000369, 2007.

Frey, K. E., Comiso, J. C., Cooper, L. W., Eisner, L. B., Gradinger, R. R., Grebmeier, J. M. and Tremblay, J. E.: Arctic Ocean Primary Productivity, Arct. Rep. Card Updat. 2011, 1–17 [online] Available from: http://www.arctic.noaa.gov/report11/primary_productivity.html, 2018.

Frings, P. J., De La Rocha, C., Struyf, E., van Pelt, D., Schoelynck, J., Hudson, M. M., Gondwe, M. J., Wolski, P., Mosimane, K., Gray, W., Schaller, J. and Conley, D. J.: Tracing silicon cycling in the Okavango Delta, a sub-tropical flood-pulse wetland using silicon isotopes, Geochim. Cosmochim. Acta, 142, 132–148, doi:10.1016/j.gca.2014.07.007, 2014.

Frings, P. J., Clymans, W., Fontorbe, G., De La Rocha, C. L. and Conley, D. J.: The continental Si cycle and its impact on the ocean Si isotope budget, Chem. Geol., 425, 12–36, doi:10.1016/j.chemgeo.2016.01.020, 2016.

Fripiat, F., Cardinal, D., Tison, J. L., Worby, A. and André, L.: Diatom-induced silicon isotopic fractionation in Antarctic sea ice, J. Geophys. Res. Biogeosciences, 112(2), doi:10.1029/2006JG000244, 2007.

Fripiat, F., Cavagna, A. J., Savoye, N., Dehairs, F., André, L. and Cardinal, D.: Isotopic constraints on the Si-biogeochemical cycle of the Antarctic Zone in the Kerguelen area (KEOPS), Mar. Chem., 123(1–4), 11–22, doi:10.1016/j.marchem.2010.08.005, 2011a.

Fripiat, F., Cavagna, A. J., Dehairs, F., Speich, S., André, L. and Cardinal, D.:

Silicon pool dynamics and biogenic silica export in the Southern Ocean inferred from Si-isotopes, Ocean Sci., 7(5), 533–547, doi:10.5194/os-7-533-2011, 2011b.

Fripiat, F., Tison, J. L., André, L., Notz, D. and Delille, B.: Biogenic silica recycling in sea ice inferred from Si-isotopes: Constraints from Arctic winter first-year sea ice, Biogeochemistry, 119(1–3), 25–33, doi:10.1007/s10533-013-9911-8, 2014.

Fripiat, F., Meiners, K. M., Vancoppenolle, M., Papadimitriou, S., Thomas, D. N., Ackley, S. F., Arrigo, K. R., Carnat, G., Cozzi, S., Delille, B., Dieckmann, G. S., Dunbar, R. B., Fransson, A., Kattner, G., Kennedy, H., Lannuzel, D., Munro, D. R., Nomura, D., Rintala, J. M., Schoemann, V., Stefels, J., Steiner, N. and Tison, J. L.: Macro-nutrient concentrations in Antarctic pack ice: Overall patterns and overlooked processes, Elementa, 5, doi:10.1525/elementa.217, 2017.

Fripiat, F., Declercq, M., Sapart, C. J., Anderson, L. G., Bruechert, V., Deman, F., Fonseca-Batista, D., Humborg, C., Roukaerts, A., Semiletov, I. P. and Dehairs, F.: Influence of the bordering shelves on nutrient distribution in the Arctic halocline inferred from water column nitrate isotopes, Limnol. Oceanogr., 63(5), 2154–2170, doi:10.1002/lno.10930, 2018.

Fripiat, F., Martínez-García, A., Marconi, D., Fawcett, S. E., Kopf, S. H., Luu, V. H., Rafter, P. A., Zhang, R., Sigman, D. M. and Haug, G. H.: Nitrogen isotopic constraints on nutrient transport to the upper ocean, Nat. Geosci., 14(11), 855–861, doi:10.1038/s41561-021-00836-8, 2021.

Garcia-Orellana, J., Rodellas, V., Tamborski, J., Diego-Feliu, M., van Beek, P., Weinstein, Y., Charette, M., Alorda-Kleinglass, A., Michael, H. A., Stieglitz, T. and Scholten, J.: Radium isotopes as submarine groundwater discharge (SGD) tracers: Review and recommendations, Earth-Science Rev., 220(December 2020), 103681, doi:10.1016/j.earscirev.2021.103681, 2021.

Geibert, W., Rutgers van der Loeff, M. M., Usbeck, R., Gersonde, R., Kuhn, G. and Seeberg-Elverfeldt, J.: Quantifying the opal belt in the Atlantic and southeast Pacific sector of the Southern Ocean by means of 230Th normalization, Global Biogeochem.

Cycles, 19(4), doi:10.1029/2005GB002465, 2005.

Georg, R. B., Reynolds, B. C., Frank, M. and Halliday, A. N.: Mechanisms controlling the silicon isotopic compositions of river waters, Earth Planet. Sci. Lett., 249(3–4), 290–306, doi:10.1016/j.epsl.2006.07.006, 2006a.

Georg, R. B., Reynolds, B. C., Frank, M. and Halliday, A. N.: New sample preparation techniques for the determination of Si isotopic compositions using MC-ICPMS, Chem. Geol., 235(1–2), 95–104, doi:10.1016/j.chemgeo.2006.06.006, 2006b.

Georg, R. B., West, A. J., Basu, A. R. and Halliday, A. N.: Silicon fluxes and isotope composition of direct groundwater discharge into the Bay of Bengal and the effect on the global ocean silicon isotope budget, Earth Planet. Sci. Lett., 283(1–4), 67–74, doi:10.1016/j.epsl.2009.03.041, 2009a.

Georg, R. B., Zhu, C., Reynolds, B. C. and Halliday, A. N.: Stable silicon isotopes of groundwater, feldspars, and clay coatings in the Navajo Sandstone aquifer, Black Mesa, Arizona, USA, Geochim. Cosmochim. Acta, 73(8), 2229–2241, doi:10.1016/j.gca.2009.02.005, 2009b.

Giesbrecht, K. E.: Biogenic Silica Dynamics of Arctic Marine Ecosystems, 2019.

Giesbrecht, K. E. and Varela, D. E.: Summertime Biogenic Silica Production and Silicon Limitation in the Pacific Arctic Region From 2006 to 2016, Global Biogeochem. Cycles, 35(1), 1–27, doi:10.1029/2020GB006629, 2021.

Giesbrecht, K. E., Varela, D. E., Wiktor, J., Grebmeier, J. M., Kelly, B. and Long, J. E.: A decade of summertime measurements of phytoplankton biomass, productivity and assemblage composition in the Pacific Arctic Region from 2006 to 2016, Deep. Res. Part II Top. Stud. Oceanogr., 162(July 2017), 93–113, doi:10.1016/j.dsr2.2018.06.010, 2019.

Giesbrecht, K. E., Varela, D. E., Souza, G. F. and Maden, C.: Natural Variations in Dissolved Silicon Isotopes Across the Arctic Ocean From the Pacific to the Atlantic,

Global Biogeochem. Cycles, 36(5), 1–23, doi:10.1029/2021gb007107, 2022.

Glibert, P. M., Wilkerson, F. P., Dugdale, R. C., Raven, J. A., Dupont, C. L., Leavitt, P. R., Parker, A. E., Burkholder, J. M. and Kana, T. M.: Pluses and minuses of ammonium and nitrate uptake and assimilation by phytoplankton and implications for productivity and community composition, with emphasis on nitrogen-enriched conditions, Limnol. Oceanogr., 61(1), 165–197, doi:10.1002/lno.10203, 2016.

Granger, J., Sigman, D. M., Needoba, J. A. and Harrison, P. J.: Coupled nitrogen and oxygen isotope fractionation of nitrate during assimilation by cultures of marine phytoplankton, Limnol. Oceanogr., 49(5), 1763–1773, doi:10.4319/lo.2004.49.5.1763, 2004.

Granger, J., Prokopenko, M. G., Sigman, D. M., Mordy, C. W., Morse, Z. M., Morales, L. V., Sambrotto, R. N. and Plessen, B.: Coupled nitrification-denitrification in sediment of the eastern Bering Sea shelf leads to 15N enrichment of fixed N in shelf waters, J. Geophys. Res. Ocean., 116(11), 1–18, doi:10.1029/2010JC006751, 2011.

Granger, J., Sigman, D. M., Gagnon, J., Tremblay, J.-E. and Mucci, A.: On the Properties of the Arctic Halocline and Deep Water Masses of the Canada Basin from Nitrate Isotope Ratios, J. Geophys. Res. Ocean., 1–16, doi:10.1029/2018JC014110, 2018.

Grasse, P., Ryabenko, E., Ehlert, C., Altabet, M. A. and Frank, M.: Silicon and nitrogen cycling in the upwelling area off Peru: A dual isotope approach, Limnol. Oceanogr., 61(5), 1661–1676, doi:10.1002/lno.10324, 2016.

Grasse, P., Brzezinski, M. A., Cardinal, D., Souza, G. F. De, Estrade, N., François, R., Frank, M., Jiang, G., Jones, J. L., Kooijman, E., Liu, Q., Lu, D., Pahnke, K., Ponzevera, E., Schmitt, M., Sun, X., Sutton, J. N., Thil, F. and Weis, D.: GEOTRACES inter-calibration of the stable silicon isotope composition of dissolved silicic acid in seawater, J. Anal. At. Spectrom., 562–578, doi:10.1039/c6ja00302h, 2017.

Grasse, P., Closset, I., Jones, J. L., Geilert, S. and Brzezinski, M. A.: Controls on Dissolved Silicon Isotopes Along the U.S. GEOTRACES Eastern Pacific Zonal Transect (GP16), Global Biogeochem. Cycles, 34(9), doi:10.1029/2020GB006538, 2020.

Grasshoff, K., Ehrhard, M. and Kremling, K.: Methods of Seawater Analysis, 2nd ed., Verlag Chemie GmbH, Weinheim., 1983.

Gruber, N.: The Dynamics of the Marine Nitrogen Cycle and its Influence on Atmospheric CO2 Variations, in The Ocean Carbon Cycle and Climate, edited by M. Follows and T. Oguz, Springer, Dordrecht., 2004.

Gruber, N. and Sarmiento, J. L.: Global patterns of marine nitrogen fixation and denitrification, Global Biogeochem. Cycles, 11(2), 235–266, 1997.

Haine, T. W. N., Curry, B., Gerdes, R., Hansen, E., Karcher, M., Lee, C., Rudels, B., Spreen, G., de Steur, L., Stewart, K. D. and Woodgate, R.: Arctic freshwater export: Status, mechanisms, and prospects, Glob. Planet. Change, 125, 13–35, doi:10.1016/j.gloplacha.2014.11.013, 2015.

Han, G., Ohashi, K., Chen, N., Myers, P. G., Nunes, N. and Fischer, J.: Decline and partial rebound of the Labrador Current 1993-2004: Monitoring ocean currents from altimetric and conductivity-temperature-depth data, J. Geophys. Res. Ocean., 115(12), 1–10, doi:10.1029/2009JC006091, 2010.

Hansen, H. P. and Koroleff, F.: Determination of nutrients, in Methods of Seawater Analysis, edited by K. Kremlingi and M. Ehrhardt, pp. 159–228, Verlag GmbH., 1999.

Hatton, J. E., Hendry, K. R., Hawkings, J. R., Wadham, J. L., Opfergelt, S., Kohler, T. J., Yde, J. C., Stibal, M. and Žárský, J. D.: Silicon isotopes in Arctic and sub-Arctic glacial meltwaters: the role of subglacial weathering in the silicon cycle, Proc. R. Soc. A Math. Phys. Eng. Sci., 475(2228), 20190098, doi:10.1098/rspa.2019.0098, 2019.

Hátún, H., Sande, A. B., Drange, H., Hansen, B. and Valdimarsson, H.: Influence of the atlantic subpolar gyre on the thermohaline circulation, Science (80-.)., 309(5742), 1841–1844, doi:10.1126/science.1114777, 2005.

Hátún, H., Azetsu-Scott, K., Somavilla, R., Rey, F., Johnson, C., Mathis, M., Mikolajewicz, U., Coupel, P., Tremblay, J., Hartman, S., Pacariz, S. V., Salter, I. and Ólafsson, J.: The subpolar gyre regulates silicate concentrations in the North Atlantic, Sci. Rep., 7(1), 1–9, doi:10.1038/s41598-017-14837-4, 2017.

Hawkings, J. R., Wadham, J. L., Tranter, M., Lawson, E., Sole, A., Cowton, T., Tedstone, A. J., Bartholomew, I., Nienow, P., Chandler, D. and Telling, J.: The effect of warming climate on nutrient and solute export from the Greenland Ice Sheet, Geochemical Perspect. Lett., 1(1), 94–104, doi:10.7185/geochemlet.1510, 2015.

Hawkings, J. R., Wadham, J. L., Benning, L. G., Hendry, K. R., Tranter, M., Tedstone, A., Nienow, P. and Raiswell, R.: Ice sheets as a missing source of silica to the polar oceans, Nat. Commun., 8(May 2016), 1–10, doi:10.1038/ncomms14198, 2017.

Hawkings, J. R., Hatton, J. E., Hendry, K. R., de Souza, G. F., Wadham, J. L., Ivanovic, R., Kohler, T. J., Stibal, M., Beaton, A., Lamarche-Gagnon, G., Tedstone, A., Hain, M. P., Bagshaw, E., Pike, J. and Tranter, M.: The silicon cycle impacted by past ice sheets, Nat. Commun., 9(1), 1–10, doi:10.1038/s41467-018-05689-1, 2018.

Hayes, C. T., Costa, K. M., Anderson, R. F., Calvo, E., Chase, Z., Demina, L. L., Dutay, J. C., German, C. R., Heimbürger-Boavida, L. E., Jaccard, S. L., Jacobel, A., Kohfeld, K. E., Kravchishina, M. D., Lippold, J., Mekik, F., Missiaen, L., Pavia, F. J., Paytan, A., Pedrosa-Pamies, R., Petrova, M. V., Rahman, S., Robinson, L. F., Roy-Barman, M., Sanchez-Vidal, A., Shiller, A., Tagliabue, A., Tessin, A. C., van Hulten, M. and Zhang, J.: Global Ocean Sediment Composition and Burial Flux in the Deep Sea, Global Biogeochem. Cycles, 35(4), 1–25, doi:10.1029/2020GB006769, 2021.

Hayes, J. M.: An Introduction to Isotopic Calculations, , (September), 1–10, 2004.

Hendry, K. R., Gong, X., Knorr, G., Pike, J. and Hall, I. R.: Deglacial diatom production in the tropical North Atlantic driven by enhanced silicic acid supply, Earth Planet. Sci. Lett., 438, 122–129, doi:10.1016/j.epsl.2016.01.016, 2016.

Henson, S. A., Sanders, R., Holeton, C. and Allen, J. T.: Timing of nutrient depletion, diatom dominance and a lower-boundary estimate of export production for Irminger Basin, North Atlantic, Mar. Ecol. Prog. Ser., 313, 73–84, doi:10.3354/meps313073, 2006.

Hölemann, J. A., Juhls, B., Bauch, D., Janout, M., Koch, B. P. and Heim, B.: The impact of the freeze-melt cycle of land-fast ice on the distribution of dissolved organic matter in the Laptev and East Siberian seas (Siberian Arctic), Biogeosciences, 18(12), 3637–3655, doi:10.5194/bg-18-3637-2021, 2021.

Holliday, N. P., Hughes, S. L., Bacon, S. and Hansen, B.: Reversal of the 1960s to 1990s freshening trend in the northeast North Atlantic and Nordic Seas, Geophys. Res. Lett., 35, 1–5, doi:10.1029/2007GL032675, 2008.

Holliday, N. P., Cunningham, S. A., Johnson, C., Gary, S. F., Griffiths, C., Read, J. F. and Sherwin, T.: Multidecadal variability of potential temperature, salinity, and transport in the eastern subpolar North Atlantic, J. Geophys. Res. Ocean., 120, 1–17, doi:10.1002/2014JC010485.Received, 2015.

Holliday, N. P., Bersch, M., Berx, B., Chafik, L., Cunningham, S., Florindo-López, C., Hátún, H., Johns, W., Josey, S. A., Larsen, K. M. H., Mulet, S., Oltmanns, M., Reverdin, G., Rossby, T., Thierry, V., Valdimarsson, H. and Yashayaev, I.: Ocean circulation causes the largest freshening event for 120 years in eastern subpolar North Atlantic, Nat. Commun., 11(1), doi:10.1038/s41467-020-14474-y, 2020.

Holmes, R. M., McClelland, J. W., Peterson, B. J., Shiklomanov, I. A., Shiklomanov, A. I., Zhulidov, A. V., Gordeev, V. V. and Bobrovitskaya, N. N.: A circumpolar perspective on fluvial sediment flux to the Arctic ocean, Global Biogeochem. Cycles, 16(4), 45-1-45–14, doi:10.1029/2001gb001849, 2002.

Holmes, R. M., Mcclelland, J. W., Peterson, B. J., Tank, S. E., Bulygina, E.,

Eglinton, T. I., Gordeev, V. V, Gurtovaya, T. Y., Raymond, P. A., Repeta, D. J., Staples, R., Striegl, R. G., Zhulidov, A. V and Zimov, S. A.: Seasonal and Annual Fluxes of Nutrients and Organic Matter from Large Rivers to the Arctic Ocean and Surrounding Seas, Estuaries and Coasts, 35, 369–382, doi:10.1007/s12237-011-9386-6, 2012.

Hopwood, M. J., Carroll, D., Dunse, T., Hodson, A., Holding, J. M., Iriarte, J. L., Ribeiro, S., Achterberg, E. P., Cantoni, C., Carlson, D. F., Chierici, M., Clarke, J. S., Cozzi, S., Fransson, A., Juul-Pedersen, T., Winding, M. H. S. and Meire, L.: Review article: How does glacier discharge affect marine biogeochemistry and primary production in the Arctic?, Cryosphere, 14(4), 1347–1383, doi:10.5194/tc-14-1347-2020, 2020.

Hughes, H. J., Delvigne, C., Korntheuer, M., De Jong, J., André, L. and Cardinal, D.: Controlling the mass bias introduced by anionic and organic matrices in silicon isotopic measurements by MC-ICP-MS, J. Anal. At. Spectrom., 26(9), 1892–1896, doi:10.1039/c1ja10110b, 2011.

Hutchins, D. A. and Bruland, K. W.: Iron-limited growth and Si:N ratios in a costal upwelling regime, Nature, 393(June), 561–564, 1998.

Ingvaldsen, R. B., Assmann, K. M., Primicerio, R., Fossheim, M., Polyakov, I. V. and Dolgov, A. V.: Physical manifestations and ecological implications of Arctic Atlantification, Nat. Rev. Earth Environ., 2(12), 874–889, doi:10.1038/s43017-021-00228-x, 2021.

IPCC: Climate Change 2021: The Physical Science Basis. Contribution of Working Group I to the Sixth Assessment Report of the Intergovernmental Panel on Climate Change, edited by V. Masson-Delmotte, P. . Zhai, A. Pirani, S. L. Connors, C. Péan, S. Berger, N. Caud, Y. Chen, L. Goldfarb, M. J. Gornis, M. Huang, K. Leitzell, E. Lonnoy, J. B. R. Matthews, T. K. Maycock, T. Waterfield, O. Yelekçi, R. Yu, and B. Zhou, Cambridge University press, Cambridge, United Kingdom and New York, NY, USA., 2021.

Ivanov, V., Varentsov, M., Matveeva, T., Repina, I., Artamonov, A. and Khavina, E.: Arctic sea ice decline in the 2010s: The increasing role of the ocean-air heat exchange in the late summer, Atmosphere (Basel)., 10(4), 1–23, doi:10.3390/atmos10040184, 2019.

Jakobsson, M.: Hypsometry and volume of the Arctic Ocean and its constituent seas, Geochemistry, Geophys. Geosystems, 3(5), 1–18, 2002.

Janout, M. A., Hölemann, J., Laukert, G., Smirnov, A., Krumpen, T., Bauch, D. and Timokhov, L.: On the Variability of Stratification in the Freshwater-Influenced Laptev Sea Region, Front. Mar. Sci., 7(September), 1–17, doi:10.3389/fmars.2020.543489, 2020.

Jenkins, W. J., Smethie, W. M., Boyle, E. A. and Cutter, G. A.: Water mass analysis for the U.S. GEOTRACES (GA03) North Atlantic sections, Deep. Res. Part II Top. Stud. Oceanogr., 116, 6–20, doi:10.1016/j.dsr2.2014.11.018, 2015.

Johnson, C., Inall, M. and Häkkinen, S.: Declining nutrient concentrations in the northeast Atlantic as a result of a weakening Subpolar Gyre, Deep. Res. Part I Oceanogr. Res. Pap., 82, 95–107, doi:10.1016/j.dsr.2013.08.007, 2013.

Kamatani, A.: Dissolution rates of silica from diatoms decomposing at various temperatures, Mar. Biol., 68(1), 91–96, doi:10.1007/BF00393146, 1982.

Karcher, M. J. and Oberhuber, J. M.: Pathways and modification of the upper and intermediate waters of the Arctic Ocean, J. Geophys. Res., 107(C6), 1–13, doi:10.1029/2000jc000530, 2002.

Karl, D. M. and Tien, G.: MAGIC: A sensitive and precise method for measuring dissolved phosphorus in aquatic environments, Limnol. Oceanogr., 37(1), 105–116, doi:10.4319/lo.1992.37.1.0105, 1992.

Kendrick, M. R., Huryn, A. D., Bowden, W. B., Deegan, L. A., Findlay, R. H., Hershey, A. E., Peterson, B. J., Beneš, J. P. and Schuett, E. B.: Linking permafrost thaw to shifting biogeochemistry and food web resources in an arctic river, Glob.

Chang. Biol., 24(12), 5738–5750, doi:10.1111/gcb.14448, 2018.

Kieke, D. and Yashayaev, I.: Studies of Labrador Sea Water formation and variability in the subpolar North Atlantic in the light of international partnership and collaboration, Prog. Oceanogr., 132, 220–232, doi:10.1016/j.pocean.2014.12.010, 2015.

Kipp, L. E., Charette, M. A., Moore, W. S., Henderson, P. B. and Rigor, I. G.: Increased fluxes of shelf-derived materials to the central arctic ocean, Sci. Adv., 4(1), 1–10, doi:10.1126/sciadv.aao1302, 2018.

Knapp, A. N., Sigman, D. M. and Lipschultz, F.: N isotopic composition of dissolved organic nitrogen and nitrate at the Bermuda Atlantic Time-series study site, Global Biogeochem. Cycles, 19(1), 1–15, doi:10.1029/2004GB002320, 2005.

Kostyleva, A. V., Polukhin, A. A. and Stepanova, S. V.: Hydrochemical Structural Patterns of the Lena River–Laptev Sea Mixing Zone in the Autumn Period, Oceanology, 60(6), 735–741, doi:10.1134/S0001437020060053, 2020.

Koul, V., Tesdal, J. E., Bersch, M., Hátún, H., Brune, S., Borchert, L., Haak, H., Schrum, C. and Baehr, J.: Unraveling the choice of the north Atlantic subpolar gyre index, Sci. Rep., 10(1), 1–12, doi:10.1038/s41598-020-57790-5, 2020.

Krause, J. ., Duarte, C. ., Marquez, I. ., Assmy, P., Fernandez-Mandez, M., Wiedmann, I., Wassmann, P., Kristiansen, S. and Agusti, S.: Biogenic silica production and diatoms dynamics in the Svalbard region during spring, Biogeosciences, 1–25, 2018.

Krause, J. W., Schulz, I. K., Rowe, K. A., Dobbins, W., Winding, M. H. S., Sejr, M. K., Duarte, C. M. and Agustí, S.: Silicic acid limitation drives bloom termination and potential carbon sequestration in an Arctic bloom, Sci. Rep., 9(1), 1–11, doi:10.1038/s41598-019-44587-4, 2019.

Krisch, S., Browning, T. J., Graeve, M., Ludwichowski, K. U., Lodeiro, P., Hopwood, M. J., Roig, S., Yong, J. C., Kanzow, T. and Achterberg, E. P.: The

influence of Arctic Fe and Atlantic fixed N on summertime primary production in Fram Strait, North Greenland Sea, Sci. Rep., 10(1), 1–13, doi:10.1038/s41598-020-72100-9, 2020.

Krom, M. D., Kress, N. and Fanning, K.: Silica cycling in the ultra-oligotrophic eastern Mediterranean Sea, Biogeosciences, 11(15), 4211–4223, doi:10.5194/bg-11-4211-2014, 2014.

Kwiatkowski, L., Naar, J., Bopp, L., Aumont, O., Defrance, D. and Couespel, D.: Decline in Atlantic Primary Production Accelerated by Greenland Ice Sheet Melt, Geophys. Res. Lett., 46(20), 11347–11357, doi:10.1029/2019GL085267, 2019.

De La Rocha, C. L., Brzezinski, M. A. and DeNiro, M. J.: Purification, Recovery, and Laser-Driven Fluorination of Silicon from Dissolved and Particulate Silica for the Measurement of Natural Stable Isotope Abundances, Anal. Chem., 68(21), 3746–3750, doi:10.1021/ac960326j, 1996.

De La Rocha, C. L., Brzezinski, M. A. and DeNiro, M. J.: Fractionation of silicon isotopes by marine diatoms during biogenic silica formation, Geochim. Cosmochim. Acta, 61(23), 5051–5056, doi:10.1016/S0016-7037(97)00300-1, 1997.

De La Rocha, C. L., Brzezinski, M. A. and Deniro, M. J.: A first look at the distribution of the stable isotopes of silicon in natural waters, Geochim. Cosmochim. Acta, 64(14), 2467–2477, 2000.

Lalande, C., Bauerfeind, E., Nöthig, E. M. and Beszczynska-Möller, A.: Impact of a warm anomaly on export fluxes of biogenic matter in the eastern Fram Strait, Prog. Oceanogr., 109, 70–77, doi:10.1016/j.pocean.2012.09.006, 2013.

Leblanc, K., Leynaert, A., Fernandez, I. C., Rimmelin, P., Moutin, T., Raimbault, P., Ras, J. and Quéguiner, B.: A seasonal study of diatom dynamics in the North Atlantic during the POMME experiment (2001): Evidence for Si limitation of the spring bloom, J. Geophys. Res. C Ocean., 110(7), 1–16, doi:10.1029/2004JC002621, 2005.

Lehmann, N., Kienast, M., Granger, J., Bourbonnais, A., Altabet, M. A. and Tremblay, J.: Remote Western Arctic Nutrients Fuel Remineralization in Deep Baffin Bay, Global Biogeochem. Cycles, 33(6), 649–667, doi:10.1029/2018GB006134, 2019.

Lehmann, N., Kienast, M., Granger, J. and Tremblay, J.: Physical and Biogeochemical Influences on Nutrients Through the Canadian Arctic Archipelago: Insights From Nitrate Isotope Ratios, J. Geophys. Res. Ocean., 127(3), 1–24, doi:10.1029/2021JC018179, 2022.

Létolle, R., Martin, J. M., Thomas, A. J., Gordeev, V. V., Gusarova, S. and Sidorov, I. S.: 18O abundance and dissolved silicate in the Lena delta and Laptev Sea (Russia), Mar. Chem., 43(1–4), 47–64, doi:10.1016/0304-4203(93)90215-A, 1993.

Letscher, R. T., Hansell, D. A., Kadko, D. and Bates, N. R.: Dissolved organic nitrogen dynamics in the Arctic Ocean, Mar. Chem., 148, 1–9, doi:10.1016/j.marchem.2012.10.002, 2013.

Li, F., Lozier, M. S., Bacon, S., Bower, A. S., Cunningham, S. A., de Jong, M. F., deYoung, B., Fraser, N., Fried, N., Han, G., Holliday, N. P., Holte, J., Houpert, L., Inall, M. E., Johns, W. E., Jones, S., Johnson, C., Karstensen, J., Le Bras, I. A., Lherminier, P., Lin, X., Mercier, H., Oltmanns, M., Pacini, A., Petit, T., Pickart, R. S., Rayner, D., Straneo, F., Thierry, V., Visbeck, M., Yashayaev, I. and Zhou, C.: Subpolar North Atlantic western boundary density anomalies and the Meridional Overturning Circulation, Nat. Commun., 12(1), 1–9, doi:10.1038/s41467-021-23350-2, 2021.

Liguori, B. T. P., Ehlert, C. and Pahnke, K.: The Influence of Water Mass Mixing and Particle Dissolution on the Silicon Cycle in the Central Arctic Ocean, Front. Mar. Sci., 7(April), 1–16, doi:10.3389/fmars.2020.00202, 2020.

Liguori, B. T. P., Ehlert, C., Nöthig, E. M., van Ooijen, J. C. and Pahnke, K.: The Transpolar Drift Influence on the Arctic Ocean Silicon Cycle, J. Geophys. Res. Ocean., 126(11), doi:10.1029/2021JC017352, 2021.

Lind, S., Ingvaldsen, R. B. and Furevik, T.: Arctic warming hotspot in the northern Barents Sea linked to declining sea-ice import, Nat. Clim. Chang., 8(634), doi:10.1038/s41558-018-0205-y, 2018.

Lozier, M. S., Li, F., Bacon, S., Bahr, F., Bower, A. S., Cunningham, S. A., De Jong, M. F., De Steur, L., DeYoung, B., Fischer, J., Gary, S. F., Greenan, B. J. W., Holliday, N. P., Houk, A., Houpert, L., Inall, M. E., Johns, W. E., Johnson, H. L., Johnson, C., Karstensen, J., Koman, G., Le Bras, I. A., Lin, X., Mackay, N., Marshall, D. P., Mercier, H., Oltmanns, M., Pickart, R. S., Ramsey, A. L., Rayner, D., Straneo, F., Thierry, V., Torres, D. J., Williams, R. G., Wilson, C., Yang, J., Yashayaev, I. and Zhao, J.: A sea change in our view of overturning in the subpolar North Atlantic, Science (80-.)., 363(6426), 516–521, doi:10.1126/science.aau6592, 2019.

Lundrigan, S. and Demirov, E.: Long-term variability of volume and heat transport in the nordic seas: A model study, Atmos. - Ocean, 50(2), 156–168, doi:10.1080/07055900.2012.683769, 2012.

Macdonald, R. W., Anderson, L. G., Christensen, J. P., Miller, L. ., Semiletov, I. P. and Stein, R.: The Arctic Ocean, in Carbon and Nutrient Fluxes in Continental Margins, edited by K. K. Liu, pp. 292–303, Springer-Verlag Berlin Heidelberg., 2010.

Macdonald, R. W., Kuzyk, Z. A. and Johannessen, S. C.: It is not just about the ice: a geochemical perspective on the changing Arctic Ocean, J. Environ. Stud. Sci., 5(3), 288–301, doi:10.1007/s13412-015-0302-4, 2015.

Maldonado, M., López-Acosta, M., Sitjà, C., García-Puig, M., Galobart, C., Ercilla, G. and Leynaert, A.: Sponge skeletons as an important sink of silicon in the global oceans, Nat. Geosci., 12(10), 815–822, doi:10.1038/s41561-019-0430-7, 2019.

Mammone, K. A.: Sediment provenance and transport on the Siberian Arctic shelf, Master thesis, 1998.

Marconi, D., Weigand, M. A., Rafter, P. A., McIlvin, M. R., Forbes, M., Casciotti,

K. L. and Sigman, D. M.: Nitrate isotope distributions on the US GEOTRACES North Atlantic cross-basin section: Signals of polar nitrate sources and low latitude nitrogen cycling, Mar. Chem., 177, 143–156, doi:10.1016/j.marchem.2015.06.007, 2015.

Marconi, D., Weigand, M. A. and Sigman, D. M.: Nitrate isotopic gradients in the North Atlantic Ocean and the nitrogen isotopic composition of sinking organic matter, Deep. Res. Part I Oceanogr. Res. Pap., 145(January), 109–124, doi:10.1016/j.dsr.2019.01.010, 2019.

Mariotti, A., Germon, J. C., Hubert, P., Kaiser, P., Letolle, R., Tardieux, A. and Tardieux, P.: Experimental determination of nitrogen kinetic isotope fractionation: some principles; illustration for the denitrification and nitrification processes, Plant Soil, 62, 413–430, 1981.

Martin, P., Lampitt, R. S., Jane Perry, M., Sanders, R., Lee, C. and D'Asaro, E.: Export and mesopelagic particle flux during a North Atlantic spring diatom bloom, Deep. Res. Part I Oceanogr. Res. Pap., 58(4), 338–349, doi:10.1016/j.dsr.2011.01.006, 2011.

März, C., Meinhardt, A. K., Schnetger, B. and Brumsack, H. J.: Silica diagenesis and benthic fluxes in the Arctic Ocean, Mar. Chem., 171, 1–9, doi:10.1016/j.marchem.2015.02.003, 2015.

Mathis, M. and Mikolajewicz, U.: The impact of meltwater discharge from the Greenland ice sheet on the Atlantic nutrient supply to the northwest European shelf, Ocean Sci., 16(1), 167–193, doi:10.5194/os-16-167-2020, 2020.

Mavromatis, V., Rinder, T., Prokushkin, A. S., Pokrovsky, O. S., Korets, M. A., Chmeleff, J. and Oelkers, E. H.: The effect of permafrost, vegetation, and lithology on Mg and Si isotope composition of the Yenisey River and its tributaries at the end of the spring flood, Geochim. Cosmochim. Acta, 191, 32–46, doi:10.1016/j.gca.2016.07.003, 2016.

Mcclelland, J. W., De, S. J., Peterson, B. J., Holmes, R. M. and Wood, E. F.: A pan-

arctic evaluation of changes in river discharge during the latter half of the 20th century, Geophys. Res. Lett., 33, 2–5, doi:10.1029/2006GL025753, 2006.

McClelland, J. W., Holmes, R. M., Dunton, K. H. and Macdonald, R. W.: The Arctic Ocean Estuary, Estuaries and Coasts, 35(2), 353–368, doi:10.1007/s12237-010-9357-3, 2012.

McDougall, T. . and P.M. Barker: Getting started with TEOS-10 and the Gibbs Seawater (GSW) Oceanographic Toolbox, , 28, doi:SCOR/IAPSO WG127, ISBN 978-0-646-55621-5, 2011.

Mctigue, N. D., Gardner, W. S., Dunton, K. H. and Hardison, A. K.: Biotic and abiotic controls on co-occurring nitrogen cycling processes in shallow Arctic shelf sediments, Nat. Commun., 7, 1–11, doi:10.1038/ncomms13145, 2016.

Meire, L., Meire, P., Struyf, E., Krawczyk, D. W., Arendt, K. E., Yde, J. C., Juul Pedersen, T., Hopwood, M. J., Rysgaard, S. and Meysman, F. J. R.: High export of dissolved silica from the Greenland Ice Sheet, Geophys. Res. Lett., 43(17), 9173–9182, doi:10.1002/2016GL070191, 2016.

Michalopoulos, P. and Aller, R. C.: Early diagenesis of biogenic silica in the Amazon delta: Alteration, authigenic clay formation, and storage, Geochim. Cosmochim. Acta, 68(5), 1061–1085, doi:10.1016/j.gca.2003.07.018, 2004.

Moore, C. M., Mills, M. M., Langlois, R., Milne, A., Achterberg, E. P., La Roche, J. and Geider, R. J.: Relative influence of nitrogen and phosphorus availability on phytoplankton physiology and productivity in the oligotrophic sub-tropical North Atlantic Ocean, Limnol. Oceanogr., 53(1), 291–305, doi:10.4319/lo.2008.53.1.0291, 2008.

Moore, C. M., Mills, M. M., Arrigo, K. R., Berman-Frank, I., Bopp, L., Boyd, P. W., Galbraith, E. D., Geider, R. J., Guieu, C., Jaccard, S. L., Jickells, T. D., La Roche, J., Lenton, T. M., Mahowald, N. M., Marañón, E., Marinov, I., Moore, J. K., Nakatsuka, T., Oschlies, A., Saito, M. A., Thingstad, T. F., Tsuda, A. and Ulloa, O.: Processes and patterns of oceanic nutrient limitation, Nat. Geosci., 6(9), 701–710,

doi:10.1038/ngeo1765, 2013.

Morley, D. W., Leng, M. J., Mackay, A. W., Sloane, H. J., Rioual, P. and Battarbee, R. W.: Cleaning of lake sediment samples for diatom oxygen isotope analysis, J. Paleolimnol., 31(3), 391–401, doi:10.1023/B:JOPL.0000021854.70714.6b, 2004.

Muglia, J., Skinner, L. C. and Schmittner, A.: Weak overturning circulation and high Southern Ocean nutrient utilization maximized glacial ocean carbon, Earth Planet. Sci. Lett., 496, 47–56, doi:10.1016/j.epsl.2018.05.038, 2018.

Nelson, D. M., Tréguer, P., Brzezinski, M. A., Leynaert, A. and Quéguiner, B.: Production and dissolution of biogenic silica in the ocean: Revised global estimates, comparison with regional data and relationship to biogenic sedimentation, Global Biogeochem. Cycles, 9(3), 359–372, doi:10.1029/95GB01070, 1995.

Neukermans, G., Oziel, L. and Babin, M.: Increased intrusion of warming Atlantic water leads to rapid expansion of temperate phytoplankton in the Arctic, Glob. Chang. Biol., 24(6), 2545–2553, doi:10.1111/gcb.14075, 2018.

Ng, H. C., Cassarino, L., Pickering, R. A., Woodward, E. M. S., Hammond, S. J. and Hendry, K. R.: Sediment efflux of silicon on the Greenland margin and implications for the marine silicon cycle, Earth Planet. Sci. Lett., 529, 115877, doi:10.1016/j.epsl.2019.115877, 2020.

Notz, D. and Community, S.: Arctic Sea Ice in CMIP6, Geophys. Res. Lett., 47(10), 1–11, doi:10.1029/2019GL086749, 2020.

Notz, D. and Stroeve, J.: Observed Arctic sea-ice loss directly follows anthropogenic CO2 emission, Science (80-.)., 354(6313), 747–750, doi:10.1126/science.aag2345, 2016.

Nürnberg, D., Stein, R., Polyakova, Y. and Pivovoarov, S. V.: Biogenic opal in shallow Eurasian shelf sediments in relation to the pelagic Arctic Ocean environment, Mitteilungen zur Kieler Polarforsch., 1997.

Olafsson, J., Olafsdottir, S. R., Takahashi, T., Danielsen, M. and Arnarson, T. S.: Enhancement of the North Atlantic CO2sink by Arctic Waters, Biogeosciences, 18(5), 1689–1701, doi:10.5194/bg-18-1689-2021, 2021.

Olsen, A., Key, R. M., Van Heuven, S., Lauvset, S. K., Velo, A., Lin, X., Schirnick, C., Kozyr, A., Tanhua, T., Hoppema, M., Jutterström, S., Steinfeldt, R., Jeansson, E., Ishii, M., Pérez, F. F. and Suzuki, T.: The global ocean data analysis project version 2 (GLODAPv2) - An internally consistent data product for the world ocean, Earth Syst. Sci. Data, 8(2), 297–323, doi:10.5194/essd-8-297-2016, 2016.

Van Oostende, N., Fawcett, S. E., Marconi, D., Lueders-Dumont, J., Sabadel, A. J. M., Woodward, E. M. S., Jönsson, B. F., Sigman, D. M. and Ward, B. B.: Variation of summer phytoplankton community composition and its relationship to nitrate and regenerated nitrogen assimilation across the North Atlantic Ocean, Deep. Res. Part I Oceanogr. Res. Pap., 121, 79–94, doi:10.1016/j.dsr.2016.12.012, 2017.

Opfergelt, S. and Delmelle, P.: Silicon isotopes and continental weathering processes: Assessing controls on Si transfer to the ocean, Comptes Rendus - Geosci., 344(11–12), 723–738, doi:10.1016/j.crte.2012.09.006, 2012.

Osadchiev, A. A., Pisareva, M. N., Spivak, E. A., Shchuka, S. A. and Semiletov, I. P.: Freshwater transport between the Kara, Laptev, and East-Siberian seas, Sci. Rep., 10(1), doi:10.1038/s41598-020-70096-w, 2020.

Oziel, L., Baudena, A., Ardyna, M., Massicotte, P., Randelhoff, A., Sallée, J. B., Ingvaldsen, R. B., Devred, E. and Babin, M.: Faster Atlantic currents drive poleward expansion of temperate phytoplankton in the Arctic Ocean, Nat. Commun., 11(1), 1–8, doi:10.1038/s41467-020-15485-5, 2020.

Pabi, S., van Dijken, G. L. and Arrigo, K. R.: Primary production in the Arctic Ocean, 1998-2006, J. Geophys. Res. Ocean., 113(8), 1998–2006, doi:10.1029/2007JC004578, 2008.

Pavlov, V. K., Timokhov, L. A., Baskakov, G. A., Kulakov, M. Y., Kurazhov, V. K., Pavlov, P. V., Pivovoarov, S. V. and Stanovoy, V. V.: Hydrometeorological regime

of the Kara, Laptev, and East-Siberian Seas, Tech. Memo. APL-UW TM, (January), 1–96, 1996.

Peng, X., Fawcett, S. E., van Oostende, N., Wolf, M. J., Marconi, D., Sigman, D. M. and Ward, B. B.: Nitrogen uptake and nitrification in the subarctic North Atlantic Ocean, Limnol. Oceanogr., 63(4), 1462–1487, doi:10.1002/lno.10784, 2018.

Peralta-Ferriz, C. and Woodgate, R. A.: Seasonal and interannual variability of pan-Arctic surface mixed layer properties from 1979 to 2012 from hydrographic data, and the dominance of stratification for multiyear mixed layer depth shoaling, Prog. Oceanogr., 134, 19–53, doi:10.1016/j.pocean.2014.12.005, 2015.

Pichevin, L. E., Ganeshram, R. S., Geibert, W., Thunell, R. and Hinton, R.: Silica burial enhanced by iron limitation in oceanic upwellling margins, Nat. Geosci., 7(July), 541–546, doi:10.1038/NGEO2181, 2014.

Piron, A., Thierry, V., Mercier, H. and Caniaux, G.: Gyre-scale deep convection in the subpolar North Atlantic Ocean during winter 2014–2015, Geophys. Res. Lett., 44(3), 1439–1447, doi:10.1002/2016GL071895, 2017.

Pohlmann, H., Sienz, F. and Latif, M.: Influence of the multidecadal Atlantic meridional overturning circulation variability on European climate, J. Clim., 19(23), 6062–6067, doi:10.1175/JCLI3941.1, 2006.

Pokrovsky, O. S., Reynolds, B. C., Prokushkin, A. S., Schott, J. and Viers, J.: Silicon isotope variations in Central Siberian rivers during basalt weathering in permafrost-dominated larch forests, Chem. Geol., 355, 103–116, doi:10.1016/j.chemgeo.2013.07.016, 2013.

Pokrovsky, O. S., Manasypov, R. M., Kopysov, S. G., Krickov, I. V., Shirokova, L. S., Loiko, S. V., Lim, A. G., Kolesnichenko, L. G., Vorobyev, S. N. and Kirpotin, S. N.: Impact of permafrost thaw and climate warming on riverine export fluxes of carbon, nutrients and metals in Western Siberia, Water (Switzerland), 12(6), doi:10.3390/w12061817, 2020.

Polyakov, I. V., Pnyushkov, A. V., Alkire, M. B., Ashik., I. M., Baumann, T. M., Carmack, E. C., Goszczko, I., Guthrie, J., Ivanov, V. V., Kanzow, T., Krishfield, R., Kwok, R., Sundfjord, A., Morison, J., Rember, R. and Yulin, A.: Greater role for Atlantic inflows on sea-ice loss in the Eurasian Basin of the Arctic Ocean, Science (80-.)., 291(April), 285–291, 2017.

Pondaven, P., Ragueneau, O., Tre, P., Hauvespre, A., Dezileau, L. and Reyss, J. L.: Resolving the “opal paradox” in the Southern Ocean, Nature, 405(May), 168–172, 2000.

Popova, E. E., Yool, A., Coward, A. C., Dupont, F., Deal, C., Elliott, S., Hunke, E., Jin, M., Steele, M. and Zhang, J.: What controls primary production in the Arctic Ocean? Results from an intercomparison of five general circulation models with biogeochemistry, J. Geophys. Res. Ocean., 117(1), 1–16, doi:10.1029/2011JC007112, 2012.

Rafter, P., Bagnell, A., Marconi, D. and Devries, T.: Global trends in marine nitrate N isotopes from observations and a neural network-based climatology, Biogeosciences, 16(13), 2617–2633, doi:10.5194/bg-16-2617-2019, 2019.

Rafter, P. A., Difiore, P. J. and Sigman, D. M.: Coupled nitrate nitrogen and oxygen isotopes and organic matter remineralization in the Southern and Pacific Oceans, J. Geophys. Res. Ocean., 118(10), 4781–4794, doi:10.1002/jgrc.20316, 2013.

Randelhoff, A., Reigstad, M., Chierici, M., Sundfjord, A., Ivanov, V., Cape, M., Vernet, M., Tremblay, J.-É., Bratbak, G. and Kristiansen, S.: Seasonality of the Physical and Biogeochemical Hydrography in the Inflow to the Arctic Ocean Through Fram Strait, Front. Mar. Sci., 5(June), 1–16, doi:10.3389/fmars.2018.00224, 2018.

Rawlins, M. A., Steele, M., Holland, M. M., Adam, J. C., Cherry, J. E., Francis, J. A., Groisman, P. Y., Hinzman, L. D., Huntington, T. G., Kane, D. L., Kimball, J. S., Kwok, R., Lammers, R. B., Lee, C. M., Lettenmaier, D. P., Mcdonald, K. C., Podest, E., Pundsack, J. W., Rudels, B., Serreze, M. C., Shiklomanov, A., Skagseth, Ø.,

Troy, T. J., Vörösmarty, C. J., Wensnahan, M., Wood, E. F., Woodgate, R., Yang, D., Zhang, K. and Zhang, T.: Analysis of the Arctic system for freshwater cycle intensification: Observations and expectations, J. Clim., 23(21), 5715–5737, doi:10.1175/2010JCLI3421.1, 2010.

Rehkämper, M., Schönbächler, M. and Stirling, C. H.: Multiple collector ICP-MS: Introduction to instrumentation, measurement techniques and analytical capabilities, Geostand. Newsl., 25(1), 23–40, doi:10.1111/j.1751-908X.2001.tb00785.x, 2001.

Reigstad, M., Wassmann, P., Wexels, C., Øygarden, S. and Rey, F.: Variations in hydrography , nutrients and chlorophyll a in the marginal ice-zone and the central Barents Sea, J. Mar. Syst., 38, 9–29, 2002.

Reynolds, B. C., Frank, M. and Halliday, A. N.: Silicon isotope fractionation during nutrient utilization in the North Pacific, Earth Planet. Sci. Lett., 244(1–2), 431–443, doi:10.1016/j.epsl.2006.02.002, 2006.

Reynolds, B. C., Aggarwal, J., Andre, L., Georg, R. B., Beucher, C., Brzezinski, M. A., Engstro, E., Land, M., Leng, M. J., Opfergelt, S., Rodushkin, I., Sloane, H. J., Boorn, S. H. J. M. Van Den and Vroon, Z.: An inter-laboratory comparison of Si isotope reference materials, J. Anal. At. Spectrom., 22, 561–568, doi:10.1039/b616755a, 2007.

Richter, M. E., Von Appen, W. J. and Wekerle, C.: Does the East Greenland Current exist in the northern Fram Strait?, Ocean Sci., 14(5), 1147–1165, doi:10.5194/os-14-1147-2018, 2018.

Rodellas, V., Garcia-Orellana, J., Masqué, P., Feldman, M., Weinstein, Y. and Boyle, E. A.: Submarine groundwater discharge as a major source of nutrients to the Mediterranean Sea, Proc. Natl. Acad. Sci. U. S. A., 112(13), 3926–3930, doi:10.1073/pnas.1419049112, 2015.

Rudels, B., Jones, E. P., Anderson, L. G. and Kattner, G.: On the Intermediate Depth Waters of the Arctic Ocean, Geophys. Monogr., (85), 33–46, doi:10.1029/gm085p0033, 1994.

Rudels, B., Fahrbach, E., Meincke, J., Budéus, G. and Eriksson, P.: The East Greenland Current and its contribution to the Denmark Strait overflow, ICES J. Mar. Sci., 59(6), 1133–1154, doi:10.1006/jmsc.2002.1284, 2002.

Rudels, B., Jones, E. P., Schauer, U. and Eriksson, P.: Atlantic sources of the Arctic Ocean surface and halocline waters, Polar Res., 23(2), 181–208, doi:10.1111/j.1751-8369.2004.tb00007.x, 2004.

Rudels, B., Björk, G., Nilsson, J., Winsor, P., Lake, I. and Nohr, C.: The interaction between waters from the Arctic Ocean and the Nordic Seas north of Fram Strait and along the East Greenland Current: Results from the Arctic Ocean-02 Oden expedition, J. Mar. Syst., 55(1–2), 1–30, doi:10.1016/j.jmarsys.2004.06.008, 2005.

Sakshaug, E.: Primary and Secondary Production in the Arctic Seas, Org. Carbon Cycle Arct. Ocean, 57–81, doi:10.1007/978-3-642-18912-8_3, 2004.

Sanders, T., Fiencke, C., Fuchs, M., Haugk, C., Juhls, B., Mollenhauer, G., Ogneva, O., Overduin, P., Palmtag, J., Povazhniy, V., Strauss, J., Tuerena, R., Zell, N. and Dähnke, K.: Seasonal nitrogen fluxes of the Lena River Delta, Ambio, 423–438, doi:10.1007/s13280-021-01665-0, 2021.

Sarmiento, J. L., Gruber, N., Brzezinski, M. A. and Dunne, J. P.: High-latitude controls of thermocline nutrients and low latitude biological productivity, Nature, 427(6969), 56–60, doi:10.1038/nature02127, 2004.

Saunders, P. M.: The dense northern overflows, in Ocean Circulation and Climate, edited by G. Siedler, J. Church, and J. Gould, pp. 401–417, Academic Press, London, UK., 2001.

Schlitzer, R.: Ocean Data View, 2021.

Schlitzer, R., Anderson, R. F., Dodas, E. M., Lohan, M., Geibert, W., Tagliabue, A., Bowie, A., Jeandel, C., Maldonado, M. T., Landing, W. M., Cockwell, D., Abadie, C., Abouchami, W., Achterberg, E. P., Agather, A., Aguliar-Islas, A., van Aken, H. M., Andersen, M., Archer, C., Auro, M., de Baar, H. J., Baars, O., Baker, A. R.,

Bakker, K., Basak, C., Baskaran, M., Bates, N. R., Bauch, D., van Beek, P., Behrens, M. K., Black, E., Bluhm, K., Bopp, L., Bouman, H., Bowman, K., Bown, J., Boyd, P., Boye, M., Boyle, E. A., Branellec, P., Bridgestock, L., Brissebrat, G., Browning, T., Bruland, K. W., Brumsack, H. J., Brzezinski, M., Buck, C. S., Buck, K. N., Buesseler, K., Bull, A., Butler, E., Cai, P., Mor, P. C., Cardinal, D., Carlson, C., Carrasco, G., Casacuberta, N., Casciotti, K. L., Castrillejo, M., Chamizo, E., Chance, R., Charette, M. A., Chaves, J. E., Cheng, H., Chever, F., Christl, M., Church, T. M., Closset, I., Colman, A., Conway, T. M., Cossa, D., Croot, P., Cullen, J. T., Cutter, G. A., Daniels, C., Dehairs, F., Deng, F., Dieu, H. T., Duggan, B., Dulaquais, G., Dumousseaud, C., Echegoyen-Sanz, Y., Edwards, R. L., Ellwood, M., Fahrbach, E., Fitzsimmons, J. N., Russell Flegal, A., Fleisher, M. Q., van de Flierdt, T., Frank, M., Friedrich, J., Fripiat, F., Fröllje, H., Galer, S. J. G., Gamo, T., Ganeshram, R. S., Garcia-Orellana, J., Garcia-Solsona, E., Gault-Ringold, M., et al.: The GEOTRACES Intermediate Data Product 2017, Chem. Geol., 493(June), 210–223, doi:10.1016/j.chemgeo.2018.05.040, 2018.

Schneider, W. and Budeus, G.: On the generation of the Northeast Water Polynya, J. Geophys. Res., 100(C3), 4269–4286, doi:10.1029/94JC02349, 1995.

Schnetger, B. and Lehners, C.: Determination of nitrate plus nitrite in small volume marine water samples using vanadium(III)chloride as a reduction agent, Mar. Chem., 160, 91–98, doi:10.1016/j.marchem.2014.01.010, 2014.

Semiletov, I. P., Savelieva, N. I., Weller, G. E., Pipko, I. I., Pugach, S. P., Gukov, A. Y. and Vasilevskaya, L. N.: The Dispersion of Siberian River Flows into Coastal Waters: Meteorological, Hydrological and Hydrochemical Aspects, in The Freshwater Budget of the Arctic Ocean, edited by E. . Lewis, E. P. Jones, P. Lemke, T. D. Prowse, and P. Wadhams, pp. 323–366, Springer, Dordrecht., 2000.

Sigman, D. M., Altabet, M. A., McCorkle, D. C., Francois, R. and Fischer, G.: The δ^{15} N of nitrate in the Southern Ocean: Nitrogen cycling and circulation in the ocean interior, J. Geophys. Res. Ocean., 105(C8), 19599–19614, doi:10.1029/2000JC000265, 2000.

Sigman, D. M., Casciotti, K. L., Andreani, M., Barford, C., Galanter, M. and Böhlke, J. K.: A bacterial method for the nitrogen isotopic analysis of nitrate in seawater and freshwater, Anal. Chem., 73(17), 4145–4153, doi:10.1021/ac010088e, 2001.

Sigman, D. M., Robinson, R., Knapp, A. N., Van Geen, A., McCorkle, D. C., Brandes, J. A. and Thunell, R. C.: Distinguishing between water column and sedimentary denitrification in the Santa Barbara Basin using the stable isotopes of nitrate, Geochemistry, Geophys. Geosystems, 4(5), 1–20, doi:10.1029/2002GC000384, 2003.

Sigman, D. M., Granger, J., DiFiore, P. J., Lehmann, M. M., Ho, R., Cane, G. and van Geen, A.: Coupled nitrogen and oxygen isotope measurements of nitrate along the eastern North Pacific margin, Global Biogeochem. Cycles, 19(4), 1–14, doi:10.1029/2005GB002458, 2005.

Sigman, D. M., Karsh, K. . and Casciotti, K. L.: Ocean process tracers: Nitrogen isotopes in the ocean, Encycl. Ocean Sci., doi:10.1016/B978-0-12-409548-9.11605-7, 2009a.

Sigman, D. M., DiFiore, P. J., Hain, M. P., Deutsch, C., Wang, Y., Karl, D. M., Knapp, A. N., Lehmann, M. F. and Pantoja, S.: The dual isotopes of deep nitrate as a constraint on the cycle and budget of oceanic fixed nitrogen, Deep. Res. Part I Oceanogr. Res. Pap., 56(9), 1419–1439, doi:10.1016/j.dsr.2009.04.007, 2009b.

Simpson, K. G., Tremblay, J. É., Gratton, Y. and Price, N. M.: An annual study of inorganic and organic nitrogen and phosphorus and silicic acid in the southeastern Beaufort Sea, J. Geophys. Res. Ocean., 113(7), 1–16, doi:10.1029/2007JC004462, 2008.

De Souza, G. F., Reynolds, B. C., Rickli, J., Frank, M., Saito, M. A., Gerringa, L. J. A. and Bourdon, B.: Southern Ocean control of silicon stable isotope distribution in the deep Atlantic Ocean, Global Biogeochem. Cycles, 26(2), 1–13, doi:10.1029/2011GB004141, 2012.

De Souza, G. F., Slater, R. D., Hain, M. P., Brzezinski, M. A. and Sarmiento, J. L.:

Distal and proximal controls on the silicon stable isotope signature of North Atlantic Deep Water, Earth Planet. Sci. Lett., 432, 342–353, doi:10.1016/j.epsl.2015.10.025, 2015.

Spivak, E. A., Osadchiev, A. A. and Semiletov, I. P.: Structure and Variability of the Lena River Plume in the South-Eastern Part of the Laptev Sea, Oceanology, 61(6), 839–849, doi:10.1134/S000143702106014X, 2021.

Srokosz, M., Baringer, M., Bryden, H., Cunningham, S., Delworth, T., Lozier, S., Marotzke, J. and Sutton, R.: Past, present, and future changes in the atlantic meridional overturning circulation, Bull. Am. Meteorol. Soc., 93(11), 1663–1676, doi:10.1175/BAMS-D-11-00151.1, 2012.

Stedmon, C. A., Amon, R. M. W., Rinehart, A. J. and Walker, S. A.: The supply and characteristics of colored dissolved organic matter (CDOM) in the Arctic Ocean: Pan Arctic trends and differences, Mar. Chem., 124(1–4), 108–118, doi:10.1016/j.marchem.2010.12.007, 2011.

Stedmon, C. A., Granskog, M. A. and Dodd, P. A.: An approach to estimate the freshwater contribution from glacial melt and precipitation in East Greenland shelf waters using colored dissolved organic matter (CDOM), J. Geophys. Res. Ocean., 1107–1117, doi:10.1002/2015JC011107.Received, 2015.

de Steur, L.: Fram Strait Cruise Report (FS2017), , (September), 2017.

de Steur, L.: Fram Strait Cruise Report (FS2018), , (September), 2018.

de Steur, L.: Fram Strait Cruise Report (FS2019), , (September), 2019.

de Steur, L., Hansen, E., Gerdes, R., Karcher, M., Fahrbach, E. and Holfort, J.: Freshwater fluxes in the East Greenland Current: A decade of observations, Geophys. Res. Lett., 36(23), L23611, doi:10.1029/2009GL041278, 2009.

Sun, X., Mörth, C. M., Porcelli, D., Kutscher, L., Hirst, C., Murphy, M. J., Maximov, T., Petrov, R. E., Humborg, C., Schmitt, M. and Andersson, P. S.: Stable silicon

isotopic compositions of the Lena River and its tributaries: Implications for silicon delivery to the Arctic Ocean, Geochim. Cosmochim. Acta, 241, 120–133, doi:10.1007/978-981-13-0589-4_20, 2018.

Sun, X., Humborg, C., Mörth, C. M. and Brüchert, V.: The Importance of Benthic Nutrient Fluxes in Supporting Primary Production in the Laptev and East Siberian Shelf Seas, Global Biogeochem. Cycles, 35(7), doi:10.1029/2020GB006849, 2021.

Sunda, W. G. and Huntsman, S. A.: Iron uptake and growth limitation in oceanic and coastal phytoplankton, Mar. Chem., 50, 189–206, 1995.

Sundfjord, A., Fer, I., Kasajima, Y. and Svendsen, H.: Observations of turbulent mixing and hydrography in the marginal ice zone of the Barents Sea, J. Geophys. Res. Ocean., 112(5), 1–23, doi:10.1029/2006JC003524, 2007.

Sutton, J. N., Varela, D. E., Brzezinski, M. A. and Beucher, C. P.: Species-dependent silicon isotope fractionation by marine diatoms, Geochim. Cosmochim. Acta, 104, 300–309, doi:10.1016/j.gca.2012.10.057, 2013.

Sutton, J. N., André, L., Cardinal, D., Conley, D. J., de Souza, G. F., Dean, J., Dodd, J., Ehlert, C., Ellwood, M. J., Frings, P. J., Grasse, P., Hendry, K., Leng, M. J., Michalopoulos, P., Panizzo, V. N. and Swann, G. E. A.: A Review of the Stable Isotope Bio-geochemistry of the Global Silicon Cycle and Its Associated Trace Elements, Front. Earth Sci., 5(January), doi:10.3389/feart.2017.00112, 2018a.

Sutton, J. N., De Souza, G. F., García-Ibáñez, M. I. and Rocha, C. L. D. La: The silicon stable isotope distribution along the GEOVIDE section (GEOTRACES GA-01) of the North Atlantic Ocean, Biogeosciences, 15(18), 5663–5676, doi:10.5194/bg-15-5663-2018, 2018b.

Tagliabue, A., Bopp, L., Roche, D. M., Bouttes, N., Dutay, J. C., Alkama, R., Kageyama, M., Michel, E. and Paillard, D.: Quantifying the roles of ocean circulation and biogeochemistry in governing ocean carbon-13 and atmospheric carbon dioxide at the last glacial maximum, Clim. Past, 5(4), 695–706, doi:10.5194/cp-5-695-2009, 2009.

Takahashi, T., Sutherland, S. C., Sweeney, C., Poisson, A., Metzl, N., Tilbrook, B., Bates, N. R., Wanninkhof, R., Feely, R. A., Sabine, C., Olafsson, J. and Nojir: Global air-sea flux of CO2 based on surface ocean pCO2, and seasonal biological and temperature effects, Deep. Res. Part II, 49, 1601–1622 [online] Available from: papers2://publication/uuid/438F305C-9B5A-493D-B7A6-7EAA86F98C00, 2002.

Takahashi, T., Sutherland, S. C., Wanninkhof, R., Sweeney, C., Feely, R. A., Chipman, D. W., Hales, B., Friederich, G., Chavez, F., Sabine, C., Watson, A., Bakker, D. C. E., Schuster, U., Metzl, N., Yoshikawa-Inoue, H., Ishii, M., Midorikawa, T., Nojiri, Y., Körtzinger, A., Steinhoff, T., Hoppema, M., Olafsson, J., Arnarson, T. S., Tilbrook, B., Johannessen, T., Olsen, A., Bellerby, R., Wong, C. S., Delille, B., Bates, N. R. and de Baar, H. J. W.: Climatological mean and decadal change in surface ocean pCO2, and net sea-air CO2 flux over the global oceans, Deep. Res. Part II Top. Stud. Oceanogr., 56(8–10), 554–577, doi:10.1016/j.dsr2.2008.12.009, 2009.

Tamborski, J., Bejannin, S., Garcia-Orellana, J., Souhaut, M., Charbonnier, C., Anschutz, P., Pujo-Pay, M., Conan, P., Crispi, O., Monnin, C., Stieglitz, T., Rodellas, V., Andrisoa, A., Claude, C. and van Beek, P.: A comparison between water circulation and terrestrially-driven dissolved silica fluxes to the Mediterranean Sea traced using radium isotopes, Geochim. Cosmochim. Acta, 238, 496–515, doi:10.1016/j.gca.2018.07.022, 2018.

Terhaar, J., Lauerwald, R., Regnier, P., Gruber, N. and Bopp, L.: Around one third of current Arctic Ocean primary production sustained by rivers and coastal erosion, Nat. Commun., 12(1), 1–10, doi:10.1038/s41467-020-20470-z, 2021.

Thibodeau, B., Bauch, D. and Voss, M.: Nitrogen dynamic in Eurasian coastal Arctic ecosystem: Insight from nitrogen isotope, Global Biogeochem. Cycles, 31(5), 836–849, doi:10.1002/2016GB005593, 2017a.

Thibodeau, B., Bauch, H. A. and Pedersen, T. F.: Stratification-induced variations in nutrient utilization in the Polar North Atlantic during past interglacials, Earth Planet. Sci. Lett., 457, 127–135, doi:10.1016/j.epsl.2016.09.060, 2017b.

Thornalley, D. J. R., Oppo, D. W., Ortega, P., Robson, J. I., Brierley, C. M., Davis, R., Hall, I. R., Moffa-Sanchez, P., Rose, N. L., Spooner, P. T., Yashayaev, I. and Keigwin, L. D.: Anomalously weak Labrador Sea convection and Atlantic overturning during the past 150 years, Nature, 556(7700), 227–230, doi:10.1038/s41586-018-0007-4, 2018.

Torres-Valdés, S., Tsubouchi, T., Bacon, S., Naveira-Garabato, A. C., Sanders, R., McLaughlin, F. A., Petrie, B., Kattner, G., Azetsu-Scott, K. and Whitledge, T. E.: Export of nutrients from the Arctic Ocean, J. Geophys. Res. Ocean., 118(4), 1625–1644, doi:10.1002/jgrc.20063, 2013.

Tréguer, P., Bowler, C., Moriceau, B., Dutkiewicz, S., Gehlen, M., Aumont, O., Bittner, L., Dugdale, R., Finkel, Z., Iudicone, D., Jahn, O., Guidi, L., Lasbleiz, M., Leblanc, K., Levy, M. and Pondaven, P.: Influence of diatom diversity on the ocean biological carbon pump, Nat. Geosci., 11(1), 27–37, doi:10.1038/s41561-017-0028-x, 2018.

Tréguer, P. J.: The Southern Ocean silica cycle, Comptes Rendus - Geosci., 346(11–12), 279–286, doi:10.1016/j.crte.2014.07.003, 2014.

Tréguer, P. J. and De La Rocha, C. L.: The World Ocean Silica Cycle, Ann. Rev. Mar. Sci., 5(1), 477–501, doi:10.1146/annurev-marine-121211-172346, 2013.

Tréguer, P. J., Sutton, J. N., Brzezinski, M., Charette, M. A., Devries, T., Dutkiewicz, S., Ehlert, C., Hawkings, J., Leynaert, A., Liu, S. M., Monferrer, N. L., López-Acosta, M., Maldonado, M., Rahman, S., Ran, L. and Rouxel, O.: Reviews and syntheses: The biogeochemical cycle of silicon in the modern ocean, Biogeosciences, 18(4), 1269–1289, doi:10.5194/bg-18-1269-2021, 2021.

Tremblay, J. É., Simpson, K., Martin, J., Miller, L., Gratton, Y., Barber, D. and Price, N. M.: Vertical stability and the annual dynamics of nutrients and chlorophyll fluorescence in the coastal, southeast Beaufort Sea, J. Geophys. Res. Ocean., 113(7), 1–14, doi:10.1029/2007JC004547, 2008.

Tremblay, J. É., Anderson, L. G., Matrai, P., Coupel, P., Bélanger, S., Michel, C. and

Reigstad, M.: Global and regional drivers of nutrient supply, primary production and CO2 drawdown in the changing Arctic Ocean, Prog. Oceanogr., 139, 171–196, doi:10.1016/j.pocean.2015.08.009, 2015.

Tsubouchi, T., Bacon, S., Naveira Garabato, A. C., Aksenov, Y., Laxon, S. W., Fahrbach, E., Beszczynska-Möller, A., Hansen, E., Lee, C. M. and Ingvaldsen, R. B.: The Arctic Ocean in summer: A quasi-synoptic inverse estimate of boundary fluxes and water mass transformation, J. Geophys. Res. Ocean., 117(1), 1–28, doi:10.1029/2011JC007174, 2012.

Tuerena, R. E., Ganeshram, R. S., Geibert, W., Fallick, A. E., Dougans, J., Tait, A., Henley, S. F. and Woodward, E. M. S.: Nutrient cycling in the Atlantic basin: The evolution of nitrate isotope signatures in water masses, Global Biogeochem. Cycles, 29, 1830–1844, doi:10.1002/2015GB005164, 2015.

Tuerena, R. E., Hopkins, J., Buchanan, P. J., Ganeshram, R. S., Norman, L., W-Jvon-Appen, Tagliabue, A., Doncila, A., Graeve, M., Ludwichowski, K., Dodd, P. A., Vega, C. de la, Salter, I. and Mahaffey, C.: An Arctic strait of two halves: The changing dynamics of nutrient uptake and limitation across the Fram Strait, Global Biogeochem. Cycles, doi:10.1029/2021gb006961, 2021a.

Tuerena, R. E., Hopkins, J., Ganeshram, R. ., Norman, L., De La Vega, C., Jeffreys, R. and Mahaffey, C.: Nitrate assimilation and regeneration in the Barents Sea: Insights from nitrate isotopes, Biogeosciences, 18(2), 637–653, doi:10.5194/bg-18-637-2021, 2021b.

Tuerena, R. E., Mahaffey, C., Henley, S. F., de la Vega, C., Norman, L., Brand, T., Sanders, T., Debyser, M., Dähnke, K., Braun, J. and März, C.: Nutrient pathways and their susceptibility to past and future change in the Eurasian Arctic Ocean, Ambio, 355–369, doi:10.1007/s13280-021-01673-0, 2021c.

Varela, D. ., Brzezinski, M. ., Beucher, C. ., Jones, J. ., Giesbrecht, K. ., Lansard, B. and Mucci, A.: Heavy silicon isotopic composition of silicic acid and biogenic silica in Arctic waters over the Beaufort shelf and the Canada Basin, Global Biogeochem.

Cycles, 30, 804–824, doi:10.1002/2015GB005277.Received, 2016.

Varela, D. E., Pride, C. J. and Brzezinski, M. A.: Biological fractionation of silicon isotopes in Southern Ocean surface waters, Global Biogeochem. Cycles, 18(1), n/a-n/a, doi:10.1029/2003GB002140, 2004.

Voss, M., Bange, H. W., Dippner, J. W., Middelburg, J. J., Montoya, J. P. and Ward, B.: The marine nitrogen cycle: Recent discoveries, uncertaintiesand the potential relevance of climate change, Philos. Trans. R. Soc. B Biol. Sci., 368(1621), doi:10.1098/rstb.2013.0121, 2013.

Ward, J. P. J., Hendry, K. R., Arndt, S., Faust, J. C., Freitas, F. S., Henley, F., Krause, J. W., März, C., Tessin, A. C. and Airs, R. L.: Benthic Silicon Cycling in the Arctic Barents Sea : a Reaction-Transport Model Study, Biogeosciences, (February), 1–34, 2022a.

Ward, J. P. J., Hendry, K. R., Arndt, S., Faust, J. C., Freitas, F. S., Henley, S. F., Krause, J. W., März, C., Ng, H. C., Pickering, R. A. and Tessin, A. C.: Stable Silicon Isotopes Uncover a Mineralogical Control on the Benthic Silicon Cycle in the Arctic Barents Sea, Geochim. Cosmochim. Acta, doi:10.1016/j.gca.2022.05.005, 2022b.

Weigand, M. A., Foriel, J., Barnett, B., Oleynik, S. and Sigman, D. M.: Updates to instrumentation and protocols for isotopic analysis of nitrate by the denitrifier method, Rapid Commun. Mass Spectrom., 30(12), 1365–1383, doi:10.1002/rcm.7570, 2016.

Wetzel, F., de Souza, G. F. and Reynolds, B. C.: What controls silicon isotope fractionation during dissolution of diatom opal?, Geochim. Cosmochim. Acta, 131, 128–137, doi:10.1016/j.gca.2014.01.028, 2014.

Woodgate, R. A.: Increases in the Pacific inflow to the Arctic from 1990 to 2015, and insights into seasonal trends and driving mechanisms from year-round Bering Strait mooring data, Prog. Oceanogr., 160(June 2017), 124–154, doi:10.1016/j.pocean.2017.12.007, 2018.

Yamamoto-Kawai, M., Carmack, E. and McLaughlin, F.: Nitrogen balance and Arctic throughflow, Nature, 443(7107), 43, doi:10.1038/443043a, 2006.

Yashayaev, I.: Hydrographic changes in the Labrador Sea, 1960-2005, Prog. Oceanogr., 73(3–4), 242–276, doi:10.1016/j.pocean.2007.04.015, 2007.

Yashayaev, I. and Loder, J. W.: Enhanced production of Labrador Sea Water in 2008, Geophys. Res. Lett., 36(1), doi:10.1029/2008GL036162, 2009.

Yashayaev, I., Seidov, D. and Demirov, E.: A new collective view of oceanography of the Arctic and North Atlantic basins, Prog. Oceanogr., 132, 1–21, doi:10.1016/j.pocean.2014.12.012, 2015.

Yi, Y., Gibson, J. J., Cooper, L. W., Hélie, J. F., Birks, S. J., McClelland, J. W., Holmes, R. M. and Peterson, B. J.: Isotopic signals (18O, 2H, 3H) of six major rivers draining the pan-Arctic watershed, Global Biogeochem. Cycles, 26(1), doi:10.1029/2011GB004159, 2012.

Yool, A. and Tyrrell, T.: Role of diatoms in regulating the ocean's silicon cycle, Global Biogeochem. Cycles, 17(4), doi:10.1029/2002GB002018, 2003.

Yool, A., Popova, E. E. and Coward, A. C.: Future change in ocean productivity: Is the Arctic the new Atlantic, J. Geophys. Res. Ocean., 120(12), 7771–7790, doi:10.1002/2015JC011167, 2015.

Young, E. D., Galy, A. and Nagahara, H.: Kinetic and equilibrium mass-dependent isotope fractionation laws in nature and their geochemical and cosmochemical significance, Geochim. Cosmochim. Acta, 66(6), 1095–1104, doi:10.1016/S0016-7037(01)00832-8, 2002.

Zhang, R., Sutton, R., Danabasoglu, G., Kwon, Y. O., Marsh, R., Yeager, S. G., Amrhein, D. E. and Little, C. M.: A Review of the Role of the Atlantic Meridional Overturning Circulation in Atlantic Multidecadal Variability and Associated Climate Impacts, Rev. Geophys., 57(2), 316–375, doi:10.1029/2019RG000644, 2019.

Zhang, S. M., Mu, C. C., Li, Z. L., Dong, W. W., Wang, X. Y., Streletskaya, I., Grebenets, V., Sokratov, S., Kizyakov, A. and Wu, X. D.: Export of nutrients and suspended solids from major Arctic rivers and their response to permafrost degradation, Adv. Clim. Chang. Res., 12(4), 466–474, doi:10.1016/j.accre.2021.06.002, 2021.